AVAILABLE TO THE PUBLIC

UNITED AIRCRAFT CORPORATION

GPO PRICE $ _____

CFSTI PRICE(S) $ _____

Hard copy (HC) _____

Microfiche (MF) _____

ff 653 July 65

United Aircraft Research Laboratories

EAST HARTFORD, CONNECTICUT

United Aircraft Research Laboratories

UNITED AIRCRAFT CORPORATION

EAST HARTFORD, CONNECTICUT

Report F-910352-13

Study of Trajectories and Upper Stage Propulsion Requirements for Exploration of the Solar System

Vol. II - Technical Report

Contract NAS2-2928
Final Report

UNCLASSIFIED

REPORTED BY _____
R. V. Ragsac

APPROVED BY _____
J. L. Cooley
Chief, Systems Analysis Section

DATE September 1967

NO. OF PAGES _____

COPY NO. 67

Report F-910352-13

Study of Trajectories and Upper Stage Propulsion Requirements for Exploration of the Solar System

Contract NAS2-2928
Vol. II - Technical Report
Final Report

TABLE OF CONTENTS

TABLE OF CONTENTS (Contd.)

TABLE OF CONTENTS (Contd.)

FOREWORD

This document is the Technical Report for the Study of Trajectories and Upper Stage Propulsion Requirements for Exploration of the Solar System. The study effort was sponsored by the Mission Analysis Division of NASA Headquarters, OART, Moffett Field, California, under Contract No. NAS2-2928.

The complete results of the study are contained in the following volumes:

Volume I - Summary
Volume II - Technical Report
Volume III - User's Manual for Power-Limited Trajectory Optimization Computer Program

The current study is an extension to the original one-year contract which began in July 1965. The period of performance for the extension was from August 1966 to September 1967. Interim quarterly reports published under the contract extension are United Aircraft Research Laboratories Report E-910352-10, November 1966, and F-910352-11, February 1967, both entitled "Study of Trajectories and Upper Stage Propulsion Requirements for Exploration of the Solar System", and F-910352-12, "Aids for Analyzing Constant-Thrust, Low-Acceleration Propulsion Systems".

ACKNOWLEDGMENT

The following personnel contributed to the preparation of this report and to the different phases of the study as indicated:

R. V. Ragsac	Program Manager Low-Thrust Planetocentric Studies Low-Thrust Propulsion System Analysis
W. R. Fimple	Variational Trajectory Analysis
R. Gogolewski	High-Low Thrust Planetocentric Studies
C. P. Van Dine	Trajectory Optimization Computer Program
T. N. Edelbaum (Consultant)	Planetocentric-Heliocentric Trajectory Matching

SECTION I

SUMMARY

This report summarizes the work accomplished under Modification No. 4 of NASA Contract No. NAS2-2928 between the United Aircraft Research Laboratories and the Mission Analysis Division, Office of Advanced Research and Technology.

Objectives and Scope

The basic objective of this research effort is to develop user-oriented computer programs for solving selected trajectory and system optimization problems characteristic of low-acceleration, power-limited, constant-thrust (electrically propelled) interplanetary vehicles. A series of heliocentric trajectory and system optimization problems was first formulated by the calculus of variations, and selected problems from this series were solved by the implicit finite-difference Newton-Raphson algorithm. The problem of combining the heliocentric trajectory phase with the planetocentric phase (for low acceleration solely or in combination with high acceleration) was analyzed to justify the computational separation of each phase in the minimization of the overall vehicle mass.

Major Results and Accomplishments

In general, the research effort produced programs which simultaneously optimized both the propulsion system and the trajectory (system-trajectory optimizations), a combined high- and low-acceleration mass minimization program, a suggested procedure for optimizing an all-electric vehicle, improvements in the previously developed constant-thrust, a single-coast system-trajectory optimization program, and complete sets of variational equations for a series of system-trajectory optimization problems of near-term and future interest. Although attempts were not made to solve all of the formulated problems of the series, those that were successfully programmed represent a considerable achievement in the economical computation of accurate, optimum, constant-thrust, multiple-coast, power-limited trajectories; especially in view of the fact that the propulsion system parameters are simultaneously optimized for given hyperbolic excess speeds and variable power.

Summarized below are specific major results and accomplishments of several programming, numerical, and analytical studies which contributed to the formulation, development, and subsequent utilization of the object computer program. Three general areas of effort are presented. These include, first, the computer programs

developed for analyzing certain power-limited, heliocentric trajectory and system optimization problems, and for minimizing the mass of mixed high- and low-acceleration propulsion vehicles. Presented next are the results of the numerical and analytical treatments concerning the problem of thrusting within the planet's sphere of influence (low acceleration solely or in combination with high acceleration) and the associated problem of calculating trajectories which transit the gravitational fields of both the planet and the sun. The third effort consists of the variational formulations for trajectory problems of interest not only to the present study but also of general interest for future programming efforts and subsequent mission mode studies.

From these several areas of study, additional problems of both a trajectory and system nature emerge which are of interest in the overall plan of analyzing electric propulsion mission modes and concepts. These important areas are presented under Recommendations for Future Studies.

Developed Computer Programs

1. Optimization of Heliocentric Power-Limited Trajectories

Planet-to-planet rendezvous is treated with an internal discrimination between one or two coast periods. One-way planetary flybys are included with either one or two coasts allowed. Hyperbolic excess speeds are to be specified at both departure and arrival for the rendezvous whereas only the departure need be given for the flyby (final hyperbolic speed is open). In both modes the option is given for optimizing either the exhaust velocity and powerplant fraction. Power, a function of heliocentric position or constant, is an option as is the choice of two- or three-dimensional trajectories.

A round-trip stopover mission can be optimized with respect to the distribution of outbound and inbound legs for fixed total trip time, planetary stay time, and given hyperbolic velocities. The hyperbolic velocities are to be specified at Earth departure, planetary arrival and departure, and either specified or left open for Earth arrival. The variable-thrust, constant-power operating mode is used.

A user's manual was developed as part of this programming effort. Sufficient information and guidelines are described to reduce the time required in familiarizing the user with the general operating characteristics of the program and to expedite the computation of desired trajectories. This manual is given in Volume III of this report and is considered to be an integral part of the heliocentric trajectory optimization program.

2. Minimization of Hybrid-Thrust Vehicle Mass

The initial mass on Earth parking orbit is minimized for a vehicle employing mixed high- and low-acceleration propulsion. The flight modes are parking

orbit to parking orbit, one-way flyby, and round-trip stopover. In the first case, high thrust is used for departure and arrival, while low-thrust is employed in between. In the second case, there is no high-thrust propulsion at planetary arrival. The third case is a combination of the first two. Actual masses (not dimensionless fraction) are computed for the high-thrust and low-thrust systems once payload mass and hyperbolic speeds are given. A search procedure is used to determine the optimum combination of high-low thrust which results in minimum vehicle mass for the given payload. A range of high-thrust propulsion is possible through the specification of certain engine parameters.

3. Improved Single-Coast Trajectory Program

The previous single-coast, constant-thrust program was improved by employing closed-form expressions for optimum exhaust velocity and powerplant fraction which are based on a given thrustor efficiency function and a simplified payload fraction definition. These expressions are used in conjunction with the trajectory optimization subroutine to obtain results of interest by themselves or for use as starting guesses for an improved payload fraction definition. This improved definition accounts for propellant tanks, tie-in structure, and thrustor mass and efficiency varying with exhaust velocity. Optimum exhaust velocity and powerplant fraction are computed for rendezvous only (specified hyperbolic velocity at departure and arrival) and for either or both payload definitions.

A closed-form expression is employed for estimating the maximum powerplant specific mass which yields zero payload for a given trajectory. Computations of specific masses greater than this maximum are avoided.

Heliocentric/Planetocentric Trajectory and System Analyses

1. Combined High-Low Thrusting Within the Planet's Sphere of Influence

A numerical analysis was performed to determine the effects of neglecting the low-thrust system's operation within the planet's activity sphere immediately after high-thrust burnout. The trajectory problem was analyzed by numerically integrating the planetocentric equations of motion for both high- and low-thrust operation until the sphere of influence is reached. In general, the time in which the low-thrust system has to act is so short that there is negligible difference in performance if the given hyperbolic excess speed is assigned to the high-thrust system, and the low-thrust system is assumed to start (heliocentrically) at the center of the massless point planet. Both departure and capture modes were investigated for Jupiter, Mercury, and Earth.

In terms of mission and systems analyses, the combining of high-thrust planetocentric and low-thrust heliocentric phases as separate regions related only by the hyperbolic excess velocity is a reasonable assumption.

2. Low-Acceleration Planetocentric Spiral

The low-thrust spiral, departure or capture, was studied by using analytic expressions available in the literature. Two aspects were studied, first, the spiral about a single gravity field which is assumed to extend to infinity and second, a spiral that accounts for properly switching the computations from the planet's gravity field to that of the sun (see Item 3 following). The spiral trajectory requirements were represented by equations giving the burnout or final mass ratio as a function of exhaust velocity and powerplant fraction. The study resulted in a procedure (not programmed) for optimizing the exhaust velocity and powerplant fraction of an all-electric vehicle that goes from parking orbit, through a heliocentric transfer, and either captures on a planetary parking orbit or attains some final heliocentric position or velocity.

3. Heliocentric/Planetocentric Trajectory Matching

A theoretical study of the motion of a low-thrust vehicle as it moves between a planetary gravity field and the solar field was performed to account for the planetary perturbations in the performance calculations. Both spiral and hyperbolic escape trajectories were considered. For the low-thrust spiral, an equation is presented for computing the performance up to the proper time at which the calculation is transferred to a heliocentric reference with no vehicle position offset with respect to the planet. Relations for the required velocity and position offsets are derived for the low-thrust hyperbolic trajectories. In both cases it is shown that the error in the approximations is on the order of the ratio of the mass of the planet to that of the sun. The effect of finite periplanet radius is also of the same order.

4. Aids for Analyzing Constant-Thrust Systems

The closed-form expressions for optimum exhaust velocity and powerplant fraction used in the improved single-coast program were plotted to develop a series of graphs for quickly estimating the performance of constant-thrust systems. Given the trajectory requirements in terms of J ($J = \int a^2\, dt$) and powered time, the optimum system parameters may be quickly estimated for a given powerplant specific mass, α_w, and thrustor efficiency parameter, d. For the same input values and parameters, a graph is used to estimate the maximum powerplant specific mass which produces zero payload. Although the foregoing graphs are for the simplified payload fraction (defined as the final mass fraction less the powerplant fraction), equations of the optimum system parameters for the improved payload definition were developed along with possible procedures for their solution. These equations were programmed as part of the improved single-coast constant-thrust optimization program.

Variational Formulations of Heliocentric Trajectory Problems

Complete sets of differential equations and related transversality conditions for the following problems were developed by use of the calculus of variations. The list is quite extensive, and not all the problems were programmed for solution by the trajectory optimization deck.

1. The first problem concerns three-dimensional trajectory and control optimization with the thrustor constrained to constant-exhaust-velocity on-off operation. The power available is a given function of position and time corresponding to decaying radioisotope power or solar power. The objective is maximum final mass fraction for given values of powerplant specific weight, powerplant fraction, and exhaust velocity. The boundary conditions correspond to (a) planetary rendezvous, (b) planetary flyby, (c) flyby at a given radius, and (d) orbital transfer.

2. This problem includes all of problem 1, but in addition, the powerplant fraction, μ_W, and the exhaust velocity, C, as well as the trajectory and the associated steering program, are to be optimized. The objective function is maximum payload fraction which is defined to be everything that is left at the end of the mission except the powerplant, thrustor, and the structure.

3. In this problem, two separate propulsion units are used, one before and one after the coast period. The exhaust velocity and powerplant fraction of each unit are optimized with respect to final payload fraction.

4. This problem is the same as problem 1 except that the thrust-acceleration vector is constrained to make a constant angle with respect to the radius vector. One constant angle is allowed before coast and another after coast. These two angles are to be separately optimized with respect to maximum final mass.

5. The round-trip stopover mission is treated for minimizing the mass of the electrically propelled vehicle (after staging of the initial high-thrust Earth departure propulsion for a given payload back at Earth). High-thrust impulses at Earth departure and planetary arrival and departure are included along with atmospheric braking at Earth return. Two power-limited propulsion systems are employed for the inbound and outbound heliocentric transfers; the latter system - including powerplant, thrustor, and tankage - is staged at the planet along with the capture high-thrust stage. The trajectory optimization includes optimizing the distribution of leg times, the launch date for fixed trip time and planetary stay time, and the directions of the hyperbolic excess velocities attributed to high thrust.

The corresponding variable-thrust solution of the round-trip stopover

mission is required as a starting approximation. Accordingly, variable-thrust transversality conditions are included corresponding to the constant-thrust case.

6. A round-trip planetary flyby is considered for the variable-thrust operating mode. The problem is treated in two parts: no constraint on the periradius, and a fixed periradius. The second part is solved if the first produces a periradius lower than the minimum bound imposed by a flight constraint; e.g., radius of the sensible atmosphere. By the use of internal transversality conditions at the planet, both the outbound and inbound legs are solved for simultaneously. The best launch date, best flyby date, and the optimum characteristics of the flyby encounter are computed.

7. Although not a calculus of variations problem, the problem of substituting analytic solutions for numerical solutions in the coast regions was investigated as a possible approach to reducing the number of mesh points. Analytic solutions for both the trajectory and the primer vector in the coast regions are developed and coupled with the numerical procedure at the switching points. These solutions, however, were not incorporated into the developed computer programs (Item 1, above).

Recommendations for Future Studies

The following list of recommended studies is a result of the background and experience obtained in the performance of the study contract. The list is limited to those activities which would directly aid in expanding current capabilities of power-limited flight analysis and in applying such capabilities to the ultimate goal of determining the role of electrically propelled spacecraft in the exploration of the solar system. It should be noted that the first three items listed are essentially study projects with the third being oriented more towards a survey. The remaining items are basically tasks which contribute to an overall goal of developing valuable study tools for power-limited systems and would therefore contribute significantly to the efforts of the first three recommended studies.

1. A system study should be initiated to determine the implications of high-plus-low-acceleration mission modes on the development of candidate power systems and thrustors and to the identification and, consequently, planning of the role of electrically propelled vehicles in solar system exploration. Such a study should have as its objective the comparison and evaluation of projected power systems and thrustors as related to a range of unmanned and, possibly, manned missions. In addition, the study should determine desirable and feasible characteristics of future primary propulsion power systems and should attempt to combine these characteristics (for different classes of powerplants) into a postulated design which would perform all or most of the missions either singly or by "clustering."

2. To ensure the broadest possible stimulation of new mission and flight mode

concepts and to expedite the evaluation of such concepts, a mission/system analysis aids manual would be an invaluable tool. The spirit and philosophy of such an aids manual would parallel that of the NASA Planetary Flight Handbook, SP-35. Because of the coupling between the propulsion system and the power-limited trajectory it is not possible to merely catalogue tables or graphs of trajectory requirements as is done for impulsive transfers. Therefore, a manual is envisioned which would include not only representative trajectory requirements but also techniques for estimating optimum constant-thrust system parameters, methods of extending payload definitions and computing the associated parameters, guidelines for determining mixed-thrust trajectory requirements, and general information and background data from past system and mission studies. An additional possibility is the inclusion of a series of computer programs for solving specific trajectory problems.

3. There presently exists several diverse computer programs for solving essentially the same power-limited trajectory problem. A survey should be made of these computer tools to identify their capabilities, limitations, and similarities such that the possibility of combining some of them could be investigated. The objective here is to develop combined programs which use the best features of each for particular problems. For example, a certain program may be capable of quickly solving the solar probe problem but requires difficult-to-obtain input guesses for certain variables. These may be provided by another program which solves essentially the same problem more slowly but requires only an unsophisticated starting solution. In other cases it may be evident that some particular power-limited trajectory problem is more conveniently and quickly solved by a certain numerical technique than that used in another program.

4. The preliminary procedure developed for optimizing the exhaust velocity and powerplant fraction with respect to payload fraction for a single-stage electric propulsion system should be programmed. This single-stage system is capable of two flight modes: 1) planetary parking orbit departure, heliocentric transfer and planetary parking orbit capture, and 2) planetary parking orbit departure and heliocentric transfer to a heliocentric position and velocity.

5. The developed multiple-coast trajectory optimization program should be modified to accept the expanded payload fraction definition in a manner similar to that accomplished in the original single-coast program. The capability of allowing for any thrustor efficiency and specific mass variation with exhaust velocity should also be included. This modification is considered to be an add-on item using the approximation techniques employed in the single-coast program modification and is not meant to be a reprogramming effort.

6. Efforts should be made to apply the basic developed computer algorithm to the problem of variable mesh point spacing. An investigation should be initiated to determine the added flexibility and broadened trajectory problem scope that variable mesh spacing produces.

7. The remaining variational problems which were formulated but not solved should be investigated by the basic computer algorithm. Of particular interest here is the constant-attitude, solar-powered trajectory, the round-trip flyby, the orbital transfer, and the staging of one (of two) electric propulsion system before coast.

8. In analyzing the implementation of the finite-difference Newton-Raphson algorithm made to date, two facts stand out very clearly. First, it is a lengthy and complex job to complete a computer code for a given problem. Although this difficulty will be eased in the future by the use of generalized subroutines now completed, this advantage will be counteracted by the necessity and desire to attack more difficult problems. Second, once a computer code has been generated to solve a problem by means of this algorithm, solutions can be generated fairly easily and quickly no matter how complicated or nonlinear the problem is. Therefore, recognizing both the difficulties of implementation and the high probability of success, future uses of this algorithm should be made in areas where the resulting data will be extremely useful or in areas where the data are currently essentially unattainable.

In trajectory analysis, three such study areas present themselves. The first is a program to choose simultaneously both the terminal hyperbolic excess speeds and the low-thrust trajectory which minimizes mass on earth orbit for a given set of vehicle parameters. This area is currently the most time-consuming process in the analysis of hybrid-thrust missions. The approach would be to incorporate the currently used approximations and matching laws into the body of the heliocentric algorithm.

The second is a program to optimize trajectories in a time-varying, n-body, gravitational field. While the usefulness of such a program might be limited to checking out currently used matching criteria, there are very little data available which have been achieved through a unified approach. The questions arising for the case of close approaches to Jupiter are certainly worth answering, and the program would also offer a convenient means to study the guidance problem of low-thrust ascent and descent.

The third is a program for minimum-total velocity increment, multiple-impulse, high-thrust trajectories. At present, only a few examples of such transfers are available. It is also extremely likely that once these data became available it would also be very useful in demonstrating both the reduction of total energy requirements needed for high-thrust missions and, probably more significantly, the broadening of the launch windows available for these missions.

SECTION II

INTRODUCTION

Objectives

The purpose of this thirteen-month study was to develop a computer algorithm to be used in optimizing space trajectories which are performed by power-limited (low-acceleration, electric) propulsion systems. This study, begun in August 1966, is an extension to the original Contract NAS2-2928, "Study of Trajectories and Upper Stage Propulsion Systems for Exploration of the Solar System", which was initiated in July 1965. The basic objective of the study extension was to develop user-oriented computer programs for solving selected trajectory and system optimization problems peculiar to low-acceleration, constant-thrust interplanetary vehicles. A secondary objective was to develop a computer program capable of minimizing the initial mass of a vehicle thrusting within the planet's sphere of influence using low acceleration solely or in combination with high acceleration.

General Approach

The general approach to the heliocentric trajectory and system optimization problems was to, first, derive the system of differential equations describing each optimization problem by the calculus of variations, and second, solve these systems of equations by the implicit finite-difference Newton-Raphson algorithm. Rather than develop complete individual computer programs for the several special problems, a series of generalized subroutines was prepared which would implement the logical and algebraic aspects of the Newton-Raphson algorithm. These subroutines represent that part of the overall programming task which is common to all the trajectory problems.

The approach to the high plus low-acceleration problem was to develop the computer programs for the heliocentric and planetocentric phases independent of each other; the two phases were related in a separate overall mass minimization program which accounts for the condition of the vehicle at the assumed transition between the planetary and heliocentric gravitational fields. The consequent computer programs for each phase provide results for input to the vehicle mass minimization program rather than attempt to integrate each program as a subroutine into a system mass computation program.

Study Scope

During the performance of the study it became evident that some of the heliocentric trajectory and system optimization problems originally scheduled were not compatible with the then-existing numerical techniques in conjunction with the requirements of computing time and machine storage capacity. The list of tasks presented in UARL Reports E-910352-10 and F-910352-11 was subsequently reduced in scope and number to result in the following list. Unless otherwise specified or implied, the listed tasks are all for constant exhaust velocity and fixed transfer time. They incorporate hyperbolic excess speeds at the boundaries and maximization of payload fraction.

I. Planet-to-planet rendezvous, internal discrimination between single and double coast periods, constant power

II. One-way planetary flyby, single or double coast, final hyperbolic velocity open, constant power

III. Tasks I and II with power a function of radial heliocentric position or of time

IV. Round-trip planetary stopover, optimum distribution of outbound and inbound leg transfer times, variable exhaust velocity, constant power.

Task I is a planet-to-planet transfer with given hyperbolic excess speeds on the terminals. The computer program is to be capable of computing the optimum trajectory and maximum payload fraction simultaneously for either one or two coasting arcs. The second task is a one-way planetary flyby with a specified hyperbolic excess speed at departure and a single final coast period.

Both of the foregoing tasks are analyzed for both constant power and variable power. The variable-power case is represented by an equation giving the power system output as a function of heliocentric position (i.e., a solar power system) or as a function of time.

The final task is analyzed under the variable-thrust operating mode rather than for constant thrust. The hyperbolic excess speeds at the terminals of the outbound leg are specified, and either the speeds at departure and arrival or the speed at departure only is fixed. The stay time at the planet is constant as is the Earth departure date.

The studies of planetocentric operations, i.e., thrusting of the electric propulsion system within the sphere of influence (with or without high thrust), attempt to evaluate the system implications and consequences of such thrusting on the dynamic condition of the vehicle at the planet's activity sphere or on the circular parking orbit. The purpose is to develop computer programs which calculate the performance of the vehicle within the planet's sphere of influence such that this performance can be related to and combined with the heliocentric trajectory.

The discussions of the programming effort and of the resulting computer programs for the heliocentric trajectory problems are presented in Section III. Also included is a discussion of the related user's manual which is a separate document intended to accompany the decks themselves. An analysis, based on numerical results, of the combined high- and low-acceleration thrusting mode within a planet's activity sphere is presented in Section IV.

Section V discusses the results of the planetocentric spiral analysis and suggests procedures for optimizing an all-electric vehicle system (no high thrust). Section VI presents an analytic treatment which justifies the use of hyperbolic velocities at planet-centered infinity and the assumption of negligible planetocentric vehicle displacement at the start of the heliocentric trajectory. Both the problems of low thrust only and of high-low thrust in combination are discussed.

Certain improvements in the previously developed single-coast, rendezvous trajectory program are detailed in Section VII along with a developed program for minimizing the mass of a combined high-low acceleration vehicle. The final technical discussion, Section VIII, gives the variational formulations of the several heliocentric, system-trajectory optimization problems.

SECTION III

GENERALIZED TRAJECTORY OPTIMIZATION COMPUTER PROGRAM

This section presents an overall picture of the three heliocentric computer programs worked on under this contract. First, the basic capabilities of each program are laid out, and, second, a general discussion of the analysis and usage of the decks is given. The detailed user's information for those decks which have been brought to a successful operating condition are presented in Volume III of this report.

Basic Program Capabilities

Program 1 - General Constant-Power Rendezvous or Flyby

Boundary conditions are given by the position and velocity of some body in a given Keplerian orbit. Initial and final hyperbolic excess speeds are specified. For the flyby mode, however, final velocity is left open. Multiple-coast arcs are accounted for except that terminal coasts may occur only at the end of a flyby. The powerplant specific mass, α_w, is specified as is the thrustor efficiency parameter, d. Specific impulse, I_{sp} (or exhaust velocity) and powerplant fraction, μ_w, may be specified or optimized in any combination. An option of running the deck in either the three-dimensional or two-dimensional mode is included.

Program 2 - General Variable-Power Rendezvous or Flyby

This program has the same characteristics as Program 1 except that the power in the exhaust beam may be specified either as a function of solar radius or as a function of time.

Program 3 - Variable-I_{sp} Round Trip.

Launch and return dates are given, and stay time at the target planet is specified. Also specified are the hyperbolic excess speeds at the beginning and end of each leg. The second, or return, leg may be considered a flyby.

Numerical and Programming Analyses

At the heart of these three heliocentric, low-thrust, computer decks is the finite-difference Newton-Raphson algorithm (Ref. III-1) for solving nonlinear, two-point boundary value problems. This algorithm operates by reducing the

boundary value problem to a sequence of large, but specially structured, algebraic systems of linear equations. Mathematically, this reduction can be viewed two ways. First, at each of many mesh points chosen along the independent variable axis between the boundary points, the nonlinear, ordinary differential equations describing the problem may be written as algebraic equations by substituting difference quotients for the derivative terms. Each of these algebraic equations will, in general, be nonlinear in the unknown dependent variables and thus will form a nonlinear system of equations. The Newton-Raphson iteration can be applied to this system. Second, however, the entire unknown solution of the differential equations can be considered as a point in function space. The generalized Newton-Raphson iteration can be applied directly to the nonlinear differential equations resulting in a system of linear differential equations. In this system the unknown variables are the corrections to be made to an approximate solution which appears as a known function on the right hand side of the same system. The standard numerical technique for solving systems of linear two-point boundary equations is to substitute difference quotients for the derivatives and solve the resulting system of linear algebraic equations.

When viewed the second way, the fact that the linear system will be specially structured becomes self-evident. The matrices involved in solving ordinary, linear, boundary value problems are of block tridiagonal form. They bear close relationship to the matrices which arise in the solution of linear partial differential equations, which have been extensively studied (Ref. III-2). From previous experience, they are known to be very well conditioned when solved by a direct-elimination method known as the block Thomas algorithm. This method is a labor-saving and convenient way of applying Gauss elimination to a block tridiagonal system.

Returning to the finite-difference Newton-Raphson algorithm itself, the theoretical studies (Ref. III-3) and computational experience both show that, through its use, solutions are very quickly and easily obtained. Given an initial approximation to the solution (to be discussed later), usually no more than 5 to 7 terms of the sequence of linear problems must be obtained. The usual terminology is that each sequential solution of the linear system is a Newton-Raphson iteration. Also, the fact that no logical decisions have to be made during the course of the iteration is of no small importance to the success of the method. The user is concerned only with providing the algorithm with an initial approximation or starting solution which is within the domain of convergence of the solution and may completely ignore the workings of the Newton iteration itself.

The computer analyst, however, can hardly ignore the Newton iteration. In the analysis and programming of the algorithm, there are two major problem areas. First is the construction of an efficient means of generating the vast numbers of coefficients which enter into the linear system. This part of the job is, of course, dependent on the particular equations being used for a given problem and

must be faced for each new problem or altered for each new modification. Second is the evaluation of the necessary formulas of linear algebra involving these coefficients in the solution of the large system of linear equations at each iteration.

Due to the magnitude of the second problem, complete advantage must be taken of any structure of the system which provides for the reduction of computations. In certain areas, the ordering of the calculations must be analyzed in order to reduce rounding errors, and, in at least one calculation, double-precision arithmetic must be used. The problems of current interest require amounts of computer storage that are usually unavailable, and the logic of using secondary storage devices must be analyzed, solved, and coded. Initially, the problem of creating a flexible means of varying the mesh point spacing was envisioned. This whole second problem area is algebraic and logical in nature and does not depend on the equations of any particular problem. It is in the area that generalized subroutines have been developed which may be used for a great variety of trajectory problems.

The first attempt to build such a generalized set of subroutines under the current contract involved the use of successive overrelaxation (SOR) as the technique used to solve the linear system. The planned inclusion of variable mesh spacing, equations containing first derivative terms, and the use of Cowell's formula for the second derivative terms, destroyed the block tridiagonal form and increased the amount of core storage needed. SOR seemed ideally suited to circumvent these difficulties. However, SOR itself is an iterative method, and it was discovered that the linear systems which arise from optimization problems are either very slowly convergent or actually divergent under SOR. The problem seems to be related to the fact that both a set of differential equations and their adjoints appear in the system. After the discovery that SOR would not be satisfactory, some reduction in the scope of the project had to be made. In terms of the algorithm, this reduction was achieved by abandoning the inclusion of variable mesh spacing and the use of Cowell's formula. These changes restored the block tridiagonal form of the system which made possible the use of the noniterative block Thomas algorithm and simplified the use of secondary storage devices. The necessity of coding the secondary storage for both the IBM 7094 DCS disk storage and the UNIVAC 1108 drum storage also created some problems.

A significant addition to the finite-difference Newton-Raphson algorithm made in this study is the inclusion of the capability to solve for the optimum values of an arbitrary set of parameters simultaneously with the differential equations of the trajectory. This capability is built into the generalized subroutines for the algorithm. Although there is an increase in the number of computations to be performed, the process is much more satisfactory than a search and also avoids the pitfalls of using approximation and extrapolation techniques based on known data. Indeed, it has been discovered, for example, that the problem of optimizing a constant-power, constant-exhaust velocity trajectory from Earth to Mercury and

simultaneously optimizing the actual value of the exhaust velocity not only results in a somewhat different value of exhaust velocity than expected, but also turns out to have a larger domain of convergence. In the constant-thrust decks, the option to optimize either or both the exhaust velocity and the powerplant fraction is available. Also, the round-trip, variable-exhaust-velocity deck uses this same capability to optimize the distribution of leg times.

Starting Solutions and Tracking

Other than the input/output routines, the other significant aspect in the programs is the computation and manipulation of the initial approximation to the solution. This area is of significant importance and interest to the users of these programs as it is in this area where the user must use his understanding of the problem and ingenuity in order to effectively use the program.

It is appropriate to return for a moment to the concept of viewing both the functions which are the solution of the differential equations and the values which are the solution of the parameters to be optimized all as a point in some function space. Under fairly general conditions, it is known that the Newton iteration will converge to the solution point from some domain of neighboring points. However, the computational work required to identify this domain is, for most practical problems, too great to be justified. Instead, a heuristic approach at obtaining initial guesses has been taken with considerable success.

The first heuristic principle is that a simple function which is a solution of the differential equations but which does not satisfy the boundary conditions of interest is very often in the domain of convergence of the desired solution. In trajectory analysis, the two-impulse ballistic trajectory immediately comes to mind as a candidate. However, the ballistic trajectory would be an extremely poor choice as a starting solution in cases where multiple coast periods turn out to be optimum. For low-thrust work, the circle start is not only extremely simple to generate, but also highly satisfactory. Very briefly, the circle start is the circular coasting trajectory which leaves the launch longitude at time zero and arrives at the longitude of the target planet at the specified time. Thus, the radius of the circle-start trajectory is determined by the central angle traversed and the trip time. Further flexibility for more complex trajectories is available by increasing the central angle by multiples of 360 degrees. Strictly speaking, the circle start is a solution only of the variable-I_{sp} equations, since any arc with no thrusted period will be singular for the constant-I_{sp} equations. Thus, the circle start is used to obtain a variable-I_{sp} trajectory, and this trajectory is then used as a starting solution for the constant I_{sp} trajectory.

The second heuristic principle used is based on the fact that the trajectories vary continuously with respect to both the boundary conditions and the specified

system parameters. Thus, once a trajectory has been obtained, it may be used as a starting solution for a trajectory which differs somewhat in either boundary conditions or system parameters. This procedure is called tracking. The important point is not the magnitude of the change of the input variables, but the magnitude and nonlinearity of the changes in the solution variables. Thus, for instance, it may be possible to change the arrival date of an Earth-Jupiter trajectory by twenty or thirty days and still converge to a solution, but a change in the arrival date of an Earth-Mercury trajectory may be limited to one or two days.

Tracking on hyperbolic excess speeds at launch and arrival can be particularly troublesome. The best opportunities for high-thrust and low-thrust trajectories occur at different dates. Thus, when the hyperbolic excess speeds are varied for a fixed trip, the nature of the trajectory may change profoundly. While this behavior is especially true for multiple-coast trips, unexpected variations have occurred even in the simplest of cases. The net result is that not only do different tracking increments have to be used in different cases but also the number and position of the coasting periods must be monitored closely.

A similar situation has been uncovered in the optimization of the exhaust velocity. The curve of optimum I_{sp} plotted against powerplant specific mass, α_w, for a given trip, starts off with a steep initial downward slope for small values of α_w. Then the function usually turns fairly sharply and exhibits a fairly gentle downslope until some maximum α_w is reached for which it is no longer possible to make the trip. Again, care must be taken to use tracking steps, in α_w, which are small enough in the steep region.

A further variation of tracking is available on the circle start. It has already been noted that the circle start is a solution of the differential equations which does not satisfy the boundary conditions of interest. However, the circle start does satisfy its own circular boundary conditions. Thus, by partitioning the difference in the boundary values between the circle start and the final trajectory in small increments, almost any variable-I_{sp} trajectory can be reached. This procedure is available in the programs and is known as an iterated circle start. It is especially useful when central angles of over 360 degrees are required.

General Program Operation

In summary then, a typical computer run goes as follows. One, the circle start trajectory will be set up. Two, a solution of a variable-I_{sp} trajectory with the specified hyperbolic excess speeds and proper boundary conditions is obtained. If difficulty is encountered at this point, the use of more iterations on the circle start boundary conditions will most always suffice. Three, the corresponding constant-thrust trajectory is obtained. This is probably the most

difficult step of the process. Very little can be done directly if this step does not work.

Remedial procedures which could be utilized are as follows. The parameters of the constant-thrust trip can be changed, especially α_w, which may be made smaller. The ratios of the estimated constant-thrust J to variable-thrust J, or of estimated thrusted time to total transfer time may be changed. The mode of simultaneously solving for I_{sp} and μ_w along with the trajectory is more likely to succeed than to specify these quantities. However, if all else fails, tracking to the desired constant-thrust trajectory from another constant-thrust trajectory will have to be employed. Four, assuming the constant-thrust trajectory is reached, another constant-thrust trajectory may be obtained by tracking. If this step fails, usually a decrease in the incremental change made in the input variables will achieve the desired result.

An example of the initial results obtained from the program is displayed in Figs. III-1 and III-2 for a 320-day constant power, Mars-to-Earth rendezvous in 1980. The first figure illustrates the position-time history of the two-coast trajectory and the times at which the thrust is turned off or on. Although the payload fraction has not been maximized with respect to specific impulse and powerplant fraction, the initial guesses made within the program are very close to optimum. For this trip it is estimated by other means that the optimum specific impulse and powerplant fraction should be 20,400 sec and 0.09, respectively, with a resulting maximum payload fraction of about 0.81. The powerplant specific mass of 1 kg/kw was chosen merely to assure convergence for the given example.

The magnitude of the primer vector is plotted in Fig. III-2 to indicate the regions of thrusting and coasting and their points of occurrence, as expected, in relation to the shape of the curve. Note that, as required for an optimum trajectory, the primer vectors are equal at the initiation and termination of a coast period.

Two warnings in the use of these programs must be noted. First, they are new programs with limited computing experience. All individual options have been checked, however all valid combinations of options have not. Therefore, it is possible that some program errors may remain. Second, and more fundamental, these programs solve equations which are intractable analytically and for which the nature of their solution is not well known. Thus, cases should arise where new knowledge concerning the basic form of the trajectories will be gained. In this respect it is impossible merely to use these programs as mission analysis tools without concurrently attempting to gain insight into the nature of the trajectories being computed.

Section III References

III-1. Van Dine, C. P., W. R. Fimple, and T. N. Edelbaum: "Application of a Finite-Difference Newton-Raphson Algorithm to Problems of Low-Thrust Trajectory Optimization." Progress in Astronautics, Vol. 17, Academic Press, Inc., New York, 1966.

III-2. Varga, R. S.: Matrix Iterative Analysis. Prentice-Hall, Inc., Englewood Cliffs, New Jersey, 1962.

III-3. Kantorovich, L. V. and G. P. Akilov: Functional Analysis in Normed Spaces. Pergamon Press, New York, 1964, Chap. XVIII.

OPTIMUM MULTIPLE - COAST, CONSTANT - THRUST TRAJECTORY

320 - DAY 1980 MARS - EARTH TRIP

$J = 20.61\ M^2/SEC^3$ $\mu_L = 0.8063$ $d = 20\ KM/SEC$

$I_{SP} = 19791\ SECS$ $\mu_W = 0.0921$ $\eta = 0.9895$

$V_A = V_B = 0$

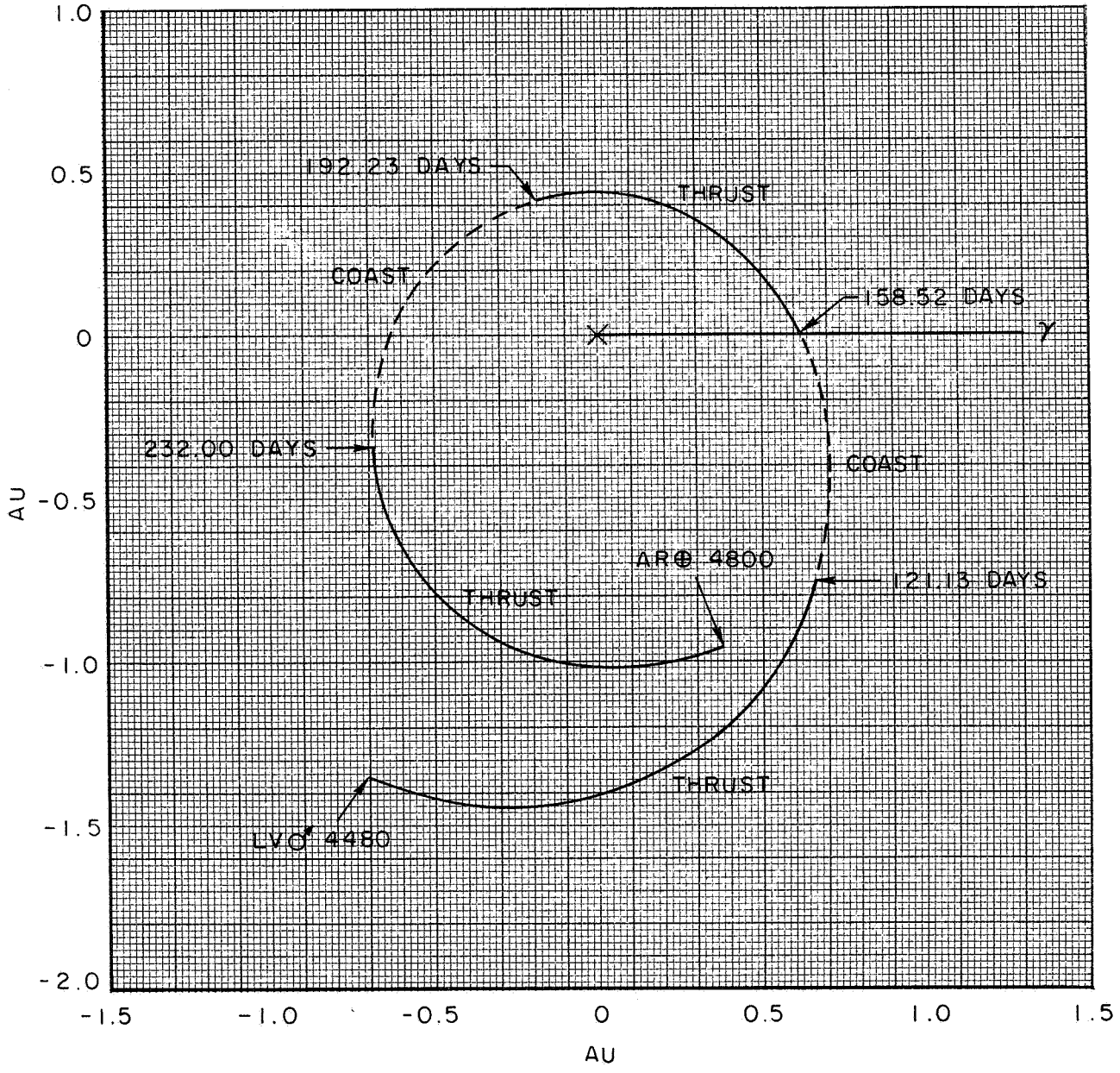

FIG. III-2

OPTIMUM MULTIPLE-COAST, CONSTANT-THRUST TRAJECTORY

PRIMER VECTOR TIME HISTORY
320-DAY 1980 MARS-EARTH TRIP

LV♂ 4480 AR⊕ 4800

$J = 20.61\ M^2/SEC^3$ $\mu_L = 0.8063$

$I_{SP} = 19791\ SEC$ $\mu_W = 0.0921$

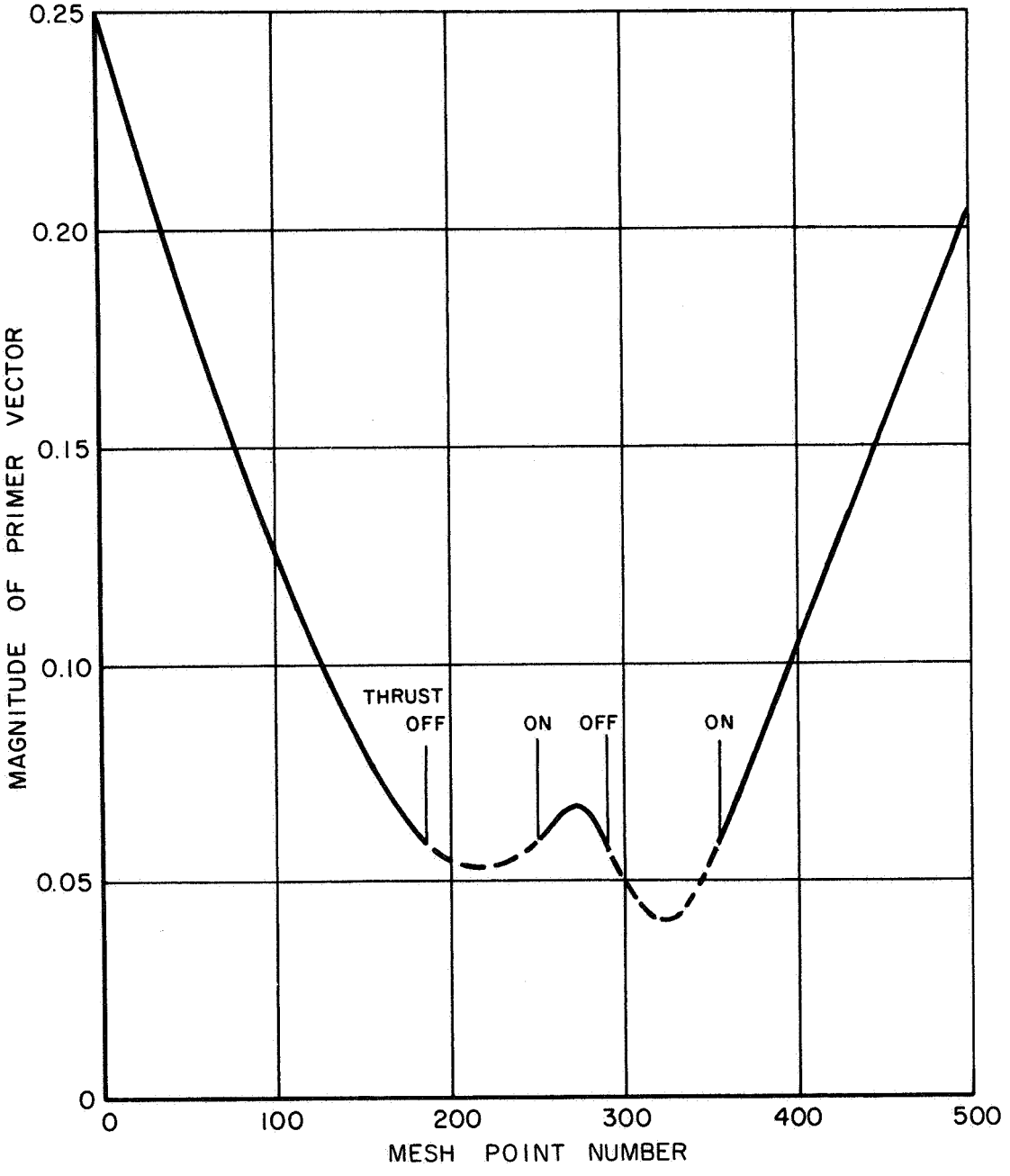

SECTION IV

HIGH-LOW THRUST PLANETOCENTRIC OPERATIONS

Introduction

The usual boundary conditions which are specified for low-thrust heliocentric trajectory analysis consider the departure and arrival planets as massless points moving through heliocentric space with known ephemeral motions. The interplanetary vehicle is assumed either to have the planet's velocity (planetocentric hyperbolic excess velocity equal to zero) or to have a heliocentric velocity which exceeds the planet's velocity by a known, required planetocentric hyperbolic excess velocity.

Also, it is assumed that the planetocentric hyperbolic excess velocity is imparted to the vehicle by a high-thrust propulsion system (to reduce mass requirements and planetocentric maneuver time) and that after high-thrust burnout the vehicle coasts on a hyperbolic trajectory to the planet's sphere of influence. Upon reaching the sphere of influence, a coordinate transformation is made and the heliocentric low-thrust mission phase is initiated. The sequence of events is reversed for planetary capture. Although this operation is labeled as a mixed high-low thrust mission mode, the high-thrust and the low-thrust operational modes are completely uncoupled and are "patched" at the planetocentric sphere of influence at departure or arrival. In many cases the planetocentric operational phase is completely neglected except for the fact that a required hyperbolic excess speed is specified at initiation and conclusion of the heliocentric trajectory. How this excess speed is produced is usually not considered in low-thrust heliocentric mission analyses.

An interesting problem arises when the vehicle is required to initiate low-thrust propulsion within the planetocentric field and to continue it through the sphere of influence. In this operational mode, the high-low mix is coupled throughout the entire mission. Low-thrust propulsion may begin at any time from high-thrust termination up to the time the vehicle passes through the sphere of influence; likewise, high-thrust vehicle propulsion parameters significantly affect the vehicle's condition upon arrival at the sphere of influence. Once the low-thrust system is assumed to operate within the planetocentric activity sphere, the structure of mixed high- low-thrust operational mode is somewhat altered from the situation in which the high- and low-thrust systems are uncoupled.

When mixed thrusting occurs within the planetocentric sphere of influence, the application of the trajectory data to the mission analysis may take one of two approaches, one affecting heliocentric operations and the other affecting planetocentric operations. The former requires that, for a given mission with specified high-thrust hyperbolic excess speeds for departure and/or capture, the vehicle arrives at the sphere of influence with greater hyperbolic excess speed. This directs that the heliocentric phase have new velocity boundary conditions; thus, the heliocentric trajectory may require shorter trip time or smaller propulsion requirements. The second approach requires that the heliocentric trajectory be specified, including the velocity boundary conditions. Therefore, the high-thrust energy requirement is reduced, a factor which may decrease initial orbital mass and/or equivalently increase arrival payload. This second approach was chosen as the method to be used in this study since it is convenient to specify an optimal heliocentric low-thrust trajectory and then incorporate the effect of the planetocentric departure/capture operation into the specific mission analysis. The inclusion of the high-low-thrust planetocentric operation into interplanetary low-thrust mission analysis creates a more sophisticated model of the sequence of events than is generally the case, and hence, its predictions are more representative of the actual mission modes under examination.

Study Approach

Since the planetary parking orbit and the planetocentric activity sphere are known for any planet under consideration, the planetocentric thrusting trajectory is calculated by an incremental integration of the first integrals of the vehicle equation of motion in differential form (Appendix B). High-thrust termination is reached when the desired high-thrust hyperbolic excess speed is acquired by the vehicle. At this time, a discontinuity in vehicle thrust acceleration and specific impulse is experienced (low-thrust propulsion initiated); although all dependent variables remain continuous, the independent variable τ (the instantaneous burn time) is set equal to zero. The vehicle's trajectory is calculated until the planetocentric activity sphere is reached.

For mixed-thrust planetocentric operations the following nondimensional constants are given.

V_{∞_H} - High-Thrust Hyperbolic Excess Speed

σ_{i_L} - Initial Low-Thrust Vehicle Acceleration

C_L - Low-Thrust Exhaust Velocity

σ_{i_H} - Initial High-Thrust Vehicle Acceleration

C_H - High-Thrust Exhaust Velocity

ζ^* - Radius of Sphere of Influence

These constants are used as input values for the existing computer programs. For the departure operation, V_∞^* (the hyperbolic excess speed achieved by the combination of high- and low-acceleration propulsion systems at arrival at the sphere of influence) may be an input in place of V_{∞_H}. If V_∞^* is an input to the departure program, a numerical Newton-Raphson technique is employed on the variable V_{∞_H} until the hyperbolic excess speed at the sphere of influence (i.e., V_∞^*) is within a desired tolerance of the input value.

For the capture operation, the computer program chooses an initial value of the final thrust acceleration σ_{B0}. A modified Newton-Raphson iterative technique acts upon the initial thrust acceleration, σ_1, until σ_1 is within a specified tolerance of the input value. This iteration technique is employed on both the high- and low-thrust initial thrust accelerations. However, once the iteration is complete, the V_∞^* is not pre-assigned; it is a dependent variable which is determined by the input vehicle parameters and the specified gravitational field.

With the available programs, the capture and departure trajectories may be computed for any planetocentric gravitational field (specific sphere-of-influence radius), initial parking orbit, and combination of high- and low-thrust vehicle parameters.

The basic assumptions made in the analysis are:

1. The departure (capture) parking orbit is <u>circular</u> and at 1.1 planetary radii from the gravitational center.

2. The vehicle thrust acceleration is in the direction of the vehicle's instantaneous velocity.

3. The departure (capture) trajectory is in the plane of the parking orbit.

4. The vehicle propulsive thrust and propulsive specific impulse of both high- and low-thrust systems are constant.

5. The radius of the planetocentric activity sphere is determined as the product of the planet's mean orbital heliocentric radius and the ratio of the planet's mass to the solar mass raised to the 0.4 power.

6. The first propulsion system employed upon departure from the parking orbit is the high-thrust system; the first propulsion system employed upon capture is the low-thrust system.

7. Immediately upon completion of the high-thrust termination (low-thrust termination), low-thrust propulsion (high-thrust propulsion) is employed until the sphere of influence (parking orbit) is reached for departure (capture) operations.

8. All variables have been nondimensionalized with respect to the parking orbit constants, i.e., the circular orbit speed, $v_{c_{p_o}}$, the circular orbit radius, r_{p_o}, and the local gravitational acceleration, g_{p_o}.

Elliptic Parking Orbits

The present formulation of the computer programs for planetary departure and capture operational modes considers the parking orbit to be circular. The introduction of nonzero eccentricity into the parking orbit poses the problem that other variables must be introduced into the problem formulation. If the parking orbit is elliptic, the eccentricity, perigee distance, and the true anomaly must be introduced unless only apsidal departure or capture is considered. Even with apsidal initiation or termination, the initial boundary conditions must be completely redefined to include the following three options.

Option 1: Circular parking orbit of radius, r_o

Option 2: Elliptic parking orbit of perigee radius, r_o; departure (capture) at perigee or apogee

Option 3: Elliptic parking orbit of apogee radius, r_o; departure (capture) at perigee or apogee

Hence, from a simplified approach of one set of initial conditions, the programs must be redefined to handle three basic options with four suboptions.

The labor involved in accomplishing this task seems unwarranted considering that the basic motivation is to determine the effect of both high and low thrusting within the planetocentric sphere and not to perform a detailed analysis of all possible variations and alternatives. The introduction of new variables would tend to complicate and obscure a basic understanding of the problem.

Discussion of Results

The results of this study are presented in two related discussions. The first deals with mixed-thrust planetocentric operations about the planets Earth, Mercury, and Jupiter. Here, a general analysis is made to show the effect of variations in planetary mass on the pertinent trajectory parameters derived from the study. The second discussion deals with mixed-thrust Earth operations only.

Planetocentric Operations

An examination of the departure and capture operational modes for Earth, Mercury, and Jupiter was made. The first was chosen because it is the most important, the latter two because they represent the extremes in planetary mass.

The high-thrust propulsion system was chosen to be either a chemical system (I_{sp} = 430 sec) or a solid-core nuclear system (I_{sp} = 800 sec). The low-thrust propulsion system is defined by a constant thrust-acceleration level of either 10^{-2}, 10^{-3}, or 10^{-4} of the Earth's surface gravitational acceleration (9.79006 x 10^{-3} km/sec^2). The initial thrust acceleration of the high-thrust system was chosen to minimize the weight of the high-thrust stage, using the results of Ref. IV-1. The data of Ref. IV-1 were approximated as linear functions of hyperbolic excess speed at high-thrust termination and are presented in Figs. IV-1 and IV-2. Although the planetary parking orbits used in Ref. IV-1 are different than those assumed here, the values of initial thrust-to-weight ratio are regarded as typical of the two types of high-thrust propulsion systems.

The definitive characteristics of the three planets and their parking orbits are summarized in Table IV-1. Although the planets may vary considerably in mass, the local gravitational acceleration at the parking orbit about Mercury is of the order of 1/3 that for Earth, while that about Jupiter is of the order of 2.5 that of Earth. The radius of the sphere of influence is 625.48, 131.68, and 40.56 times the parking orbit radius for Jupiter, Earth, and Mercury, respectively. Since all operational modes begin (or terminate, for capture) at a nondimensional radius of 1.0, there is considerable increase in thrusting time available for the low-thrust system when comparing the Jupiter operations with those about Mercury.

The increase in hyperbolic excess speed due to low acceleration within the sphere of influence of Earth, Mercury, and Jupiter is shown in Figs. IV-3, IV-4, and IV-5, respectively. For a given hyperbolic excess speed at high-thrust termination (V_{∞_H}), the hyperbolic excess speed at the sphere of influence (V_∞^*) is essentially a function of the low-thrust acceleration only, since negligible dependence on high-thrust specific impulse was found. The functional form of V_∞^* appears to be hyperbolic (quadratic) with respect to V_{∞_H} and is asymptotic to a 45-deg line passing through the origin and representing a limit of no low-thrust operation.

The difference in V_∞^* for the departure and capture modes is directly proportional to the low-thrust acceleration and planetary mass and inversely proportional to V_{∞_H}.

Although Figs. IV-3 through IV-5 illustrate the added energy at the sphere of influence due to low-thrust acceleration; these figures also indicate the required reduction in the energy imparted by the high-thrust system to achieve a given energy (V_∞^2) at the sphere of influence. As an example, an Earth-escape maneuver using

mixed high- and low-thrust systems must provide a hyperbolic excess speed of 0.40 EMOS. From Fig. IV-3, a low-thrust system with an acceleration of 10^{-4} g's reduces the high-thrust V_∞ requirement to 0.395 EMOS, while a low-thrust system providing 10^{-3} g's reduces the high-thrust V_∞ requirement to 0.375 EMOS. If the "low-thrust" acceleration is 10^{-2} g's, it can be seen that there is no requirement for a high-thrust system. In fact, the "low-thrust" system alone will provide a $V_\infty = 0.45$ EMOS. Therefore, the powered time of the "low-thrust" system would have to be reduced to provide a $V_\infty = 0.40$ at the sphere of influence. The other alternative is to use only a high-thrust system.

Similarly, Fig. IV-4 shows the relative insensitivity of the acceleration level of the low-thrust system at Mercury as compared to Earth operations. Conversely, the Jupiter data shown in Fig. IV-5 indicates that the acceleration level of the low-thrust system is quite critical. For a low-thrust level of 10^{-4} g's, the low-thrust system alone will provide 0.25 EMOS. Therefore, any mission requiring a $V_\infty > 0.25$ would use a high- and low-thrust planetary escape system. Conversely, for V_∞ requirements less than 0.25 EMOS, either a high-thrust system or the low-thrust system would suffice.

The low-thrust powered time is shown in Figs. IV-6 through IV-9 as a function of the hyperbolic excess speed provided by the high-thrust system. This powered time is directly proportional to the planetary mass and inversely proportional to V_{∞_H} and low-thrust acceleration. The difference in powered time between the departure and capture modes is directly proportional to planetary mass and low-thrust acceleration and inversely proportional to V_{∞_H}, for values of V_{∞_H} less than 4.0. This limiting value is in nondimensional form as are Figs. IV-6 through IV-9. In this form, the researcher can use these figures universally. As an example, the abscissa of each figure is actually $V_{\infty_H}/V_{c_{PO}}$, where $V_{c_{PO}}$ is the circular velocity of the planetary parking orbit. Therefore, the researcher can use the data universally for any size parking orbit he may be using in his analysis. Likewise, the powered-time parameter, τ, can be expressed as

$$\tau = t\left(\frac{V_{c_{PO}}}{r_{PO}}\right)$$

Where: t = powered time, sec
$V_{c_{PO}}$ = planetary parking orbit radius, ft/sec or km/sec
R_{PO} = planetary parking orbit radius, ft or km

the powered time of the low-thrust system is then

$$t = \frac{\tau}{86400}\left(\frac{r_{PO}}{V_{c_{PO}}}\right) \quad \text{days}$$

It appears that the planetary departure and capture low-thrust operating times are nearly identical in the region where $V_{\infty_H}/V_{c_{PO}} = 4.0$. For a low parking orbit about Earth, this is equivalent to about 1.05 EMOS. Since this velocity is far above normal values for missions of interest, the above analogy is academic. Likewise, for Jupiter, a value of $V_{\infty_H}/V_{c_{PO}} = 4.0$ is equivalent to about 5.4 EMOS. However, for Mercury, an equivalent value would be about 0.38 EMOS, which corresponds to typical Mercury missions.

When $V_{\infty_H}/V_{c_{PO}}$ becomes greater than 4.0, the high-thrust burn time becomes a significant fraction of the total operational powered time, and, consequently, the dependence on the high-thrust specific impulse and operational mode becomes pronounced. From an operational standpoint, it should be noted that most interplanetary hyperbolic excess speeds are kept below 0.50 EMOS by judicious trajectory selection. Likewise, when considering mixed-thrust systems, the V_∞ delegated to the high-thrust system by various optimization techniques seldom exceeds 0.3 EMOS.

Figures IV-10 and IV-11 display vehicle flight path angle at the sphere of influence as a function of hyperbolic excess speed and high-thrust burnout. Above a V_{∞_H} of 0.2 EMOS the dependence on low-thrust acceleration and operational mode rapidly becomes negligible. Below this value the flight path angle is directly proportional to low-thrust acceleration and is slightly larger for the capture mode as compared to the departure operational mode. For the three planets examined, the flight path angle remains reasonably constant for V_{∞_H} greater than 0.2 EMOS and maintains a value above 88 deg. Therefore, the approximation that the vehicle velocity is radially oriented upon reaching the sphere of influence is valid ($V_{\infty_H} \geq 0.2$ EMOS).

To summarize the above statements for the general discussion of high- and low-thrust planetocentric operations, the following conclusions are made:

1. The hyperbolic excess speed attained by the vehicle at the planetocentric sphere of influence, V_∞^*, is a function of the low-thrust acceleration and the hyperbolic excess speed at high-thrust burnout, V_{∞_H}, only; high-thrust specific impulse does not appreciably affect the augmentation of hyperbolic excess speed.

2. The functional form of V_∞^* is hyperbolic (in a quadratic sense) and is asymptotic to the limiting case of no low-thrust operation as hyperbolic excess speeds at high-thrust burnout become large.

3. $V_\infty^* - V_{\infty_H}$ is directly proportional to low-thrust acceleration and planetary mass and inversely proportional to V_{∞_H}.

4. The difference in V_∞^* for the capture and departure modes is directly proportional to low-thrust acceleration and planetary mass and inversely proportional to V_{∞_H}.

5. An arbitrary choice of vehicle parameters cannot be made if a specific V_∞^* is to result from a designated V_{∞_H}.

6. Low-thrust powered time is directly proportional to planetary mass and inversely proportional to low-thrust acceleration and V_{∞_H}.

7. The difference in low-thrust operating time between capture and departure operational modes is directly proportional to low-thrust acceleration and planetary mass. This difference is inversely proportional to V_{∞_H}/V_{co} until V_∞/V_{co} exceeds a value of 4.0; above this value the dependence becomes direct.

8. Vehicle flight path angle at the activity sphere is directly proportional to low-thrust acceleration and slightly larger for the capture mode, as compared with the departure mode, for V_{∞_H} less than 0.2 EMOS. Above this value the flight path angle remains essentially constant and is a slight function of high-thrust specific impulse.

9. For a value of V_{∞_H} greater than 0.2 EMOS the vehicle flight path angle is greater than 88 deg, thereby implying that the assumption of radial velocity direction at the activity sphere is valid.

Earth Operations

An examination of the departure and capture operational modes for the planet Earth was made. The data of this part of the study are more detailed inasmuch as a larger range of initial low-thrust accelerations is examined and the low-thrust propulsion system is now characterized by constant thrust and constant specific impulse.

The high-thrust propulsion system was chosen to be either a chemical system (I_{sp} = 430 sec) or a solid-core nuclear system (I_{sp} = 800 sec). The low-thrust system was defined by a range of specific impulses from 2000 sec to 10,000 sec. The initial thrust acceleration of the low-thrust stage was either 10^{-2}, 10^{-3}, 10^{-4}, or 10^{-6} of the Earth's surface gravitational acceleration. The radius of the Earth's activity sphere is 131.68 Earth parking orbit radii. The parking orbit has a radius of 1.1 times the radius of the Earth. The fundamental constants of the problem are found in Table IV-I. The basic assumptions which formulate the planetocentric mixed-thrust model are found in the 'Study Approach'.

The increase in hyperbolic excess speed due to low-thrust operation within the Earth's activity sphere can be obtained from Figs. IV-12 to IV-14. For a given hyperbolic excess speed with high thrust only, V_{∞_H}, the hyperbolic excess speed at the sphere of influence, V_∞^*, is a strong function of the low-thrust initial acceleration

and a weak function of the low-thrust specific impulse. There is no dependence on the high-thrust specific impulse in the examined range. The functional form of V_∞^* appears to be hyperbolic (quadratic) with respect to V_{∞_H} and is asymptotic to a 45-deg line commencing at the origin (i.e., the limiting case of no low-thrust propulsion). For both Earth departure and capture, once the low-thrust initial acceleration is less than 10^{-3} times the Earth surface gravitational acceleration, the effect of low-thrust specific impulse on V_∞^* becomes negligible. Figure IV-17 displays an enlarged view of Figs. IV-12 and IV-13 to 0.30 EMOS. The curve showing 10^{-6} for initial low-thrust acceleration may be taken as equivalent to no low-thrust operation since, when V_{∞_H} has the value 0.0182 EMOS, V_∞^* has the value 0.0187 EMOS, and when V_{∞_H} has the value 0.3005, V_∞^* has the value 0.3005.

Low-thrust operating time as a function of hyperbolic excess speed at high-thrust burnout is shown in Figs. IV-15 to IV-18. Low-thrust operating time is inversely proportional to V_{∞_H} and initial low thrust-acceleration and directly proportional to the low-thrust specific impulse. When the low-thrust initial acceleration is less than 10^{-3}, there is no effect of low-thrust specific impulse on the low-thrust operating time for either the capture or departure operational mode.

Figures IV-19 and IV-20 display high-thrust characteristic speeds for Earth departure/capture and for both chemical and solid-core nuclear propulsion systems. These characteristic speeds include the effect of 'gravity loss' due to the finite thrusting time of the high-thrust propulsion system and are calculated in the manner of Ref. IV-2. As would be expected, the characteristic speed of the solid-core nuclear system is greater than that of the chemical system for a given hyperbolic excess speed at high-thrust termination, since characteristic speed increases with increasing specific impulse (increase in thrusting time).

The difference between the vehicle's instantaneous path speed, V^*, and its hyperbolic excess speed, V_∞^*, at the sphere of influence is presented in Figs. IV-21 and IV-22. When the low-thrust initial acceleration is less than 10^{-3} times the Earth's surface gravitational acceleration, there is no effect on this difference due to low-thrust specific impulse.

For a hyperbolic excess speed at the end of high-thrust operation of 1.0 EMOS, $V^*-V_\infty^*$ is of the order of one-fortieth of one percent of the nominal heliocentric speed of any of the initial low-thrust accelerations examined. When the hyperbolic excess speed at high-thrust termination is zero (parabolic conditions), this difference with respect to nominal heliocentric speed ranges from about one-tenth of one percent to about 2.7% for initial low-thrust accelerations of 10^{-2} to 10^{-6}, respectively.

SECTION IV REFERENCES

IV-1. Titus, R. R., R. V. Ragsac, R. P. Gogolewski, and G. Thrasher: "Study of Trajectories and Upper-Stage Propulsion Requirements for Exploration of the Solar System". Contract NAS2-2928, United Aircraft Research Laboratories Report E-910352-9, July 1966.

IV-2. Gogolewski, R. P.: "The Impulsive Approximation and the Problem of Gravity Loss". United Aircraft Research Laboratories Report F-110058-23, January 1967.

TABLE IV-I

PHYSICAL PARAMETERS OF PLANETS

Parameter	Planet		
	Earth	Mercury	Jupiter
Planetary Radius, km	6.37839×10^3	2.50×10^3	6.988×10^4
Parking Orbit Radius (1.1 x Planetary Radius, km)	7.01623×10^3	2.750×10^3	7.6868×10^4
Parking Orbit Altitude, km	6.3784×10^2	2.50×10^2	6.988×10^3
Radius of Activity Sphere (Parking Orbit Radii)	131.68185	40.55530	625.477
Parking Orbit Circular Speed, km/sec	7.53713	2.80580	40.56664
Local Gravitational Constant at Parking Orbit, g	0.82645	0.29220	2.18516
Multiplicative Time Conversion, days	1.07742×10^{-2}	1.13439×10^{-2}	2.19311×10^{-2}

FIG. IV-1

HIGH-LOW THRUST PLANETOCENTRIC OPERATIONS

INITIAL HIGH-THRUST ACCELERATION

HIGH-THRUST I_{SP} = 430 SEC

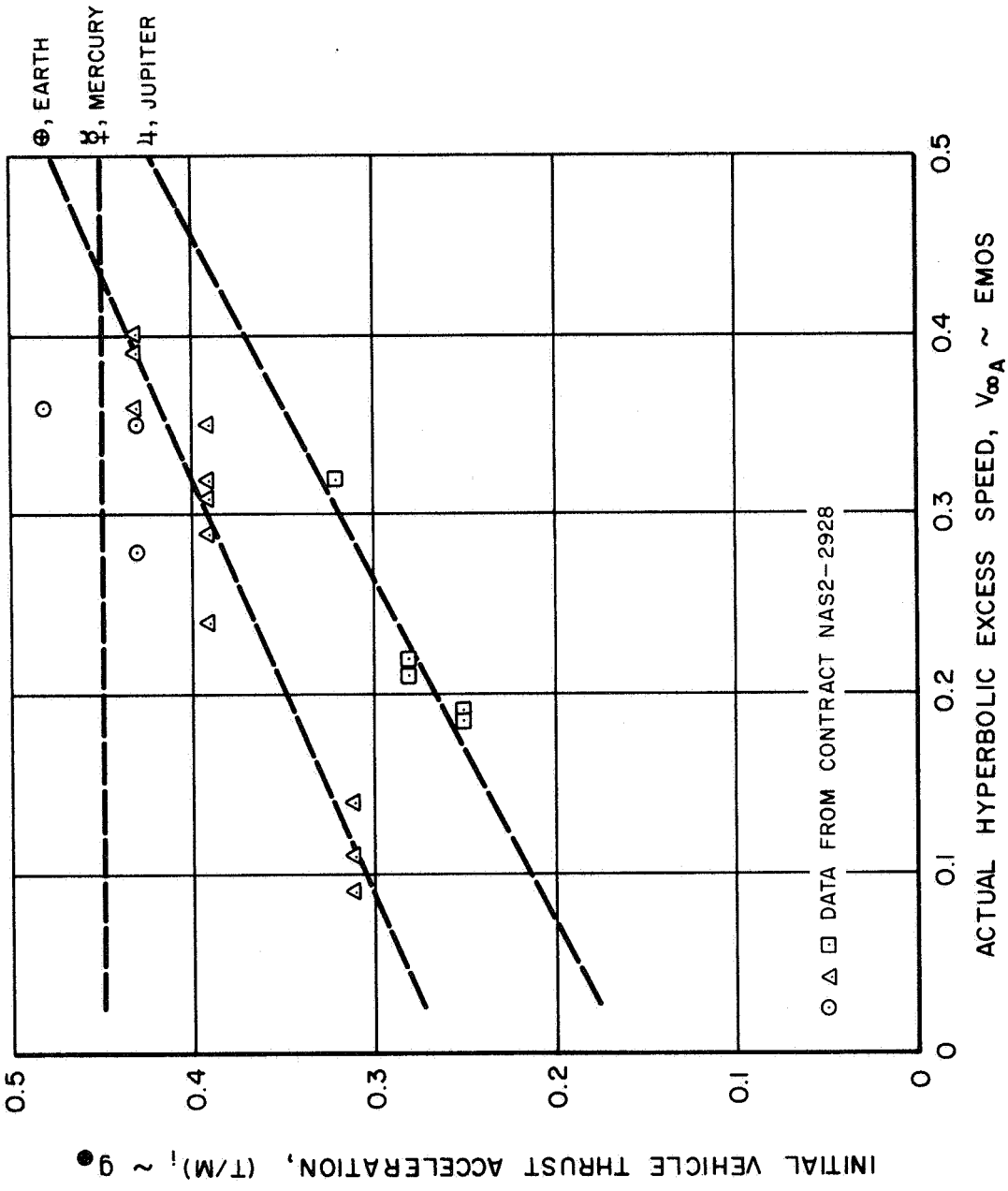

FIG. IV - 2

HIGH-LOW THRUST PLANETOCENTRIC OPERATIONS

INITIAL HIGH-THRUST ACCELERATION

HIGH-THRUST I_{SP} = 800 SEC

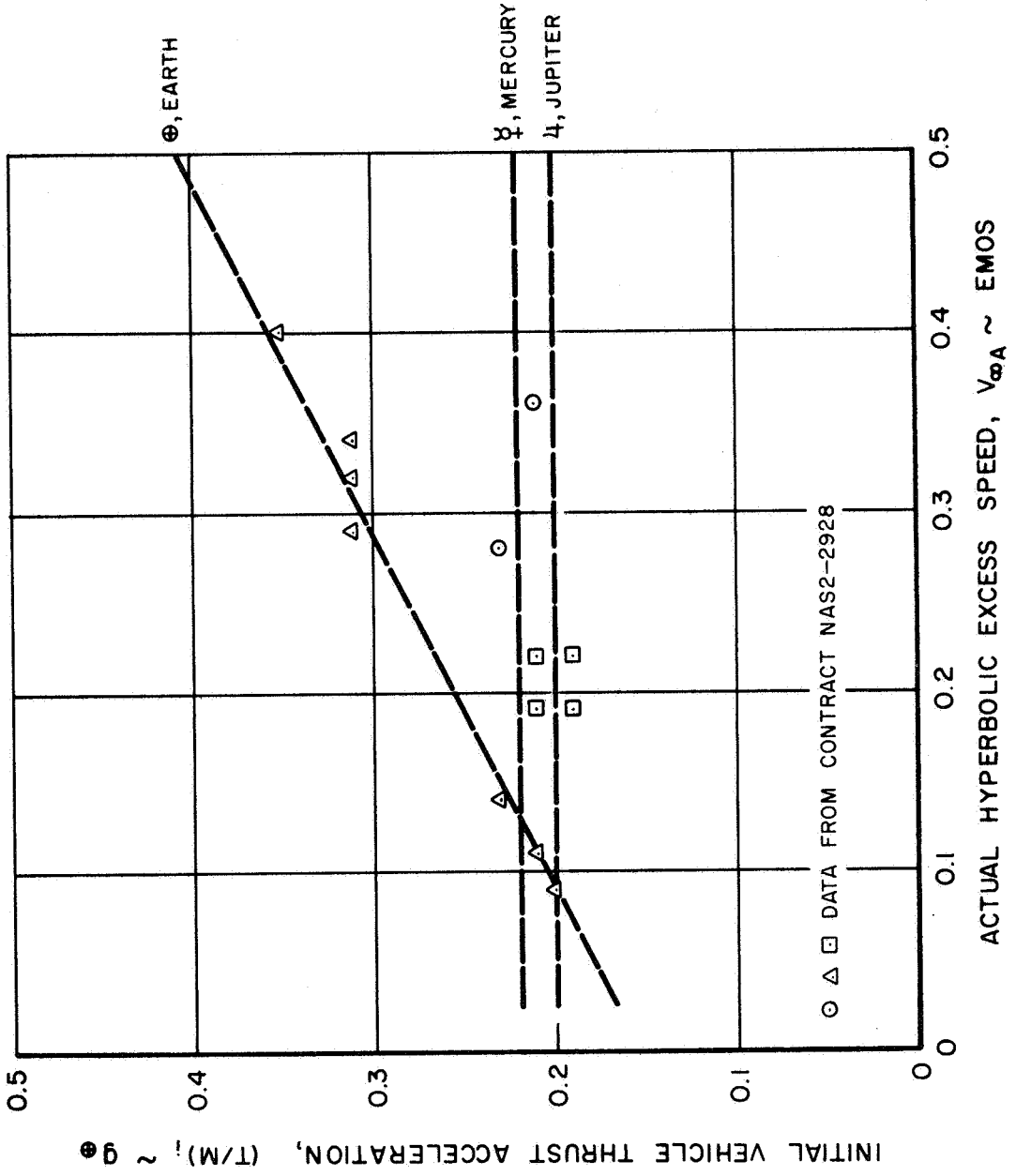

HIGH-LOW THRUST PLANETOCENTRIC OPERATIONS

HYPERBOLIC EXCESS SPEEDS ATTAINED WITH HIGH- AND LOW-THRUST PROPULSION WITHIN SPHERE OF influence

EARTH ESCAPE

$r_0 = 1.1$

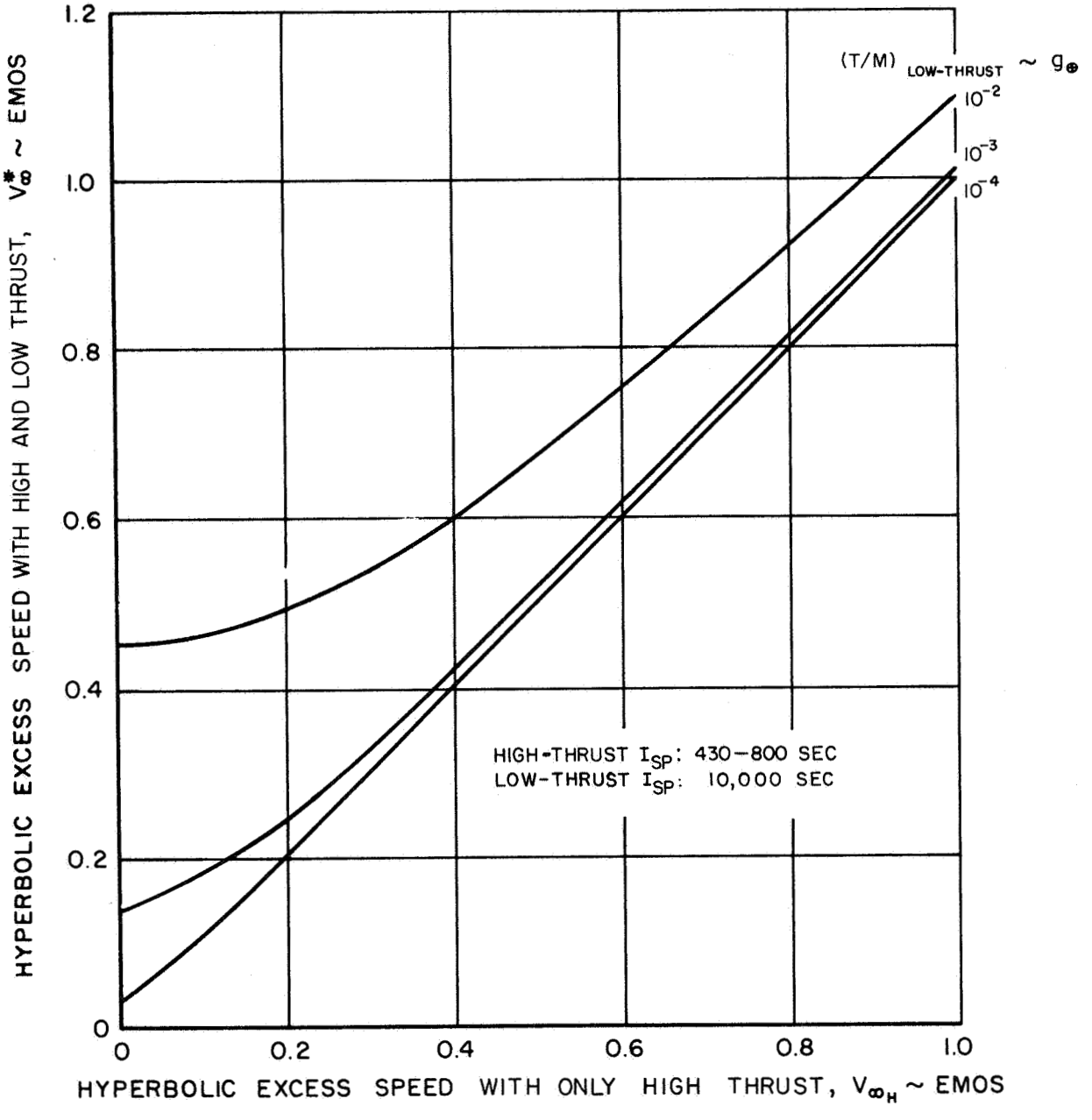

HIGH—LOW THRUST PLANETOCENTRIC OPERATIONS

HYPERBOLIC EXCESS SPEEDS ATTAINED WITH HIGH- AND LOW-THRUST PROPULSION WITHIN SPHERE OF INFLUENCE

PLANET - MERCURY

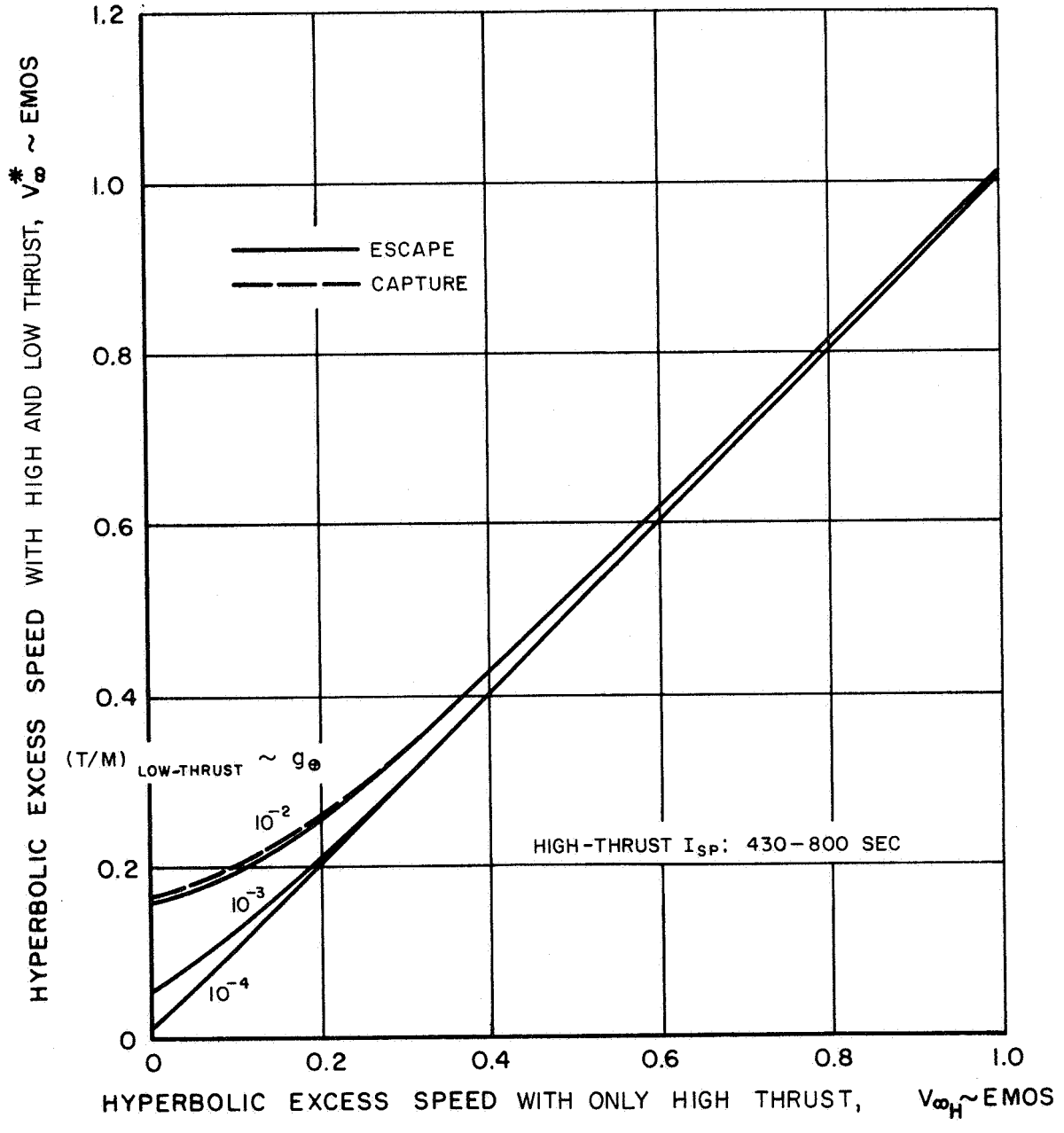

HIGH-LOW THRUST PLANETOCENTRIC OPERATIONS

HYPERBOLIC EXCESS SPEEDS ATTAINED WITH HIGH- AND LOW-THRUST PROPULSION WITHIN SPHERE OF INFLUENCE

PLANET - JUPITER

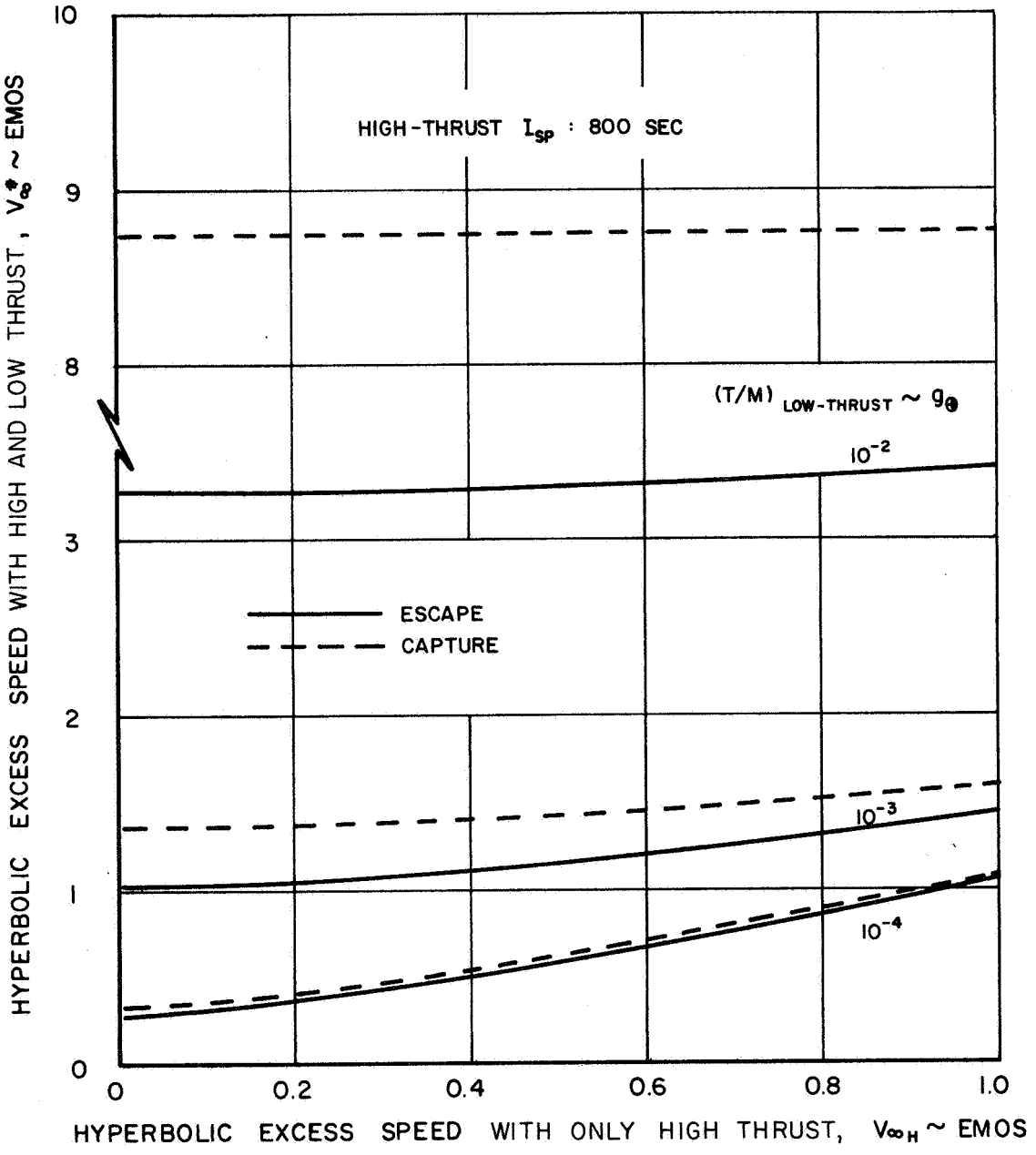

FIG. IV-6

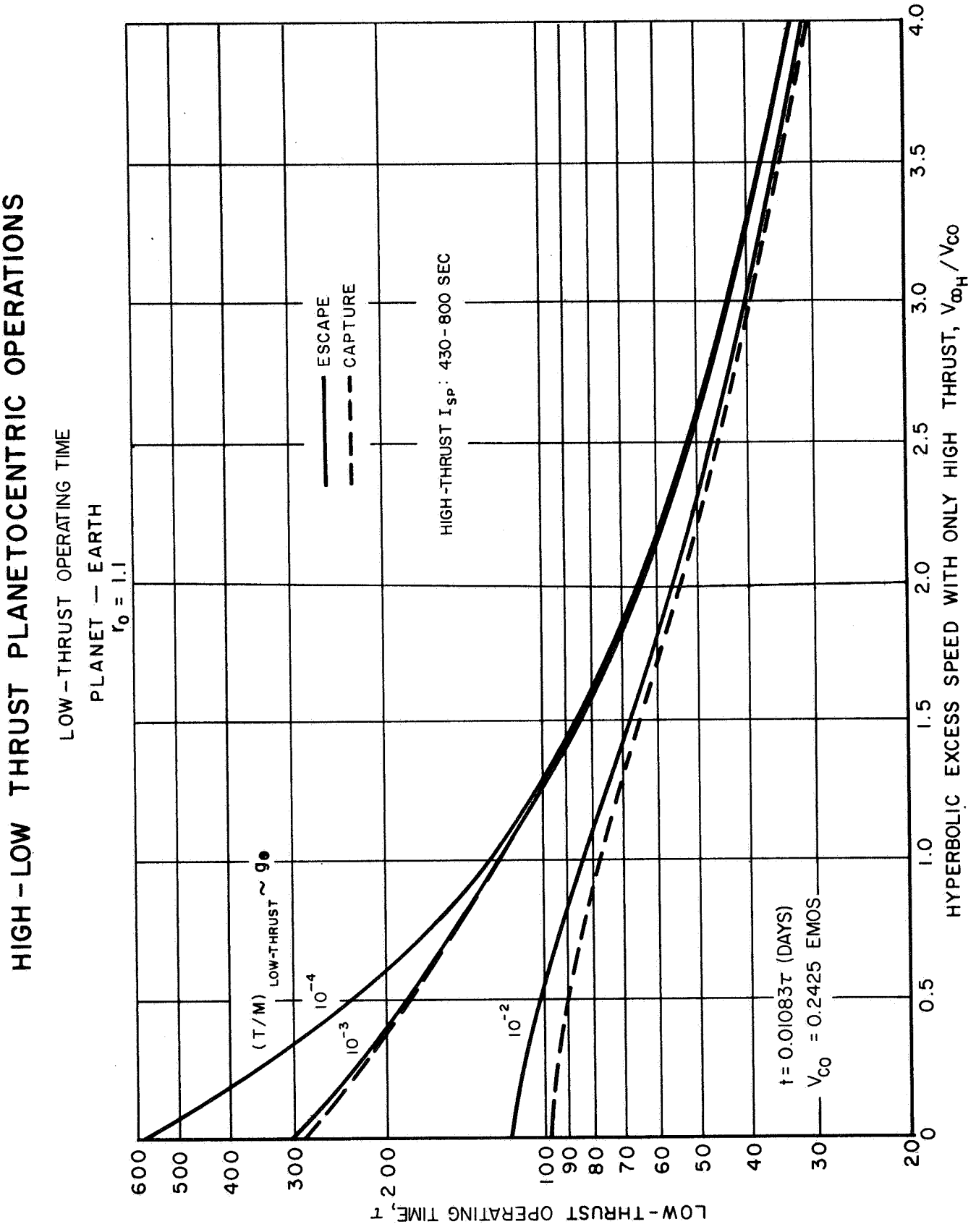
HIGH-LOW THRUST PLANETOCENTRIC OPERATIONS
LOW-THRUST OPERATING TIME
PLANET — EARTH
r_0 = 1.1
ESCAPE
CAPTURE
HIGH-THRUST I_{sp}: 430-800 SEC
$(T/M)_{LOW-THRUST} \sim g_\oplus$
10^{-4}
10^{-3}
10^{-2}
t = 0.01083τ (DAYS)
V_{CO} = 0.2425 EMOS
LOW-THRUST OPERATING TIME, τ
HYPERBOLIC EXCESS SPEED WITH ONLY HIGH THRUST, V_{∞_H}/V_{CO}
600
500
400
300
200
100
90
80
70
60
50
40
30
20
0
0.5
1.0
1.5
2.0
2.5
3.0
3.5
4.0

HIGH-LOW THRUST PLANETOCENTRIC OPERATIONS

LOW-THRUST OPERATING TIME
HIGH-THRUST I_{SP} = 430 SEC

PLANET - MERCURY

r_0 = 1.1

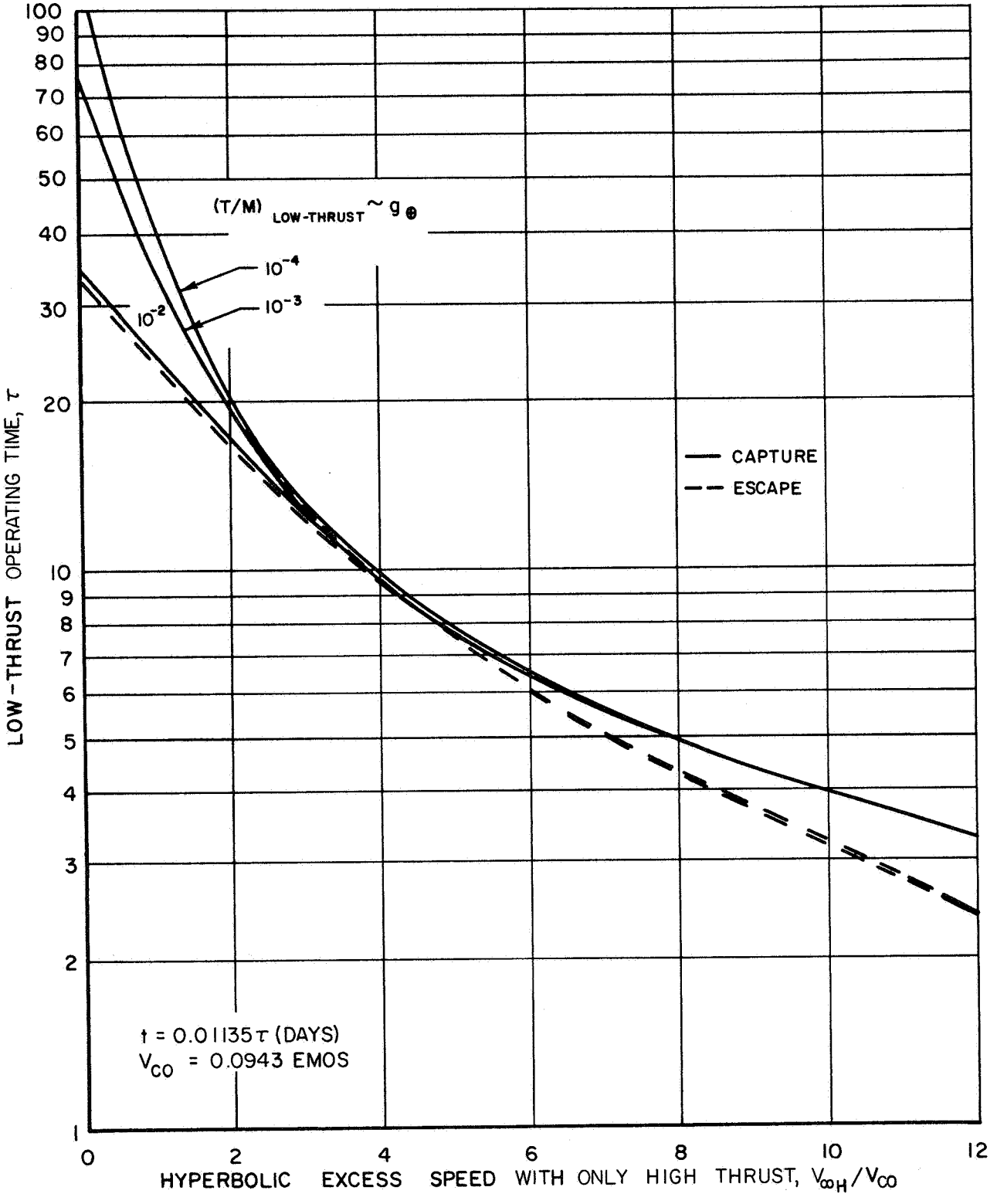

HIGH - LOW THRUST PLANETOCENTRIC OPERATIONS

LOW-THRUST OPERATING TIME
HIGH-THRUST I_{SP} = 800 SEC

PLANET - MERCURY

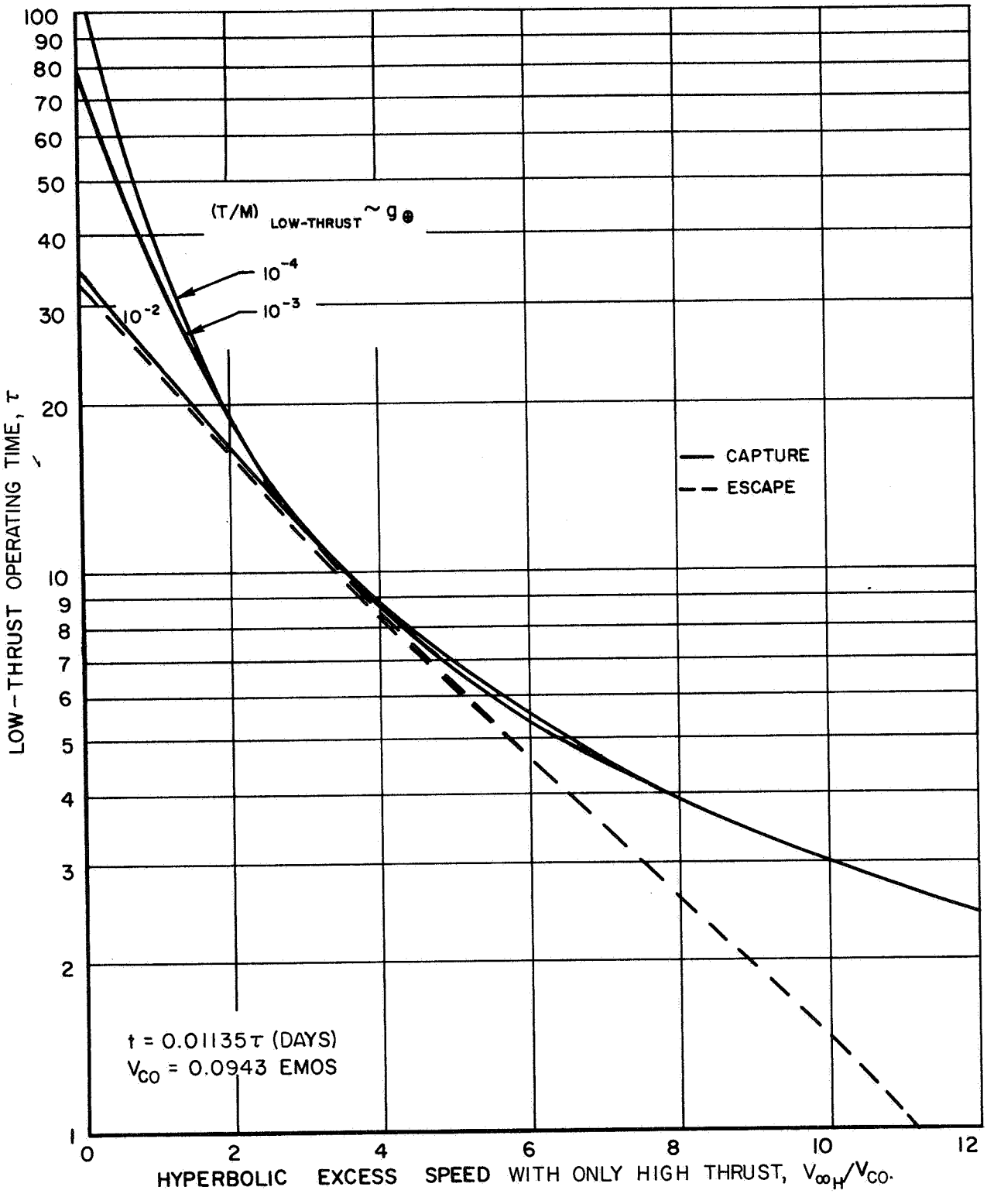

HIGH-LOW THRUST PLANETOCENTRIC OPERATIONS

LOW-THRUST OPERATING TIME
HIGH-THRUST I_{SP} = 800 SEC

PLANET - JUPITER

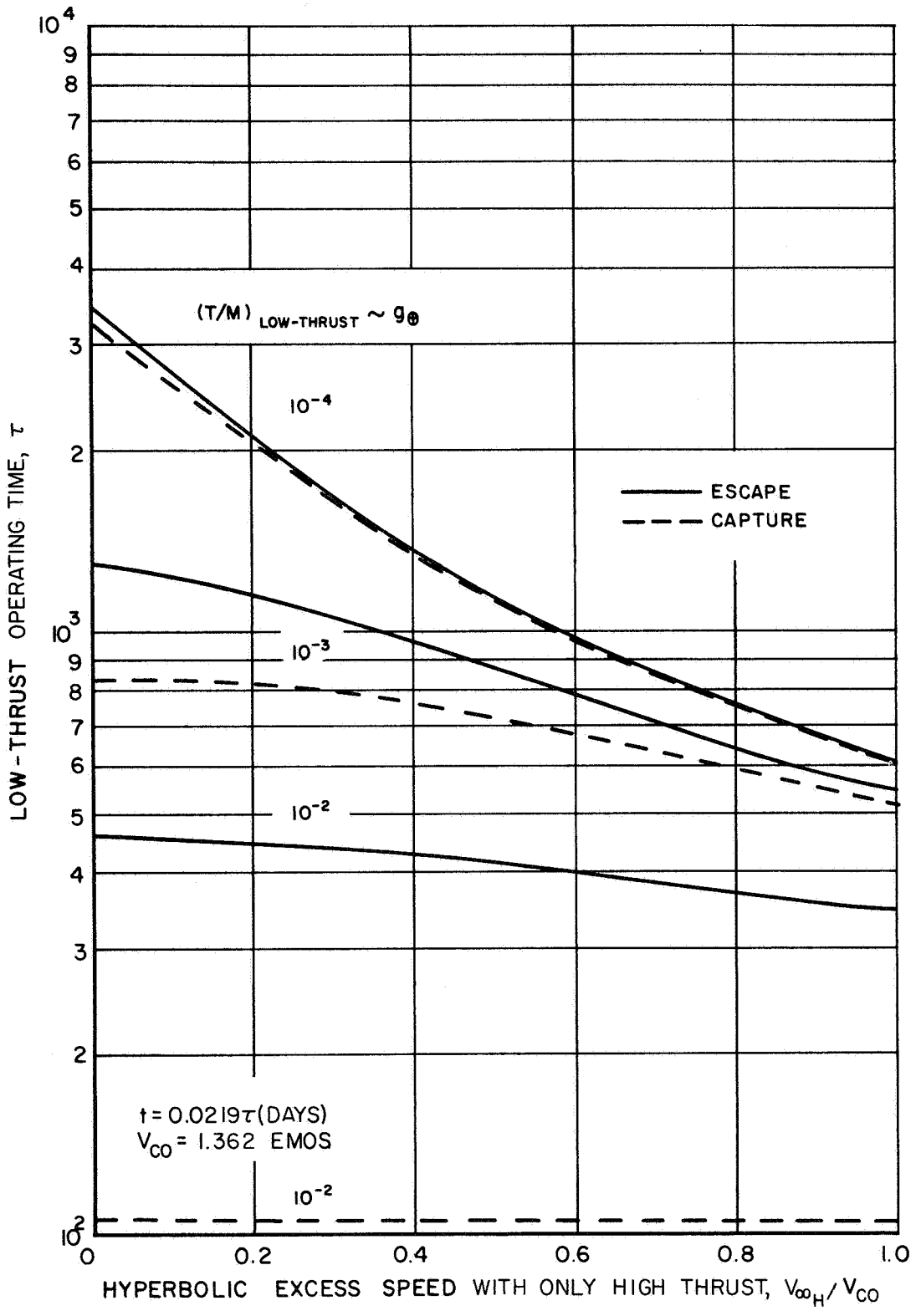

FIG. IV-10

HIGH-LOW THRUST PLANETOCENTRIC OPERATIONS

VEHICLE FLIGHT PATH ANGLE AT SPHERE OF INFLUENCE

HIGH-THRUST I_{SP} = 800 SEC

PLANET—EARTH

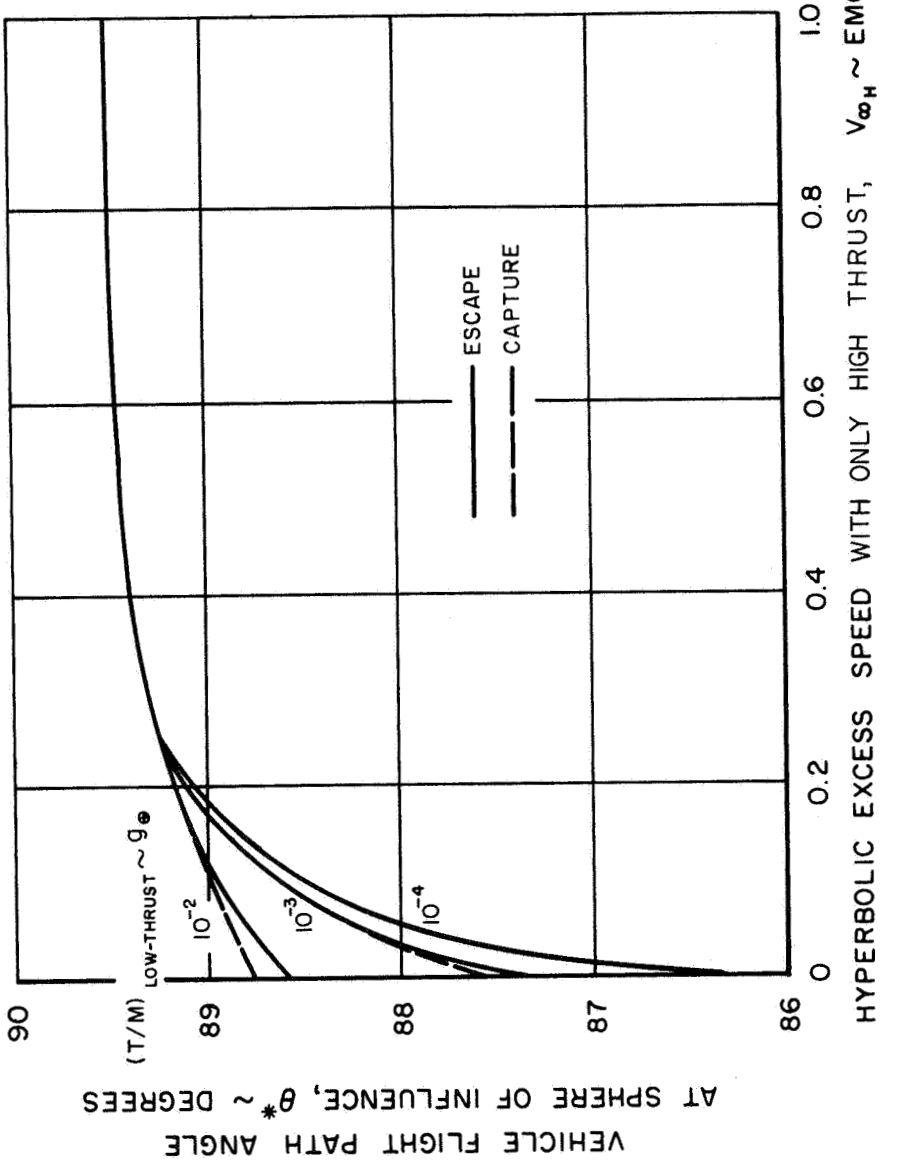

FIG. IV-11

HIGH-LOW THRUST PLANETOCENTRIC OPERATIONS

VEHICLE FLIGHT PATH ANGLE AT SPHERE OF INFLUENCE

HIGH-THRUST I_{SP} = 800 SEC

PLANET — MERCURY

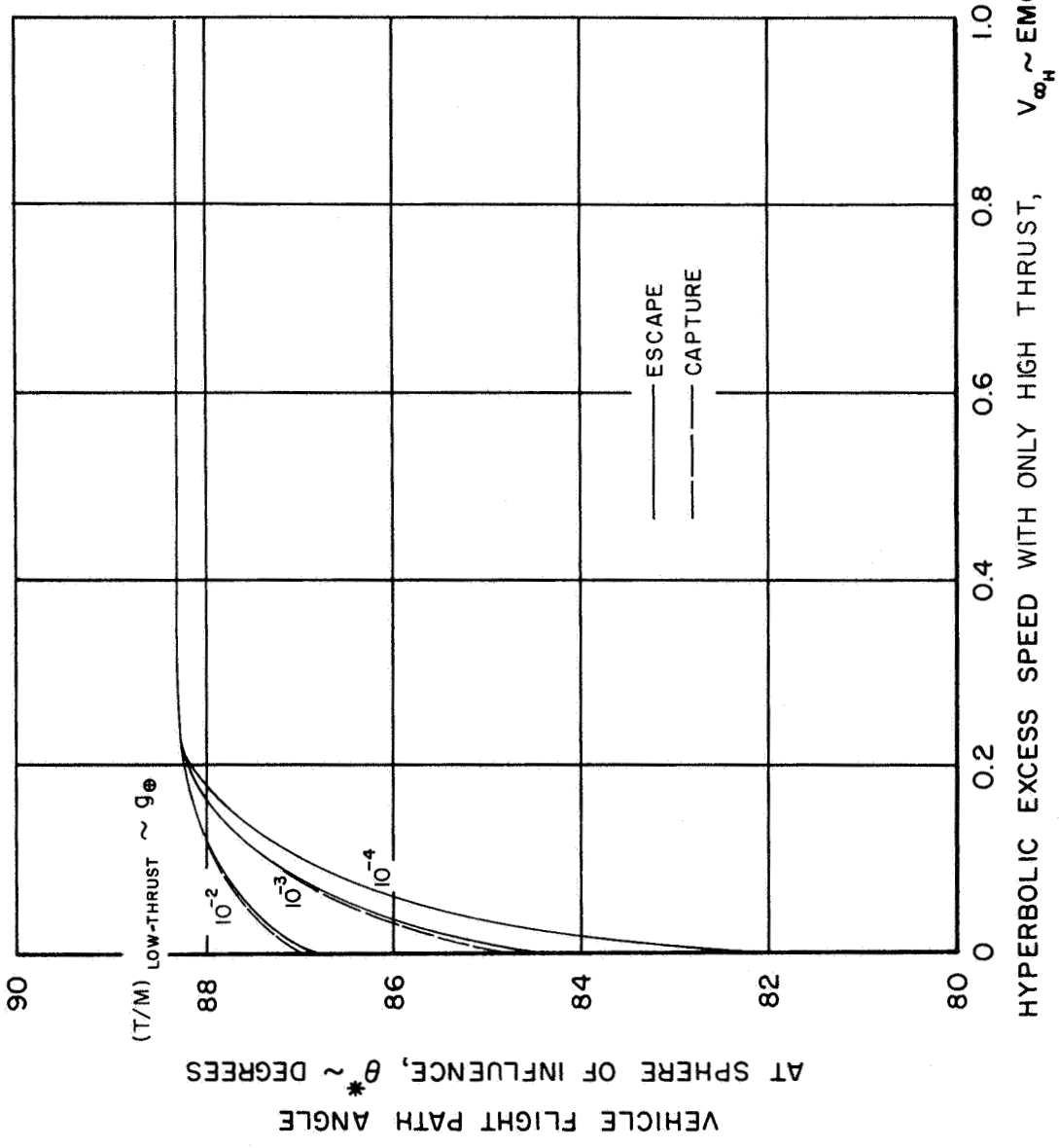

HIGH-LOW THRUST PLANETOCENTRIC OPERATIONS

HYPERBOLIC EXCESS SPEEDS ATTAINED WITH HIGH- AND LOW-THRUST PROPULSION WITHIN SPHERE OF INFLUENCE

EARTH DEPARTURE

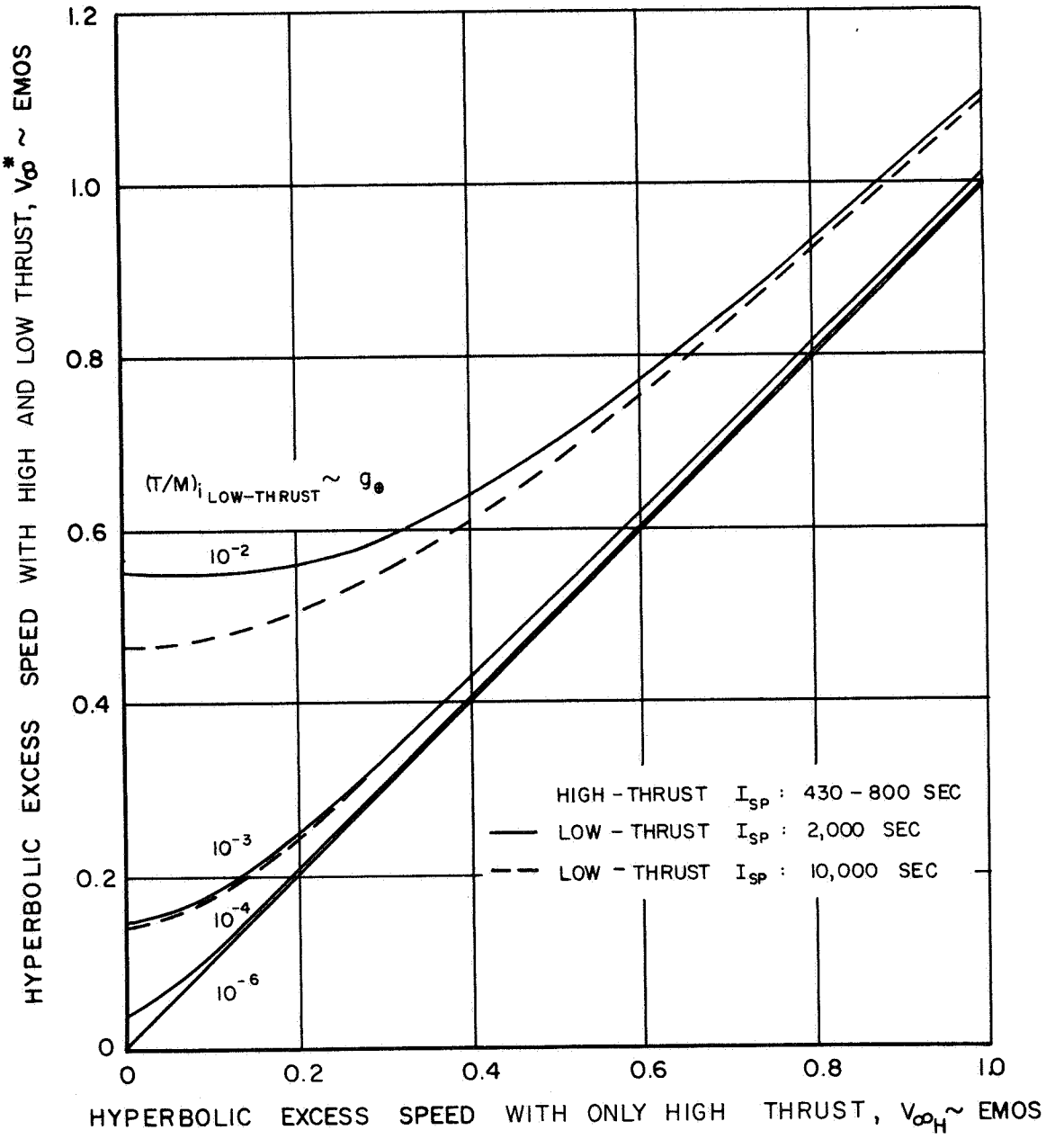

HIGH-LOW THRUST PLANETOCENTRIC OPERATIONS

HYPERBOLIC EXCESS SPEEDS ATTAINED WITH HIGH- AND LOW-THRUST PROPULSION WITHIN SPHERE OF INFLUENCE

EARTH CAPTURE

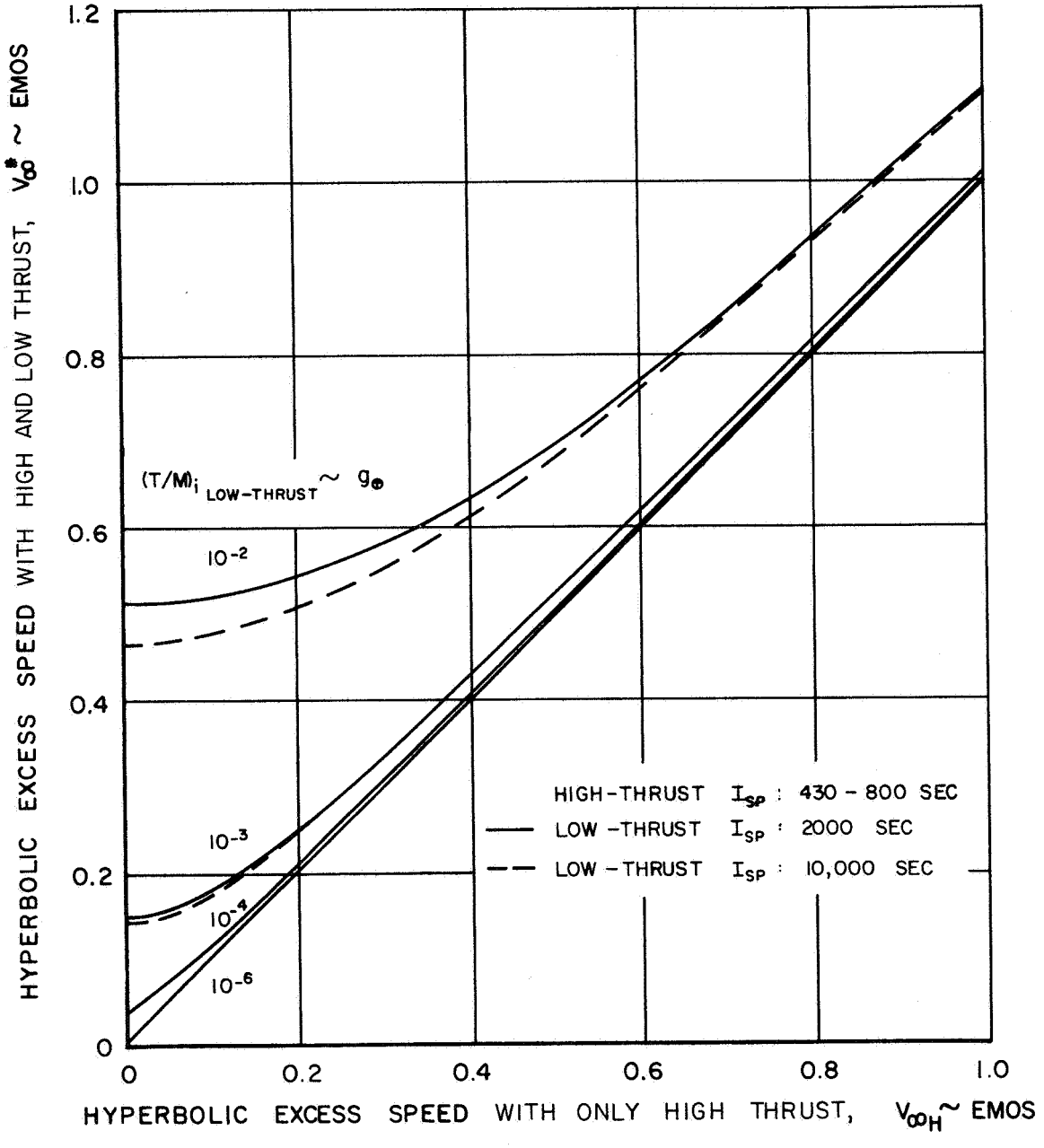

HIGH-LOW THRUST PLANETOCENTRIC OPERATIONS

EARTH DEPARTURE AND CAPTURE

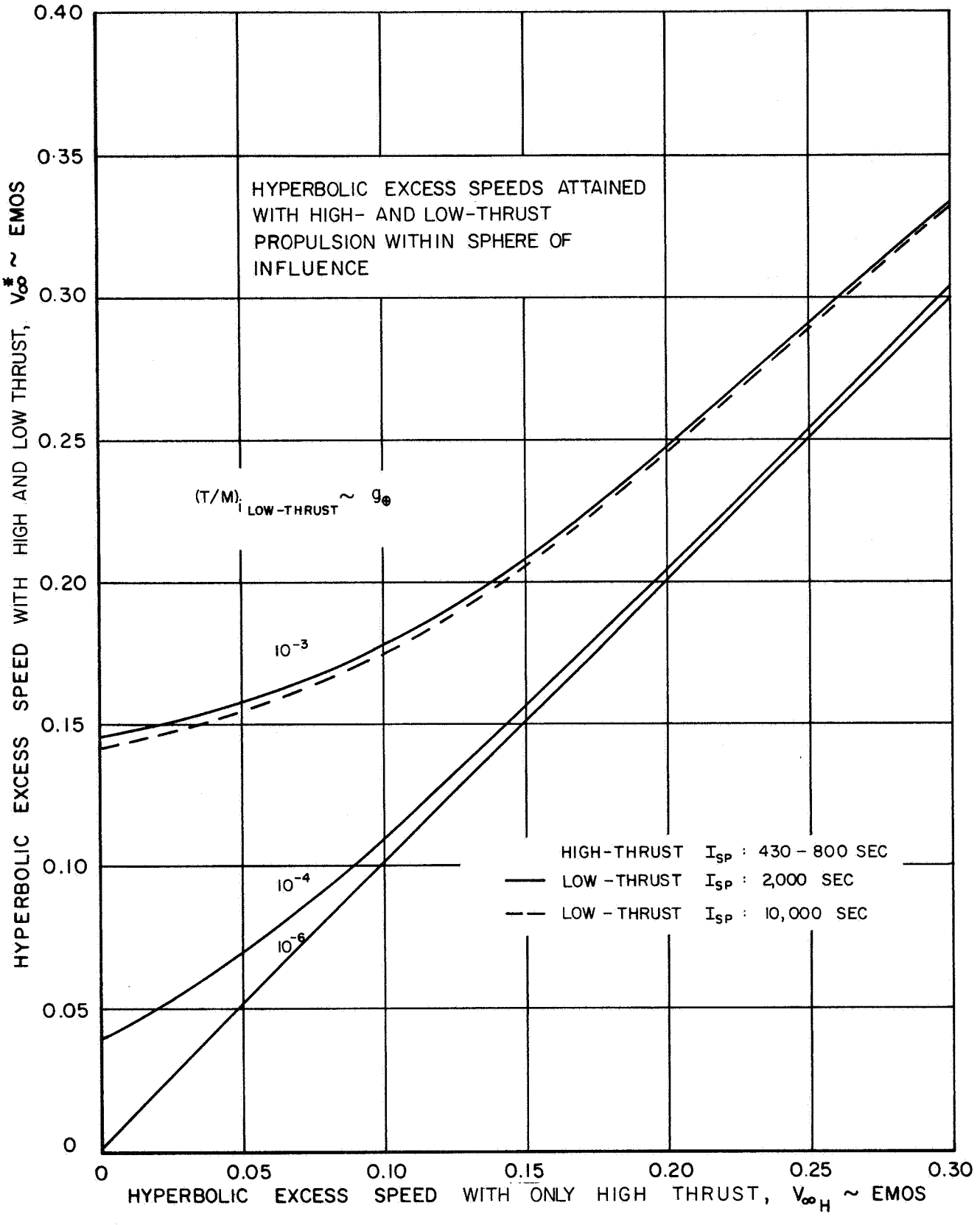

HIGH - LOW THRUST PLANETOCENTRIC OPERATIONS

LOW-THRUST OPERATING TIME

HIGH-THRUST I_{SP} = 430 SEC

EARTH DEPARTURE

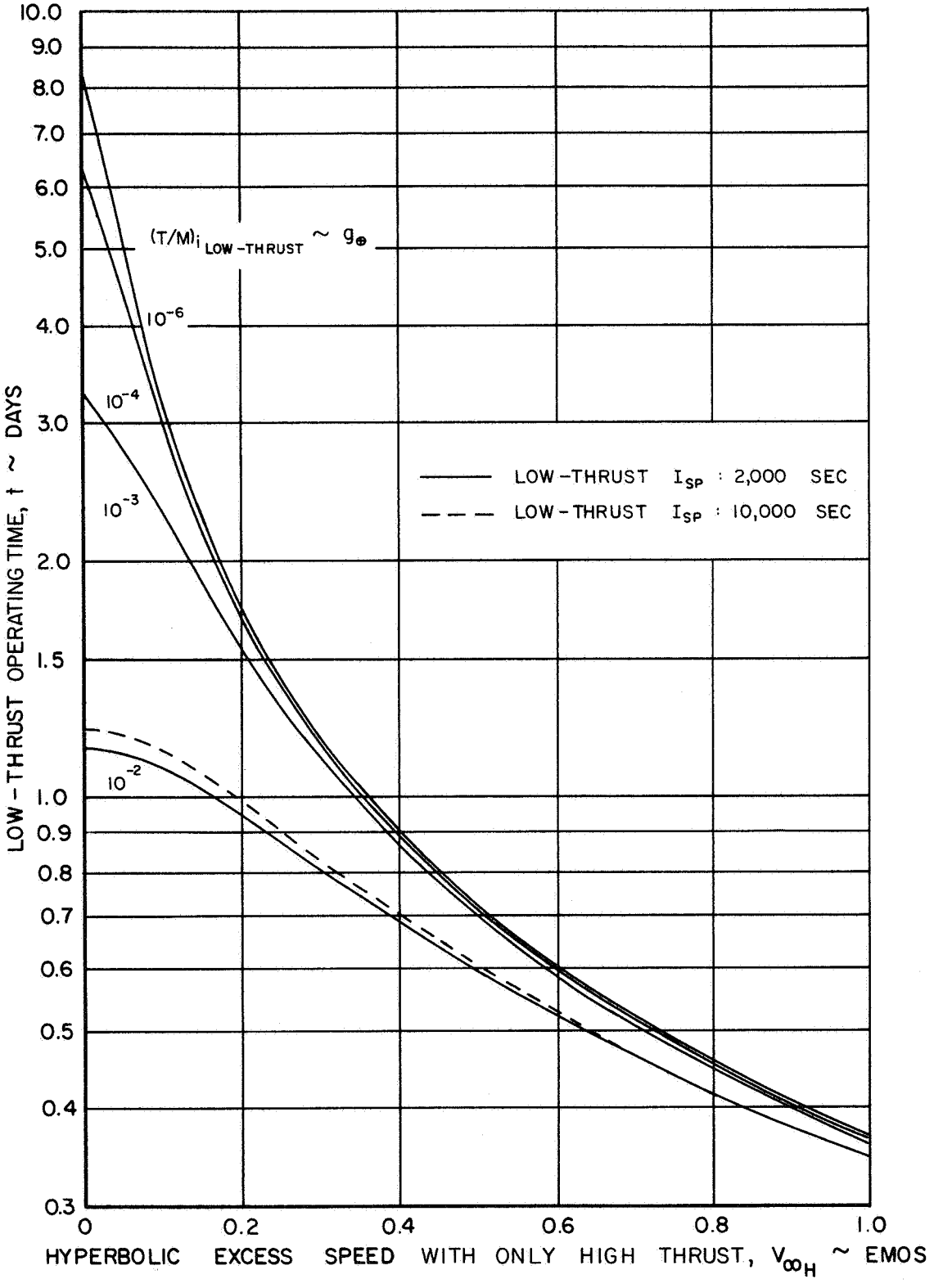

HIGH - LOW THRUST PLANETOCENTRIC OPERATIONS

LOW-THRUST OPERATING TIME
HIGH-THRUST I_{SP} = 800 SEC

EARTH DEPARTURE

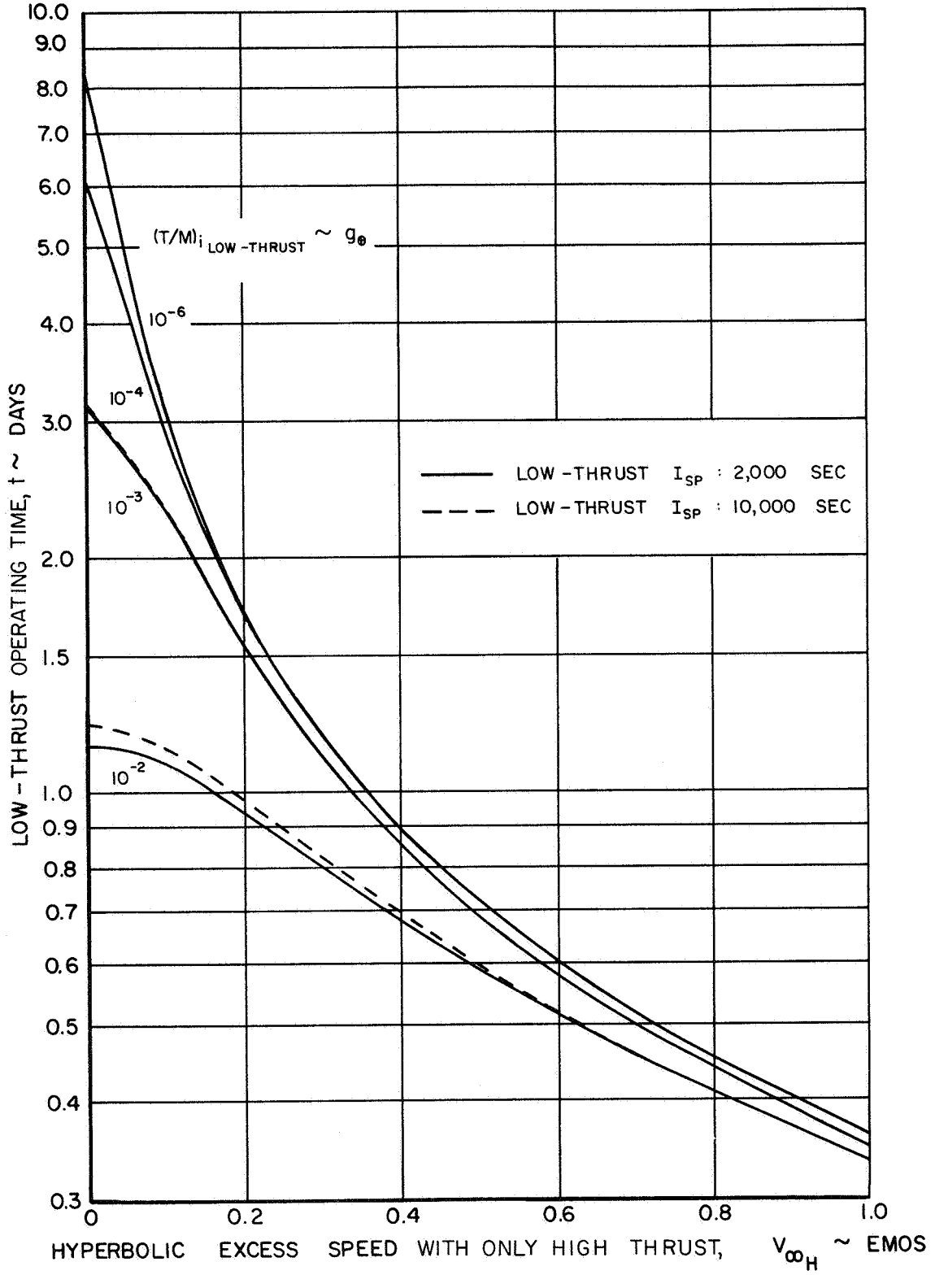

HIGH-LOW THRUST PLANETOCENTRIC OPERATIONS

LOW-THRUST OPERATING TIME
HIGH-THRUST I_{SP} = 430 SEC

EARTH CAPTURE

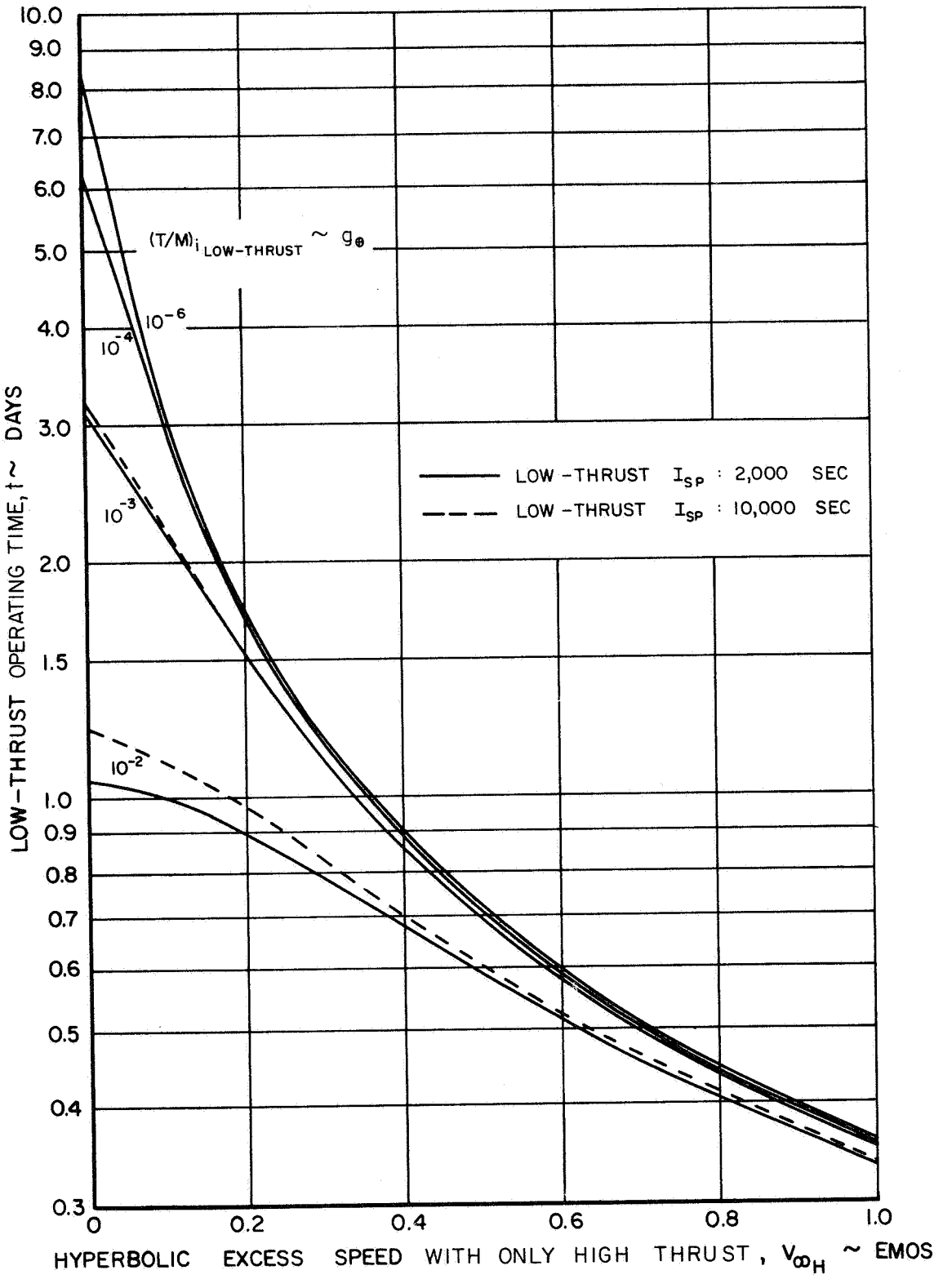

HIGH - LOW THRUST PLANETOCENTRIC OPERATIONS

LOW - THRUST OPERATING TIME
HIGH-THRUST I_{SP} = 800 SEC

EARTH CAPTURE

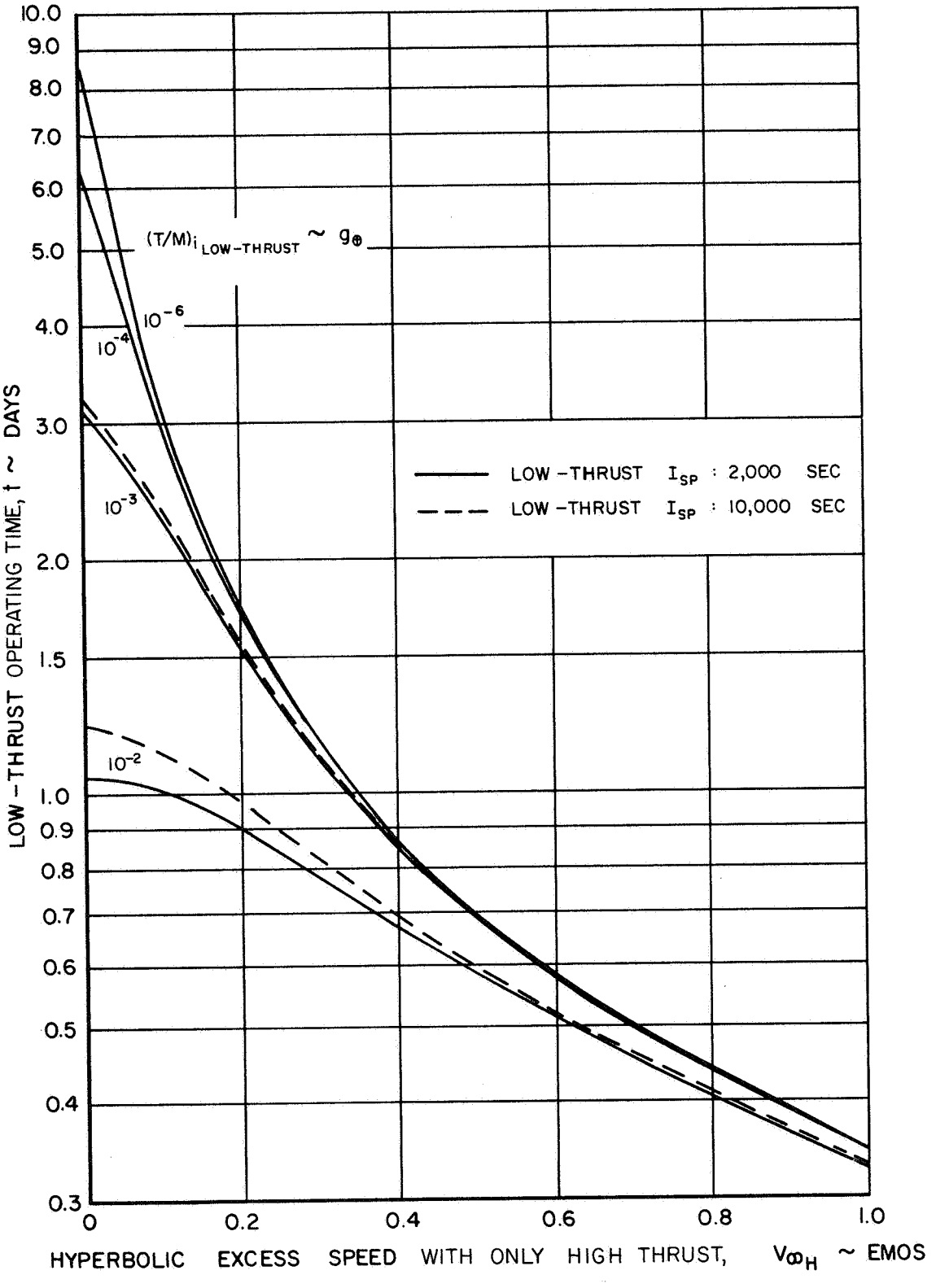

HIGH - LOW THRUST PLANETOCENTRIC OPERATIONS

HIGH-THRUST CHARACTERISTIC SPEEDS

EARTH DEPARTURE

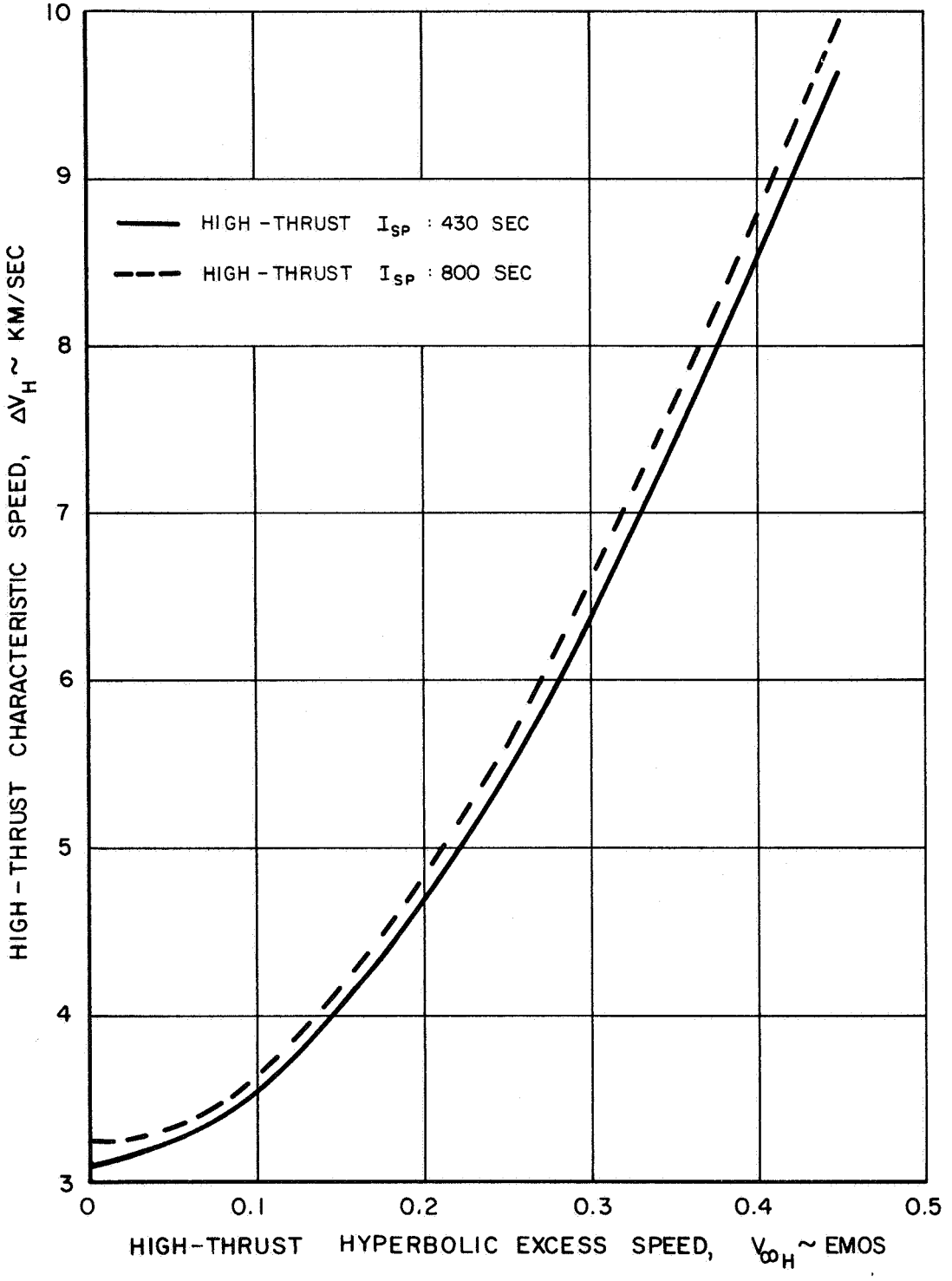

HIGH-LOW THRUST PLANETOCENTRIC OPERATIONS

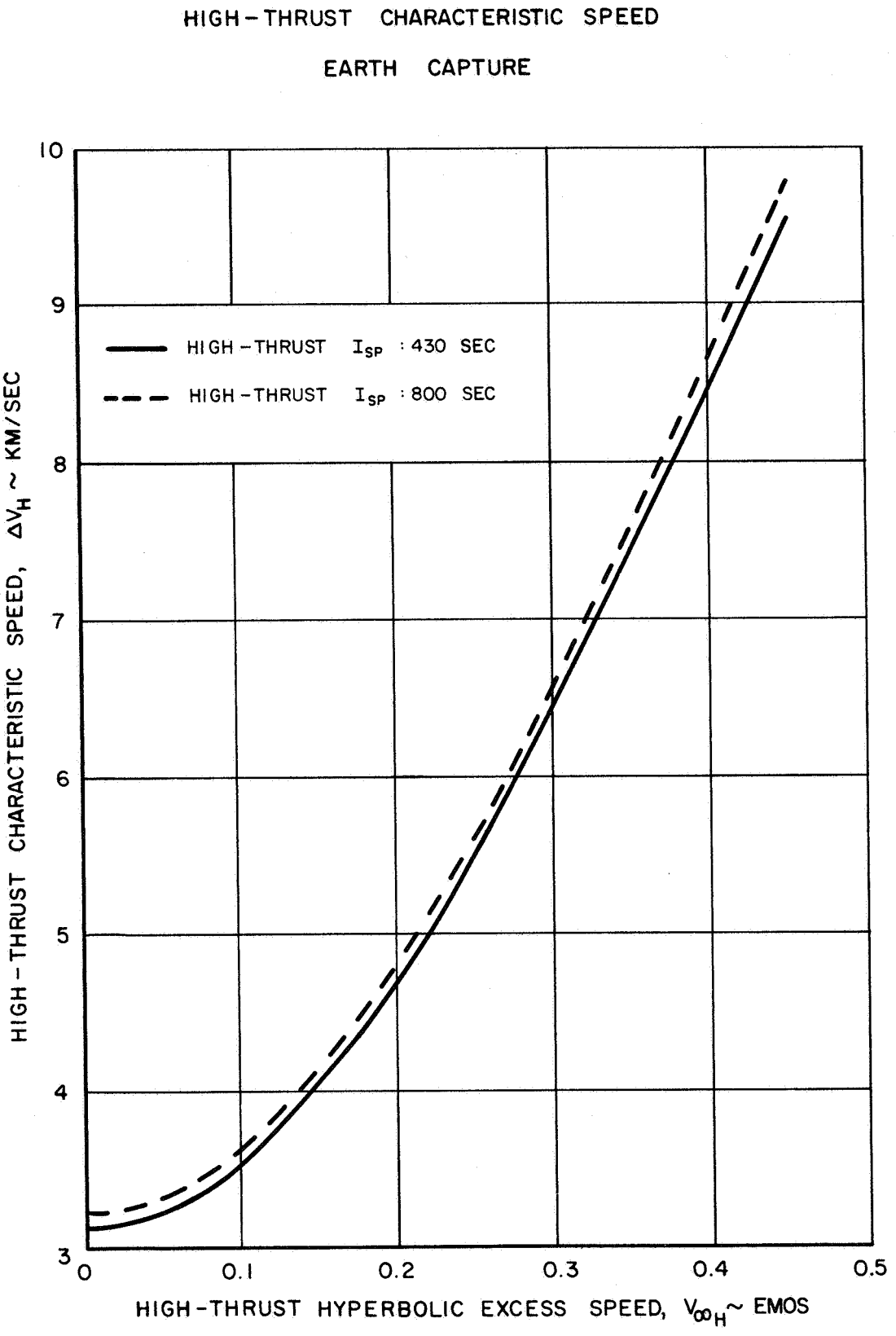

HIGH-LOW THRUST PLANETOCENTRIC OPERATIONS

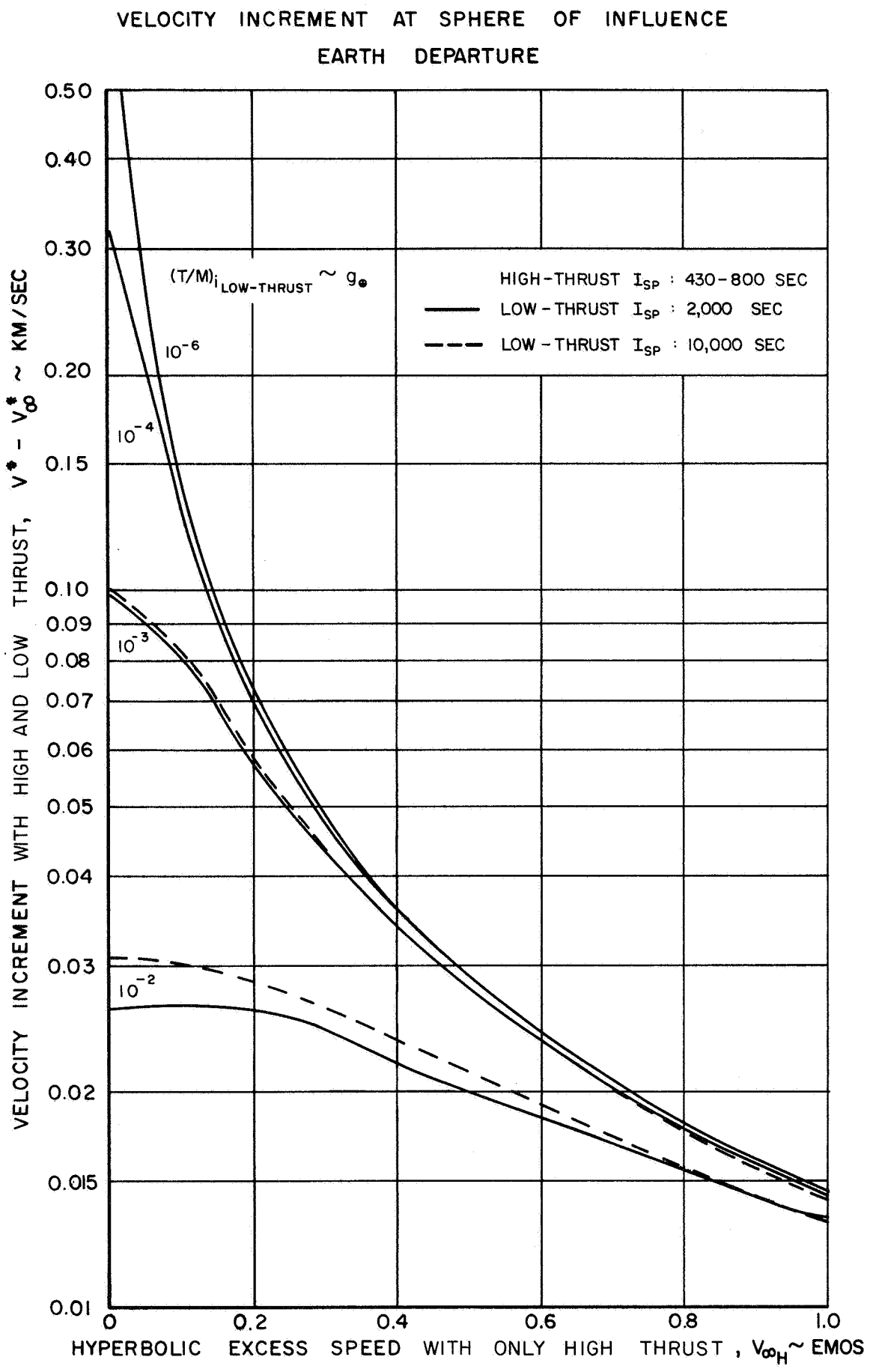

HIGH-LOW THRUST PLANETOCENTRIC OPERATIONS

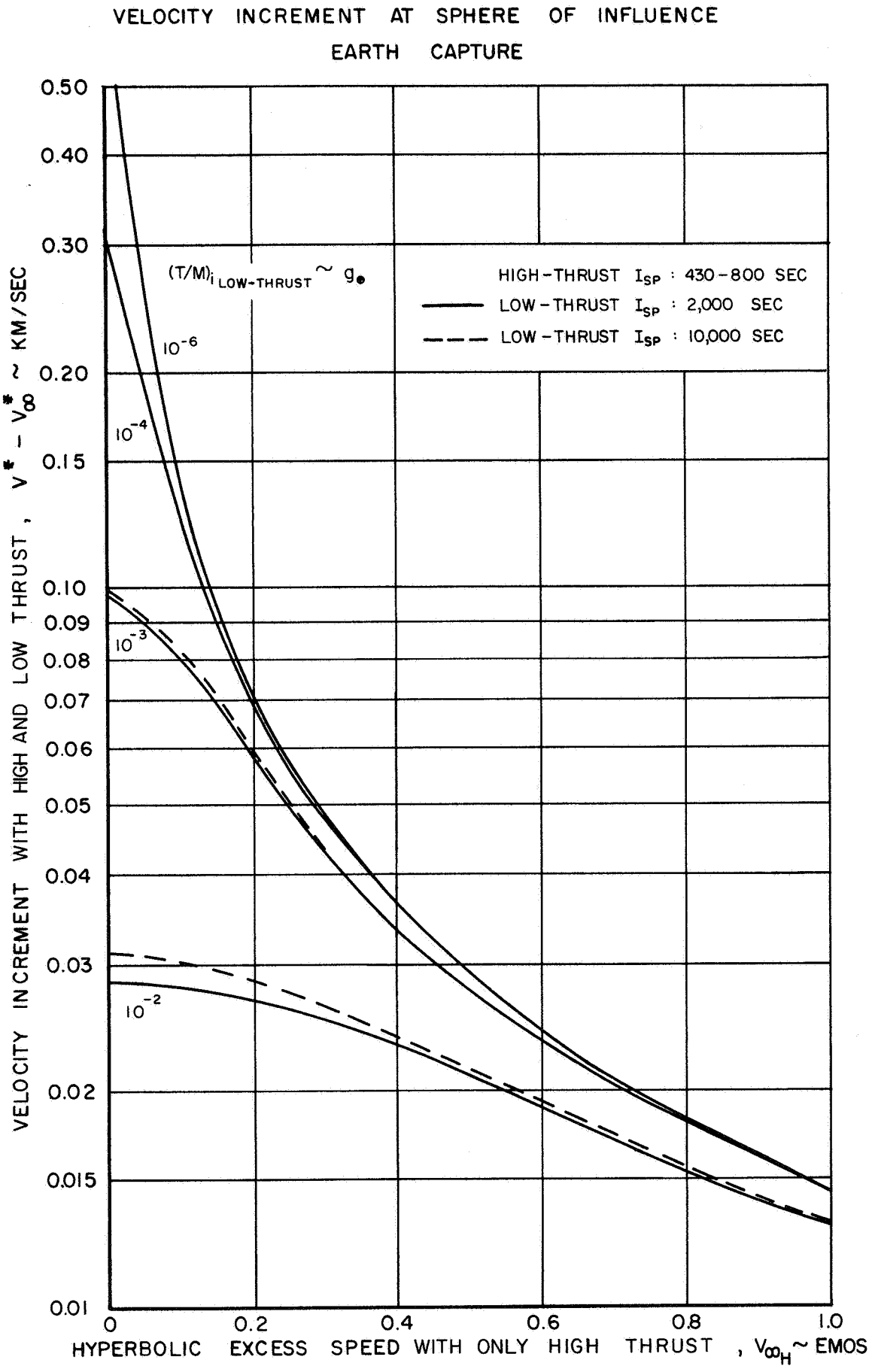

SECTION V

LOW-THRUST PLANETOCENTRIC SPIRAL

The purpose of the planetocentric low-thrust analysis is to develop an insight into the low-thrust system parameters for departure from or capture onto a circular parking orbit. The goal is to combine the planetocentric spirals with the heliocentric trajectory so procedures may be developed to optimize a single propulsion system which is to operate successively in both gravity fields. The general approach is based on the work of Perkins (Ref. V-1) and Edelbaum (Ref. V-2).

In review, two linear forms of the equations relating the nondimensional velocity parameter and the mass parameter were found for the planetary low-thrust spiral involving departure from or capture onto a circular parking orbit with a specified hyperbolic velocity at, respectively, the terminal or initial points. These linear equations, once translated into vehicle system and trajectory terms, relate the burnout mass fraction required to accommodate a given hyperbolic velocity for a specified initial thrust-to-mass ratio, circular parking orbit, and planet. The equations are simple and straightforward and require, at most, an elementary iteration for mass fraction (See Appendix C).

The foregoing approach is limited by two aspects: the magnitude of the circular and hyperbolic velocities imposed by the linearization of the dimensionless equations, and the fact that the vehicle does not necessarily attain the specified hyperbolic velocity at the sphere of influence. It is the purpose of the following to discuss in detail the implications of the above two aspects. Comparisons are made between the present method and exact numerical results for payload mass fractions and thrusting times (planet-centered only). The utility of the method is shown for planetocentric payload optimization under various hyperbolic velocities to be achieved by a low-thrust spiral departure from Earth. Justification for neglecting the sphere of influence approach and position offset for combining planetocentric and heliocentric phases is developed in Section VI, Calculation of Interplanetary Trajectories in the Vicinity of the Planets. These latest results are used in the study of a single propulsion system performing parking orbit-to-parking orbit missions. In this case the transition point, as it influences the vehicle, between the planetocentric and heliocentric phases is taken into account.

Summary of Mass Ratio Equations

For convenience, the mass ratio equations derived in Refs. V-1 and V-2 (and given in Appendix C) are summarized below. It should be remembered that these

equations apply only to a planet-centered spiral and do not include the effects of other perturbing bodies. The equations for thrusting time and payload ratio are also presented.

Circular Orbit to Escape Velocity

$$\frac{m_C}{m_E} = \exp\left\{ \frac{V_C}{C} \left[1 - 0.805 \left(\frac{F/m_C}{\mu/R_C^2} \right)^{1/4} \left(\frac{m_C}{m_E} \right)^{1/4} \right] \right\}$$

The term m_C is the initial mass on the circular orbit, V_C is the circular speed, C is the jet exhaust speed, and m_E is the mass at escape; F/m_C is the initial thrust-to-weight ratio, μ is the planet's gravitational parameter, and R_C is the radius of the circular orbit.

Circular Orbit to Hyperbolic Velocity

$$\frac{m_C}{m_H} = \exp\left\{ \frac{V_H}{C} + \frac{V_C}{C} \left[1 - 1.746 \left(\frac{F/m_C}{\mu/R_C^2} \right)^{1/4} \left(\frac{m_C}{m_E} \right)^{1/4} \right] \right\}$$

The term m_C/m_E is found from the previous equation (circular orbit to escape velocity). The asymptotic (hyperbolic) velocity, V_H, must not be zero; this restriction is a consequence of combining the linear dimensionless equations for the two modes: circular-to-escape and escape-to-hyperbolic. Note that setting $V_H = 0$ in the above equation does not yield the proper mass ratio which is given by the previous equation (circular orbit to escape).

Escape Velocity to Circular Orbit

$$\frac{m_E}{m_C} = \exp\left\{ \frac{V_C}{C} \left[1 - 0.805 \left(\frac{F/m_E}{\mu/R_C^2} \right)^{1/4} \right] \right\}$$

F/m_E is the initial thrust-to-mass ratio; i.e., the value at initiation of the planetocentric phase where the vehicle is at local escape velocity.

Hyperbolic Velocity to Circular Orbit

$$\frac{m_H}{m_C} = \exp\left\{ \frac{V_H}{C} + \frac{V_C}{C} \left[1 - 1.746 \left(\frac{F/m_H}{\mu/R_C^2} \right)^{1/4} \left(\frac{m_H}{m_E} \right)^{1/4} \right] \right\} \quad , V_H \neq 0$$

The terms m_H and F/m_H are, respectively, the mass and thrust-to-mass ratio at the initiation of planetocentric phase when the vehicle is at the specified asymptotic velocity, V_H. The ratio m_H/m_E is given by

$$\frac{m_H}{m_E} = \exp\left[\frac{V_H}{C} - \frac{0.941}{C} \left(\mu \frac{F}{m_H} \right)^{1/4} \left(\frac{m_H}{m_E} \right)^{1/4} \right]$$

This is the mass ratio required to decelerate from an asymptotic velocity to local escape velocity.

Limitations on Velocity

Because it is assumed that the dimensionless parametric equations are linear (See Appendix A), a region of validity can be described which actually places a limitation on the circular and hyperbolic velocities depending on the system parameters. Thus for:

circular-to-escape; $$V_C \geq 1.8 \left(\mu \frac{F}{m_C}\right)^{1/4} \left(\frac{m_C}{m_E}\right)^{1/4}$$

escape-to-hyperbolic; $$V_H \geq 1.95 \left(\mu \frac{F}{m_E}\right)^{1/4}$$

escape-to-circular; $$V_C \geq 1.8 \left(\mu \frac{F}{m_E}\right)^{1/4}$$

hyperbolic-to-escape; $$V_H \geq 1.95 \left(\mu \frac{F}{m_E}\right)^{1/4} \left(\frac{m_H}{m_E}\right)^{1/4}$$

The foregoing limitations correspond to an allowable error of about 5% between the linear and actual forms of the dimensionless parametric equations. As can be seen, the lower limits on the velocities depend primarily on the initial thrust-to-weight ratios. The importance of this dependence is pointed out later.

Time and Payload Ratio

The time, T, spent in thrusting during the low-thrust spiral (departure or capture) is the time necessary to expend the propellant so that the burnout mass fraction (as required by the foregoing equations) is achieved. It remains to specify the initial thrust-to-weight ratio and specific impulse or, equivalently, the powerplant-to-gross mass fraction and exhaust velocity.

$$T = \frac{\alpha_W}{2} \frac{C^2}{\eta} \frac{(1-\mu_1)}{\mu_W}$$

where C is the exhaust velocity, μ_W the powerplant mass fraction, η the thruster efficiency, and α_W the powerplant specific mass. The final mass fraction, μ_1, is the reciprocal of the mass ratio obtained from the appropriate mass ratio equations listed above.

Note that the initial thrust-to-mass ratio, in terms of the vehicle system parameters, is given by

$$\left(\frac{F}{m}\right)_i = \frac{2\eta\mu_W}{\alpha_W C}$$

This notation is preferred in the present analysis because of the importance of thruster efficiency and the dependence of efficiency on exhaust velocity. These considerations are also intimately related to the payload fraction for the planetocentric phase, the heliocentric phase, or both combined.

Regardless of which operational phase is considered, the most inclusive definition of payload fraction accounts for the mass of the propellant tanks, the thrusters, the tie-in structure, and the power source (including power conversion equipment). The payload fraction μ_L, is thus

$$\mu_L = 1 - \frac{(1+\sigma)}{\rho}(1-\mu_1) - (1+\sigma)\left[1 + \frac{\alpha_F(C)}{\alpha_W}\right]\mu_W$$

where α_F (C) is the ratio of the thruster mass to input power (a function of C), and ρ is the tank propellant mass fraction (assumed constant) defined as the ratio of propellant mass to the mass of the propellant plus tanks. The tie-in and miscellaneous structure is represented by the proportionality constant, σ, which, when multiplied by the mass of the other inert hardware, yields the structure. It can be seen that the payload is a function of C and μ_W, the two parameters which must be optimally chosen to maximize μ_L for a given thrusting phase (planetocentric, heliocentric, or both).

If the mass of the propellant tanks is to be ignored, then $\rho \rightarrow 1$. Additionally, if the thruster mass is assumed constant, rather than a function of exhaust velocity, it may be included as a part of the powerplant by redefining α_W. For the special case where the propellant tanks and structure are negligible and the thrusters are either part of the powerplant or simply ignored, the payload fraction simplifies to

$$\mu_L = \mu_1 - \mu_W$$

This definition was used in the payload fraction calculation presented below.

Comparison of Analytical and Numerical Results

The following presents the results of a brief study performed to investigate the accuracy of the approximate mass ratio equations. Two overall comparisons are made: one for departure from a circular orbit to varying hyperbolic velocities (including zero) and the other for departure from a circular orbit to escape velocity for varying powerplant mass fractions. The two approaches are employed in order to check the validity of the equations for the overall problems of circular orbit-to-hyperbolic velocity and for the special case of departure to only escape velocity. In the latter case another analytical method, previously discussed in the literature, is also studied.

Circular Orbit to Hyperbolic Velocity

The basis of comparison for this mode of operation is the work of Moeckel (Ref. V-3) published in 1959 by NASA, Lewis Research Center. Precisely the same thrusting program (constant, tangential) as assumed in the current study was used and applied to both outward (departure) and inward (capture) paths. Trajectory data are presented in Ref. V-3 for a range of thrust-to-weight ratios from 10 to 10^{-4} and a range of exhaust velocities from those attainable by chemical rockets to infinity. Departure from or capture onto a circular parking orbit is assumed.

The approximate mass ratio equations in this report were applied to the case of departure from a 1.1-radii circular parking orbit about Earth to hyperbolic velocities ranging from zero to about 1.6 times initial circular velocity. Two initial thrust accelerations were used, 10^{-4} and 10^{-2} g_o (g_o = acceleration of gravity at the parking orbit); for each thrust acceleration an exhaust velocity of 5 and 3 times circular velocity was assumed. The parameter used for comparisons is Moeckel's nondimensional time, τ, defined as the circular velocity times time divided by the orbit radius.

The results are depicted in the following table using Moeckel's nondimensional notation. It should be noted that Moeckel's results are presented on logarithmic graphs, thereby limiting the accuracy with which his results may be read, although it is sufficient for comparison purposes.

COMPARISON OF TIME PARAMETERS BETWEEN APPROXIMATE (PERKINS/ EDELBAUM) AND EXACT (MOECKEL) METHODS; OUTWARD PATHS

Square of local Hyperbolic Velocity V_H^2	Initial Acceleration = $10^{-4} g_o$				Initial Acceleration = $10^{-2} g_o$			
	V_j = 5		V_j = 3		V_j = 5		V_j = 3	
	Time Parameter, τ							
	Approx	Exact*	Approx	Exact*	Approx	Exact*	Approx	Exact*
0	8368	8400	7873	7900	68.43	68.4	64.76	64.8
0.1	10,140	10,100	9067	9400	69.08	77.0	64.76	72.5
0.2	11,170	11,200	9961	10,200	80.22	85.0	74.81	79.0
0.3	11,940	11,900	10,620	10,800	88.58	91.0	82.23	84.5
0.4	12,580	12,600	11,160	11,200	95.49	97.0	88.30	89.8
0.5	13,140	13,100	11,670	11,600	101.5	102	93.50	94.8
1.0	15,240	15,200	13,330	13,300	124.2	124	112.7	113
1.5	16,760	16,800	14,540	14,600	140.7	140	126.2	126
2.0	18,000	18,000	15,480	15,700	154.0	154	136.9	137
2.5	19,050	19,000	16,270	16,300	165.4	165	145.7	146

* = Read from Figs. 3a and 3c, Ref. V-3
g_0 = acceleration of gravity at initial circular orbit
V_j = exhaust velocity/circular velocity of initial orbit
V_H = hyperbolic velocity/circular velocity of initial orbit
τ = circular velocity x time/initial orbit radius, nondimensional time

In general the lower the initial thrust acceleration the closer the agreement for all hyperbolic velocities, with the exhaust velocity having a secondary effect. This is a fortunate set of circumstances since, in a practical sense, the thrust accelerations are not expected to be greater than $10^{-4} g_0$ and the operating exhaust velocities should be not less than 3 times the circular velocity. Consequently, is is expected that, regardless of the hyperbolic velocities to be achieved by the electric propulsion system, the approximate mass equations used herein are sufficiently accurate for mission analysis purposes.

It should be noted also that, regardless of the thrust acceleration and exhaust velocity, the higher the hyperbolic velocity the closer the agreement between the two methods. This result is as expected from the derivation of the approximate mass ratio equations.

An example of the limitation on hyperbolic velocity discussed previously is shown in the table for the initial acceleration of $10^{-2} g_0$. For the zero-hyperbolic velocity case the agreement is very close, becuase a mass ratio equation is available for this special case of escape. To obtain a mass equation for the nonzero-hyperbolic velocity case, two linear dimensionless equations must be combined, thereby giving rise to the restriction on hyperbolic velocity. It is expected that for hyperbolic velocities near zero the error would be large since this range of velocities falls near the nonlinear form of the original dimensionless parameteric equations. This fact is shown clearly in the table for $V_H^2 = 0.1, 0.2, 0.3$ and an initial thrust acceleration of $10^{-2} g_0$.

Circular Orbit to Escape Velocity

In this comparison, the analytical technique developed by Melbourne (Ref. V-4) was applied to the operation of departing from a 1.1 Earth radii parking orbit to escape velocity. Constant, tangentially applied thrust is again the basic thrusting program. The Melbourne mass ratio equation is employed complete with the empirically derived correction factor on thrusting time. To facilitate the computation, a curve fit was employed for the correction factor, rather than the graph (Fig. 25 p. 59, Ref. V-4).

Particular system parameters chosen were an exhaust velocity, C, of 30 km/sec and a powerplant specific mass of 20 kg/kw. The thruster efficiency was taken to vary with exhaust velocity according to $1/[1+(20/C)^2]$. The payload fraction

(simplified definition) and thrusting time were computed for powerplant mass fractions ranging from 0.1 to 1.0.

The following table displays the results and indicates the closeness of the two methods. The advantage of the approximate method is the absence of a correction factor for time, although a simple iteration is required on the mass ratio. Either method, however, can be easily employed; the Perkins/Edelbaum formulation is preferred because of the relationship to the hyperbolic velocity equations.

TIME TO REACH ESCAPE FROM 1.1 EARTH RADII PARKING ORBIT

Exhaust Velocity, C = 30 km/sec
Thrustor Efficiency = $1/[1+(20/C)^2]$
Powerplant Specific Mass = 20 kg/kw

Powerplant Mass Fraction	Perkins/Edelbaum		Melbourne	
	Payload Fraction	Time, Days	Payload Fraction	Time, Days
0.1	0.6900	316.0	0.6903	315.6
0.2	0.5923	156.0	0.5926	156.0
0.3	0.4938	103.4	0.4942	103.2
0.4	0.3950	77.13	0.3954	76.90
0.5	0.2959	61.42	0.2964	61.25
0.6	0.1967	50.98	0.1973	50.83
0.7	0.0974	43.54	0.0981	43.40
0.8	-0.0019	37.98	-0.0013	37.85
0.9	-0.1013	33.66	-0.1006	33.54
1.0	-0.2008	30.22	-0.2000	30.10

Influence of Propulsion Systems Parameters

To develop insight into the importance of exhaust velocity and powerplant mass fraction, the variation of the planetocentric payload-to-gross mass fraction was computed for departure from a circular Earth parking orbit to hyperbolic excess speeds of zero, 2.0, and 4.5 km/sec. The problems of thrusting through the sphere of influence and into heliocentric space are neglected; the analysis applies only to the planet. Actually, the objective of this computation is two-fold: the first is to understand the behavior of the planetocentric payload fraction for varying system and trajectory parameters, and the second is to relate the planetocentric departure and capture phases to the heliocentric

transfer wherein one propulsion system is utilized for the entire mission. The latter objective is important since the ultimate goal of the low-thrust spiral analyses is to combine the planetocentric and heliocentric flight profiles for maximizing the overall payload fraction.

The low-thrust vehicle is assumed to start in a 1.1 Earth radii parking orbit with a powerplant specific mass fixed at 20 kg/kw. An assumed variation of thruster efficiency with exhaust velocity was utilized, and the payload is simply defined as the difference between the burnout mass fraction and the powerplant mass fraction. The approximate (Perkins/Edelbaum) mass ratio equations were employed. The final results for payload fraction and thrusting time are displayed in Figs. V-1 to V-6 which include two figures for each of the three hyperbolic velocities.

Several observations may be made with the aid of these figures. It can be seen from Figs. V-1, V-3, and V-5 that, if the mission objective is to deliver a payload to a given hyperbolic velocity, there are optimal choices for C and μ_W depending on the desired (or required) thrusting time. Further, under a given set of dynamic and system conditions (excluding C and μ_W), there is an absolute minimum time for which optimal C and μ_W yield zero payload. This can be seen in Fig. V-1 wherein the minimum time is about 35 days for C = 20 km/sec and μ_W = 0.71. Also for times greater than the minimum, there are two sets of (nonoptimal) values for the pair (C, μ_W) which produce zero payload. For times less than the minimum the payload is negative regardless of the values for C and μ_W.

Therefore, one would expect that, given a thrusting time, the values for both C and μ_W must have co-related upper and lower bounds; i.e., the values at which payload is zero. This is true for C but not for μ_W. Taking the 50-day case in Fig. V-1, C must be between about 12 and 60 km/sec; for these limits μ_W must be 0.54 and 0.89, respectively. However, note that μ_W could be decreased (with a corresponding increase in C and μ_L) to almost 0.51, which is the minimum μ_W for that thrusting time. This effect can be noticed for longer thrusting times.

Besides providing higher payload fractions, the increased thrusting times cause the payload fractions to become less sensitive to changes in C and μ_W about their optimal values. This effect is most noticeable in Fig. V-1 and becomes less as the hyperbolic velocity increases, Fig. V-3. Thus if the desired thrusting time is 100 days for a departure to escape velocity, the exhaust velocity can range between 20 and 50 km/sec and the corresponding powerplant fraction between 0.27 and 0.43; this results in a payload fraction decrease of not more than 10%. If the vehicle is to achieve 2.0 km/sec hyperbolic speed within 100 days, the exhaust velocity can range between 20 and 40 km/sec and the corresponding powerplant fraction between 0.31 and 0.47 for a payload decrease not exceeding 10%.

A summary of the payload fraction data is shown in Fig. V-7, wherein the maximum payload fraction is plotted against hyperbolic velocity. In this plot, the minimum time for zero payload is clearly indicated at given hyperbolic velocities. The absolute minimum time for zero payload and zero hyperbolic velocity is about 34.5 days.

In the evaluation of candidate power systems, the problem arises as to what values of C and μ_W should be employed to maximize the corresponding payload mass (not fraction) for a fixed time. The characteristics usually associated with a certain class of powerplant are its power rating and specific mass or, equivalently, its mass. Given the mass of the powerplant, m_W, the corresponding payload, m_L is given by

$$m_L = m_W\left(\frac{\mu_L}{\mu_W}\right)$$

Hence the appropriate choices for C and μ_W should be those that maximize the ratio μ_L/μ_W; this is true in general, regardless of the definition for payload fraction. If the simplified definition for payload fraction were employed, then the ratio μ_1/μ_W should be maximized. A numerical example of this fixed-mass powerplant problem is given in the accompanying table.

MAXIMIZATION OF PAYLOAD FOR FIXED POWERPLANT MASS

Circular to Escape Velocity
Powerplant Specific Mass = 20 kg/kw
Parking Orbit = 1.1 Earth radii

C, km/sec	μ_L	μ_W	μ_L/μ_W
10	0.22	0.289	0.761
15	0.37	0.270	1.37
20	0.44	0.270	1.63
30	0.48	0.310	1.55
32*	0.49	0.320*	1.53
40	0.48	0.362	1.33
60	0.39	0.500	0.780
80	0.28	0.640	0.437

* Optimal for maximum payload fraction

In this case, for a powerplant having a specific mass of 20 kg/kw (the data were generated for this specific mass) and a given mass or power rating, the optimum value for C is about 20 km/sec and for μ_W about 0.27. For the simplified payload fraction definition the vehicle can deliver a payload whose mass is 1.63 times that of the powerplant. Note that the optimum values for C and μ_W are quite different from those for maximum payload fraction. Furthermore, for other hyperbolic speeds and at a given thrusting time, it can be seen that the optimum μ_W does not necessarily correspond to its minimum value. An important side effect is that the initial vehicle mass becomes high since payload is maximized with respect to the powerplant mass.

For the case of applying a given thruster capable of a fixed specific impulse, the problem is to either fix a μ_W and accept the resulting time or fix the time and accept the μ_W. Fixing either μ_W or T is somewhat arbitrary unless there are auxiliary system constraints which would perforce determine either parameter. An alternative approach would be to seek the value of μ_W which maximizes the ratio μ_L/T for the given exhaust velocity (specific impulse). An example of this technique is given in Fig. V-8, wherein a 30 km/sec exhaust velocity was assumed for the thruster operating under the conditions given in Fig. V-1. For this case, a μ_W of 0.4 maximizes μ_L/T resulting in a time of about 78 days (Fig. V-2). The corresponding payload fraction is 0.4.

It is no coincidence that the optimum value of μ_W equals the corresponding payload fraction. This fact can be shown by forming the ratio μ_L/T and differentiating with respect to μ_W. The resulting equation for optimum μ_W is

$$\mu_W(1-\mu_W)\frac{d\mu_1}{d\mu_W} + (1-\mu_1)(\mu_1 - 2\mu_W) = 0$$

This is a nonlinear equation in μ_W wherein μ_1 is a function of μ_W. A simplification can be employed by using the sample results of Fig. V-9. Note that the burnout mass fraction, μ_1, is essentially independent of μ_W for practical thrusting times. Consequently, as a first approximation, $d\mu_1/d\mu_W \approx 0$, and the above equation yields $\mu_{W_{opt}} = \mu_1/2$. Putting this result into the simplified payload fraction definition, $\mu_L = \mu_1 - \mu_W$, produces $\mu_L = \mu_W$ at maximum μ_L/T.

Consequently, to obtain a first guess of the optimal value for μ_W at any C, a line joining equal values of μ_L and μ_W could be overlaid on the plots of Figs. V-1, V-3, and V-5. The corresponding times then can be found from Figs. V-2, V-4, and V-6. Alternatively, a line connecting the optimal μ_W for a given C can be placed on the plots of Figs. V-2, V-4, and V-6.

The fact that $d\mu_1/d\mu_W$ is approximately zero produces another interesting aspect; namely the slope of the μ_L vs μ_W curves should be about -1 for any C (simplified payload definition). This feature is shown in Fig. V-10 for a Mars

spiral to escape velocity. A plot of the data on linear coordinates shows that the constant C lines have a slope of approximately -1. Furthermore, the curve of maximum payload fraction is seen to be almost linear (dotted line). In this example case, for times varying between 20 and 100 days, the optimum value of C ranges between 23 and 35 km/sec respectively.

The line of optimum μ_W for maximum μ_L/T is indicated by the solid line of slope +1. The corresponding times are given in Fig. V-11. Note that under the condition of maximum μ_L/T, there exists a unique minimum time; in Fig. V-11 it is about 27.5 days, occurring at a C of about 25 km/sec and a μ_W of about 0.45. This is the point at which the maximum μ_L/T line intersects the maximum μ_L line in Fig. V-10. Furthermore this point is the highest maximum value that μ_L/T can achieve if C is unrestricted.

Combined Planetocentric and Heliocentric Missions

The major restriction associated with the mass ratio equations employed previously is the fact that thrusting may continue well outside the planet's sphere of influence and into the heliocentric field. Accordingly, the performance computations will be in error. This problem is circumvented by employing the concept of "matched asymptotic expansions" which is discussed in detail in the low-thrust spiral portion of Section VI, Calculation of Interplanetary Trajectories in the Vicinity of the Planets. No sphere of influence definition is necessary, and the position offset with respect to the planet is ignored.

From the latest results of trajectory studies described in Section VI, the corresponding mass ratio equations for the low-thrust planetocentric trajectory are as follows:

Departure:
$$\frac{m_c}{m_m} = \exp\left\{\frac{V_c}{C}\left[1 - 1.84\left(\frac{F/m_c}{\mu/R_c^2}\right)^{1/4}\left(\frac{m_c}{m_m}\right)^{1/4}\right]\right\}$$

Capture:
$$\frac{m_m}{m_c} = \exp\left\{\frac{V_c}{C}\left[1-1.84\left(\frac{F/m_m}{\mu/R_c^2}\right)^{1/4}\right]\right\}$$

where m_m is considered to be the mass of the vehicle at the initiation or termination of the planetocentric phase; i.e., at the matching point. The initial thrust accelerations for departure and capture are F/m_c and F/m_m, respectively. This formulation is used to agree with the computational model discussed below. The above equations imply that the boundary conditions for the heliocentric trajectory are the planet's heliocentric position and velocity; this latter condition corresponds to zero velocity relative to the planet.

In the mass ratio equation for thrusting between a circular orbit and a hyperbolic velocity, V_H, the constant previously employed was 1.746 based on the original work by Perkins and Edelbaum. Later refined analysis indicated that the constant should be 1.757. Both constants are based on tangential thrusting. If optimal steering is utilized the appropriate constant is 1.84, which is used herein.

For thrusting solely in the planet's field, the V_H term appears as indicated by the appropriate equation in the Summary of Mass Ratio Equations. In the above mass ratio equation to be used for combining the planetocentric and heliocentric trajectories, the hyperbolic speed V_H does not appear. This is because in the asymptotic matching technique employed here, the hyperbolic velocity is assigned to the heliocentric trajectory close to the massless planet (see Section VI).

With the foregoing equations and assumptions the problem of analyzing the combined planetocentric and heliocentric mission becomes straightforward. It is assumed herein that one propulsion system performs the entire mission from departure parking orbit to capture parking orbit. The payload is delivered onto a circular parking orbit about the destination planet in a fixed total time (parking orbit to parking orbit). The total mission duration consists of the departure time, the heliocentric transfer time (assumed constant for a given optimization) and the capture time. The problem is thus to choose C and μ_W and the corresponding distribution of planetocentric thrusting time which maximizes the overall payload-to-gross mass fraction for a given total mission duration. A schematic presentation of this mission profile is given in Sketch A.

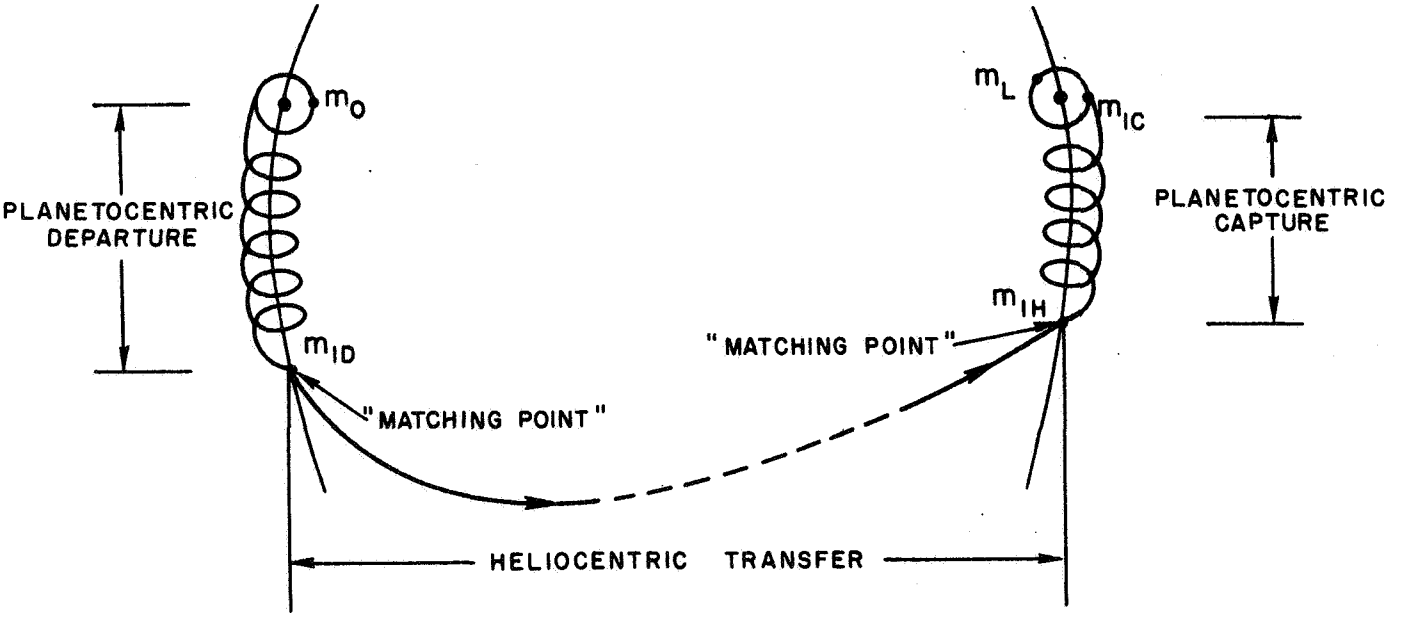

Sketch A

Single Electric Propulsion Systems, Parking Orbit to Parking Orbit Mission

An initial mass m_0 is accelerated to the matching point at which time the mass is m_{1D}; this becomes the initial mass for the heliocentric transfer which terminates with mass m_{1H}. The start of the capture phase occurs at the matching point with mass m_{1H} and finally ends on the parking orbit with mass m_{1C}. The payload is m_L. Note that the fixed value of C and powerplant mass m_w is employed throughout three different gavity fields. For the normalized mass fraction equations to be used it should be pointed out that the powerplant fraction at the beginning of each thrusting phase is different and determined by the initial value of μ_W assigned at the departure point. The corresponding computation for burnout mass fraction in each thrusting phase must take this into account.

The relationships between the three thrusting phases and the three powerplant fractions are depicted in Sketch B. Given a μ_{WD} (which actually is the powerplant fraction μ_W to be used in the payload fraction) and a C, the departure thrusting time, T_D, and terminal (or departure) mass fraction, μ_{1D}, may be computed. Thus the powerplant fraction, μ_{WH}, for the heliocentric portion may be found in addition to the terminal heliocenteic mass fraction μ_{WH}. The planetocentric capture powerplant fraction, μ_{WC}, is now obtained and used to compute the final mass fraction at capture, μ_{1C}, and the capture thrusting time, T_C. The corresponding payload fraction is $\mu_L = \mu_{1D}\ \mu_{1H}\ \mu_{1C} - \mu_{WD}$ (simplified definition) and the resulting total trip time is $T = T_D + T_H + T_C$. (T is not the total thrusting time since coast periods may occur in the heliocentric transfer).

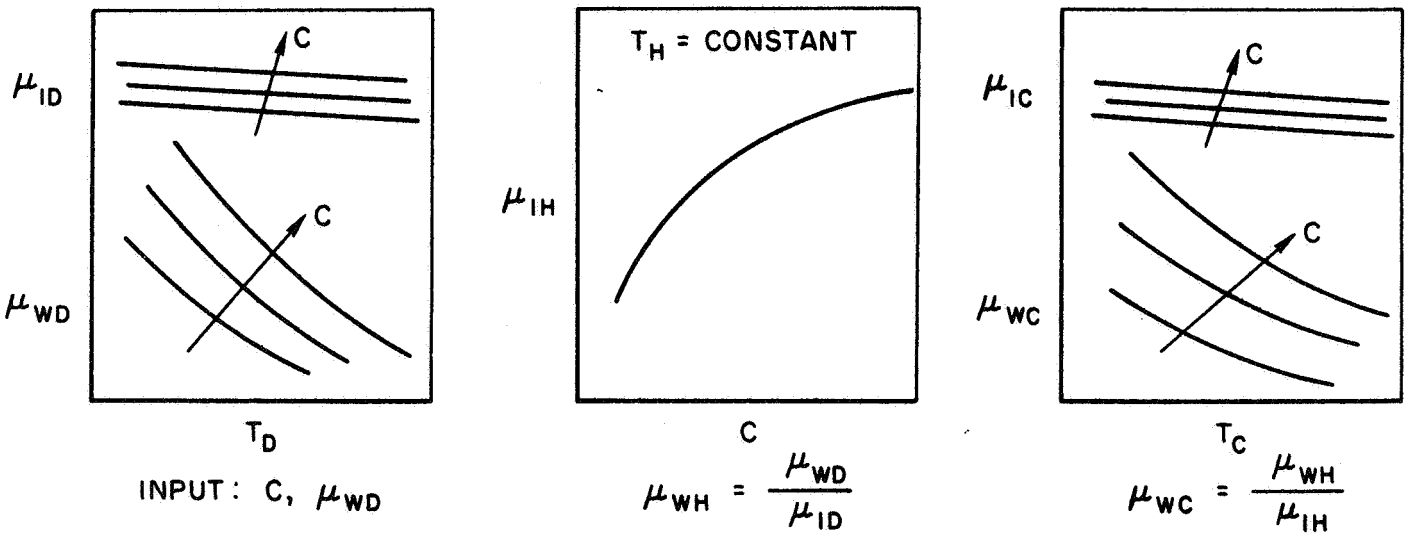

Sketch B

Relationship Between Departure, Heliocentric, and Capture Phases

The middle plot of Sketch B is obtained from the heliocentric trajectory optimization program with optimum coasts, zero hyperbolic speeds on the boundaries, and no optimization of C and μ_{WH} (since these are specified as part of the overall problem). The fixed heliocentric trip time, T_H, is the difference between the Julian dates of departure and arrival. The two planetocentric plots are represented by the two mass ratio equations given above along with the time equation.

A possible procedure, formulated by a brief study of the affected equations as depicted by Sketch B, would make use of the fact that the terminal mass fractions (μ_{1D}, μ_{1H}, and μ_{1C}) are affected only slightly by changes in the related powerplant mass fraction. Furthermore, the planetocentric terminal fraction changes slowly with variations in either the powerplant fraction or time, for a given exhaust velocity. For a given total trip time, T, the approach is thus to pick a C, guess T_D and compute μ_{WD}. Then μ_{WH}, μ_{1H}, and μ_{WC} are easily computed. The burnout mass fraction at the end of capture, μ_{1C}, is computed and used to find T_C. In general, T_C added to T_H and T_D will not give the required time, T. An iteration is suggested which involves solving for a new T_D using the recently computed T_C; i.e., $T_D = (T - T_H) - T_C$. This value of T_D is then compared with the original input value and, if the comparison does not satisfy a given tolerance, the current value of T_D becomes the new input for the planetocentric departure calculation and the iteration continues.

At convergence for T_D (provided a solution exists for the given C and fixed T) enough information is now available to compute μ_L. However, this is only for a selected value of C which, in general, will not yield maximum payload fraction. Therefore, a search on C is required wherein, for each trial C, the foregoing iteration for T_D must be completed. The above suggested procedure did not reach the computer programming phase.

For the case of an unmanned probe to be delivered to some terminal heliocentric position and velocity, no capture phase is required, and the problem degenerates to a flight profile consisting of a planetocentric (Earth) departure and a heliocentric transfer to the final boundary. Examples of such a mode would be an inclined 1-AU heliocentric orbit, a solar probe or planetary flyby, and a solar synchronous orbit. The corresponding schematic for the two-phase mission is depicted in Sketch C.

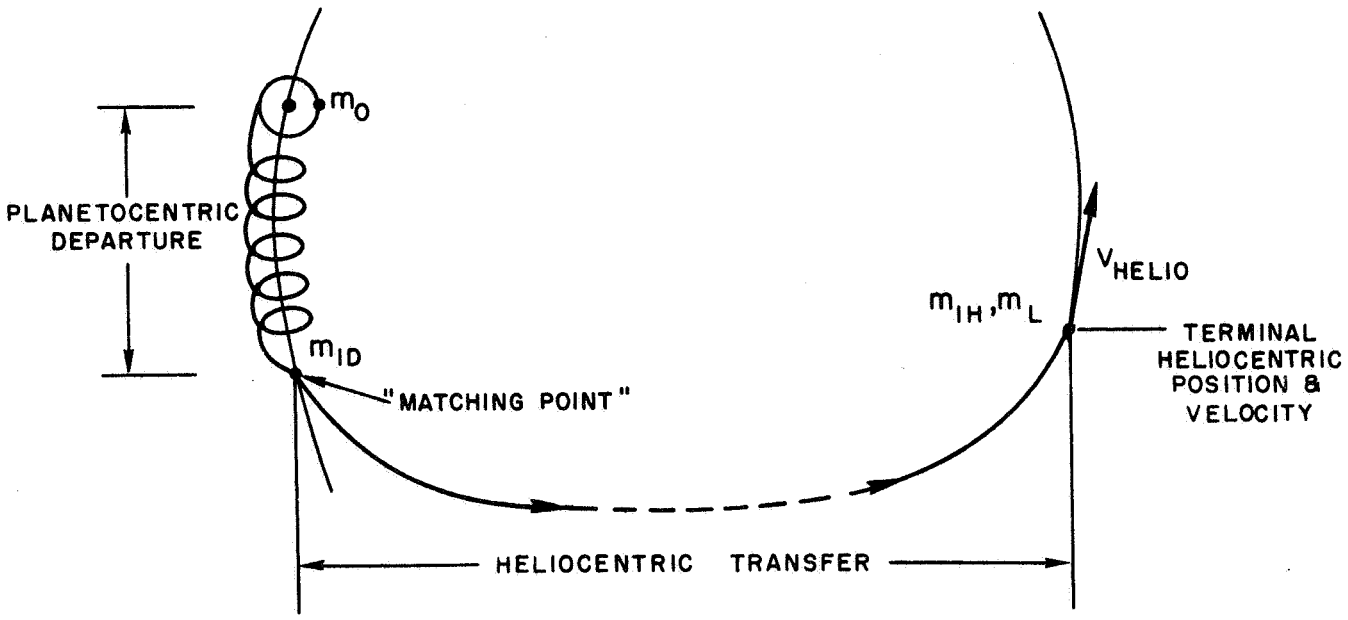

Sketch C

Profile for Parking Orbit to Heliocentric Position and Velocity Mission

Section V References

V-1. Perkins, F. M.: Flight Mechanics of Low-Thrust Spacecraft. Journal of Aerospace Sciences, Vol. 26, No. 5, May 1959, p. 291-297.

V-2. Edelbaum, T. N.: A Comparison of Nonchemical Propulsion Systems for Round-Trip Mars Missions. United Aircraft Research Laboratories Report E-1383-2, October 1960.

V-3. Moeckel, W. E.: Trajectories with Constant Tangential Thrust in Central Gravitational Fields. NASA Technical Report R-53, Lewis Research Center, Cleveland, Ohio, 1959.

V-4. Melbourne, W. G.: Interplanetary Trajectories and Payload Capabilities of Advanced Propulsion Vehicles. JPL Technical Report No. 32-68, March 31, 1961.

FIG. V-1

LOW-THRUST EARTH DEPARTURE TO ESCAPE VELOCITY

EFFECT OF POWERPLANT MASS FRACTION AND EXHAUST VELOCITY ON PAYLOAD RATIO

HYPERBOLIC VELOCITY = 0.0 KM/SEC

POWERPLANT SPECIFIC MASS = 20 KG/KW

THRUSTOR EFFICIENCY = $1/[1+(20/C)^2]$

PARKING ORBIT = 1.1 EARTH RADII

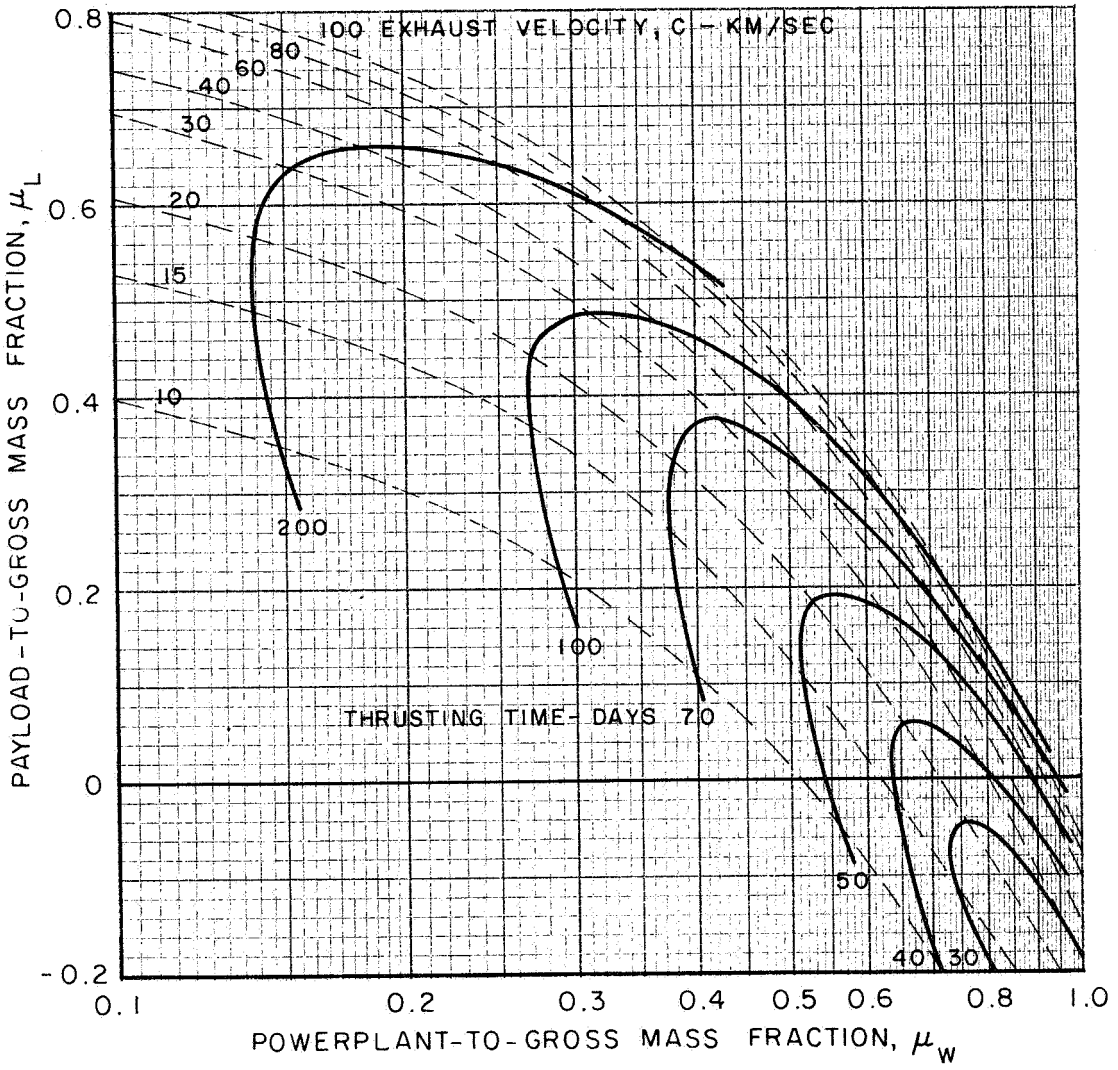

LOW-THRUST EARTH DEPARTURE TO ESCAPE VELOCITY

REQUIRED THRUSTING TIME

HYPERBOLIC VELOCITY = 0.0 KM/SEC

PARKING ORBIT = 1.1 EARTH RADII

POWERPLANT SPECIFIC MASS = 20 KG/KW

THRUSTOR EFFICIENCY = $1/[1+(20/C)^2]$

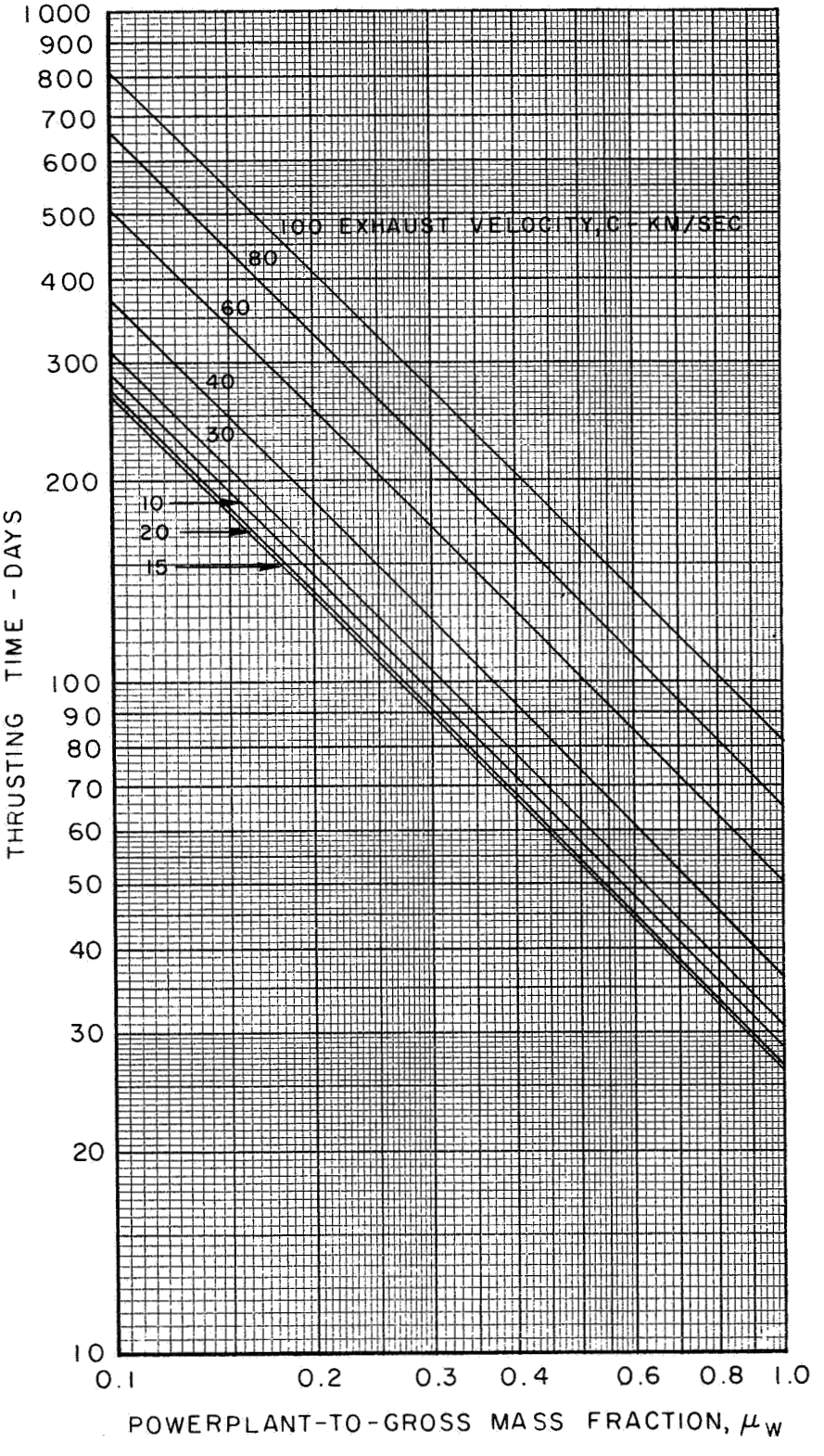

LOW-THRUST EARTH DEPARTURE TO HYPERBOLIC VELOCITY

EFFECT OF POWERPLANT MASS FRACTION AND EXHAUST VELOCITY ON PAYLOAD RATIO

HYPERBOLIC VELOCITY = 2.0 KM/SEC

POWERPLANT SPECIFIC MASS = 20 KG/KW

THRUSTOR EFFICIENCY = $1/[1+(20/C)^2]$

PARKING ORBIT = 1.1 EARTH RADII

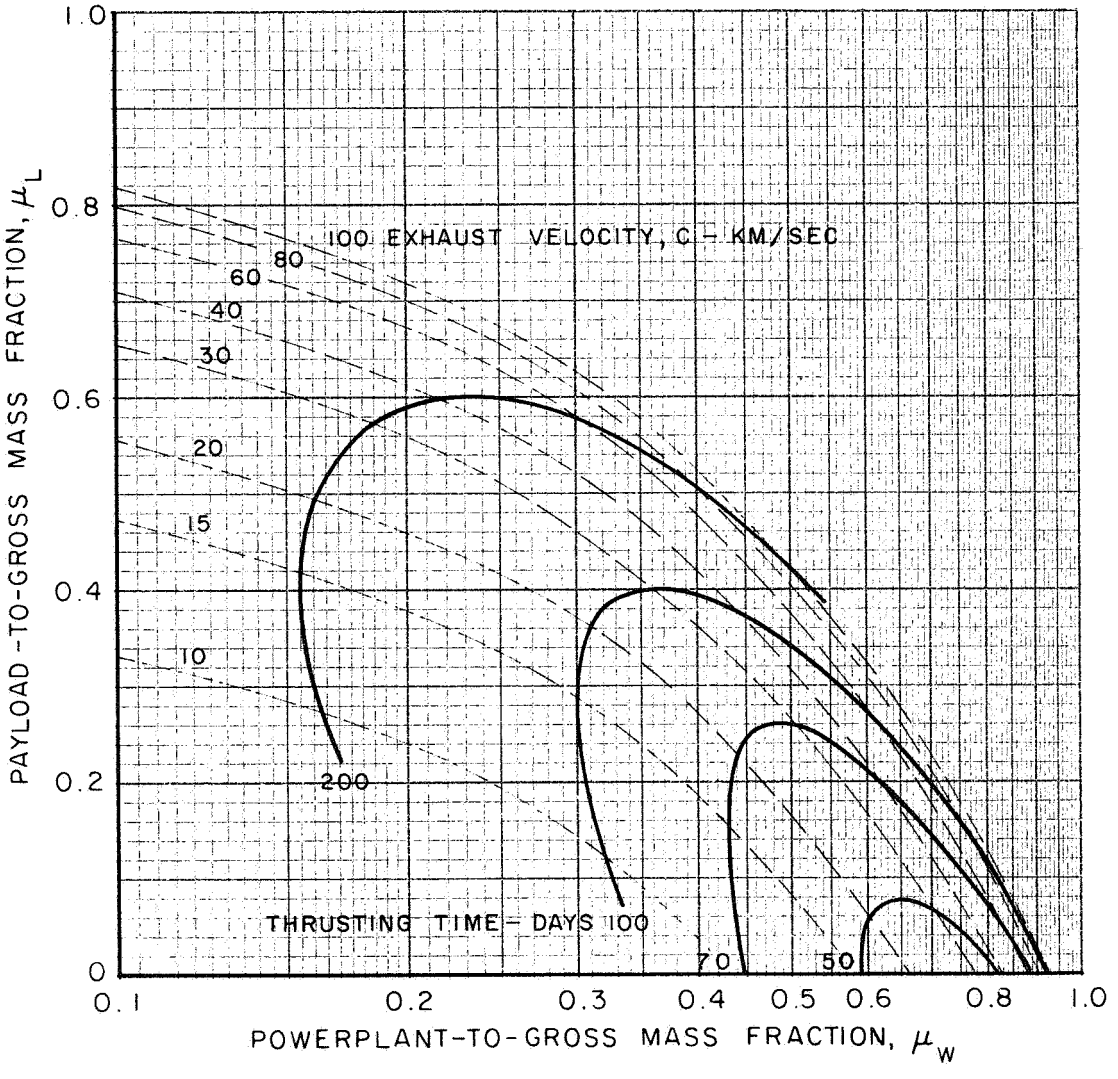

LOW-THRUST EARTH DEPARTURE TO HYPERBOLIC VELOCITY

REQUIRED THRUSTING TIME

HYPERBOLIC VELOCITY = 2.0 KM/SEC

PARKING ORBIT = 1.1 EARTH RADII

POWERPLANT SPECIFIC MASS = 20 KG/KW

THRUSTOR EFFICIENCY = $1/[1+(20/C)^2]$

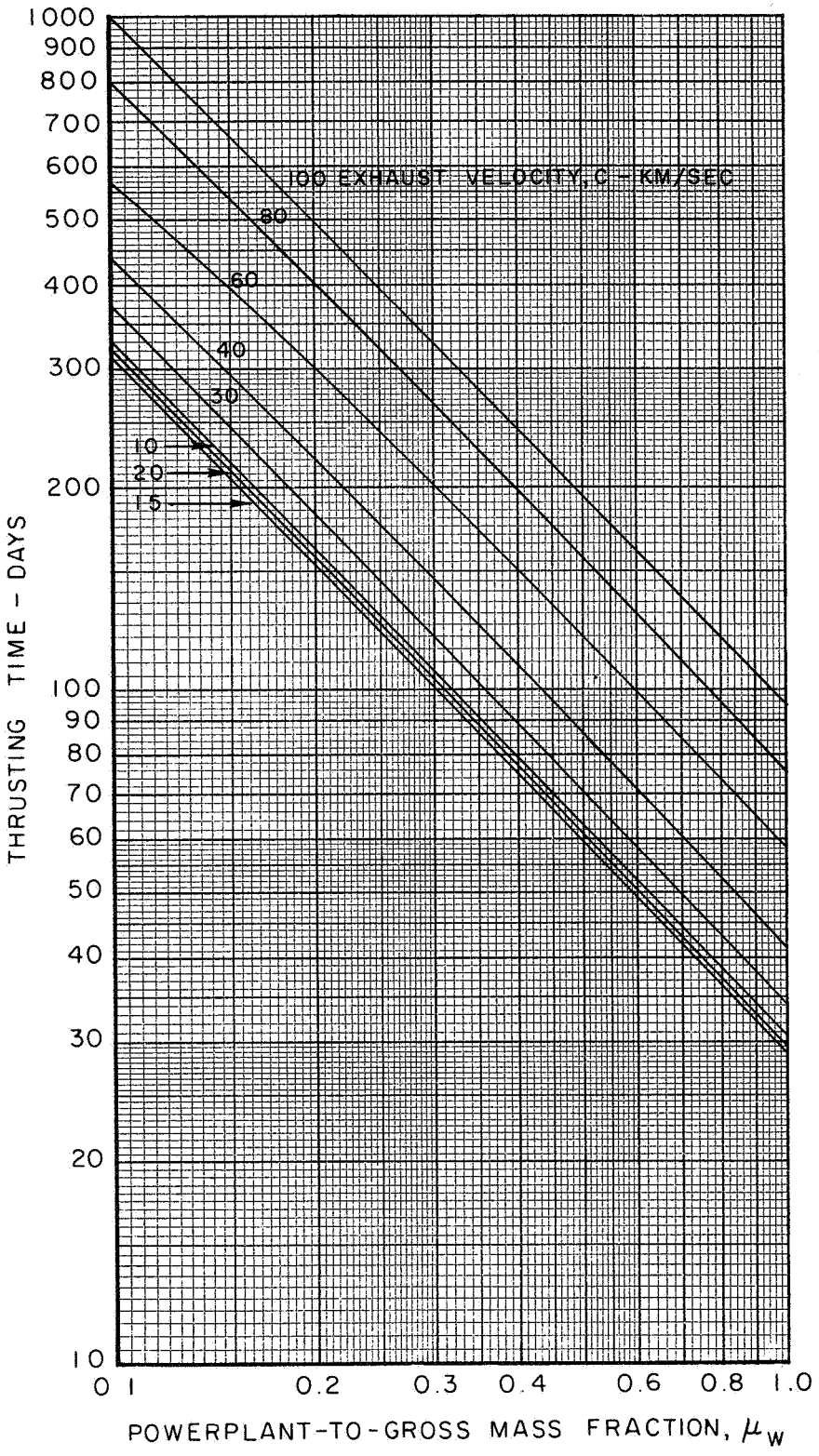

LOW-THRUST EARTH DEPARTURE TO HYPERBOLIC VELOCITY

EFFECT OF POWERPLANT MASS FRACTION AND EXHAUST VELOCITY ON PAYLOAD RATIO

HYPERBOLIC VELOCITY = 4.5 KM/SEC

POWERPLANT SPECIFIC MASS = 20 KG/KW

THRUSTOR EFFICIENCY = $1/[1+(20/C)^2]$

PARKING ORBIT = 1.1 EARTH RADII

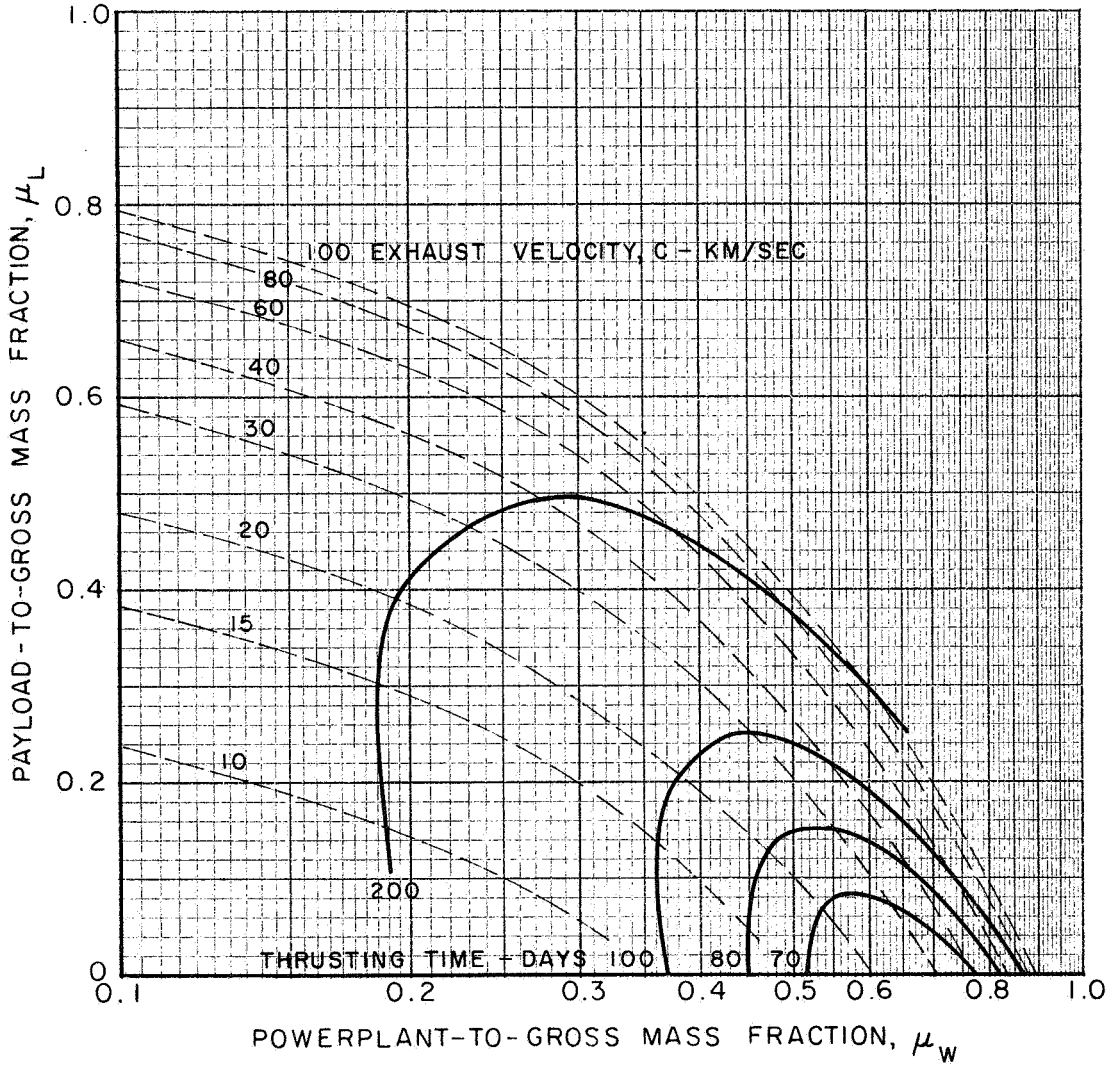

LOW-THRUST EARTH DEPARTURE TO HYPERBOLIC VELOCITY

REQUIRED THRUSTING TIME

HYPERBOLIC VELOCITY = 4.5 KM/SEC

PARKING ORBIT = 1.1 EARTH RADII

POWERPLANT SPECIFIC MASS = 20 KG/KW

THRUSTOR EFFICIENCY = $1/[1+(20/C)^2]$

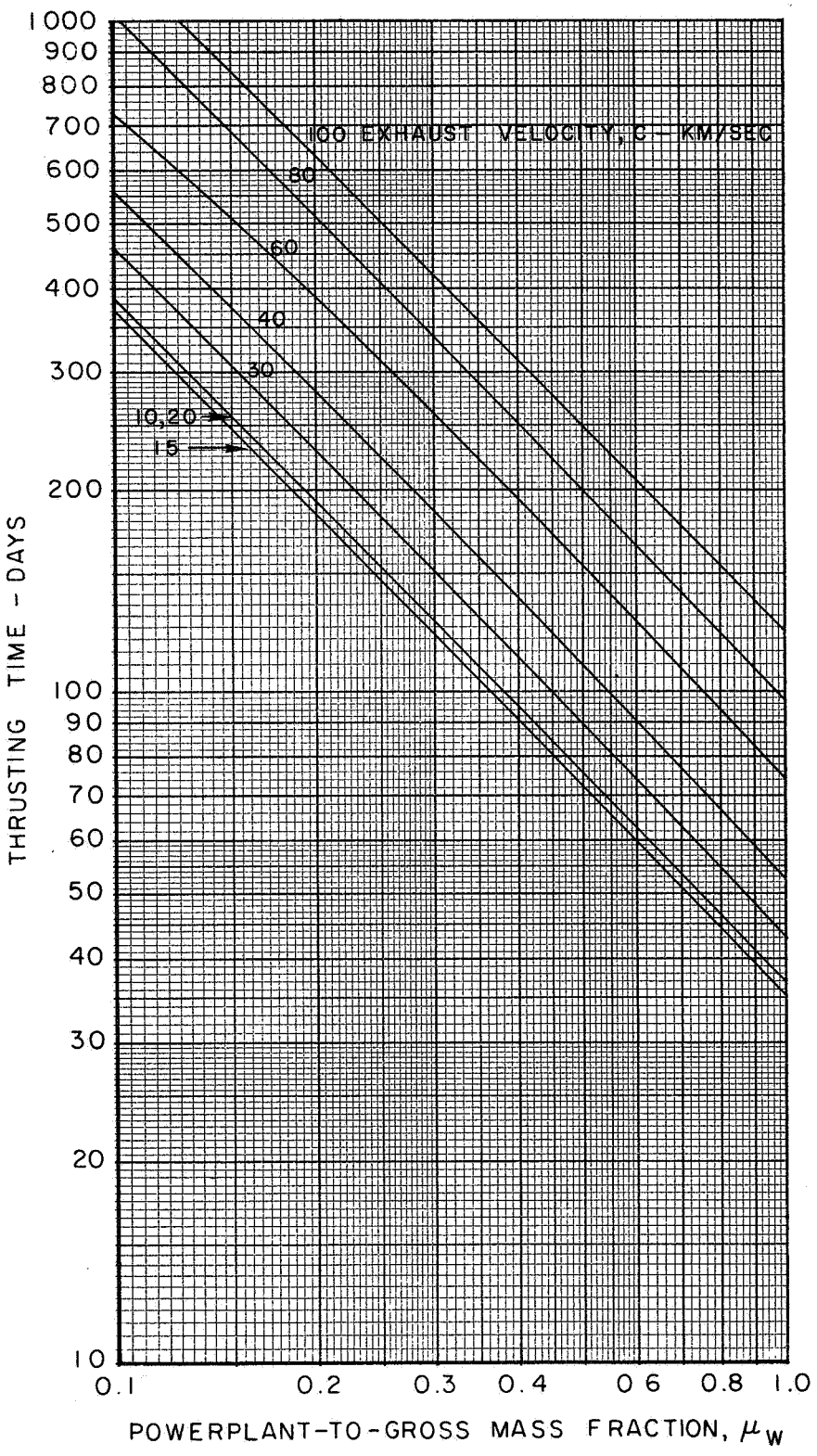

LOW-THRUST DEPARTURE TO HYPERBOLIC VELOCITY

INFLUENCE OF THRUSTING TIME AND VELOCITY

PERKINS/ EDELBAUM EQUATIONS

POWERPLANT SPECIFIC MASS = 20 KG/KW

THRUSTOR EFFICIENCY = $1/[1+(20/C)^2]$

PARKING ORBIT = 1.1 EARTH RADII

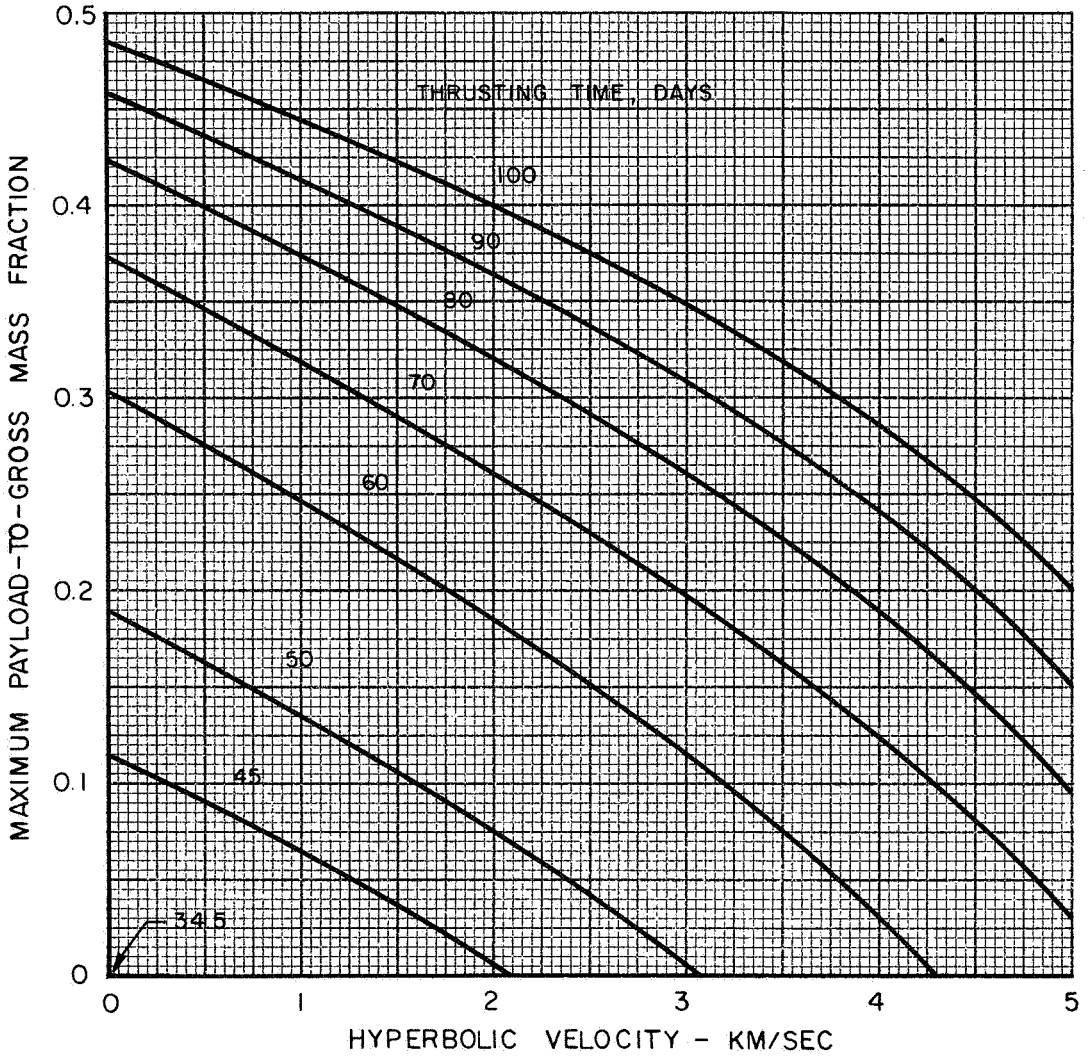

MAXIMIZATION OF μ_L / T FOR GIVEN C

EXHAUST VELOCITY = 30 KM/SEC
HYPERBOLIC VELOCITY = 0.0 KM/SEC
POWERPLANT SPECIFIC MASS = 20 KG/KW
THRUSTOR EFFICIENCY = $1/[1+(20/C)^2]$
PARKING ORBIT = 1.1 EARTH RADII

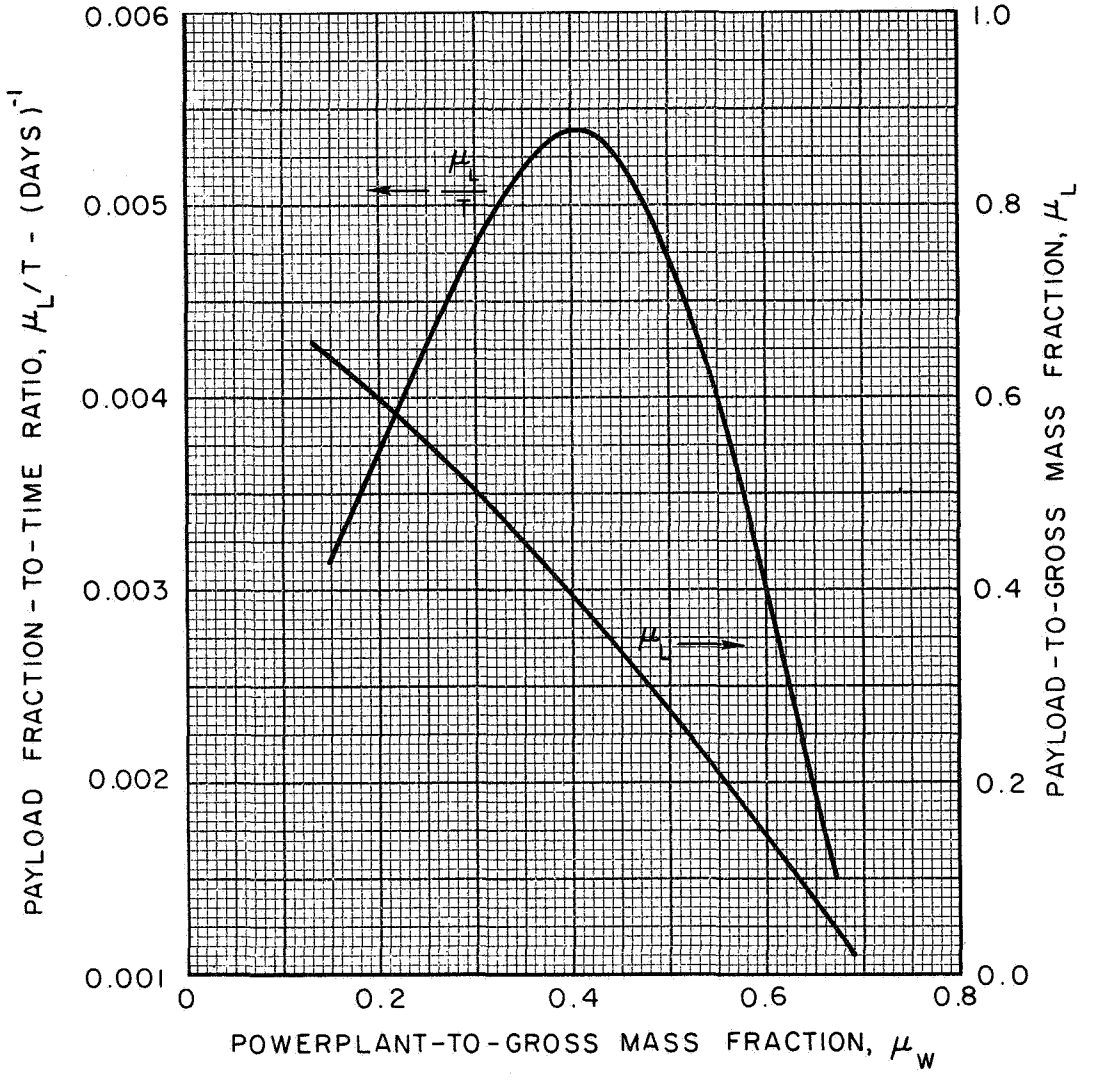

LOW-THRUST EARTH DEPARTURE TO HYPERBOLIC VELOCITY

INFLUENCE OF THRUSTING TIME ON SYSTEM MASS FRACTION

HYPERBOLIC VELOCITY = 2.0 KM/SEC
POWERPLANT SPECIFIC MASS = 20 KG/KW
THRUSTOR EFFICIENCY = $1/[1+(20/C)^2]$
PARKING ORBIT = 1.1 EARTH RADII

EXHAUST VELOCITY
——— 30 KM/SEC
— — — 60 KM/SEC

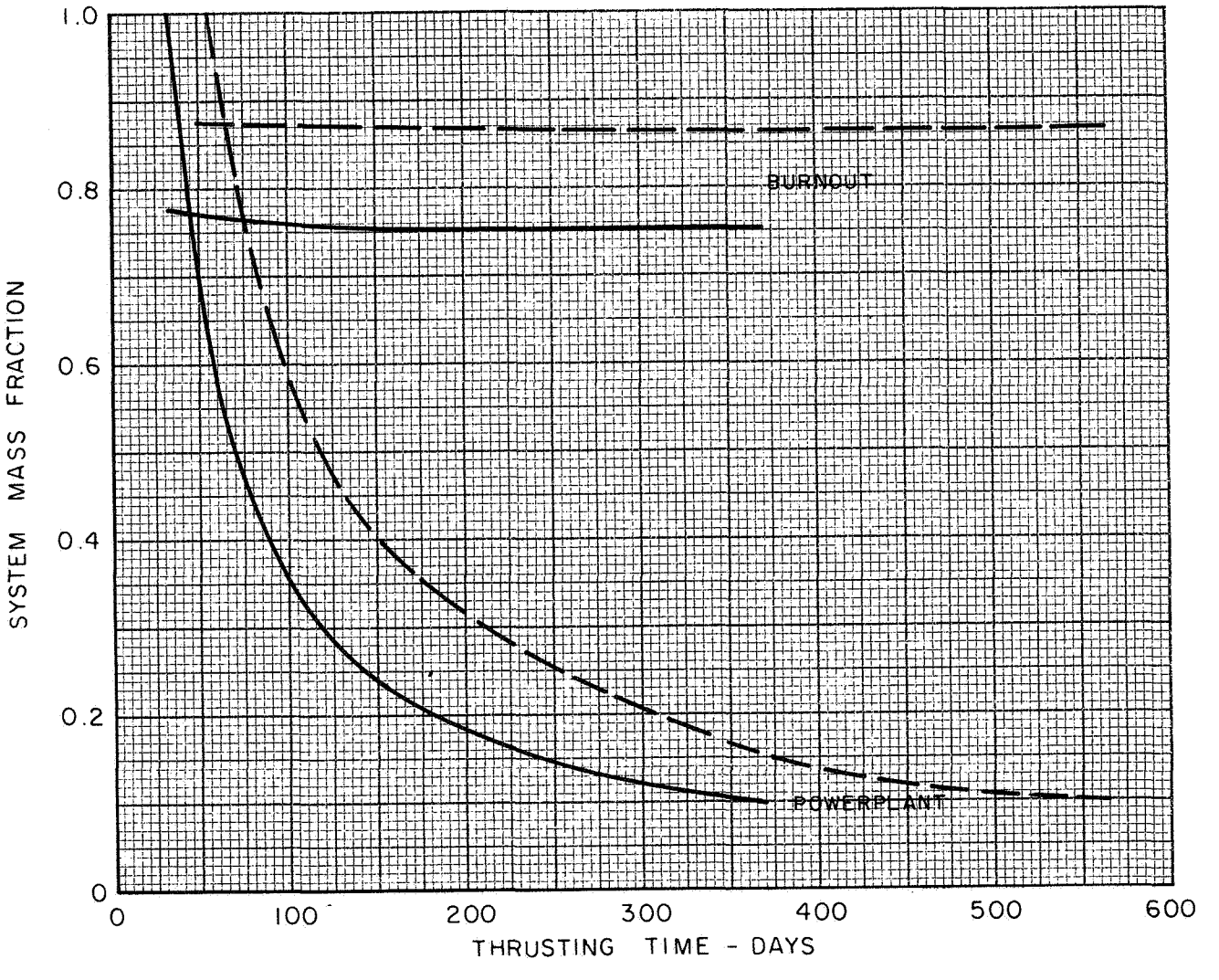

LOW-THRUST MARS DEPARTURE TO ESCAPE VELOCITY

EFFECT OF POWERPLANT MASS FRACTION AND EXHAUST VELOCITY ON PAYLOAD RATIO

HYPERBOLIC VELOCITY = 0.0 KM/SEC

POWERPLANT SPECIFIC MASS = 20 KG/KW

THRUSTOR EFFICIENCY = $1/[1+(20/C)^2]$

PARKING ORBIT = 1.28 MARTIAN RADII

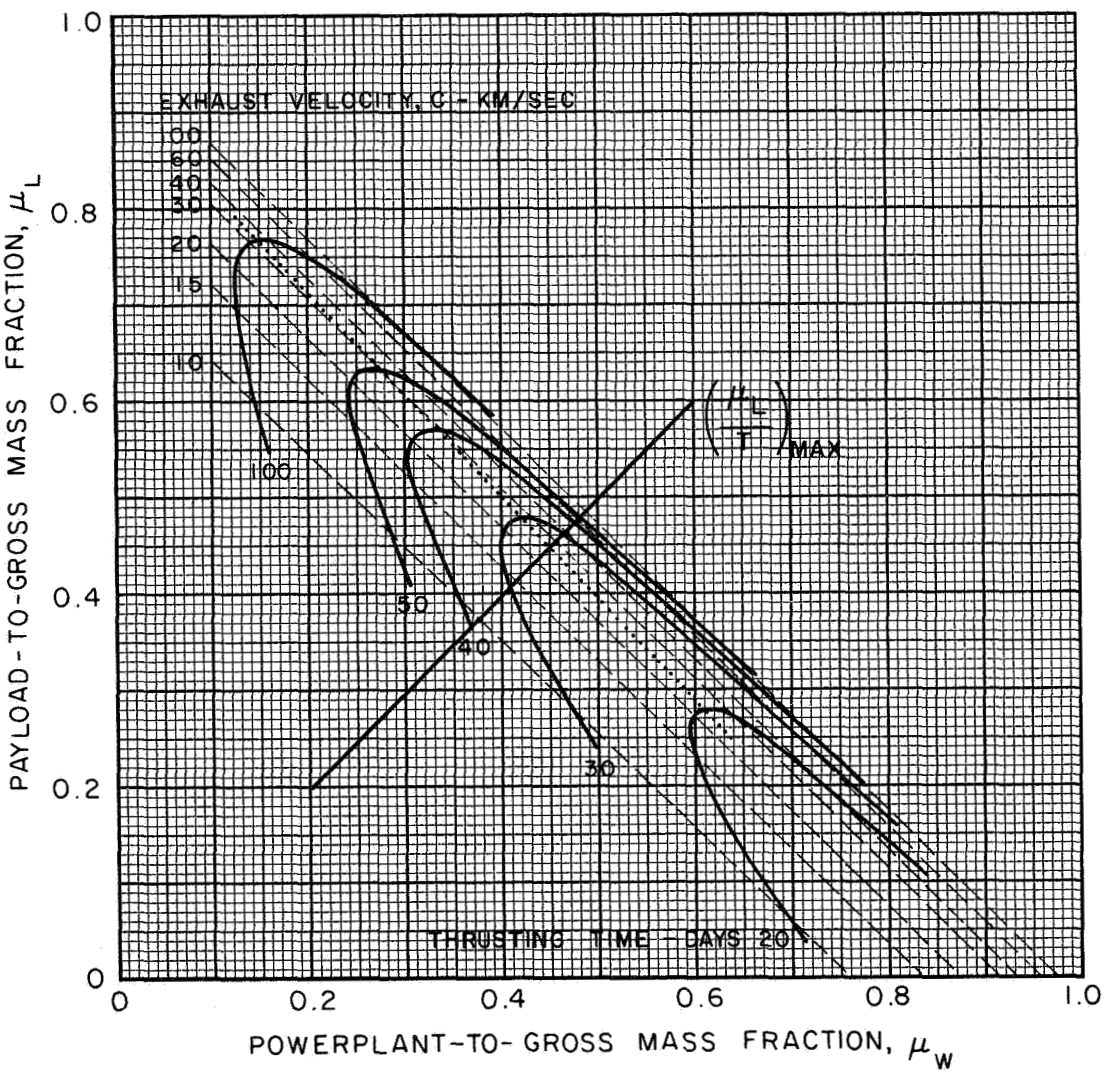

FIG. V-11

LOW-THRUST MARS DEPARTURE TO ESCAPE VELOCITY

REQUIRED THRUSTING TIME

HYPERBOLIC VELOCITY = 0.0 KM/SEC

PARKING ORBIT = 1.28 MARTIAN RADII

POWERPLANT SPECIFIC MASS = 20 KG/KW

THRUSTOR EFFICIENCY = $1/[1+(20/C)^2]$

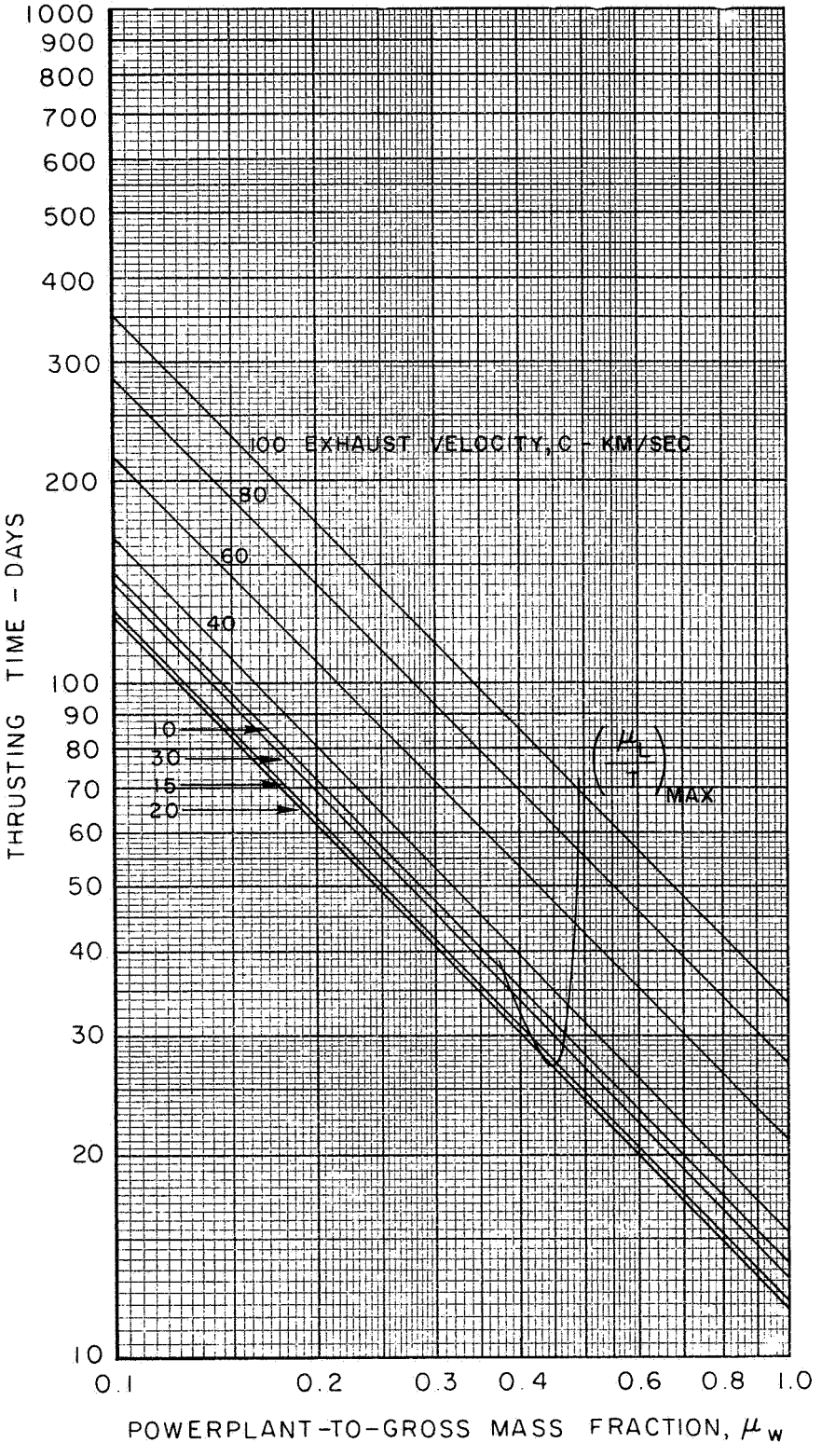

SECTION VI

CALCULATION OF INTERPLANETARY TRAJECTORIES IN THE VICINITY OF THE PLANETS

Introduction

The calculation of interplanetary trajectories, either powered or unpowered, involves the solution of an N-body problem. This N-body problem can be well approximated as a slightly perturbed two-body problem as long as the space vehicle is far from any of the planets. However, when the space vehicle passes close to a planet, the third-body effects become important, and some way of approximating this three-body problem is necessary for routine performance calculations. Two different methods have been developed for the approximate solution of this problem. The first of these is the patched conic approximation, while the second is the method of matched asymptotic expansions. The similarity of the words matching and patching has produced considerable confusion between the two methods, and the methods are often not as well understood as they should be. The distinctions are actually quite simple.

In the patched conic approximation, a two-body trajectory is calculated in the vicinity of the planet until the sphere of influence is reached. At the sphere of influence, the position and velocity are used as initial conditions for a heliocentric two-body trajectory. The patching consists of keeping the position the same on both sides of the sphere of influence and of vectorially adding the planet's velocity to the velocity relative to the planet to determine the heliocentric velocity on the outside of the sphere of influence. The patched conic method usually neglects all third-body perturbations on both legs of the trajectory, but the patching of the two conics does simulate many of the important phenomena in the three-body problem. There is no rigorous theory of the error in the patched conic approximation, but numerical calculations have shown that it is generally adequate for performance purposes.

The use of the patched conic method for interplanetary trajectories requires the solution of a multipoint boundary value problem because the positions and times at which the spheres of influence of both planets are pierced are not known. Because the solution of this multipoint boundary value problem is time consuming even with conic trajectories, the patched conic approximation has not been used very widely for interplanetary trajectories. The patched conic approximation may be used without change for powered low-thrust trajectories, except that here the trajectories on either side of the sphere of influence will be powered two-body trajectories and not unpowered conics.

The method of approximating the three-body problem that has been more widely used for calculating interplanetary trajectories is the method of matched asymptotic expansions. This is a systematic perturbation procedure which can be carried out to various orders of approximation. The basic idea is that the trajectory close to the planet is expanded in powers of a small parameter, such as the mass ratio of the planet to the sun (μ). Another expansion is made of the heliocentric trajectory in the vicinity of the planet, carried out to the same order of approximation in powers of the same parameter. These two asymptotic expansions are then matched in a suitable region near the planet, such that both solutions will give the same answer in this intermediate or "boundary layer" region. In this way, a composite solution is obtained for the whole problem, close to the planet, in the boundary layer region, and far from the planet.

Systematic theories of interplanetary trajectories based on this idea have been developed for the unpowered case by Breakwell and Perko (Ref. VI-1) and for the power-limited spiral low-thrust case by Breakwell and Rauch (Ref. VI-2). The zero-order term in the Breakwell-Perko theory is an analysis that has been widely used for performance calculations, for example in the Interplanetary Trajectory Handbook (Ref. VI-3). The zero-order term consists of calculating a heliocentric elliptic or hyperbolic trajectory which goes from the center of a massless planet to the center of another massless planet. This is the outer solution. The inner solution consists of a hyperbola around each of the planets. The outer limit of this inner solution is the hyperbolic excess velocity at infinity. This hyperbolic excess velocity at infinity is then matched to the center of the massless planet. The Breakwell-Perko theory shows that the error in this approximation is of order μ. This error is acceptable for most performance calculations and is retained in the analysis to follow. The Breakwell-Perko theory does carry out the next approximation to order μ with error of order μ^2, but this process requires numerical evaluation of several integrals for each trajectory.

The Breakwell-Rauch theory for low-thrust trajectories is carried out through terms of order $\mu^{\frac{1}{4}}$ and $\mu^{\frac{1}{2}}$ with errors on the order of μ so that it is comparable to the widely used analysis for high-thrust trajectories. The term of order $\mu^{\frac{1}{4}}$ is quite important for all the planets and should be included in performance calculations. The term of order $\mu^{\frac{1}{2}}$ is quite small for the inner planets and has been neglected in the past. It may be important for trajectories that spiral around the larger planets. The great advantage of using matched asymptotic expansions for trajectory calculations is that the solution of the multipoint boundary value problem is partially carried out in the process of matching, so all that is necessary to produce a trajectory is a solution of a two-point boundary-value problem. Also there is no need to define a "sphere of influence" for each planet.

Powered Phases of High-Thrust Trajectories

The powered flight time for typical high-thrust propulsion systems is so short compared with a year that high-thrust operations in heliocentric space can usually be well approximated by impulses. However, these thrusting times are often not too much shorter than the period of a satellite orbit so that it is necessary to provide corrections for the characteristic velocity losses of finite-thrust trajectories in the vicinity of planets. A very simple and accurate theory for this problem has recently been developed by Howard Robbins (Ref. VI-4). Robbins' theory is a general one which can be used for multistage operations and for multiple thrusting periods. The ΔV for a single, finite-thrust maneuver is given by Robbins in the general relationship of Eq. (VI-1).

$$\Delta V = \Delta V_I + \frac{1}{2}\left[\frac{\mu_P}{r^3}\left(1 - 3\sin^2\theta\right) - \dot{\bar{\lambda}}\cdot\dot{\bar{\lambda}}\right]\frac{\Delta V_I k t^2}{12} + \ldots \qquad \text{(VI-1)}$$

In this equation, ΔV_I is the required impulsive velocity, μ_P is the gravitational constant of the planet, C (Eq. (VI-2)) is the exhaust velocity, r is the radius at the initiation of the impulsive thrust, θ is the angle with the horizontal, $\bar{\lambda}$ is the primer vector of Lawden (the adjoint to the velocity vector), t is the thrusting time of the stage (of initial mass, M_0) given by Eq. (VI-2), and k is the correction factor for the second moment of a constant-thrust burn which is given very accurately by the series in Eq. (VI-3).

$$t = \left(1 - e^{-\Delta V/C}\right)\frac{m_0 C}{T} \qquad \text{(VI-2)}$$

$$k \equiv \frac{6C}{\Delta V}\left[-\frac{2C}{\Delta V} + \coth\frac{\Delta V}{2C}\right] = 1 - \frac{1}{60}\left(\frac{\Delta V}{C}\right)^2 + \frac{1}{1920}\left(\frac{\Delta V}{C}\right)^4 + \ldots \qquad \text{(VI-3)}$$

For injection onto the perigee of an escape hyperbola from the pericenter of a co-planar ellipse, the following two equations are satisfied:

$$\theta = 0 \qquad \text{(VI-4)}$$

$$\dot{\bar{\lambda}}\cdot\dot{\bar{\lambda}} = \frac{\mu_P^2}{r_0^4\left(V_\infty^2 + \frac{2\mu_P}{r_0}\right)} \qquad \text{(VI-5)}$$

and the resulting expression for the ΔV is given by Eq. (VI-6).

$$\Delta V = \left[\left(V_\infty^2 + \frac{2\mu_P}{r_0}\right)^{1/2} - V_0\right]\left[1 + \frac{kt^2}{24}\cdot\frac{\mu_P}{r_0^3}\cdot\frac{V_\infty^2 + \frac{\mu_P}{r_0}}{V_\infty^2 + \frac{2\mu_P}{r_0}} + \cdots\right] \qquad \text{(VI-6)}$$

Where r_0 and V_0 are the pericenter radius and velocity, respectively, at the initiation of thrust, and V_∞ is the required hyperbolic excess speed.

This equation is based on an optimum steering program. The time may be calculated from the ΔV for the impulsive case, thereby eliminating the need for iteration, because the time is used only in the small correction term and errors in it have a higher-order effect. Precisely this same equation may be used for injection from a hyperbolic approach trajectory into an elliptic orbit at perigee.

It should be noted the Eq. (VI-1) is perfectly general and may be used for any single-burn maneuver which is optimal in the time-open and angle-open case. Equation (VI-6) is the generalization to the constant-thrust case of the constant-acceleration analysis developed by Long in Ref. VI-5.

Low-Thrust Spiral Trajectories

A systematic theory of low-thrust trajectories which start from a circular orbit around the planet and go into heliocentric space has been developed by Breakwell and Rauch in Ref. VI-2. The basic idea of their analysis is illustrated in Fig. VI-1. At a time t_1, the vehicle is assumed to start from rest at the offset point and to be thrusting in the direction of the asymptote to the spiral trajectory. The heliocentric trajectory is then calculated from the offset point at time t_1 with the gravity field of the planet assumed nonexistent. For an approach spiral, the effect of the planet would be to place the vehicle on the spiral at the point shown at time t_1 rather than to reach the offset point at the same time. Thus t_1 is the point at which the computation of vehicle performance for the planetocentric portion of the flight ceases for departure or starts for capture. This point is sought by the trajectory analysis so as to make the calculation of performance agree with the actual trajectory profile. The analysis in Ref. VI-2 is for variable-thrust power-limited trajectories but has been extended to the constant-acceleration case in unpublished work by Rauch. For the constant-acceleration case with optimal steering, the incremental velocity required to reach time t_1 is given by Eq. (VI-7).

$$\Delta V_1 = V_c - 1.84\left(\frac{T}{m_1}\mu_P\right)^{1/4} \qquad \text{(VI-7)}$$

where V_c is the circular velocity of the parking orbit, T the thrust, and m_1 the vehicle mass at point t_1.

The constant in this equation is different from the one given earlier in Ref. VI-6 and 7 because the earlier result was for tangential steering. The difference in these two constants (1.84 and 1.757) is the difference between tangential thrusting and optimum steering. The position offset from the center of the planet contributes a change in propellant consumption to the whole trajectory of order $\mu^{\frac{1}{2}}$ which is on the order of the square of the velocity correction term in ΔV_1. This term can be neglected in performance calculations for trajectories around the inner planets.

Equation (VI-7) may be used without change for constant-thrust trajectories as well as constant-acceleration trajectories if the mass in the equation is taken to be the mass at time t_1. The reason for this interchangeability is that in the early part of the spiral, ΔV_1 is completely independent of the specific impulse of the engine and the (small) magnitude of the thrust acceleration. This is also true on the latter part of the trajectory when it approaches a straight line. The only time that the thrust acceleration affects the ΔV is the relatively short time around time t_1. The validity of this approximation is borne out by the numerical results in Ref. VI-8.

Low-Thrust Hyperbolic Trajectories

An approximate analysis for constant-acceleration trajectories with hyperbolic energy under the influence of low thrust has been developed independently in Ref. VI-7 and Ref. VI-9. Both of these references approximate the actual trajectory by a straight-line trajectory which starts at the center of the planet, Fig. VI-2. With this approximation, the equations can be integrated exactly and the theory developed through the $\mu^{\frac{1}{4}}$ and the $\mu^{\frac{1}{2}}$ terms. (μ is the ratio of the mass of the planet to that of the sun.) As in the Breakwell-Rauch theory, the error of this approximation will be of order μ. The effect of the planet is replaced by a velocity offset and a position offset at the initial (or terminal) time. The required velocity δV, and position, δR, offsets are given by Eqs. (VI-8) and (VI-9).

For $V_\infty \leq 2\left(\frac{T}{m}\mu_P\right)^{1/4}$:

$$\delta V = \left[2\sqrt{2}\,E(k) - \sqrt{2}\,K(k)\right]\left(\frac{T}{m}\mu_P\right)^{1/4} \qquad \text{(VI-8a)}$$

Where $$k^2 = \frac{1}{2} - \frac{V_\infty^2}{8}\sqrt{\frac{m}{T\mu_P}}$$

and $$\delta R = \frac{(\delta V)^2 - V_\infty^2}{2\frac{T}{m}} \qquad \text{(VI-9a)}$$

For $V_\infty \geq 2\left(\frac{T}{m}\mu_P\right)^{1/4}$:

$$\delta V = \left[\left(\sqrt{\frac{V_\infty^4}{4}\frac{m}{T\mu_P}} + \sqrt{\frac{V_\infty^4}{4}\frac{m}{T\mu_P} - 4}\right)^{1/2} E(k)\right]\left(\frac{T}{m}\mu_P\right)^{1/4} \qquad \text{(VI-8b)}$$

Where $$k^2 = \frac{2\sqrt{\frac{V_\infty^4}{4}\frac{m}{T\mu_P} - 4}}{\sqrt{\frac{V_\infty^4}{4}\frac{m}{T\mu_P}} - \sqrt{\frac{V_\infty^4}{4}\frac{m}{T\mu_P} - 4}}$$

and $$\delta R = \frac{(\delta V)^2 - V_\infty^2}{2\frac{T}{m}} \qquad \text{(VI-9b)}$$

In these equations, K and E are the complete elliptic integrals of the first and second kind. The velocity offset, δV, is in the direction of the initial heliocentric thrust direction and is always larger than the initial hyperbolic excess velocity, V_∞. The difference between these two quantities is shown in Fig. VI-3. The velocity offset, δV, is thus the total velocity of the vehicle due to the initial hyperbolic excess speed, V_∞, plus that due to the low-thrust system acting within the planet's activity sphere, $(T\mu_P/m)^{\frac{1}{4}} D$. The effect of the planet on the vehicle is obtained through the velocity correction factor, D, evaluated from Eqs. (VI-8a) and (-8b). Note that either Eq. (VI-8a) or (-8b) is used depending on whether the value of $V_\infty(T\mu_P/m)^{-\frac{1}{4}}$, the abscissa of Fig. VI-3, is respectively less than, or greater than 2.0. For a value exactly equal to 2.0, both equations yield identical results.

The units depend on the units taken for μ_P. If the unit of distance is the AU and the unit of time, T, is the time required for Earth to traverse one radian in its

orbit, then μ_p will be AU^3/T^3 and the resulting velocities are in AU/T or EMOS (Earth's mean orbital speed). In these units, μ_p is equal to μ, the mass ratio of the planet to the Sun. The position offset is a positive offset in the same direction. It is quite small and can be neglected for the inner planets.

These equations may once again be used without change for the case of constant thrust provided the mass is taken to be the initial (or terminal) mass of the vehicle at the start (or end) of low-thrust operation.

Analysis of Finite Periapsis Radius

The foregoing analysis was based on an approximation that the initial periapsis radius was zero; that is, the trajectory was assumed to start at the center of the planet. The following analysis corrects for this and shows the effect of starting at a finite periapsis radius. The vehicle is assumed to be injected by the high-thrust rocket onto the periapsis of a hyperbolic orbit. At this point, low-thrust propulsion is started. The analysis to follow shows that the effect of the finite periapsis radius is of order μ, the ratio of the mass of the planet to that of the sun. This is a higher-order effect and may be neglected for purposes of performance analysis, along with the other higher-order terms (also of order μ) which were neglected in the analysis given above.

The effect of the initial periapsis radius is analyzed by considering the difference in a linear analysis of having an initial eccentricity of unity or an initial eccentricity corresponding to the actual trajectory which starts at the parking orbit radius. The acceleration due to thrust is assumed to be constant in magnitude and to be directed tangentially. Under this perturbation, the linear theory predicts that the increase in energy of the orbit will be proportional to the arc length of the hyperbola. Equations for the radius, time, and arc length of a hyperbolic orbit are given by the first three equations to follow. In these equations, the semimajor axis, a, is taken to be positive and H is the hyperbolic eccentric anomaly. F and E are the incomplete elliptic integrals of the first and second kind, respectively. The unit of distance is the AU and the unit of time is the time required for Earth to traverse one radian in its orbit. Thus the gravitational parameter of the sun is unity and the gravitational parameter of the planet, μ_p, is given in terms of this unit solar gravitational parameter. Consequently, in the expressions following, μ_p represents the mass ratio of the planet to the sun.

$$r = a(e \cosh H - 1) \tag{VI-10}$$

$$t = \frac{\mu}{V_\infty^3}(e \sinh H - H) \tag{VI-11}$$

$$s = a e \left[\frac{e^2 - 1}{e^2} F(\phi, k) + e \sin\phi \cosh H \right] \qquad \text{(VI-12)}$$

$$e = 1 + \frac{r_P V_\infty^2}{\mu_P} \qquad k = \frac{1}{e} \qquad \sin\phi = \frac{e \sinh H}{\sqrt{e^2 + e^2 \sinh^2 H - 1}}$$

What is of interest is the change in time and the change in arc length (due to the change in periapsis radius) as the vehicle gets far from the origin. Accordingly, the limits of Eqs. (VI-11) and (VI-12) as given by Eqs. (VI-13) and (VI-14) are used.

for $H >> 1$

$$t \approx \frac{\mu_P}{V_\infty^3} \left[\frac{r+a}{a} - \ln\left(2 \frac{r+a}{a}\right) + \ln e \right] \qquad \text{(VI-13)}$$

$$s \approx r + a \left[1 + \frac{e^2 - 1}{e} K\left(\frac{1}{e}\right) - eE\left(\frac{1}{e}\right) \right] \qquad \text{(VI-14)}$$

The effect of the finite planetary radius will be assumed to be reflected in a change in the initial hyperbolic excess velocity of the trajectory. In order to calculate this, consider the difference in hyperbolic excess velocity between a trajectory with unit eccentricity and the actual trajectory. Equation (VI-15) considers the changes due to both the time required to get to a given radius and the difference in arc length traveled in getting to that same radius.

$$\delta V_\infty = \frac{T}{m} \frac{1}{V_\infty} \left(s - s_{e=1}\right) - \frac{T}{m} \left(t - t_{e=1}\right) \qquad \text{(VI-15)}$$

If the values obtained from Eqs. (VI-13) and (VI-14) are substituted into Eq. (VI-15), the result is Eq. (VI-16) which gives an approximate indication of the perturbation in initial hyperbolic excess velocity due to a finite periapsis radius. It should be noted that this perturbation is of order μ and will generally be small enough to be neglected for performance calculations.

$$\delta V_\infty = \frac{\mu_P}{V_\infty^3} \frac{T}{m} \left[1 - \ln e + \frac{e^2 - 1}{e} K\left(\frac{1}{e}\right) - eE\left(\frac{1}{e}\right) \right] \qquad \text{(VI-16)}$$

Section VI References

VI-1. Breakwell, J. V. and L. M. Perko: "Matched Asymptotic Expansions, Patched Conics, and the Computation of Interplanetary Trajectories," in Methods in Astrodynamics and Celestial Mechanics, Vol. 17 of the AIAA Series, "Progress in Astronautics and Aeronautics," ed. by Duncombe and Szebehely, Academic Press, N.Y., 1966.

VI-2. Breakwell, J. V. and H. E. Rauch: "Asymptotic Matching in Power-Limited Interplanetary Transfers." AAS preprint 66-114, 1966.

VI-3. Ross, S. E., et al: "Space Flight Handbooks, Vol. 3 - Planetary Flight Handbook," NASA SP-35, 1963.

VI-4. Robbins, H. M.: "An Analytical Study of the Impulsive Approximation." AIAA Journal, Vol. 4, No. 8, p. 1417-1423, 1966.

VI-5. Long, R. L.: "Escape from a Circular Orbit with Finite Velocity at Infinity." Astronautica Acta, Vol. V, Fasc. 3-4, p. 159-162, 1959.

VI-6. Fimple, W. R. and T. N. Edelbaum: "Applications of SNAP-50 Class Powerplants to Selected Unmanned Electric Propulsion Missions." AIAA Paper No. 64-494. NASA Contract NASw-737, 1964.

VI-7. Melbourne, W. G. and C. G. Sauer: "Performance Computations with Pieced Solutions of Planetocentric and Heliocentric Trajectories of Low-Thrust Missions." JPL Space Programs Summary No. 37-36, Vol. IV, December 1965.

VI-8. Edelbaum, T. N.: "A Comparison of Nonchemical Propulsion Systems for Round Trip Mars Missions." UA Research Laboratories Report R-1383-2, October 1960.

VI-9. Ragsac, R. V., et al: "Study of Low-Acceleration Space Transportation Systems." UA Research Laboratories Report D-910262-3, July 1965, NASA Contract NAS 8-11309.

EFFECT OF PLANETARY GRAVITATIONAL FIELD ON LOW-THRUST TRAJECTORY

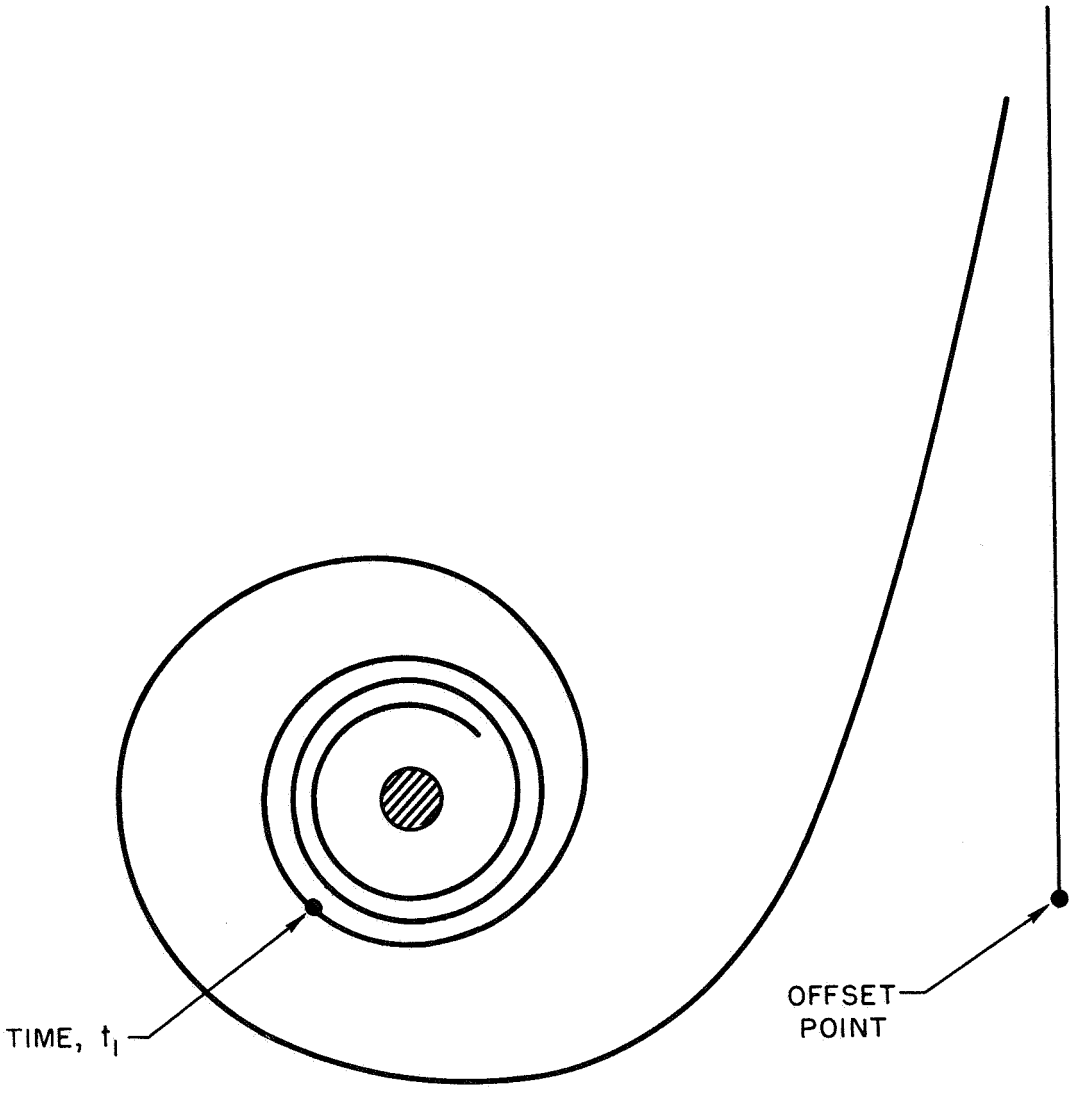

FIG. VI - 2

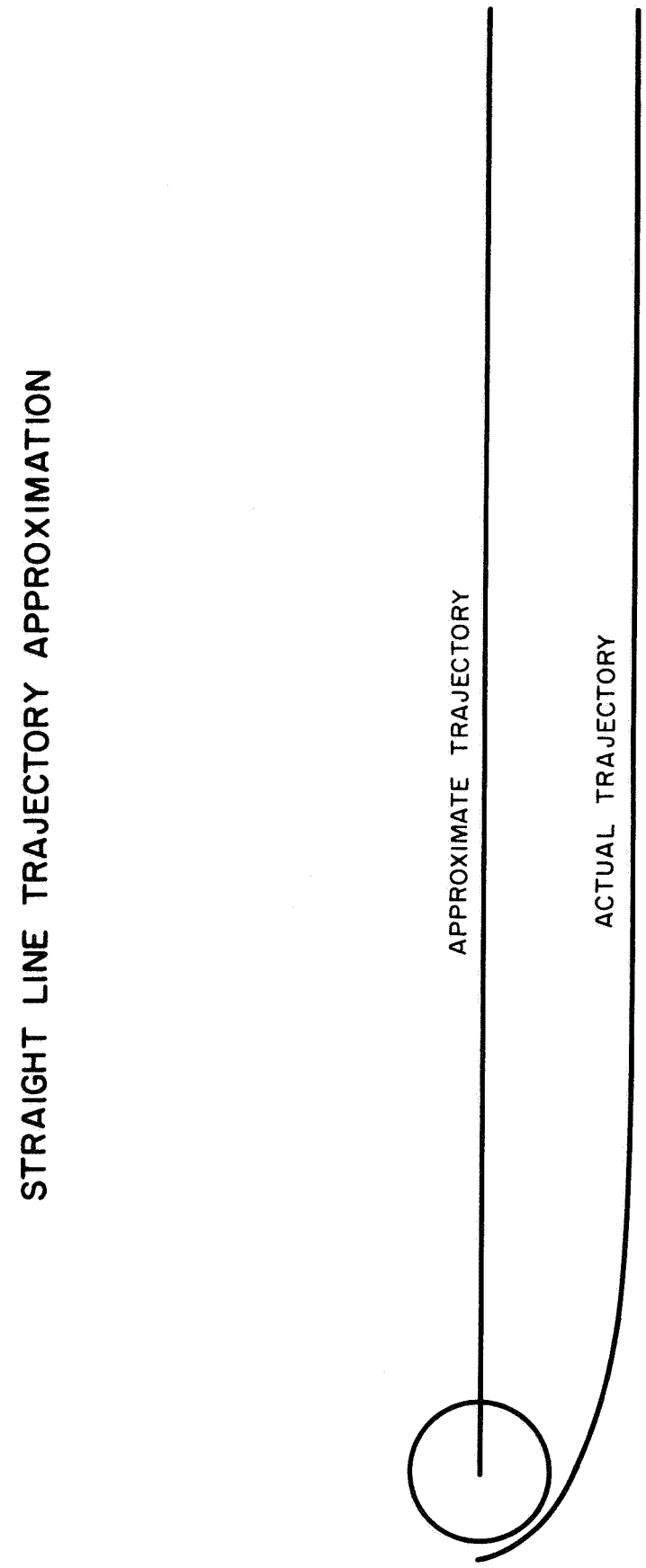
STRAIGHT LINE TRAJECTORY APPROXIMATION
APPROXIMATE TRAJECTORY
ACTUAL TRAJECTORY

VELOCITY CORRECTION TO HYPERBOLIC LOW-THRUST TRAJECTORIES DUE TO PLANETARY ATTRACTION

$$\delta V \equiv \left(\frac{T}{m}\mu_P\right)^{1/4} D + V_\infty$$

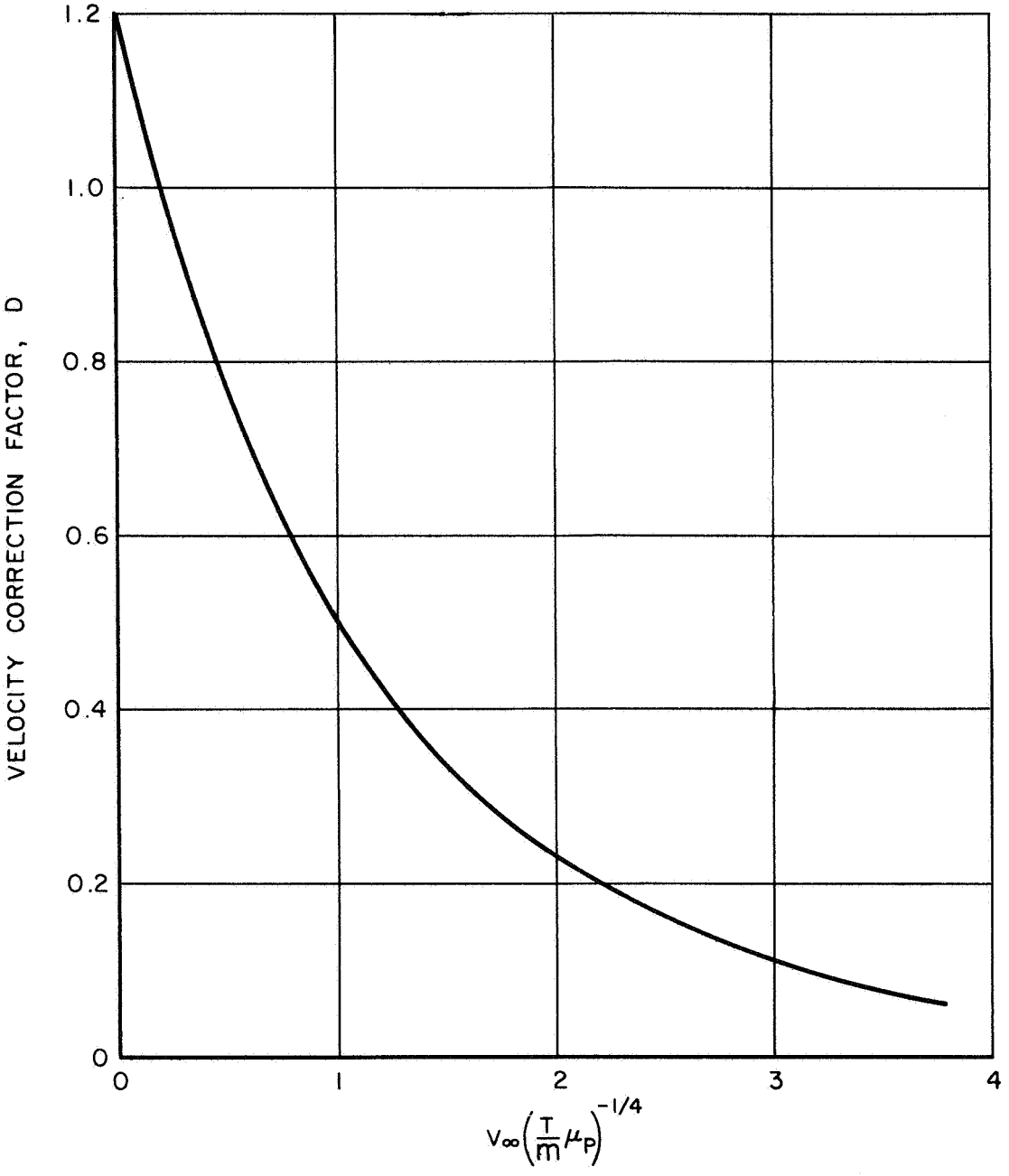

SECTION VII

MASS OPTIMIZATION PROGRAMS

The analysis of low-acceleration propulsion systems usually centers on the proper selection of exhaust jet velocity (or the specific impulse) and powerplant mass fraction which together maximize payload fraction for a given flight profile. The purpose of this discussion is to describe some techniques which were developed to expedite the analysis of low-acceleration systems operating under constant thrust with optimum coast. The main features of the procedures are the utilization of computer-developed trajectory data to estimate system parameters for a more refined payload fraction definition and the refinements made in the current constant-thrust, single-coast, payload optimization computer program.

Newly developed, but not thoroughly checked, is the hybrid-thrust mass optimization program. Because of the limitations on time which were precipitated by numerical difficulties early in the project, the hybrid-thrust program could not be applied to as many sample and trial cases as was originally desired. A discussion of the program is presented below.

In general, the analytical work was based primarily on the work by Melbourne and Sauer in JPL Space Programs Summary No. 37-17.

Analysis of Payload Fraction Optimization

The simplest definition for payload fraction recognizes that the final mass fraction, μ_1, (the ratio of final mass to initial mass) consists of the payload fraction, μ_L, and powerplant mass fraction, μ_W. If necessary, inert masses of tanks, tie-in structure, etc., may be assumed as part of the powerplant. Thus,

$$\mu_L = \mu_1 - \mu_W$$

The final mass fraction depends on the trajectory being executed, i.e., J, the efficiency, η, of the thrustor in converting input power to jet power, the powerplant specific mass, α_w, and powerplant mass fraction, μ_w. The rocket equation for power-limited systems is

$$\mu_1 = \frac{1}{1 + \frac{\gamma^2}{\eta \mu_w}} \quad , \quad \gamma^2 \equiv \frac{\alpha_w J}{2}$$

In the analysis of a given mission, J is usually known and α_w is given. The efficiency depends, generally, on the exhaust velocity and the type of thrustor employed. For convenience, a hypothetical thrustor efficiency curve of the following form is assumed for all the analyses in this report.

$$\eta = \frac{1}{1 + \left(\frac{d}{c}\right)^2}$$

where $10 < d < 40$ km/sec depending on the desired form of the curve, Fig. VII-1.

An electric propulsion system operating at high specific impulse retains most of its initial mass; thus, variations in the powerplant mass do not drastically change the final mass or thrust-acceleration profile. Under these conditions it is assumed that the minimum value of $J = \int a^2 \, dt$ and the average thrust acceleration over a minimum-J trajectory do not change with μ_w. The use of the geometric mean for the average thrust acceleration is particularly suited to the purposes here and is employed throughout.

$$\bar{a} = (a_0 a_1)^{1/2} = \left(\frac{J}{T_p}\right)^{1/2} , \quad a = \frac{2 \eta \mu_w}{\alpha_w C \mu}$$

where a_0 and a_1 are, respectively, the thrust accelerations at the beginning and end of the mission and T_p is the powered time.

With the foregoing equations the payload fraction may be maximized. Hence, the optimum powerplant fraction is given by

$$\mu_{w\,OPT} = \frac{\mu_1 (1 - \mu_1)}{1 - \frac{1 + \mu_1}{2} \left(\frac{\eta' C}{\eta}\right)}$$

where $\eta' \equiv d\eta/dC$. This equation must be solved iteratively with the foregoing equations if the efficiency curve is different from that presented above. If, however, the given form is employed, then closed-form equations for C, μ_W, and μ_L may be written in terms of only J, T_p, d, and α_W. These formulas are summarized in Table I.

For a given trajectory and mission it is helpful to know the value of powerplant specific mass which yields zero payload. By setting $\mu_{L_{opt}} = 0$, the maximum α_W may be found; the resulting equation is given at the bottom of Table I.

Because the system parameters of interest are given by simplified expressions, graphs are easily constructed for C, μ_W, μ_1, and μ_L at various values of d and the product JT_p. This has been done for values of γ^2, JT_p, and d = 10, 20, 30, and 40 km/sec. The graphs are displayed in Figs. VII-2 to -9. The chart giving the value of α_W at zero payload has been constructed in nomograph form and is shown in Fig. VII-10.

Use of Charts

The series of graphs is useful for quickly estimating system performance for constant-thrust operation and under the assumed simplified payload fraction definition. Since d and α_W are usually known, it is necessary to obtain values for J and T_p before using the curves. Two methods are currently available for estimating J and T_p; one involves the constant-thrust, single-coast computer program, and the other is based on variable-thrust data.

In the present computer program the constant-thrust J, powered time, and the corresponding system parameters are computed for given arrival and departure dates and a series of powerplant specific masses. Both J and T_p change but slightly with α_W and are almost constant at high values of α_W (> 10 kg/kw); thus an average J and T_p may be used. Given the above information the charts may be used to estimate system performance at different values of d, which may be interpreted to represent different types of thrustors, and for other values of α_W. In addition the limiting powerplant specific mass for the given mission may be estimated.

The alternative method of estimating J and T_p employs estimates based on precomputed values which are compared to the variable-thrust J (J_V) and the trip time, T. These comparisons lead to the ratio $K = J/J_V$ and $\tau = T/T_p$, which are bases for estimating J and T_p for different missions. Based on the results detailed in UARL Report F-910352-12, June 1967, for Earth-Mars trips, the best guess for τ is approximately 1.8 to 2.0 while for K it is about 1.2 to 1.4

Further comparisons are necessary to determine the ranges of K and τ for other missions. Although this latter method of estimating K and τ to obtain J and T_p is quite empirical, the major advantage is the relative ease with which variable-thrust data are obtained for different flight profiles. Trips to Mars, in particular, have been computed for variable-thrust operation and were given in Report F-910352-12. The major assumption is that zero hyperbolic excess speeds are used on the end points of the low-acceleration trajectory.

Improved Payload Definition

An improved definition of payload fraction may be made to account for the mass of the thrustors, the propellant tanks, the tie-in structure, and miscellaneous hardware. For this purpose it is convenient to employ the following design parameters: ρ, the mass fraction of a loaded tank which is propellant, and σ, the proportionality constant which gives the structure and miscellaneous hardware mass as a proportion of the total powerplant, thrustor, tank, and propellant masses. The mass of the thrustors is obtained from the specific mass, α_F, which is the mass per unit of power input to the thrustors. In general, α_F is a function of the specific impulse or jet exhaust velocity delivered by the thrustor.

The improved definition of payload mass is thus

$$m_L = m_1 - (m_W + m_F + m_T + m_S)$$

where m_1 = burnout mass

m_W = powerplant

m_F = thrustor

m_T = tank

m_S = structure and miscellaneous

Normalizing with respect to initial mass and using the foregoing design parameters, the new payload fraction becomes

$$\mu_L = 1 - \frac{(1+\sigma)}{\rho}(1-\mu_1) - (1+\sigma)\left[1 + \frac{\alpha_F(C)}{\alpha_W}\right]\mu_W$$

which is also summarized in Table II. This is the form that is to be maximized with respect to exhaust velocity and powerplant mass fraction.

The only new addition, besides the constants σ and ρ, is the thrustor specific mass as a function of C. An example of the relationships for electron-bombardment and contact-type thrustors is illustrated in Fig. VII-11 for two levels of technology. To derive an expression for the empirical data, an analytic fit was employed using a sum of two exponentials. The results are tabulated in Table III. Thus, in principle, the optimum values of C and μ_W may be determined for the improved payload definition.

Using the standard procedure and employing the geometric mean for average thrust acceleration, the optimum powerplant fraction is

$$\mu_{W\ OPT} = \frac{\mu_1(1-\mu_1)/\rho}{\left[1+\frac{\alpha_F(C)}{\alpha_W}\right]\left[1-\frac{1+\mu_1}{2}\left(\frac{\eta' C}{\eta}\right)\right]+\frac{1+\mu_1}{2}\left(\frac{\alpha_F' C}{\alpha_W}\right)}$$

The complete system of equations to be solved is listed in Table IV. Because of the complicated relationship between α_F and C, it is not possible to derive closed-form expressions for the optimum system parameters. As the equations stand in Table IV, it is not necessary to accept the efficiency function given therein; any relationship could be part of the iteration procedure. The last equation in Table IV, giving the exhaust velocity, is a consequence of the average thrust-acceleration (geometric mean) assumption.

An iterative procedure, which appears to work for a few check cases, is to first pick or guess a value of C (it is assumed that J, T_p, d, α_W, σ, and ρ are given). A value is assumed for μ_1 and the first two equations between μ_W and μ_1 (Table IV) are solved by successive substitution. That is, for the assumed C, substitute μ_1 to find $\mu_{W\,opt}$; substitute this to find μ_1, etc., until μ_1 converges. With this μ_1, an updated value for C is obtained from the remaining equation and the entire procedure is repeated. This nested iteration procedure is time-consuming and may encounter convergence problems. The solution could be enhanced by employing a "false position" technique or, preferably, by utilizing a direct-search procedure on an augmented function which combines the system of equations.

The obvious values for C and μ_1 to use as first guesses are those obtained from the closed-form equations of the simplified payload fraction analysis. For the few cases so far analyzed, these initial guesses are close to the answers and therefore provide excellent starting points.

Since the foregoing analysis is based essentially on the same assumptions used in the preceding discussion of the simplified payload fraction, the equations of Table IV may also be solved using J and T_p obtained from the computer program (which is based on the simplified system) or from the ratios K and τ.

Improvements in Computer Programs

The current single-coast program has been modified to solve the closed-form equations for the simplified payload fraction as an integral part of the Newton-Raphson iteration. The form of the efficiency function given above is used exclusively, and the additional input required is the "efficiency parameter", d. This modified program is identified as deck F530.

At the first input value of α_W in the program (usually 1 kg/kw), the corresponding values of J and T_p are used to determine the powerplant specific mass which would yield zero payload. If the next input value of α_W is less than this $\alpha_{W\ max}$, the computation continues; if not, the program goes to a new case. This avoids computing trajectory and system parameters which, because α_W is greater than $\alpha_{W\ max}$ lead to negative or zero payloads. Because of the above two features, no iterations of the system equations are required, therby eliminating convergence problems in the powerplant optimization, and unnecessary computations for negative or zero payloads are avoided.

Further refinements, leading to a separate and more general deck (F487), incorporate the system equations for both the simplified and improved payload definitions. This second program contains that part of the foregoing program which employs the closed-form equations as part of the Newton-Raphson iterations. In addition, for each α_W the corresponding J and T_p are used in a subroutine which directly solves the optimization equations for the improved payload definition, external to the N-R algorithm. The additional inputs necessary are d, σ, ρ, and the type of thrustor specific mass relationship that is desired (of the four discussed previously). This modification includes the foregoing program, since σ and ρ may be zero and one, respectively, and α_F may be a constant or zero.

Note that the optimizing equations are solved external to the N-R algorithm and utilize the J and T_p corresponding to the simplified payload definition. A more accurate solution would require that the equations be solved at each iteration of the algorithm. However, based on the results showing the accuracy of the basic assumptions and procedure (as developed by Melbourne and Sauer), it is believed that, by using machine-computed J's and T_p's, the same approach as applied to the improved-payload case is at least more than adequate for mission studies and rapid system analyses.

A recently uncovered characteristic of all present versions of the single-coast computer programs is the dependence of computed values of powered time and exhaust velocity upon the input guesses for the ratio of powered time to trip time and the ratio of constant-thrust J to variable-thrust J. Iterations on these ratios using the computed powered time and constant-thrust J are not part of the internal

iterations between the exhaust velocity (and powerplant fraction) and the trajectory optimization subroutine. The result is that the computed system mass fractions agree quite well with exact solutions (from the multiple-coast program) but the specific impulse is slightly in error and the powered time even more so. These latter two approximations may not be sufficiently accurate for detailed analysis of operating lifetime and system design requirements.

A byproduct of the foregoing characteristic is that the powered time has practically no effect on the maximum payload fraction near the optimum specific impulse. Thus the powered time may be reduced from its optimum value to mitigate the lifetime and operating requirements of the thrustor with no significant reduction in payload capability.

Additional Curve Fits for Thrustor Specific Mass

The sum-of-exponentials approach used above for determing the analytic approximation to the thrustor specific mass function is quite accurate and yields a smooth curve for the function and its first derivative. Although this approach is suitable for any curve of the same form, it is time-consuming to determine the appropriate coefficients in the analytic approximation.

To expedite the analysis of other types of thrustors which may have somewhat different curves than those presented herein, an alternative analytic approximation was studied which quickly yields the necessary constants. It is necessary to specify the sample points of the given curve at exhaust velocities of 20, 40, 60, 80, and 100 km/sec. A fourth-degree polynomial is fitted through the five sample points using exact matching. Thus the coefficient matrix can be determined immediately by multiplying the data matrix (of sample points) by a transformation matrix, D. If the five sample points are chosen at the specified exhaust velocities, the matrix D remains the same for any other thrustor curve.

Table V gives the polynomial, the required input, the equation for the coefficients, and the transformation matrix, D. The analytic approximation and the required first derivative are quickly obtained and may be substituted in the iteration procedure for the equations of Table IV. The coefficients for the four thrustor curves displayed in Fig. VII-11 are presented in Table VI.

The polynomial approximation has the disadvantage of producing wavy forms for the function and its first derivative and of not yielding accurate values between the data points. However, these characteristics are probably well within the accuracy probably desired for mission and system analyses.

Hybrid-Thrust Mass Optimization Program

Capabilities

The purpose of the mixed high- and low-thrust mass optimization program is to minimize the gross vehicle mass on Earth (or planet) parking orbit for a given

payload to be delivered at the termination of the mission. The program handles three (one-way) flight modes and a round-trip mission:

1. Planet-to-planet orbits
2. Planet-to-no capture
3. Planet-to-planetary entry
4. Earth-to-planet-to-Earth

The first mode is the usual parking-orbit-to-parking-orbit mission between two planets. The second includes terminal conditions such as planetary flyby, solar probe, out-of-the-ecliptic, etc., wherein the final conditions are specified as heliocentric position or velocity. The third mode is similar to the first except that the capture at the planet is accomplished by a direct entry with atmospheric braking. The final case, the round-trip mission, is essentially a combination of the first and third modes. In all cases the mass of the payload to be delivered at the planet is to be specified as well as a range of values for the appropriate hyperbolic excess speeds and propulsion system parameters.

General Characteristics

In general, the program is a mass computation procedure that determines the mass of the entire vehicle before departure from the initial parking orbit (either from Earth or a planet). For a given final payload mass, final hyperbolic excess speed (if any) and departure hyperbolic speed, the initial mass of the vehicle is computed taking into account the mass of the life support system mission modules, solar shelter, basic structure and radiation shielding.

For mixed-acceleration systems the overall payload fraction μ_L of the entire vehicle is given, in general, by

$$\mu_L = \mu_{LD}\, \mu_{LH}\, \mu_{LC}$$

where subscript C represents the payload fraction of the capture system (either high-thrust propulsion or atmospheric entry) which delivers the final payload mass, H denotes the payload fraction of the heliocentric low-thrust system which delivers the capture system plus final payload to some final hyperbolic excess speed, and D signifies the departure high-thrust system which accelerates the final payload plus the capture system plus the electric system to a given initial hyperbolic excess speed. If the flight mode is (2) above the factor μ_{LC} would not appear.

The coupling between the heliocentric phase and the boundary phases is through the hyperbolic excess speed. The payload fraction, μ_{L_H}, is computed by the heliocentric trajectory optimization program for various values of the hyperbolic excess speeds on the boundaries. These data are entered into the program in the form of a table.

The minimization of the initial gross vehicle mass on parking orbit is accomplished by a direct search technique on the hyperbolic excess speeds relating the high-thrust and low-thrust propulsion phases. At each trial set for the hyperbolic speeds, the gross mass is computed and compared with previous values to determine appropriate speeds which tend to decrease the mass. This procedure has been found to be quite efficient in problems of this type.

The high-thrust step mass computation subroutine is an improved version of that developed under the initial phase of Contract NAS2-2928 (Report UARL E-910352-9, July 1966). The subroutine includes gravity losses and optimum thrust-to-weight ratio for minimum step mass. Various types of high-thrust propulsion systems may be employed (chemical, solid-core nuclear, liquid-core nuclear, etc.) by the proper specification of engine parameters such as specific impulse, thrust-to-weight ratio, minimum engine mass, and maximum thrust.

The additional mass for a manned spacecraft employs the scaling laws reported in E-910352-9. In these laws the life support system mass is given as a function of the total mission duration and the number of men in the crew. Fixed masses are assumed for the mission and living modules, shelter, etc.

The scaling of the entry follows the convenient law

$$\frac{m_A}{m_A'} = e^{\zeta\left(\frac{V_E^2}{V_E'^2} - 1\right)}$$

where m_A and m_A' are the masses of the ablative entry system and a reference system, respectively, and V_E and V_E' are the atmospheric entry velocities, required and reference, respectively. The factor ζ is an entry system growth parameter which predicts the growth of the reference system mass as higher entry velocities are accommodated. This growth parameter can be determined by matching the theoretical curve with one of interest. The above scaling law is merely representative of ablative systems and is employed here for convenience. Provision is made in the program for adding a storable propellant retrorocket if V_E exceeds a maximum entry speed limit.

The low-thrust mass computation subroutine employs the usual low-thrust mass equations for constant-thrust operation. The change envisioned herein is the

utilization of an improved definition for payload fraction which includes the mass of the thrustors, propellant tanks, and miscellaneous structure as well as the powerplant. This procedure is utilized in order to maintain compatible detail between the high-thrust and low-thrust mass computations and, consequently, to compute a fairly realistic vehicle mass and its associated subsystems.

The variation of thrustor efficiency and specific mass with exhaust velocity utilized are those given in Figs. VII-1 and -11.

TABLE VII-1

CONSTANT—THRUST OPTIMUM SYSTEM PARAMETERS

SIMPLIFIED PAYLOAD FRACTION DEFINITION

$$C_{OPT} = \left\{ 0.0864 \frac{JT_P}{\gamma^2} \left(1 + \frac{\gamma^2}{0.0864} \frac{d^2}{JT_P} \right) \left[1 - \frac{\gamma}{\left(1 + \frac{\gamma^2}{0.0864} \frac{d^2}{JT_P} \right)^{1/2}} \right] \right\}^{1/2}$$

$$\mu_{W\,OPT} = \gamma \left[\frac{1 + \frac{2\gamma^2}{0.0864} \frac{d^2}{JT_P}}{\left(1 + \frac{\gamma^2}{0.0864} \frac{d^2}{JT_P} \right)^{1/2}} - \gamma \right]$$

$$\mu_{L\,MAX} = 1 - 2\gamma \left(1 + \frac{\gamma^2}{0.0864} \frac{d^2}{JT_P} \right)^{1/2} + \gamma^2$$

WHERE: $\gamma^2 \equiv \frac{\alpha_W J}{2000}$

C, KM/SEC

J, m^2/SEC^3

T_P, DAYS

α_W, KG/KW

d, KM/SEC

α_W AT ZERO μ_L: $\alpha_{W\,MAX} = \dfrac{2000/J}{1 + \sqrt{\frac{1}{0.0216} \cdot \frac{d^2}{JT_P}}}$

TABLE VII-2

IMPROVED PAYLOAD FRACTION DEFINITION

$$\mu_L = 1 - \frac{1+\sigma}{\rho}(1-\mu_1) - (1+\sigma)\left(1 + \frac{\alpha_F(C)}{\alpha_W}\right)\mu_W$$

WHERE:

$$\sigma = \frac{m_{STRUCT}}{m_W + m_F + m_{TANKS} + m_{PROP}}$$

$$\rho = \frac{m_{PROP}}{m_{TANKS} + m_{PROP}}$$

$\alpha_F(C)$ = THRUSTOR SPECIFIC MASS FUNCTION

α_W = POWERPLANT SPECIFIC MASS

μ_1 = TERMINAL MASS FRACTION

μ_W = POWERPLANT MASS FRACTION

μ_L = PAYLOAD FRACTION

TABLE VII-3

EXPONENTIAL APPROXIMATION TO THRUSTOR SPECIFIC MASS FUNCTION

$$\alpha_F(C) = a_1 e^{-\sigma_1\left(\frac{C}{20}-1\right)} + a_2 e^{-\sigma_2\left(\frac{C}{20}-1\right)}$$

α_F, KG/KW C, KM/SEC

	a_1	σ_1	a_2	σ_2
ELECTRON BOMBARDMENT, 1	1.63542	0.406626	2.46479	1.92452
" " , 2	0.429867	0.403804	1.05991	1.06851
CONTACT, 1	−0.0197516	−0.357073	1.10985	0.342079

CONTACT, 2 :

$$\alpha_F(C) = e^{-0.600736\left(\frac{C}{20}-1\right)}\left\{0.590562\cos\left[\left(13^\circ\,14.428'\right)\left(\frac{C}{20}-1\right)\right] + 0.275432\sin\left[\left(13^\circ\,14.428'\right)\left(\frac{C}{20}-1\right)\right]\right\}$$

TABLE VII-4

CONSTANT—THRUST OPTIMUM SYSTEM PARAMETERS

IMPROVED PAYLOAD FRACTION DEFINITION

$$\mu_{W\,OPT} = \frac{\mu_1(1-\mu_1)/\rho}{\left(1+\frac{\alpha_F(C)}{\alpha_W}\right)\left[1-\frac{1+\mu_1}{2}\left(\frac{\eta' C}{\eta}\right)\right]+\frac{1+\mu_1}{2}\left(\frac{\alpha_F' C}{\alpha_W}\right)}$$

$$\mu_1 = \frac{1}{1+\frac{\gamma^2}{\eta\,\mu_W}}\;; \qquad \eta = \frac{1}{1+\left(\frac{d}{C}\right)^2}$$

$$C = \frac{\left[(0.0864)\,J\,T_P\right]^{1/2}}{1-\mu_1}$$

WHERE $\gamma^2 = \frac{\alpha_W J}{2000}$

AND

J, m^2/SEC^3

T_P, DAYS

C, KM/SEC

d, KM/SEC

α_F, KG/KW

α_W, KG/KW

TABLE VII-5

DETERMINATION OF COEFFICIENTS FOR THRUSTOR SPECIFIC MASS FUNCTION

$$\alpha_F(C) = a_0 + a_1\left(\frac{C}{20}\right) + a_2\left(\frac{C}{20}\right)^2 + a_3\left(\frac{C}{20}\right)^3 + a_4\left(\frac{C}{20}\right)^4$$

α_F, KG/KW

C, KM/SEC

INPUT:

C	20	40	60	80	100
α_F	α_{F0}	α_{F1}	α_{F2}	α_{F3}	α_{F4}

$$\begin{pmatrix} a_0 \\ a_1 \\ a_2 \\ a_3 \\ a_4 \end{pmatrix} = D \times \begin{pmatrix} \alpha_{F0} \\ \alpha_{F1} \\ \alpha_{F2} \\ \alpha_{F3} \\ \alpha_{F4} \end{pmatrix}$$

WHERE

$$D = \begin{pmatrix} 5 & -10 & 10 & -5 & 1 \\ -6.41665 & 17.83331 & -19.50 & 10.16667 & -2.08333 \\ 2.95833 & -9.83333 & 12.25 & -6.83333 & 1.45833 \\ -0.58333 & 2.16667 & -3.0 & 1.83333 & -0.41667 \\ 0.041667 & -0.16667 & 0.25 & -0.16667 & 0.041667 \end{pmatrix}$$

TABLE VII-6

POLYNOMIAL APPROXIMATION FOR THRUSTOR SPECIFIC MASS

$$\alpha_F(C) = a_0 + a_1\left(\frac{C}{20}\right) + a_2\left(\frac{C}{20}\right)^2 + a_3\left(\frac{C}{20}\right)^3 + a_4\left(\frac{C}{20}\right)^4$$

α_F, KG/KW

C, KM/SEC

THRUSTOR TYPE	a_0	a_1	a_2	a_3	a_4
ELECTRON BOMBARDMENT, I	11.73	−11.467	4.6271	−0.84750	0.057916
2	3.44	−2.68666	0.88670	−0.13833	0.008333
CONTACT, I	1.55	−0.54083	0.089583	−0.091662	0.0004167
2	1.00	−0.53167	0.14333	−0.023333	0.0016667

FIG. VII - 1

DEPENDENCE OF THRUSTOR EFFICIENCY ON EXHAUST VELOCITY

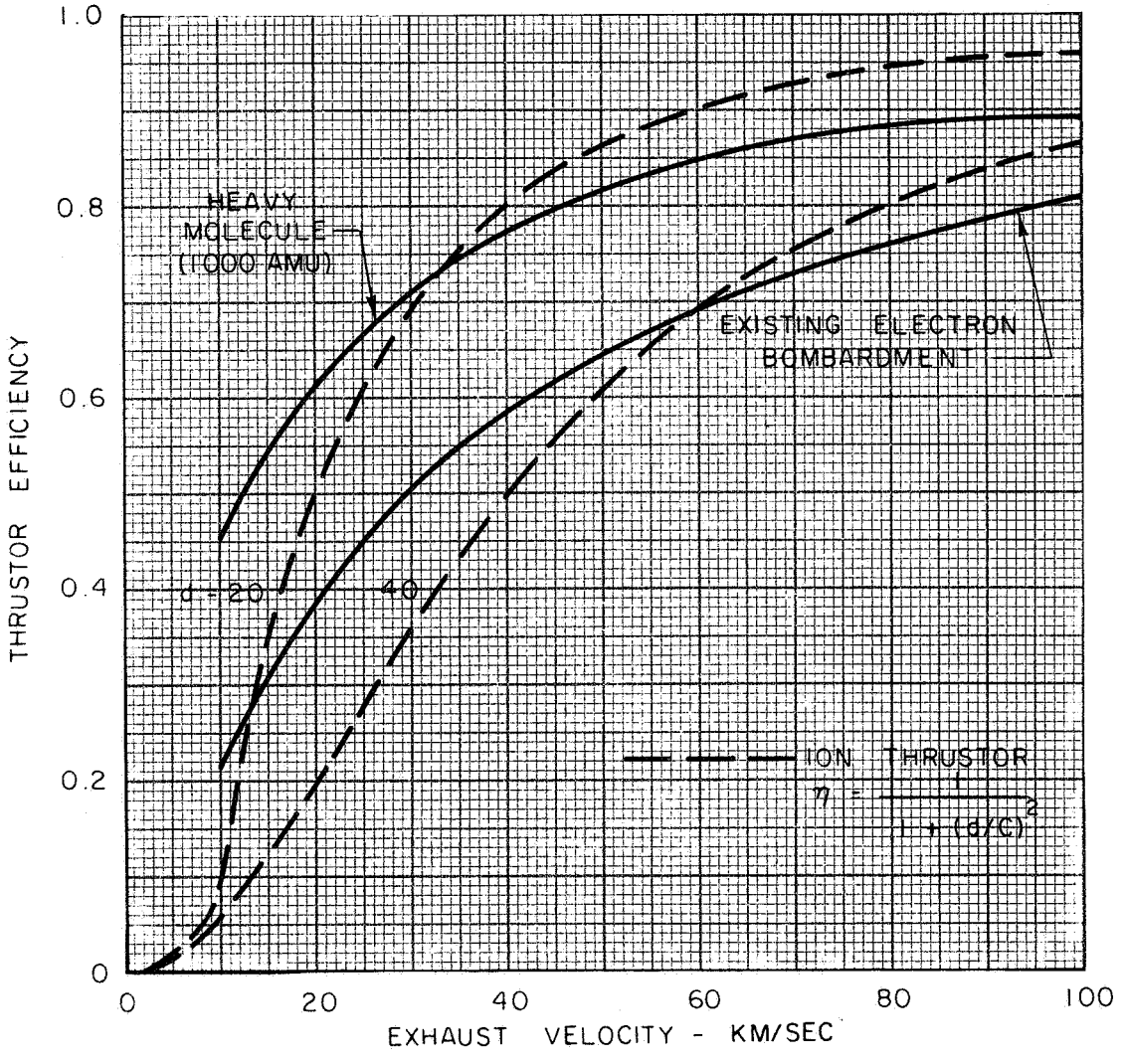

PAYLOAD AND POWERPLANT FRACTIONS FOR CONSTANT-THRUST OPERATION

d = 10 KM/SEC

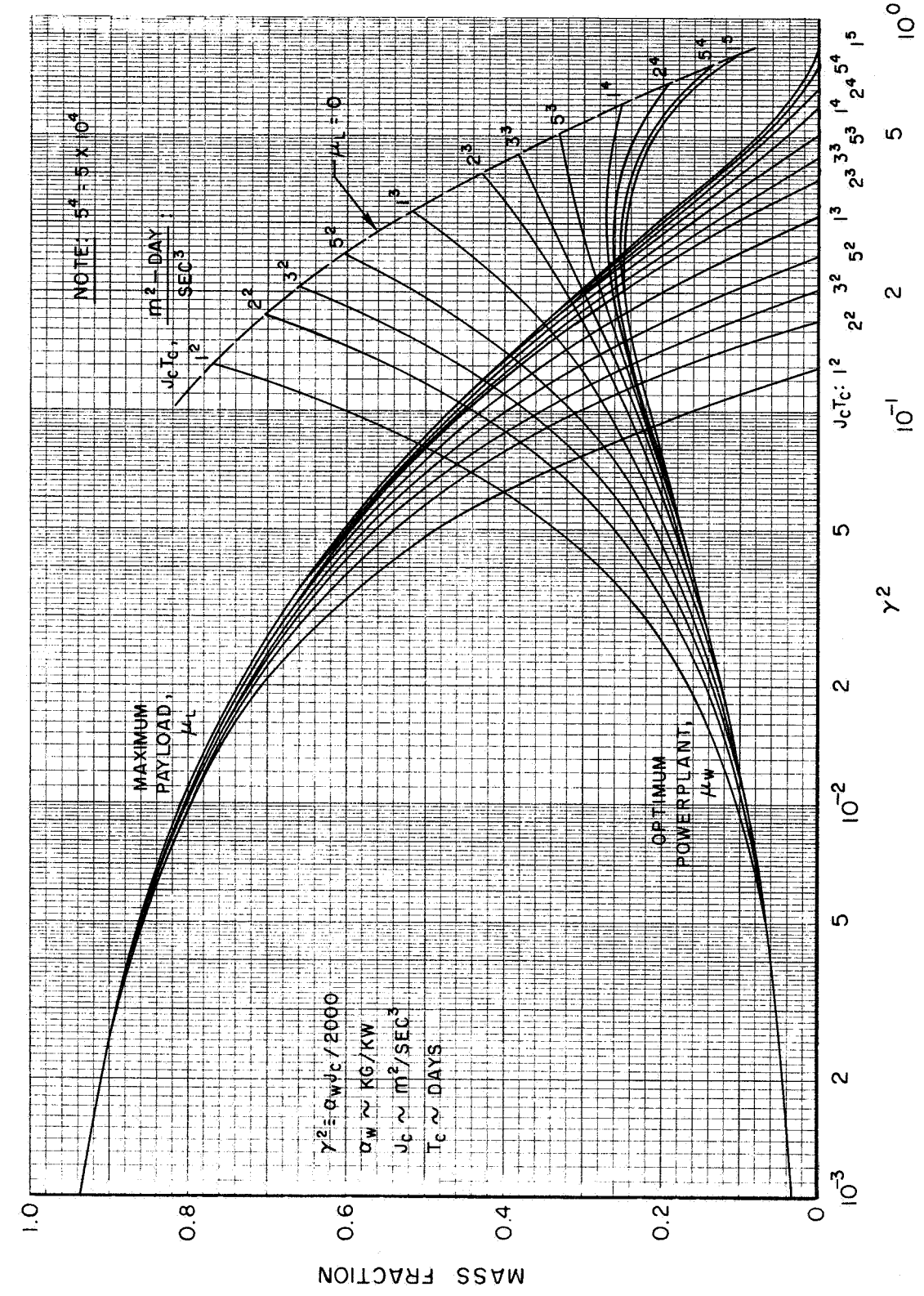

FIG. VII-3

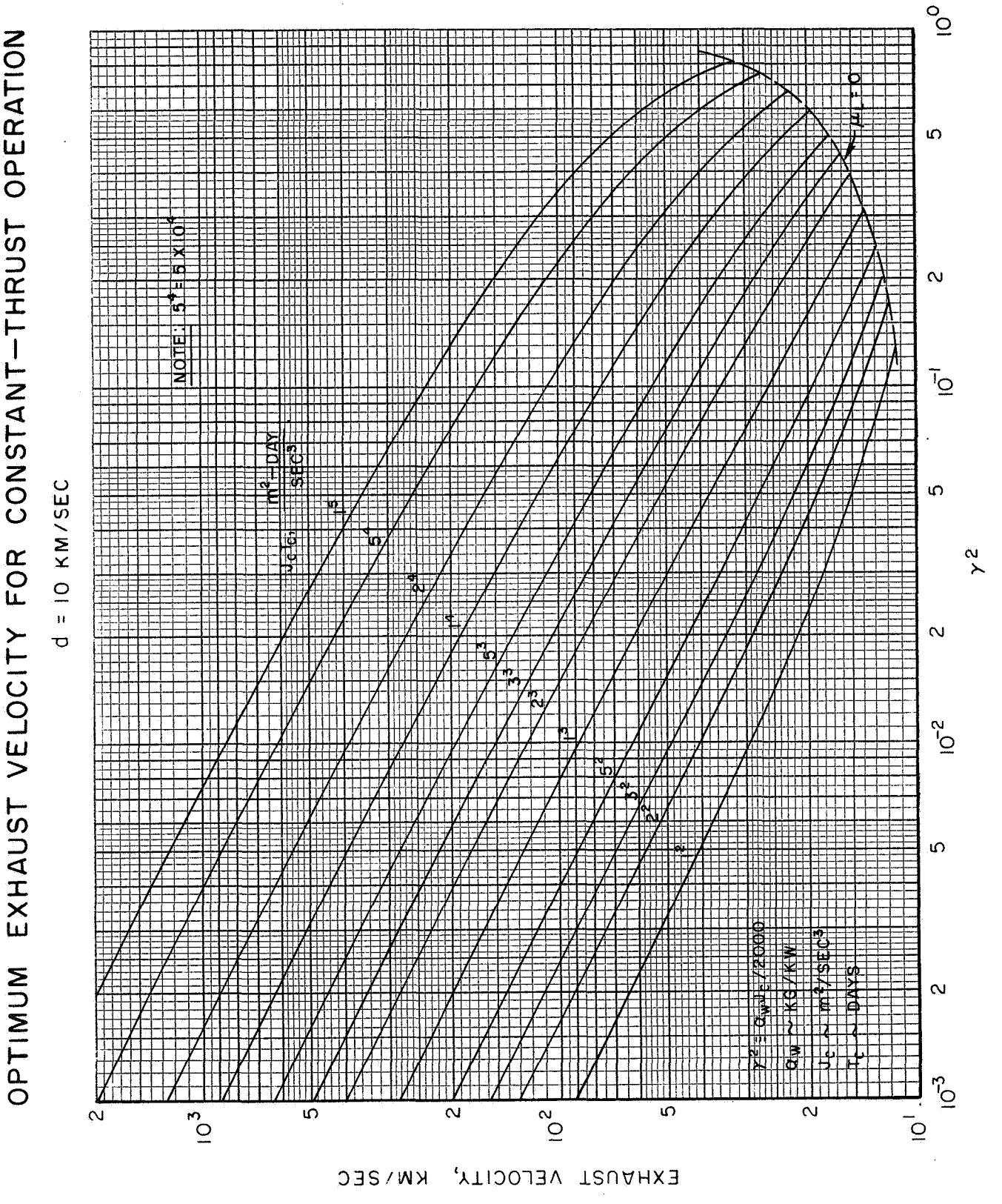
OPTIMUM EXHAUST VELOCITY FOR CONSTANT-THRUST OPERATION
d = 10 KM/SEC
NOTE: $\delta^4 = 5 \times 10^{-4}$
$J_c T_c$, m^2-DAY / SEC^3
$\mu_L = 0$
$\gamma^2 = \alpha_w T_c / 2000$
$\alpha_w \sim$ KG/KW
$J_c \sim m^2/SEC^3$
$T_c \sim$ DAYS
EXHAUST VELOCITY, KM/SEC
γ^2

FIG. VII-4

PAYLOAD AND POWERPLANT FRACTIONS FOR CONSTANT-THRUST OPERATION

d = 20 KM/SEC

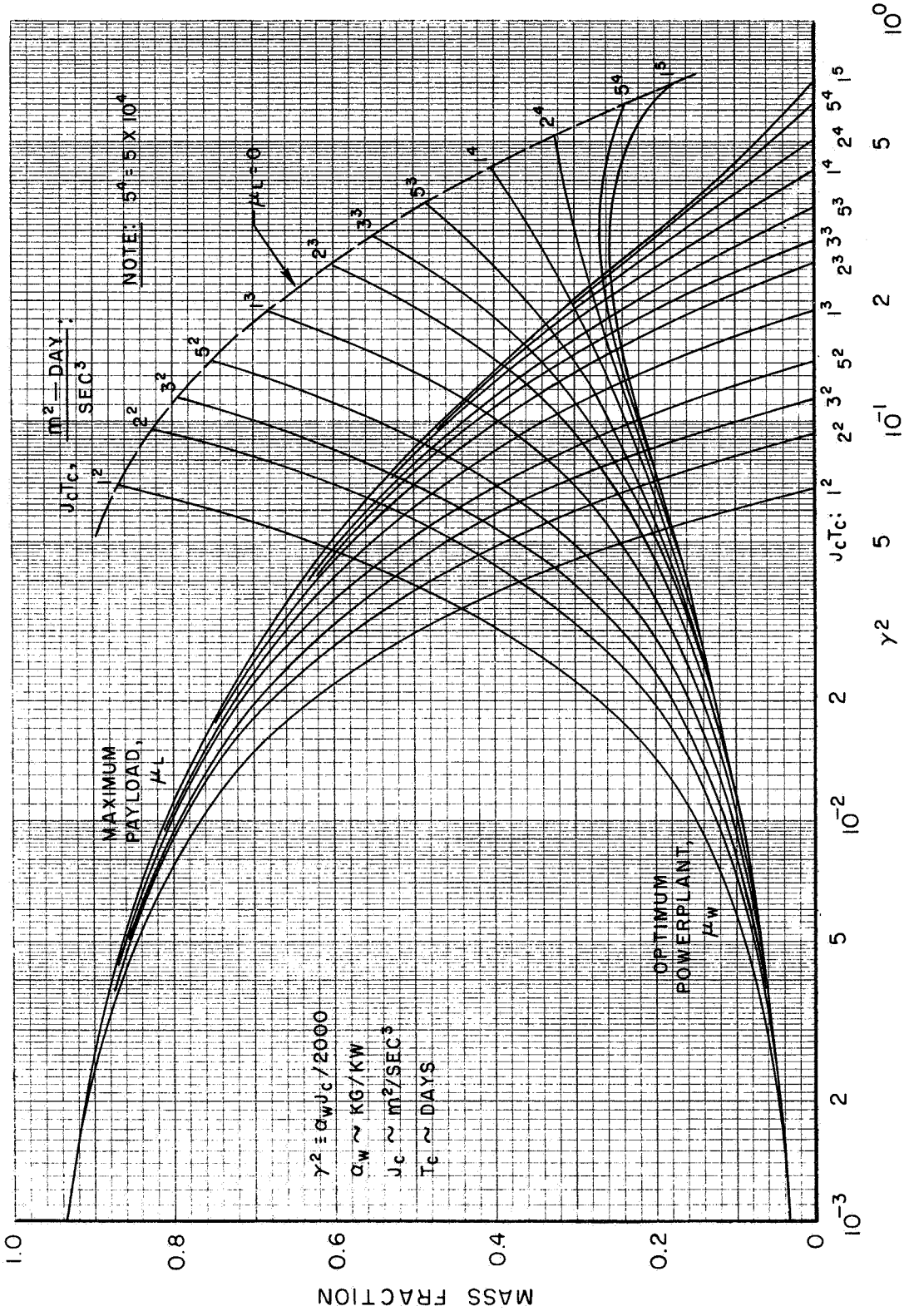

FIG. VII – 5

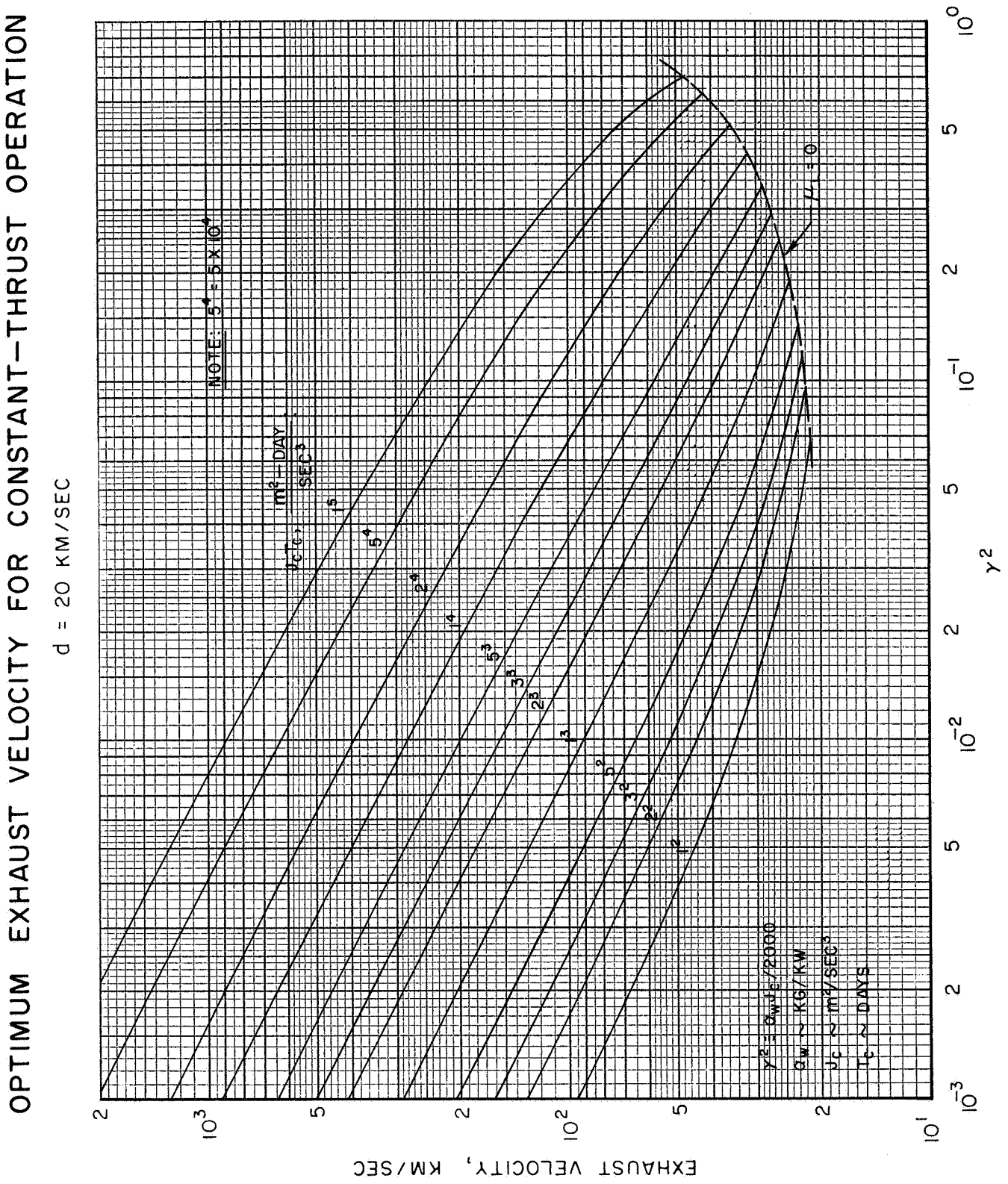
OPTIMUM EXHAUST VELOCITY FOR CONSTANT–THRUST OPERATION
d = 20 KM/SEC
NOTE: $5^4 = 5 \times 10^4$
m^2–DAY / $\mu_c T_c$, SEC^3
$\mu_c = 0$
$\gamma^2 = \alpha_w J_c / 2000$
$\alpha_w \sim$ KG/KW
$J_c \sim m/SEC^2$
$T_c \sim$ DAYS
EXHAUST VELOCITY, KM/SEC
γ^2

FIG. VII - 6

PAYLOAD AND POWERPLANT FRACTIONS FOR CONSTANT-THRUST OPERATION

d = 30 KM/SEC

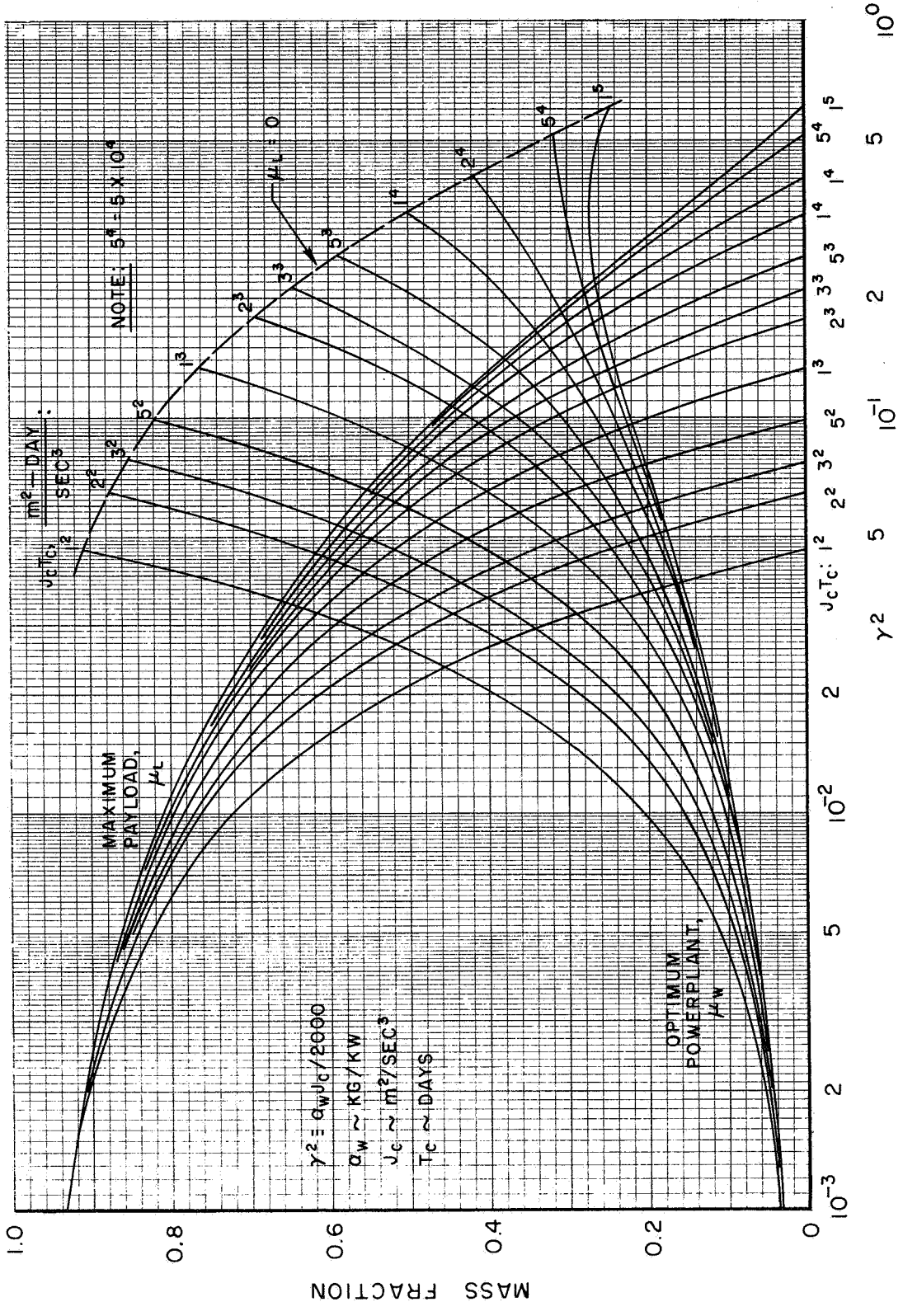

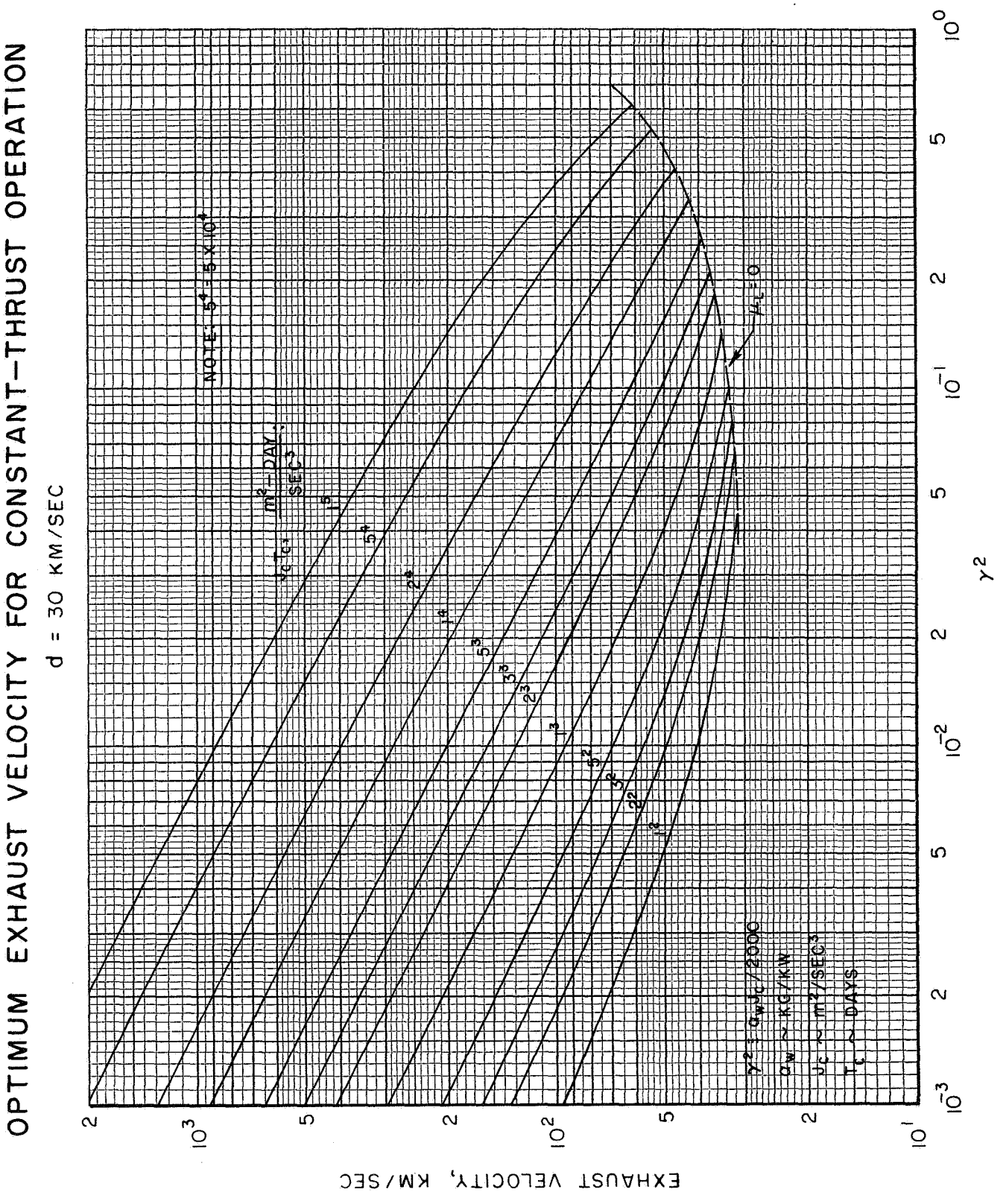
OPTIMUM EXHAUST VELOCITY FOR CONSTANT-THRUST OPERATION
d = 30 KM/SEC
NOTE: $5^4 = 5 \times 10^4$
$\frac{m^2 - DAY}{SEC^3}$
$\mu_1 = 0$
$\gamma^2 = \alpha_w t_c / 2000$
$\alpha_w \sim$ KG/KW
$t_c \sim$ DAYS
EXHAUST VELOCITY, KM/SEC
γ^2

FIG. VII-8

PAYLOAD AND POWERPLANT FRACTIONS FOR CONSTANT-THRUST OPERATION

d = 40 KM/SEC

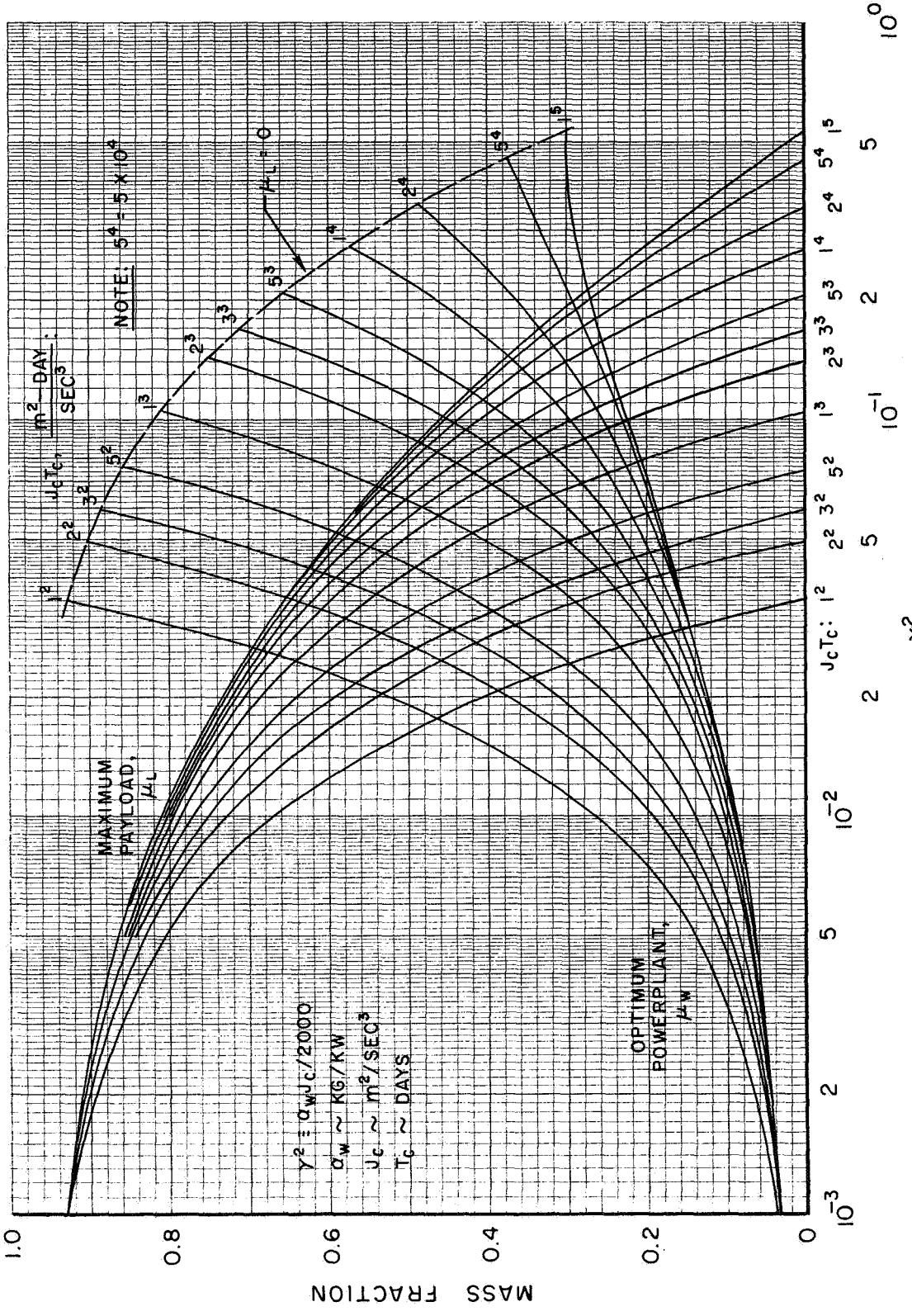

FIG. VII – 9

OPTIMUM EXHAUST VELOCITY FOR CONSTANT–THRUST OPERATION

d = 40 KM/SEC

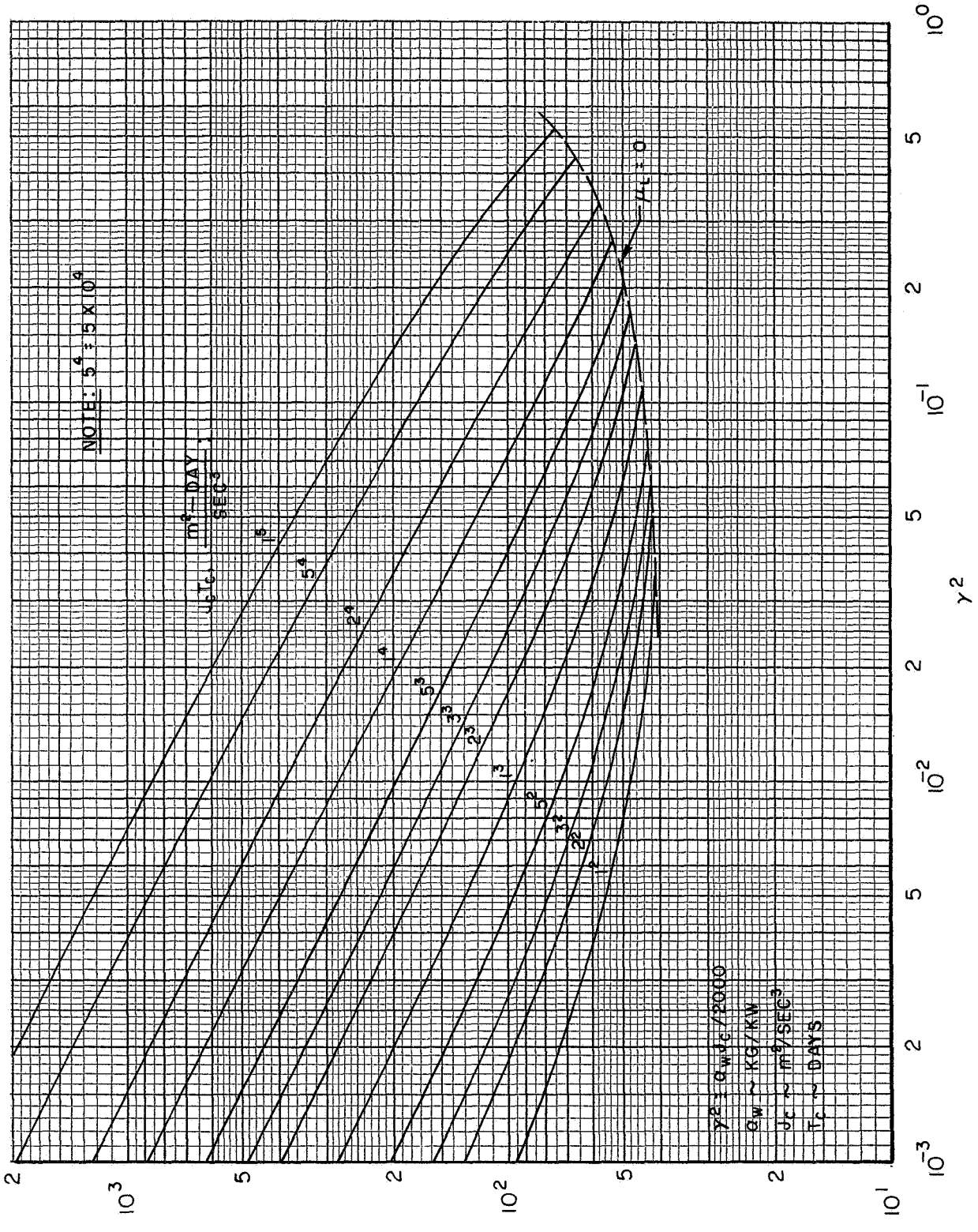

F-910352-13

FOLDOUT FRAME 1

FOLDOUT FRAME 2

FIG. VII-10

POWERPLANT SPECIFIC WEIGHT AT ZERO PAYLOAD FRACTION

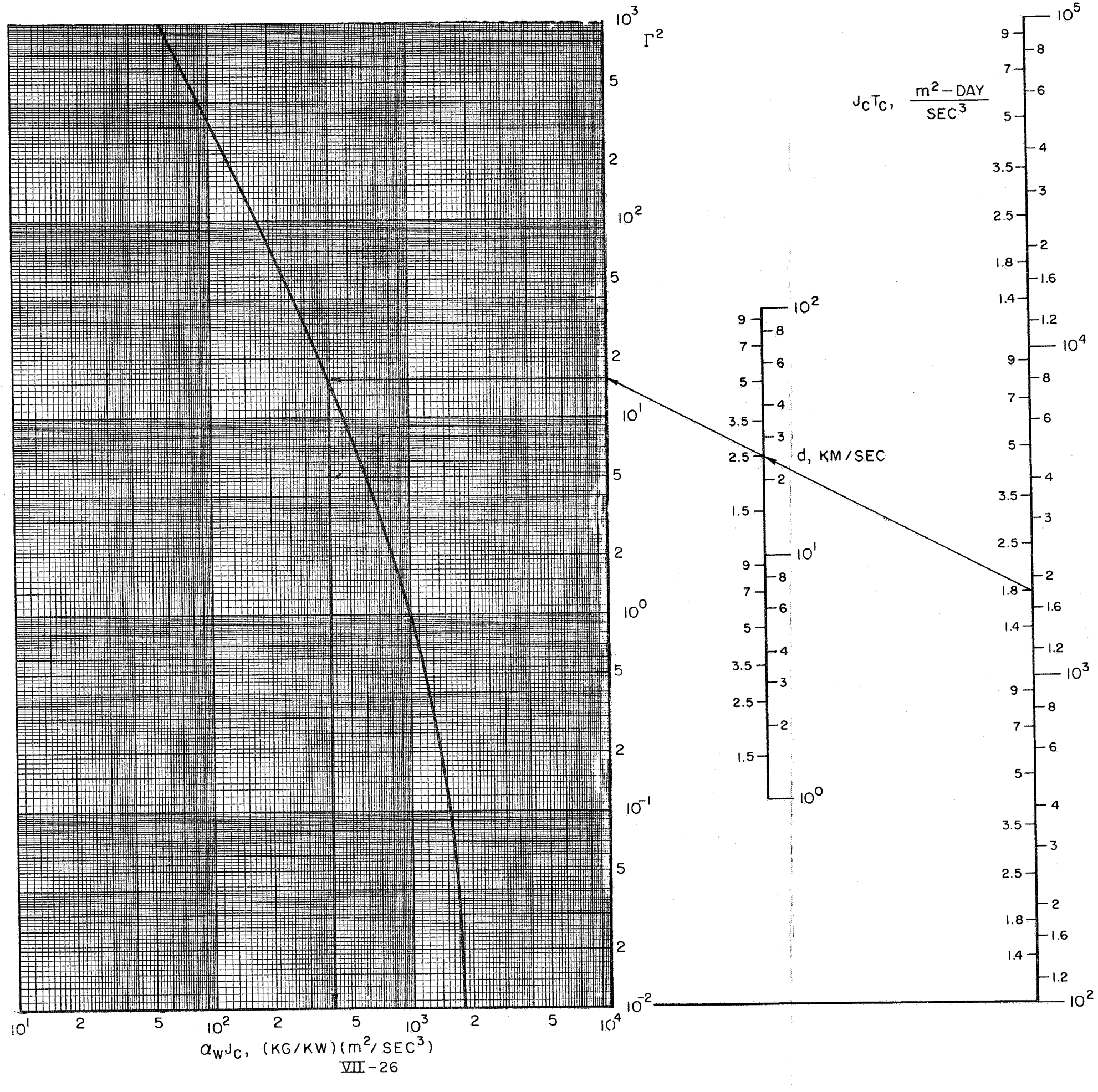

d = THRUSTOR EFFICIENCY PARAMETER, KM/SEC

J_C = CONSTANT THRUST J, m^2/SEC^3

T_C = POWERED TIME, DAYS

EXAMPLE:

d = 25, $J_CT_C = 1.8 \times 10^3$;

$\therefore \Gamma^2 = 15.7$,

& $\alpha_{WMAX} = \frac{3.95 \times 10^2}{J_C}$, KG/KW

THRUSTOR SPECIFIC MASS

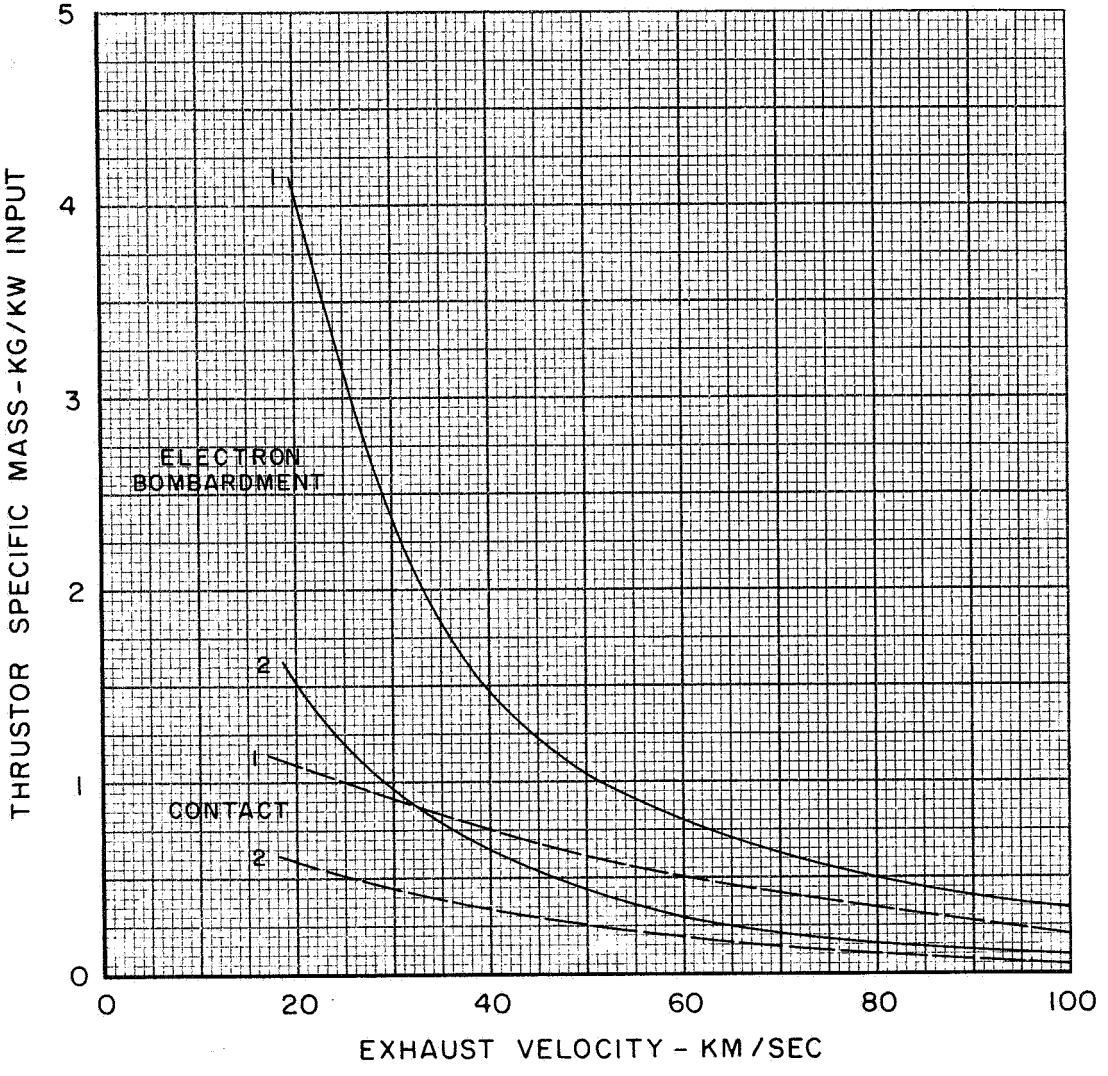

SECTION VIII

VARIATIONAL FORMULATIONS OF POWER-LIMITED TRAJECTORY AND PROPULSION-SYSTEM OPTIMIZATION PROBLEMS

Introduction

The original application of the Newton-Raphson algorithm to solve the two-point boundary value problem associated with low-thrust trajectory optimization was presented in Ref. VIII-1. In that work only the simplest problem was treated, the two-dimensional trajectory optimization problem for a power-limited propulsion system that is completely unconstrained in thrusting direction and magnitude of exhaust velocity. Subsequently, more complicated problems have been solved including constant-thrust, minimum-time rendezvous (Ref. VIII-2); maximum final mass for constant-thrust with optimum-coast, fixed-time rendezvous; and variable thrust with power given as $P_o e^{-\alpha t}/r^n$, (Ref. VIII-3).

In the present study more realistic constant-thrust problems involving additional complexities and constraints have been considered. Optimization of propulsion system parameters which are constant in time along with the trajectory and thrusting program has been analyzed, closely following the original analysis of Ref. VIII-4.

In the initial analyses performed during the early portion of the contract period, several constant-thrust flight modes were completely analyzed. The variational analysis treats any continuous power-available function of position and time The boundary and transversality conditions considered in the study include fixed-time planetary flyby, fixed-time flyby at a given radius, optimum fixed-time orbital transfer, and optimum fixed-time round trips. The effect of discarding inert mass during coasting periods has been investigated. Finally, the problem has been considered wherein the thrust vector is constrained to make a constant angle with the radius vector in three dimensions. The equations for those problems of immediate interest resulting from this initial analysis are summarized below. Part 2 of Appendix A details the derivations for all the problems cited above.

Immediately after the summary of the initial problem set, the development of two additional problems is presented. The first is the round-trip stopover mission with optimum launch and arrival dates at both planets for prescribed values of total trip time and stay time. The second problem is the variable-thrust round-trip flyby including the effect of the intermediate planetary perturbation. The corresponding constant-thrust case was not formulated. In the interest of brevity,

only the major results of the analysis are presented here. The analysis is based upon the developments in Appendix A of this report. A complete, though non-rigorous, derivation of the general variational calculus results upon which these formulations are based is presented in Appendix A, Part 1.

A final problem treated is the substitution of the analytic solutions for the numerical solutions in the coast regions. This problem arose as the result of the computer storage requirements; the use of analytic solution reduces the number of mesh points and, consequently, the amount of core storage needed.

Summary of Initial Problem Set

The several flight modes summarized herein are distinguished by the appropriate boundary and transversality conditions. These include planetary rendezvous, planetary flyby, flyby at a given heliocentric radius, and optimum orbital transfer, all for a fixed-time transfer. These foregoing conditions correspond, respectively, to the following flight modes: a planet-to-planet rendezvous, one-way flyby of a planet, a solar probe passing at some heliocentric radius, and, finally, an optimum transfer between any two heliocentric orbits. In all of the following equations the objective function to be maximized is the final payload-to-gross mass fraction with respect to exhaust velocity (specific impulse) and powerplant fraction.

For the rendezvous mode, only constant power is considered although single or double coast periods are treated. In the case of the flyby, constant power is again considered with a single final coast period or an intermediate and a final coast. The solar probe is treated with power ranging as a function of heliocentric position. In this instance three cases involving coast periods are considered: (1) single final coast, (2) intermediate and final coasts, and (3) two intermediate and one final coast. In the final problem, optimum orbital transfer, the power is considered to be a function of heliocentric position and one or two intermediate coast perios are treated.

Problem 1: <u>Constant-exhaust velocity, constant-power, rendezvous in fixed time with multiple coasts.</u>

Final payload fraction is maximized with respect to powerplant fraction and exhaust velocity.

<u>Differential Equations:</u>

$$\ddot{\chi}_i = \frac{2\mu_w \eta \beta}{\alpha_w c \mu} \quad \frac{\lambda_{i+3}}{\rho} - \frac{\chi_i}{r^3} \qquad (i = 1, 2, 3)$$

$$\ddot{\lambda}_{i+3} = - \frac{\lambda_{i+3}}{r^3} + \frac{3\chi_i}{r^5} \sum_{j=1}^{3} \lambda_{j+3} \chi_j$$

where $$\mu(t) = 1 - \frac{2\mu_w \eta}{\alpha_w c^2} \int_0^T \beta(\tau)\, d\tau$$

Switching Times:

(a) Case 1. Single intermediate coast - switching times at T_1 and T_2.

$$p(T_1) = p(T_2)$$

$$\beta = \begin{cases} 1 \text{ for } t \le T_1 \text{ and } t \ge T_2 \\ 0 \text{ for } T_1 < t < T_2 \end{cases}$$

(b) Case 2. Double intermediate coast - switching times at T_1, T_2, T_3 and T_4

$$p(T_1) = p(T_2)$$

$$p(T_3) = p(T_4)$$

$$\frac{p(T_3)}{\mu(T_3)} = \frac{p(T_2)}{\mu(T_2)} + \frac{2\eta\mu_w}{\alpha_w c^2} \int_{T_2}^{T_3} \frac{p}{\mu^2}\, dT$$

$$\beta = \begin{cases} 1 \text{ FOR } 0 \le t \le T_1, \quad T_2 \le t \le T_3, \quad T_4 \le t \le T \\ 0 \text{ FOR } T_1 < t < T_2, \quad T_3 < t < T_4 \end{cases}$$

(c) Case 3. Single intermediate thrust period, switching times at T_1 and T_2.

$$\frac{p(T_2)}{\mu(T_2)} = \frac{p(T_1)}{\mu(T_1)} + \frac{2\eta\mu_w}{\alpha_w c^2} \int_{T_1}^{T_2} \frac{p}{\mu^2}\, dT$$

$$\beta = \begin{cases} 1 & \text{FOR} \quad T_1 \le t \le T_2 \\ 0 & \text{FOR} \quad 0 \le t < T_1, \quad \text{AND} \quad T_2 < t \le T \end{cases}$$

Boundary Conditions

$$X_i(0) = g_i(0) \qquad (i = 1, 2, 3)$$

$$\dot{X}_i(0) = \dot{g}_i(0) + V_\infty(0) \frac{\lambda_{i+3}(0)}{p(0)}$$

$$X_i(T) = g_i(T)$$

Either

$$\dot{X}_i(T) = \dot{g}_i(T) - V_\infty(T) \frac{\lambda_{i+3}(T)}{p(T)}, \quad \text{OR} \quad \lambda_{i+3}(T) = 0$$

Subsidiary Conditions:

$$\lambda_\mu(T) = \frac{c\,p(T_L)}{\mu(T_L)} + \frac{2\eta\mu_w}{a_w c} \int_{T_L}^{T} \frac{p\beta}{\mu^2}\, dT$$

$$\lambda_\mu(0) = \frac{c\,p(T_F)}{\mu(T_F)} - \frac{2\eta\mu_w}{a_w c} \int_{0}^{T_F} \frac{p\beta}{\mu^2}\, dT$$

where T_L denotes conditions at the time of launch and T_F denotes the conditions at final time.

$$\left[\mu(T) - \mu_w\left(1 + \frac{\partial \mu_F}{\partial \mu_w}\right)\right] \lambda_\mu(T) - \lambda_\mu(0) = 0$$

$$\lambda_\mu(T)\frac{\partial \mu_F}{\partial C} + \frac{2\mu_w \eta}{a_w C^3}\left[\int_0^T \left(1 - C\frac{d\ln\eta}{dC}\right)\frac{Cp}{\mu}\beta\, dt\right.$$

$$\left. - \left(2 - C\frac{d\ln\eta}{dC}\right)\left(\lambda_\mu(0)\int_0^T \beta\, dt + \frac{2\mu_w\eta}{a_w C}\int_0^T (T-t)\frac{p\beta}{\mu^2}\, dt\right)\right] = 0$$

Objective Function:

$$\mu_{PL} = \mu(T) - \mu_w - \mu_F(\mu_w, C) - \mu_s$$

Problem 2: Problem 1, only with flyby

Boundary Conditions

Differential Equations

Same as for Problem 1.

Switching Times

(a) Case 1. Single final coast - switching time at T_1.

$$\beta = \begin{cases} 1 \text{ FOR } t \le T_1 \\ 0 \text{ FOR } t > T_1 \end{cases}$$

(b) Case 2. Intermediate and final coasts - switching times at T_1, T_2, and T_3.

$$\beta = \begin{cases} 1 \text{ FOR } 0 \le t \le T_1, \quad T_2 \le t \le T_3 \\ 0 \text{ FOR } T_1 < t < T_2, \quad t > T_3 \end{cases}$$

$$p(T_1) = p(T_2)$$

$$\frac{p(T_3)}{\mu(T_3)} = \frac{p(T_2)}{\mu(T_2)} + \frac{2\mu_w \eta}{\alpha_w C^2} \int_{T_2}^{T_3} \frac{p}{\mu^2}\, dt$$

Boundary Conditions

$$\chi_i(0) = g_i(0) \qquad (i = 1, 2, 3)$$

$$\dot{\chi}_i(0) = \dot{g}_i(0) + V_\infty(0)\, \frac{\lambda_{i+3}(0)}{p(0)}$$

$$\chi_i(T) = g_i(T)$$

$$\vec{p}(T) = 0$$

Subsidiary Conditions

$$\lambda_\mu(T) = \frac{Cp(T_L)}{\mu(T_L)}$$

$$\lambda_\mu(0) = \frac{Cp(T_F)}{\mu(T_F)} - \frac{2\mu_w \eta}{\alpha_w C} \int_0^{T_F} \frac{p}{\mu^2}\, dt$$

$$\left[\mu(T) - \mu_w \left(1 + \frac{\partial \mu_F}{\partial \mu_w}\right)\right] \lambda_\mu(T) - \lambda_\mu(0) = 0$$

$$\lambda_\mu(T)\, \frac{\partial \mu_F}{\partial C} + \frac{2\mu_w \eta}{\alpha_w C^3} \left[\int_0^T \left(1 - \frac{C\, d \ln \eta}{dC}\right) \frac{Cp}{\mu}\, \beta\, dt \right.$$

$$\left. - \left(2 - C\, \frac{d \ln \eta}{dC}\right)\left(\lambda_\mu(0) \int_0^T \beta\, dt + \frac{2\mu_w \eta}{\alpha_w C} \int_0^T (T - t)\, \frac{p\beta}{\mu^2}\, dt\right)\right] = 0$$

Problem 3: Solar Probe with Power a function of position.

Final payload fraction is maximized. The function of position is denoted by f.

Differential Equations

$$\ddot{\chi}_i = \frac{2\mu_w \eta f \beta}{a_w C \mu} \frac{\lambda_{i+3}}{p} - \frac{\chi_i}{r^3}$$

$$\dot{\lambda}_{i+3} = -\frac{\lambda_{i+3}}{r^3} + \frac{3\chi_i}{r^5} \sum_{k=1}^{3} \lambda_{k+3} \chi_k + \frac{2\eta\mu_w\beta}{a_w C^2} \frac{\partial f}{\partial \chi_i} \left(\frac{Cp}{\mu} - \lambda_\mu \right)$$

$$\dot{\lambda}_\mu = \frac{\dot{p}\lambda_\mu}{p} + \frac{2}{C}\sqrt{\frac{2\eta\mu_w f}{a_w C}} \left(\frac{\lambda_\mu^3}{p} \right)^{1/2} \quad \text{FOR } \beta = 1$$

$$\lambda_\mu = \lambda_\mu(T_1) \quad \text{FOR } \beta = 0$$

$$\mu = \sqrt{\frac{2\eta\mu_w f p}{a_w C \lambda_\mu}} \quad \text{FOR } \beta = 1$$

$$\mu = \mu(T_1) \quad \text{FOR } \beta = 0$$

where T_1 is the time at the beginning of the coast period.

Switching Times

(a) Case 1. Single final coast - switching time at T_1.

$$\beta = \begin{cases} 1 & \text{FOR } 0 \le t \le T_1 \\ 0 & \text{FOR } T_1 < t \le T \end{cases}$$

(b) Case 2. Intermediate and final coasts - switching times at T_1, T_2, and T_3.

$$\beta = \begin{cases} 1 \text{ FOR } 0 \le t \le T_1 \text{ AND } T_2 \le t \le T_3 \\ 0 \text{ FOR } T_1 < t < T_2 \text{ AND } T_3 < t \le T \end{cases}$$

$$p(T_1) = p(T_2)$$

$$\frac{p(T_3)}{\mu(T_3)} = \frac{p(T_2)}{\mu(T_2)} + \frac{2\mu_w \eta}{a_w C} \int_{T_2}^{T_3} \frac{pf\beta}{\mu^2}\, dt$$

(c) Case 3. Two intermediate and one final coast - switching times at T_1, T_2, T_3, T_4, and T_5.

$$\beta = \begin{cases} 1 \text{ FOR } 0 \le t \le T_1;\ T_2 \le t \le T_3;\ T_4 \le t \le T_5 \\ 0 \text{ FOR } T_1 < t < T_2;\ T_3 < t < T_4;\ T_5 < t \le T \end{cases}$$

$$p(T_1) = p(T_2)$$

$$\frac{p(T_3)}{\mu(T_3)} = \frac{p(T_2)}{\mu(T_2)} + \frac{2\mu_w \eta}{a_w C} \int_{T_2}^{T_3} \frac{pf\beta}{\mu^2}\, dt$$

$$p(T_3) = p(T_4)$$

$$\frac{p(T_5)}{\mu(T_5)} = \frac{p(T_4)}{\mu(T_4)} + \frac{2\mu_w \eta}{a_w C} \int_{T_4}^{T_5} \frac{pf\beta}{\mu^2}\, dt$$

Boundary Conditions

$$\chi_i(0) = g_i(0) \qquad (i = 1, 2, 3)$$

$$\dot{\chi}_i(0) = \dot{g}_i(0) + \frac{V_\infty(0)\,\lambda_{i+3}(0)}{p(0)}$$

$$\sum_{i=1}^{3} \left[\chi_i(T)\right]^2 = R^2$$

$$\frac{\dot{\lambda}_4(T)}{\dot{\lambda}_5(T)} = \frac{\chi_1(T)}{\chi_3(T)}\,; \qquad \frac{\dot{\lambda}_5(T)}{\dot{\lambda}_6(T)} = \frac{\chi_2(T)}{\chi_3(T)}$$

$$\vec{p}(T) = 0$$

Subsidiary Conditions

$$\lambda_\mu(T) = \frac{Cp(T_L)}{\mu(T_L)}$$

$$\lambda_\mu(0) = \frac{Cp(T_F)}{\mu(T_F)} - \frac{2\mu_w\eta}{a_w C}\int_0^{T_F} \frac{pf}{\mu^2}\,dt$$

$$\left[\mu(T) - \mu_w\left(1 + \frac{\partial\mu_F}{\partial\mu_w}\right)\right]\lambda_\mu(T) - \lambda_\mu(0) = 0$$

$$\lambda_\mu(T)\,\frac{\partial\mu_F}{\partial C} + \frac{2\mu_w\eta}{a_w C^3}\int_0^T \left[\left(2 - \frac{Cd\ln\eta}{dC}\right)\left(\frac{Cp}{\mu} - \lambda_\mu\right) - \frac{Cp}{\mu}\right] f\beta\,dt = 0$$

Problem 4: Fixed-time optimum orbital transfer, solar power, multiple coasts.

Final payload fraction is maximized.

Differential Equations

Same as for Problem 3.

Switching Times

Same as for Problem 1.

Boundary Conditions

$$\chi_i(0) = g_i(\xi_1); \quad \chi_i(T) = g_i(\xi_2)$$

$$\dot{\chi}_i(0) = \dot{g}_i(\xi_1); \quad \dot{\chi}_i(T) = \dot{g}_i(\xi_2)$$

$$\sum_{i=1}^{3} \left(\lambda_{i+3} \frac{d\dot{g}_i}{d\xi_1} - \dot{\lambda}_{i+3} \frac{dg_i}{d\xi_1} \right)_{t=0} = 0$$

$$\sum_{i=1}^{3} \left(\lambda_{i+3} \frac{d\dot{g}_i}{d\xi_2} - \dot{\lambda}_{i+3} \frac{dg_i}{d\xi_2} \right)_{t=T} = 0$$

Subsidiary Conditions

Same as for Problem 3.

The Round-Trip Stopover Mission

The mission profile has the following characteristics. Use is made of high-thrust impulses departing Earth, arriving at the destination planet, and departing the destination planet. The magnitudes of these impulses are fixed input, and no optimization is carried out with respect to them internal to the algorithm. Atmospheric braking is employed back at Earth. Two power-limited propulsion systems constrained to constant-thrust-with-coast operation are employed, one for the outbound leg and the other for the inbound leg. The first propulsion system - including powerplant, thruster, and tankage - is staged at the destination planet along with a high-thrust rocket, tankage, and an intermediate payload.

The objective function for the algorithm is minimum initial mass of the space vehicle after staging of the initial high-thrust rocket and tankage, for a given final payload mass back at Earth. If desired, the optimum distribution between high thrust and low thrust can be obtained by running a sequence of cases with

varying amounts of high thrust. For each case in such a sequence, the algorithm optimizes the low-thrust propulsion not only with respect to the trajectory, but also with respect to the two sets of propulsion system parameters. The trajectory optimization includes optimization of the distribution of leg times and of launch date for fixed trip time and stay time at the destination planet. It also includes optimization of the directions of the hyperbolic excess velocities due to the high thrust.

Governing Equations for Constant-Thrust Case

Because the objective function for this problem is minimum initial mass for a given final payload, the mass fraction is defined somewhat differently than in the previous formulations. The objective function

$$Z = K\mu(0) \tag{VIII-1}$$

is to be minimized where the mass fraction is

$$\mu(t) = \frac{m(t)}{m_p} \tag{VIII-2}$$

and m_p is the final payload mass. The differential equations that must be satisfied in thrusting regions are the following.

$$\ddot{X}_i = \left(\frac{2\eta\mu_{w\upsilon}}{a_{w\upsilon}c_\upsilon}\right)^{1/2}\left(\frac{\dot{\lambda}_\mu}{p}\right)^{1/2}\frac{\lambda_i+3}{p} - \frac{X_i}{r^3}\,,\quad i = 1,2,3 \tag{VIII-3}$$

$$\ddot{\lambda}_{i+3} = -\frac{\lambda_{i+3}}{r^3} + \frac{3X_i}{r^5}\sum_{j=1}^{3}\lambda_{j+3}X_j \tag{VIII-4}$$

$$\ddot{\lambda}_\mu = \frac{2}{c_\upsilon}\left(\frac{2\eta_\upsilon\mu_{w\upsilon}}{a_{w\upsilon}c_\upsilon}\right)^{1/2}\frac{\dot{\lambda}_\mu^{3/2}}{p^{1/2}} + \frac{\dot{\lambda}_\mu\dot{p}}{p} \tag{VIII-5}$$

where $\nu = \begin{cases} 1 \text{ for outbound leg } (0 \le t \le T_a),\ T_a = \text{planetary arrival time} \\ 2 \text{ for inbound leg } (T_b \le t \le T),\ T_b = \text{planetary departure time} \end{cases}$

During coasting periods the system becomes

$$\ddot{x}_i = - \frac{x_i}{r^3} \tag{VIII-6}$$

$$\dot{\lambda}_\mu = 0 ; \quad \lambda_\mu(t) = \lambda_\mu(T_1) \tag{VIII-7}$$

in addition to Eq. (VIII-4) which remains the same. In Eq. (VIII-7), T_1 is the time at the beginning of the coast period.

The switching times between thrusting and coasting periods are governed by the switching function

$$\gamma = \frac{c_v p}{\mu} - \lambda_\mu$$

where

$$\mu = \left(\frac{2 \eta_v \mu_{wv} p}{a_{wv} c_v \dot{\lambda}_\mu} \right)^{1/2} \tag{VIII-8}$$

during thrusting periods and $\mu(t) = \mu(T_1)$ during coasting periods.

The transversality conditions that must be satisfied relating conditions at T_a and T_b (the times of arrival and departure at the destination planet) are the following.

$$\sum_{i=1}^{3} \left[V_\infty(a) \lambda_{i+3}(a) \frac{\lambda_{i+3}(a)}{p(a)} + V_\infty(b) \dot{\lambda}_{i+3}(b) \frac{\lambda_{i+3}(b)}{p(b)} \right]$$

$$+ \frac{2 \eta_1 \mu_{w_1}}{a_{w_1} c_1^2} \gamma_1(a) - \frac{2 \eta_2 \mu_{w_2}}{a_{w_2} c_1^2} \gamma_2(b) = 0 \tag{VIII-9}$$

$$\lambda_\mu(a) = \lambda_\mu(b) \tag{VIII-10}$$

From the fact that

$$\mu(b) = \mu(a) - (\mu_{w_1} + \mu_{F_1} + \mu_{s_1} + \mu_I) \qquad \text{(VIII-11)}$$

an additional relationship is obtained,

$$\dot{\lambda}_\mu(b) = \frac{2\eta_2 \mu_{w_2} p(b)}{a_{w_2} c_2} \left[\left(\frac{2\eta_1 \mu_{w_1} p(a)}{a_{w_1} c_1 \dot{\lambda}_\mu(a)} \right)^{1/2} - (\mu_{w_1} + \mu_{F_1} + \mu_{s_1} + \mu_I) \right]^{-1} \qquad \text{(VIII-12)}$$

Furthermore the boundary values of x_i and $\dot{x}_i$ must be related to the planetary position and velocity components, g_i and $\dot{g}_i$, at the times T_a and T_b.

$$x_i(a) = g_i(a); \; x_i(b) = g_i(b) \qquad \text{(VIII-13)}$$

$$\dot{x}_i(a) = \dot{g}_i(a) - V_\infty(a) \frac{\lambda_{i+3}(a)}{p(a)} ; \; \dot{x}_i(b) = \dot{g}_i(b) + V_\infty(b) \frac{\lambda_{i+3}(b)}{p(b)} \qquad \text{(VIII-14)}$$

Equations (VIII-9) through (VIII-14) provide sufficient internal boundary conditions for the system of differential equations, Eqs. (VIII-3), (VIII-4), and (VIII-5).

These conditions determine the optimum distribution of leg times for a given total trip time. It remains to provide information concerning the optimum launch date for the trip. This is provided by the following additional transversality condition.

$$\sum_{i=1}^{3} \left\{ \dot{\lambda}_{i+3}(T) \left[\dot{x}_i(T) - \dot{g}_i(T) \right] - \dot{\lambda}_{i+3}(0) V_\infty(0) \frac{\lambda_{i+3}(0)}{p(0)} \right\}$$

$$+ \frac{2\eta_1 \mu_{w_1}}{a_{w_1} c_1^2} \gamma_1(0) - \frac{2\eta_2 \mu_{w_2}}{a_{w_2} c_2^2} \gamma_2(T) = 0 \qquad \text{(VIII-15)}$$

$$2\lambda_\mu(a)\frac{\partial \mu_{F_1}}{\partial c_1} + \frac{2\eta_1\mu_{w_1}}{a_{w_1}c_1^3}\int_0^{Ta}\left[\left(2 - c_1\frac{d\ln\eta_1}{dc_1}\right)\left(\frac{c_1 p}{\mu} - \lambda_\mu\right) - \frac{c_1 p}{\mu}\right] dt = 0 \quad \text{(VIII-16)}$$

$$\lambda_\mu(a)\left(1 + \frac{\partial \mu_F}{\partial \mu_{w_1}}\right) - \frac{1}{\mu_{w_1}}\left[\mu(a)\lambda_\mu(a) - \mu(0)\lambda_\mu(0)\right] = 0 \quad \text{(VIII-17)}$$

$$\lambda_\mu(T)\frac{\partial \mu_{F_2}}{\partial c_2} + \frac{2\eta_2\mu_{w_2}}{a_{w_2}c_2^3}\int_{Tb}^{T}\left[\left(2 - c_2\frac{d\ln\eta_2}{dc_2}\right)\left(\frac{c_2 p}{\mu} - \lambda_\mu\right) - \frac{c_2 p}{\mu}\right] dt = 0 \quad \text{(VIII-18)}$$

$$\lambda_\mu(T)\left(1 + \frac{\partial \mu_{F_2}}{\partial \mu_{w_2}}\right) - \frac{1}{\mu_{w_2}}\left[\mu(T)\lambda_\mu(T) - \mu(b)\lambda_\mu(b)\right] = 0 \quad \text{(VIII-19)}$$

Transversality Conditions for Variable-Thrust Case

The corresponding variable-thrust solution of the round-trip stopover mission is required as a starting approximation. The system of differential equations is the same as usual. Corresponding to Eqs. (VIII-9) and (VIII-15) for the constant-thrust case, the variable-thrust transversality conditions are

$$\frac{p^2(a)}{2} - \frac{p^2(b)}{2} + \sum_{i=1}^{3}\left[\dot{\lambda}_{i+3}(a)V_\infty(a)\frac{\lambda_{i+3}}{p}(a) + \dot{\lambda}_{i+3}(b)V_\infty(b)\frac{\lambda_{i+3}}{p}\right] = 0 \quad \text{(VIII-20)}$$

$$\frac{p^2(0)}{2} - \frac{p^2(T)}{2} + \sum_{i=1}^{3}\lambda_{i+3}(T)\left[\dot{x}_i(T) - \dot{g}_i(T)\right] - \sum_{i=1}^{3}\lambda_{i+3}(0)V_\infty(0)\frac{\lambda_{i+3}(0)}{p(0)} = 0 \quad \text{(VIII-21)}$$

Round-Trip Flyby Mission (Variable Thrust)

The only way to avoid large amounts of machine time and tedious matching of boundary conditions at the destination planet in the optimization of the trajectory for the round-trip flyby is to employ internal transversality conditions and solve the outbound and inbound legs simultaneously. Unfortunately these conditions for the variable-thrust starting solution are sufficiently complicated to raise the question of whether the corresponding constant-thrust system may defy numerical solution. If such is the case, an alternative would be to use the variable-thrust solution to supply fixed internal boundary conditions for the constant-thrust solution. Such boundary conditions would be very close to optimum, and if the exact optimum is desired a numerical search procedure could be employed.

The effect of the planetary encounter at flyby is to change the space vehicle's velocity vector. In the standard approximation of separating heliocentric and planetocentric motion, this velocity change is considered to be impulsive. As a result of the encounter, the velocity vector in the planetocentric frame undergoes an orthogonal transformation, the matrix of which depends upon the periradius of the planetary encounter, the planetocentric energy, and the orientation of the plane of the planetocentric hyperbola.

If the planet ideally were considered to be a mathematical focus of gravitational attraction, then any $\vec{V}_\infty$ vector could be rotated into any direction by proper selection of the periradius. However, one must consider the inequality constraint imposed by the fact that the periradius cannot be less than a lower bound imposed by the radius of the sensible atmosphere of the planet.

Instead of optimizing subject to the inequality constraint, the problem can be treated in two parts. First, the problem is solved subject to no constraint on the periradius. If the optimum periradius turns out to be less than the imposed lower bound, the problem is solved again fixing the periradius at the lower bound. This is the same procedure used to handle the inequality constraint on the final reentry velocity. The technique also allows one to specify any desired value for the periradius.

General Transversality Conditions for Round-Trip Flyby

Since the variable-thrust equations of motion and Euler-Lagrange equations for this mission are the standard ones, only the various transversality conditions will be given. The general transversality conditions for the round-trip flyby are

$$\left[- H dt + \sum_{i=1}^{3} (- \dot{\lambda}_{i+3} dx_i + \lambda_{i+3} d\dot{x}_i) \right]_0^T = 0 \qquad \text{(VIII-22)}$$

$$\left[- H dt + \sum_{i=1}^{3} (- \dot{\lambda}_{i+3} dx_i + \lambda_{i+3} d\dot{x}_i) \right]_{T_a - \epsilon}^{T_a + \epsilon} = 0$$

(VIII-23)

where T_a is the time of flyby. Equation (VIII-22) determines the best launch date for the round trip. For the case of a given V_∞ at t = o and velocity open (flyby) at t = T, Eq. (VIII-22) gives

$$\lambda_{i+3}(T) = 0 \qquad (i = 1, 2, 3.)$$

(VIII-24)

$$- \frac{p(T)^2}{2} + \sum_{i=1}^{3} \dot{\lambda}_{i+3}(T) \left[\dot{x}_i(T) - \dot{g}_i(T) \right] + \frac{p(0)^2}{2} - \sum_{i=1}^{3} \dot{\lambda}_{i+3}(0) V_\infty(0) \frac{\lambda_{i+3}(0)}{p(0)} = 0$$

(VIII-25)

The second condition, Eq. (VIII-23), determines the best flyby time and the optimum characteristics of the planetary encounter. The latter, of course, depend upon the constraint on the periradius. It is instructive to first consider the case where there is no planetary perturbation. This corresponds to a very large periradius of the encounter. For this case Eq. VIII-23 gives

$$\vec{p}(T_a + \epsilon) = \vec{p}(T_a - \epsilon)$$

(VIII-26)

and

$$\vec{\dot{p}} \cdot (\vec{\nu} - \vec{\dot{g}}) \Big|_{T_a - \epsilon}^{T_a + \epsilon} = 0$$

(VIII-27)

The more general conditions must reduce to Eqs. (VIII-26) and (VIII-27) in the limit as the periradius goes to infinity.

Transversality Conditions for Periradius Unconstrained

Next, consider the case where the periradius is completely unconstrained. In the planetocentric frame of reference the orthogonal transformation of the $\vec{V}_\infty$ vector is represented by a 3 x 3 matrix $A \equiv [a_{ij}]$.

$$\vec{V}_\infty(T_a + \epsilon) = AV_\infty(T_a - \epsilon) \tag{VIII-28}$$

The orthogonal, unimodular matrix A can be specified by three independent Euler angles ψ, θ, and φ.

$$A = \begin{pmatrix} \cos\Psi\cos\phi - \cos\theta\sin\phi\sin\Psi & -\sin\Psi\cos\phi - \cos\theta\sin\phi\cos\Psi & \sin\theta\sin\phi \\ \cos\Psi\sin\phi + \cos\theta\cos\phi\sin\Psi & -\sin\Psi\sin\phi + \cos\theta\cos\phi\cos\Psi & -\sin\theta\cos\phi \\ \sin\theta\sin\Psi & \sin\theta\cos\Psi & \cos\theta \end{pmatrix} \tag{VIII-29}$$

In terms of heliocentric vectors, Eq. (VIII-28) is

$$\vec{\nu}(T_a + \epsilon) = \vec{\bar{g}}(T_a + \epsilon) + A\left[\vec{\nu}(T_a - \epsilon) - \vec{\bar{g}}(T_a - \epsilon)\right] \tag{VIII-30}$$

which becomes upon differentiation

$$d\vec{\nu}(T_a + \epsilon) = \dot{\vec{\bar{g}}}(T_a + \epsilon)\,dt(T_a + \epsilon) + A\left[d\vec{\nu}(T_a - \epsilon) - \dot{\vec{\bar{g}}}(T_a - \epsilon)\,dt(T_a - \epsilon)\right]$$
$$+ dA\left[\vec{\nu}(T_a - \epsilon) - \vec{\bar{g}}(T_a - \epsilon)\right] \tag{VIII-31}$$

where the matrix $dA = [da_{ij}]$. For example,

$$da_{11} = -(\sin\Psi\cos\phi + \cos\Psi\sin\phi\cos\theta)d\Psi - (\cos\Psi\sin\phi + \sin\Psi\cos\phi\cos\theta)d\phi + \sin\Psi\sin\phi\sin\theta\, d\theta, \text{ etc.} \tag{VIII-32}$$

When the components of Eq. (VIII-31) are substituted into the general transversality condition, Eq. (VIII-23), and the coefficients of the independent variations, $dt(T_a - \epsilon)$, $d\dot{x}_i\ (T_a - \epsilon)$, $d\psi$, $d\varphi$, and $d\theta$, are set equal to zero, the following conditions result.

$$\vec{p}(T_a + \epsilon) = A\vec{p}(T_a + \epsilon) \tag{VIII-33}$$

$$\vec{\vec{p}}\cdot(\vec{\nu} - \vec{\vec{g}})\Big|_{T_a - \epsilon}^{T_a + \epsilon} = 0 \tag{VIII-34}$$

$$B\vec{p}(T_a + \epsilon) = 0 \tag{VIII-35}$$

where

$$B = \left[b_{ij}\right] \quad (i, j = 1, 2, 3) \quad \text{and}$$

$$b_{11} = a_{21}\dot{X}_1(T_a - \epsilon) + a_{22}\dot{X}_2(T_a - \epsilon) + a_{23}\dot{X}_3(T_a - \epsilon) \tag{VIII-36}$$

$$b_{12} = -a_{11}\dot{X}_1(T_a - \epsilon) - a_{12}\dot{X}_2(T_a - \epsilon) - a_{13}\dot{X}_3(T_a - \epsilon) \tag{VIII-37}$$

$$b_{13} = 0 \tag{VIII-38}$$

$$b_{21} = -a_{12}\dot{X}_1(T_a - \epsilon) + a_{11}\dot{X}_2(T_a - \epsilon) \qquad \text{(VIII-39)}$$

$$b_{22} = -a_{22}\dot{X}_1(T_a - \epsilon) + a_{21}\dot{X}_2(T_a - \epsilon) \qquad \text{(VIII-40)}$$

$$b_{23} = -a_{32}\dot{X}_1(T_a - \epsilon) + a_{31}\dot{X}_2(T_a - \epsilon) \qquad \text{(VIII-41)}$$

$$b_{31} = a_{13}a_{31}\dot{X}_1(T_a - \epsilon) + a_{13}a_{32}\dot{X}_2(T_a - \epsilon) + a_{13}a_{33}\dot{X}_3(T_a - \epsilon) \qquad \text{(VIII-42)}$$

$$b_{32} = a_{23}a_{31}\dot{X}_1(T_a - \epsilon) + a_{23}a_{32}\dot{X}_2(T_a - \epsilon) + a_{23}a_{33}\dot{X}_3(T_a - \epsilon) \qquad \text{(VIII-43)}$$

$$b_{33} = a_{31}a_{33}\dot{X}_1(T_a - \epsilon) + a_{32}a_{33}\dot{X}_2(T_a - \epsilon) + (1 - a_{33}^2)\dot{X}_3(T_a - \epsilon) \qquad \text{(VIII-44)}$$

Equation (VIII-33) corresponds to Eq. (VIII-26) for the unperturbed case, and Eq. (VIII-34), which determines the optimum flyby time, has exactly the same form as its opposite for the unperturbed case, Eq. (VIII-27). The additional vector equation, Eq. (VIII-35), has to do with determining the optimum values of the three Euler angles, ψ, φ, and θ, in the rotation matrix A. Altogether at the flyby point, thirteen quantities must be determined, i.e., the time, 3 position coordinates, 6 velocity components (3 at $T_a - \epsilon$ and 3 at $T_a + \epsilon$), and the three Euler angles. The equations of transversality, Eqs. (VIII-33), (VIII-34), and (VIII-35), supply 7 of the required 13 conditions. Equation (VIII-30), relating the vehicle velocity at $T_a + \epsilon$ to that at $T_a - \epsilon$, supplies 3 more of them. Finally the ephemeris equation, $\vec{r} = \vec{g}(t)$, supplies the remaining 3 conditions for the position coordinates. Thus the equations presented above supply sufficient information to determine the internal boundary values at the flyby point.

Round-Trip Flyby Transversality with Periplanet Radius Fixed

Finally it is shown how the above conditions must be modified in order to constrain the periplanet radius to a fixed value. For given values of periplanet radius and hyperbolic excess velocity, the angle θ between the incoming and out-

going asymptotes is fixed. This means that only two of the three Euler angles in the rotation matrix A may be varied independently. This additional constraint may be expressed as a constraint on the trace of A.

$$\chi \equiv a_{11} + a_{22} + a_{33} = 1 + 2\cos\theta = 3 - \frac{4}{e^2} \qquad \text{(VIII-45)}$$

where e is the eccentricity of the planetocentric hyperbola. The eccentricity is related to the hyperbolic excess velocity simply by

$$e = 1 + K^2 V_\infty^2 = 1 + K^2(\vec{\nu}(T_a - \epsilon) - \vec{g}(T_a))^2 \qquad \text{(VIII-46)}$$

where V_∞ is in EMOS and $K = \sqrt{\mu_s r_p / \mu_p (1\,AU)}$. Substituting Eq. (VIII-46) into Eq. (VIII-45),

$$(1 + K^2 V_\infty^2)^2 \chi = 3(K^2 V_\infty^2 + 2) K^2 V_\infty^2 - 1 \qquad \text{(VIII-47)}$$

and differentiating,

$$(1 + K^2 V_\infty^2)^2 d\chi = \frac{8k^2}{1 + k^2 V_\infty^2} dV_\infty^2 \qquad \text{(VIII-48)}$$

In terms of the Euler angles

$$\chi = (1 + \cos\theta)\cos(\Psi + \phi) + \cos\theta \qquad \text{(VIII-49)}$$

and

$$d\chi = -(1 + \cos\theta)\sin(\Psi + \phi)(d\Psi + d\phi) - \left[1 + \cos(\Psi + \phi)\right]\sin\theta\, d\theta \qquad \text{(VIII-50)}$$

while

$$dV_\infty^2 = \sum_{i=1}^{3} \left\{ \left[2\dot{X}_i(T_a - \epsilon) - 2\dot{g}_i \right] d\dot{X}_i(T_a - \epsilon) + \left[2\dot{g}_i - 2\dot{X}_i(T_a - \epsilon) \right] \ddot{g}_i \, dt(T_a) \right\} \tag{VIII-51}$$

Using Eq. (VIII-48), the variation $d\theta$ can be solved for in terms of the other variations. Then this can be substituted for the variation $d\theta$ in the general transversality condition, Eq. (VIII-23). The difference between this case and the unconstrained case is that, in the latter, $d\theta$ was another independent variation. Since the algebra is rather involved only the resulting conditions will be presented. To shorten the notation the following functions are defined.

$$F(\theta, \Psi, \phi) \equiv -\frac{(1+\cos\theta)\sin(\Psi+\phi)}{\sin\theta(1+\cos(\Psi+\phi))} \tag{VIII-52}$$

$$G(\Psi, \phi, \theta, \dot{X}_i(-\epsilon)) = -\frac{8k^2}{\left[1+\cos(\Psi+\phi)\right]\sin\theta\,(1+K^2V_\infty^2)^2} \tag{VIII-53}$$

$$b'_{31} \equiv \frac{b_{31}}{\sqrt{1-a_{33}^2}} \; ; \quad b'_{32} \equiv \frac{b_{32}}{\sqrt{1-a_{33}^2}} \; ; \quad b'_{33} \equiv \frac{b_{33}}{\sqrt{1-a_{33}^2}} \tag{VIII-54}$$

$$G' \equiv G\left[b'_{31}\lambda_4(T_a+\epsilon) + b'_{32}\lambda_5(T_a+\epsilon) + b'_{33}\lambda_6(T_a+\epsilon) \right] \tag{VIII-55}$$

Employing the above definitions, the resulting transversality conditions for the constrained periradius case may be written as follows.

$$\vec{p}\,(T_a+\epsilon) = A\vec{p}\,(T_a-\epsilon) - 2G'A\left[\vec{\nu}\,(T_a-\epsilon) - \vec{\dot{g}}(T_a)\right] \tag{VIII-56}$$

$$\left[-\frac{p^2}{2} + \dot{\vec{p}} \cdot (\vec{\nu} - \dot{\vec{g}}) \right]_{T_a - \epsilon}^{T_a + \epsilon} = 0 \qquad \text{(VIII-57)}$$

$$\sum_{i=1}^{2} b_{1i} \lambda_{i+3}(T_a + \epsilon) + F \sum_{i=1}^{3} b'_{3i} \lambda_{i+3}(T_a + \epsilon) = 0 \qquad \text{(VIII-58)}$$

$$\sum_{i=1}^{3} (b_{2i} + F b_{3i}) \lambda_{i+3}(T_a + \epsilon) = 0 \qquad \text{(VIII-59)}$$

It is seen from Eq. (VIII-56) that the primer vector no longer undergoes a simple orthogonal transformation at flyby, but the norm of $\vec{p}$ changes depending in part on the hyperbolic excess velocity. This being the case, the norm of $\vec{p}$ appears in Eq. (VIII-57), but otherwise Eq. (VIII-57) has the same form as for the unconstrained case, Eq. (VIII-34). The three equations determining the optimum values of the Euler angles are Eqs. (VIII-47), (VIII-58), and (VIII-59). Again there are 13 internal boundary conditions to be specified and 13 equations.

Analysis of Analytic Coast Solutions

A major limitation to the finite difference Newton-Raphson algorithm for solving systems of nonlinear differential equations with split boundary conditions is its large requirement of computer storage. Among other factors, the storage requirement depends directly upon the number of mesh points employed for a particular problem. In the particular case of constant-thrust-with-coast trajectory optimization problems the algorithm has always been used to numerically solve the whole trajectory including the coasting regions. But it is well known that analytic solutions exist for both the trajectory and the associated primer vector in coasting regions. If these analytic solutions could be coupled with the numerical problem at the switching points a great many mesh points would no longer be needed, thereby permitting a reduction of computer storage requirements for a given problem.

Generally speaking, the cases that make the most severe demands upon computer storage are the trajectories to the outer solar system (Jupiter and beyond) and these trajectories usually involve coast periods which constitute a major portion

of the trip. Consequently, while the great majority of these cases cannot be handled conventionally within the limitations of core storage, substitution of the analytic solutions for the numerical solutions in the coast region will permit the treatment of many of these difficult cases within the confines of core storage.

Analytic Solution of the Equations of Motion

Let the two switching times with a coast between them be T_1 and T_2. The state and primer vector at T_1 ($\vec{r}_1$, $\vec{v}_1$, $\vec{p}_1$, $\dot{\vec{p}}_1$) completely determine these same quantities at T_2 ($\vec{r}_2$, $\vec{v}_2$, $\vec{p}_2$, $\dot{\vec{p}}_2$) through the analytic solutions of the equations of motion and the Euler-Lagrange equations over the coasting arc. Including the three components of the position, velocity, the primer vectors, the time derivative of the primer vector, and the time, there are thirteen quantities to be related across the coast period. The same number of equations is needed for the analytic solutions.

The first six equations relating the states at T_1 and T_2 are provided by Ref. VIII-6 in the form of the two vector equations,

$$\vec{r}_2 = \left[1 - \frac{r_2}{|\vec{r}_1 \times \vec{v}_1|}\left(1 - \frac{\vec{r}_1 \cdot \vec{r}_2}{r_1 r_2}\right)\right]\vec{r}_1 + \frac{|\vec{r}_1 \times \vec{r}_2|}{|\vec{r}_1 \times \vec{v}_1|}\,\epsilon(\vec{r}_1, \vec{r}_2)\,\vec{v}_1 \qquad \text{(VIII-60)}$$

and

$$\vec{v}_2 = \left[\frac{\vec{r}_1 \cdot \vec{v}_1}{r_1 |\vec{r}_1 \times \vec{v}_1|^2}\left(1 - \frac{\vec{r}_1 \cdot \vec{r}_2}{r_1 r_2}\right) - \frac{|\vec{r}_1 \times \vec{r}_2|}{r_1^2 r_2 |\vec{r}_1 \times \vec{v}_1|}\right]\vec{r}_1 + \left[1 - \frac{r_1}{|\vec{r}_1 \times \vec{v}_1|^2}\left(1 - \frac{\vec{r}_1 \cdot \vec{r}_2}{r_1 r_2}\right)\right]\vec{v}_1$$

(VIII-61)

where

$$\epsilon(\vec{r}_1, \vec{r}_2) = \begin{cases} +1 \text{ if } (\vec{r}_1 \times \vec{r}_2)_3 \geq 0 \\ -1 \text{ if } (\vec{r}_1 \times \vec{r}_2)_3 < 0 \end{cases}$$

Depending upon the total energy, the switching times are related by one of the following two equations.

$$T_2 - T_1 = a^{3/2}\left[\sin^{-1}\left(\frac{\vec{r}_2\cdot\vec{v}_2}{e\sqrt{a}}\right) - \sin^{-1}\left(\frac{\vec{r}_1\cdot\vec{v}_1}{e\sqrt{a}}\right) - \frac{1}{\sqrt{a}}\left(\vec{r}_2\cdot\vec{v}_2 - \vec{r}_1\cdot\vec{v}_1\right)\right] \tag{VIII-62}$$

$$T_2 - T_1 = a^{3/2}\left[-\sinh^{-1}\left(\frac{\vec{r}_1\cdot\vec{v}_1}{e\sqrt{a}}\right) + \sinh^{-1}\left(\frac{\vec{r}_2\cdot\vec{v}_2}{e\sqrt{a}}\right) + \frac{1}{\sqrt{a}}\left(\vec{r}_2\cdot\vec{v}_2 - \vec{r}_1\cdot\vec{v}_1\right)\right] \tag{VIII-63}$$

where

$$e = \left[|\vec{r}_1 \times \vec{v}_1|^2\left(\frac{\vec{r}_1\cdot\vec{v}_1}{r_1}\right)^2 + \left(\frac{|\vec{r}_1 \times \vec{v}_1|^2}{r_1} - 1\right)^2\right]^{1/2} \tag{VIII-64}$$

and

$$a = \frac{|\vec{r}_1 \times \vec{v}_1|^2}{|(1-e^2)|}$$

Equations VIII-62 and VIII-63 are applicable for $e < 1$ and $e > 1$ respectively.

Analytic Solution of the Euler-Lagrange Equations

The primer vector solution is taken from Ref. VIII-5. In addition to a and e, a number of other auxiliary parameters are employed in expressing the solution but all of these parameters are directly expressible in terms of $\vec{r}_1$, $\vec{v}_1$ $\vec{r}_2$, and $\vec{v}_2$.

These additional auxiliary parameters are Ω, I, ω, f_1, f_2. First, it is shown how each is expressible exlusively in terms of the state at T_1 and T_2. Define a unit vector $\vec{n}$ normal to the plane of the coasting arc.

$$\vec{n} = \frac{\vec{r}_1 \times \vec{r}_2}{r_1 r_2} \tag{VIII-66}$$

Then $\cos I = \vec{n} \cdot \vec{k}$ (1st quadrant) (VIII-67)

Let $\vec{n}'$ be the projection of $\vec{n}$ on the x-y plane.

$$\vec{n}' = \vec{i}\, n_x + \vec{j}\, n_y \tag{VIII-68}$$

Then for the longitude of the ascending node,

$$\cos \Omega = \frac{(\vec{n} \times \vec{n}')_1}{|\vec{n} \times \vec{n}'|} \tag{VIII-69}$$

and

$$\sin \Omega = \frac{(\vec{n} \times \vec{n}')_2}{|\vec{n} \times \vec{n}'|} \tag{VIII-70}$$

The true anomalies at the switching times T_1 and T_2 are given by

$$\cos f_1 = \frac{|\vec{r}_1 \times \vec{v}_1|^2}{r_1 e} - \frac{1}{e}, \quad \cos f_2 = \frac{|\vec{r}_2 \times \vec{v}_2|^2}{r_2 e} - \frac{1}{e} \tag{VIII-71}$$

where r, v are vectors at the respective switching points.

In Ref. VIII-5, Lawden gives the following analytic solution for the primer vector over a coasting arc.

$$\begin{aligned} \vec{p}' = {} & A - B\sin f + C(I_1 \cos f - I_2)\sin F - \frac{(D - A\sin f)\sin f}{1 + \cos F} \quad B(e + \cos f) \\ & + C(I_1 \sin^2 f + I_2)\cos f + \frac{(D - A\sin f)\cos f}{1 + e\cos f} \quad \frac{E\cos f + F\sin f}{1 + e\cos f} \end{aligned} \tag{VIII-72}$$

where I_1 and I_2 are defined below.

$$I_1 = \frac{1}{2(1-e^2)}\tan\frac{f}{2} - \frac{1}{2(1+e)}\cot\frac{f}{2} - \frac{6e^2}{(1-e^2)^{5/2}}\tan^{-1}\left(\sqrt{\frac{1-e}{1+e}}\tan\frac{f}{2}\right) + \frac{e^3}{(1+e^2)^2}\frac{\sin f}{1+e\cos f}; \quad (e<1) \tag{VIII-73}$$

$$I_1 = \frac{1}{2(e^2-1)}\tan\frac{f}{2} - \frac{1}{2(e+1)}\cot\frac{f}{2} - \frac{6e^2}{(e^2-1)^{5/2}}\tanh^{-1}\left(\sqrt{\frac{e-1}{e+1}}\tan\frac{f}{2}\right) + \frac{e^3}{(e^2+1)^2}\frac{\sin f}{1+e\cos f}; \quad (e>1) \tag{VIII-74}$$

$$I_1 = \frac{1}{40}\tan^5\frac{f}{2} + \frac{1}{8}\tan^3\frac{f}{2} + \frac{3}{8}\tan\frac{f}{2} - \frac{1}{8}\cot\frac{f}{2}; \quad (e=1) \tag{VIII-75}$$

$$I_2 = \frac{\cot f}{e(1+e\cos f)} + (1+e\cos f)\frac{I_1}{e}; \quad (e\neq 0) \tag{VIII-76}$$

In Eq. VIII-72, A through F are constants of integration to be determined by boundary conditions. Actually it is not necessary to determine any of these constants since what is required is an expression relating the primer vectors at T_1 with that at T_2 of the same coasting arc.

The components of $\vec{p}'$ in Eq. VIII-72 are referred to a coordinate system where the x and y axes are in the plane of the coasting arc and the x axis is in the direction of the perihelion. Since, in the Newton-Raphson algorithm, the primer vector is expressed in the standard frame with the x axis in the direction of the

vernal equinox and the z axis perpendicular to ecliptic plane, it is necessary to transform p into this system. For this purpose the following three rotation matrices are defined.

$$Q \equiv \begin{pmatrix} \cos w & -\sin w & 0 \\ \sin w & \cos w & 0 \\ 0 & 0 & 1 \end{pmatrix} \tag{VIII-77}$$

$$A \equiv \begin{pmatrix} 1 & 0 & 0 \\ 0 & \cos I & -\sin I \\ 0 & \sin I & \cos I \end{pmatrix} \tag{VIII-78}$$

$$S \equiv \begin{pmatrix} \cos\Omega & -\sin\Omega & 0 \\ \sin\Omega & \cos\Omega & 0 \\ 0 & 0 & 1 \end{pmatrix} \tag{VIII-79}$$

$$\vec{p} = QRS\,\dot{\vec{p}} \tag{VIII-80}$$

Now, in order to relate the primer vector at T_1 with the same at T_2, it is necessary to solve Eq. VIII-72 and its time derivative for the 6-dimensional column vector of integration constants. To facilitate this operation the following matrix elements are defined.

$$a_{11}(\vec{r},\vec{v}) = 1 + \frac{\sin^2 f}{1 + e\cos f} \tag{VIII-81}$$

$$a_{12} = -\sin f \qquad \text{(VIII-82)}$$

$$a_{13} = I_1(f)\cos f - I_1(f) \qquad \text{(VIII-83)}$$

$$a_{14} = \frac{\sin f}{1 + e\cos f} \qquad \text{(VIII-84)}$$

$$a_{15} = a_{16} = 0 \qquad \text{(VIII-85)}$$

$$a_{21} = -\frac{\sin f \cos f}{1 + e\cos f} \qquad \text{(VIII-86)}$$

$$a_{22} = e + \cos f \qquad \text{(VIII-87)}$$

$$a_{23} = \sin^2 f\, I_1(f) + \cos f\, I_2(f) \qquad \text{(VIII-88)}$$

$$a_{24} = \frac{\cos f}{1 + e\cos f} \qquad \text{(VIII-89)}$$

$$a_{25} = a_{26} = 0 \qquad \text{(VIII-90)}$$

$$a_{31} = a_{32} = a_{33} = a_{34} \equiv 0 \qquad \text{(VIII-91)}$$

$$a_{35} = \frac{\cos f}{1 + e\cos f} \qquad \text{(VIII-92)}$$

$$a_{36} = \frac{\sin f}{1 + e\cos f} \qquad \text{(VIII-93)}$$

$$a_{41} = \frac{|\vec{r} \times \vec{v}|}{r^2}\left[\frac{2\sin f\cos f}{1 + e\cos f} - \frac{e\sin^3 f}{(1 + e\cos f)^2}\right] \qquad \text{(VIII-94)}$$

$$a_{42} = \frac{|\vec{r} \times \vec{v}|}{r^2}\cos f \qquad \text{(VIII-95)}$$

$$a_{43} = \frac{|\vec{r} \times \vec{v}|}{r^2}\left[\cos f\left(I_1 + \frac{dI_1}{df}\right) - \sin f\, I_1 - \frac{dI_2}{df}\right] \qquad \text{(VIII-96)}$$

$$a_{44} = -\frac{|\vec{r} \times \vec{v}|}{r^2}\left[\frac{e\cos 2f + e\cos f}{(1 + e\cos f)^2}\right] \qquad \text{(VIII-97)}$$

$$a_{45} = a_{46} = 0 \qquad \text{(VIII-98)}$$

$$a_{51} = \frac{|\vec{r} \times \vec{v}|}{r^2}\left[\frac{e\cos^3 f - \cos 2f}{(1+e\cos f)^2}\right] \qquad \text{(VIII-99)}$$

$$a_{52} = -\frac{|\vec{r} \times \vec{v}|}{r^2}\sin f \qquad \text{(VIII-100)}$$

$$a_{53} = \frac{|\vec{r} \times \vec{v}|}{r^2}\left[\sin^2 f I_1 + \sin^2 f \frac{dI_1}{df} - \sin f\, I_2 + \cos f \frac{dI_2}{df}\right] \qquad \text{(VIII-101)}$$

$$a_{54} = -\frac{|\vec{r} \times \vec{v}|}{r^2}\frac{\sin f}{(1+e\cos f)^2} \qquad \text{(VIII-102)}$$

$$a_{55} = a_{56} = 0 \qquad \text{(VIII-103)}$$

$$a_{61} = a_{62} = a_{63} = a_{64} = 0 \qquad \text{(VIII-104)}$$

$$a_{65} = -\frac{\sin f}{|\vec{r} \times \vec{v}|} \qquad \text{(VIII-105)}$$

$$a_{66} = \frac{e + \cos f}{|\vec{r} \times \vec{v}|} \qquad \text{(VIII-106)}$$

These elements a_{ij} define a 6 x 6 matrix.

$$N \equiv (a_{ij}) \quad (i,j = 1,2,\ldots,6) \tag{VIII-107}$$

If further the six-dimensional column vectors $\vec{P}$ and $\vec{C}$ are defined by

$$\vec{p}' \equiv \begin{pmatrix} p_1' \\ p_2' \\ p_3' \\ \dot{p}_1' \\ \dot{p}_2' \\ \dot{p}_3' \end{pmatrix} \quad ; \quad \vec{C} \equiv \begin{pmatrix} A \\ B \\ C \\ D \\ E \\ F \end{pmatrix} \tag{VIII-108}$$

then,

$$\vec{P}' = N\vec{C} \tag{VIII-109}$$

Since the matrices Q, R, and S, given in Eqs. VIII-77 to VIII-79, do not depend on time, differentiating Eq. VIII-80 simply gives

$$\dot{\vec{p}} = Q\,R\,S\,\dot{\vec{p}}' \tag{VIII-110}$$

Equations VIII-80 and VIII-110 are both expressed by

$$\vec{P} = M\vec{P}' \tag{VIII-111}$$

where M is a 6 x 6 matrix defined by

$$M \equiv \begin{pmatrix} QRS & 0 \\ 0 & QRS \end{pmatrix} \tag{VIII-112}$$

Eliminating $\vec{P}'$ between Eqs. VIII-109 and VIII-111 gives

$$\vec{P} = M N \vec{C} \qquad \text{(VIII-113)}$$

Equation VIII-113 is a function of time which can be written for the two switching times T_1 and T_2

$$\vec{P}(T_1) = M N(T_1) \vec{C} \qquad \text{(VIII-114)}$$

$$\vec{P}(T_2) = M N(T_2) \vec{C} \qquad \text{(VIII-115)}$$

Note that the 6 x 6 matrix M and the six-dimensional column vector of integration constants C are independent of time. Now $\vec{C}$ can be eliminated between Eq. VIII-14 and VIII-115 giving the relation between $\vec{P}(T_1)$ and $\vec{P}(T_2)$ that is sought.

$$\vec{P}(T_2) = MN(T_2) N^{-1}(T_1) M^{-1} \vec{P}(T_1) \qquad \text{(VIII-116)}$$

Both of the 6 x 6 matrices M and N can be easily inverted symbolically using Kramer's rule or Gaussian elimination.

The 13 equations that must be satisfied across a coast period are Eqs. VIII-60, -61, -62, and VIII-116. These 13 equations provide the same information as the numerical solution of the equations of motion and the Euler-Lagrange equations.

Section VIII References

VIII-1. Van Dine, C. P., W. R. Fimple, and T. N. Edelbaum: "Applications of a Finite-Difference Newton-Raphson Algorithm to Problems of Low-Thrust Trajectory Optimization". Progress in Astronautics and Aeronautics - Vol. 17 edited by R. L. Duncombe and V. G. Szebehely (Academic Press, Inc., New York, 1966) p. 377-400.

VIII-2. Fimple, W. R. and C. P. Van Dine: "Low Thrust Guidance Study" United Aircraft Research Laboratories Report E-910350-11 (Contract NAS8-20119) July 1966.

VIII-3. Titus, R. R., et al: "Study of Trajectories and Upper Stage Propulsion Requirements for Exploration of the Solar System", United Aircraft Research Laboratories Report E-910352-9 (Contract NAS2-2928), July 1966.

VIII-4. Melbourne, W. G. and C. G. Sauer, Jr.: "Payload Optimization for Power-Limited Vehicles". American Rocket Society Preprint 2370-62, March 1962.

VIII-5. Lawden, D. F.: Optimal Trajectories for Space Navigation (Butterworths, London, 1963).

VIII-6. Battin, B. H.: Astronautical Guidance, Ch. 2. McGraw-Hill, New York 1964.

Section VIII Nomenclature

a_{ij}	Matrix elements of rotation matrix
A	Rotation matrix
b_{ij}	Matrix elements defined by Eqs. (VIII-36) through (VIII-44)
B	Matrix $[b_{ij}]$
C	Exhaust velocity
e	Eccentricity
F	Function defined by Eq. (VIII-52)
$\bar{g}$	Planetary position vector
G	Function defined by Eq. (VIII-53)
H	Variational Hamiltonian
K	Arbitrary constant and also used as defined following Eq. (VIII-46)
m	Mass
$\bar{p}$	Primer vector = $\begin{matrix}\lambda_4\\ \lambda_5\\ \lambda_6\end{matrix}$
r	Radius
r_p	Periplanet radius
t	Time
T	Specific instant of time
$\bar{v}$	Velocity vector
$\bar{V}_\infty$	Hyperbolic excess velocity vector
x	Position coordinate
z	Objective function
α_w	Powerplant specific mass

Section VIII Nomenclature (contd.)

γ	Switching function defined by Eq. VIII-8
ϵ	Small change in time used in limit as $\epsilon \rightarrow 0$
η	Thrustor efficiency (function of exhaust velocity)
θ	Standard Euler angle
Θ	Rotation angle of $\bar{V}_\infty$
λ_i, λ_μ	Adjoint variable ($i = 1,\ldots 6$), adjoint variable or mass ratio
μ	Mass ratio defined by Eq. (VIII-2)
μ_F	Thrustor ratio (in the sense of Eq. VIII-2)
μ_I	Intermediate payload ratio
μ_S	Structure ratio
μ_W	Powerplant mass ratio
μ_s	Gravitational constant of the sun
μ_p	Gravitational constant of planet
ϕ	Standard Euler angle
X	Trace of rotation matrix
ψ	Standard Euler angle

APPENDIX A - PART 1

THE CALCULUS OF VARIATIONS APPLIED TO LOW-THRUST TRAJECTORY OPTIMIZATION

The objective of low-thrust propulsion system and trajectory optimization is generally to maximize that part of the final mass of the spacecraft defined as useful payload for a given mission (defined mathematically be a set of boundary conditions on position, velocity, and time). If the propulsion system is specified, and only the trajectory and control are to be optimized, the objective function is generally chosen to be maximum final mass.

Derivation of the Rocket Equation

The power limited constraint specifies that the power in the exhaust beam shall not exceed the power available, that is

$$\eta_c P \leq -\frac{1}{2}\dot{m}c^2 \tag{A-1}$$

It has been demonstrated that one always wants to use all of the power available so the equality of Eq. (A-1) must be used (Ref. A-1). The thrust acceleration is given by

$$a = -\frac{\dot{m}c}{m} \tag{A-2}$$

Eliminating the exhaust velocity between Eqs. (A-1) and (A-2) one obtains

$$\frac{dm}{m^2} = -\frac{1}{2}\frac{a^2}{\eta_c P}\,dt \tag{A-3}$$

and integrating from initial to final time gives the final mass.

$$\frac{1}{m(T)} = \frac{1}{m(0)} + \frac{1}{2}\int_0^T \frac{a^2}{\eta_c P}\,dt \tag{A-4}$$

The final mass is maximized if the integral in Eq. (A-4) is minimized. This is the problem of Lagrange in the calculus of variations, and is the most convenient way to express the completely unconstrained problem. When constraints are imposed on the thrust (magnitude and/or direction), however, it proves to be more convenient to express the problem in the Mayer form where it is desired to extremize a given function of the endpoints. The Lagrange problem can always be transformed into the Mayer problem by introducing an auxiliary state variable.

For example, the Lagrange problem of Eq. (A-4) is to minimize the functional

$$J = \int_0^T \frac{a^2}{2\eta_c P}\, dt \tag{A-5}$$

Introducing a new state variable, z , satisfying the constraint,

$$\dot{z} - \frac{a^2}{2\eta_c P} = 0 \tag{A-6}$$

then the new functional is

$$J = z(T) - z(0) \tag{A-7}$$

which is a function of the endpoints and therefore in the Mayer form. It is not surprising to find that

$$\dot{z} = \frac{a^2}{2\eta_c P}\ \frac{\dot{m}c^2}{2\eta_c P m^2} = -\frac{\dot{m}}{m^2} = \frac{d}{dt}\left(\frac{1}{m}\right) \tag{A-8}$$

i.e., the new state variable z is just the instantaneous reciprocal mass of the vehicle.

The Lagrange Problem

The basic problem of the calculus of variations is the Lagrange problem of determining n state functions x_i (t), (i = 1,...,n) which must take on certain prescribed boundary values at say t = 0 and t = T, such that the functional,

$$I = \int_0^T F(\dot{x}_i, x_i, t)\, dt \tag{A-9}$$

is stationary. In other words, find a path through phase space, x_i (t), such that weak variations about the path produce only higher-order changes in the functional, I.

These weak variations of the functions x_i (t) are denoted parametrically as follows:

$$x_i(\alpha_i, t) = x_i(0, t) + \alpha_i \eta_i(t) \tag{A-10}$$

$$\dot{x}_i(\alpha_i, t) = \dot{x}_i(0, t) + \alpha_i \dot{\eta}_i(t) \tag{A-11}$$

where the x_i (0,t) are by definition the functions which render I stationary, the α_i are a set of parameters, and the η_i (t) are a set of arbitrary functions which vanish at the endpoints 0 and T. The case where this restriction is removed will be treated later. The shorthand notation, $\delta x_i = \eta_i(t)\, d\alpha_i$ and $\delta \dot{x}_i = \dot{\eta}_i(t)\, d\alpha_i$ is useful where the δx_i are called the variations in the functions x_i (t).

If the functional I is stationary,

$$\delta I = 0 = \sum_{i=1}^{n} \left(\frac{\partial I}{\partial \alpha_i} \right)_{\alpha_i = 0} d\alpha_i \tag{A-12}$$

and

$$\begin{aligned} 0 &= \int_0^T \sum_{i=1}^{n} \left(\frac{\partial F}{\partial \dot{x}_i}\, \dot{\eta}_i + \frac{\partial F}{\partial x_i}\, \eta_i \right) d\alpha_i\, dt \\ 0 &= \int_0^T \sum_{i=1}^{n} \left(\frac{\partial F}{\partial \dot{x}_i} \delta \dot{x}_i + \frac{\partial F}{\partial x_i} \delta x_i \right) dt \end{aligned} \tag{A-13}$$

The first set of terms in the integral of Eq. (A-13) can be integrated by parts.

$$\sum_{i=1}^{n} \int_0^T \frac{\partial F}{\partial \dot{x}_i} \delta \dot{x}_i \, dt = \sum_{i=1}^{n} \frac{\partial F}{\partial \dot{x}_i} \delta x_i \Big|_0^T - \int_0^T \sum_{i=1}^{n} \frac{d}{dt} \left(\frac{\partial F}{\partial \dot{x}_i} \right) \delta x_i \, dt \qquad \text{(A-14)}$$

The first term on the right of Eq. (A-14) vanishes because the variations vanish at the endpoints. Substituting Eq. (A-14) back into Eq. (A-13) and multiplying by -1 gives

$$0 = \int_0^T \sum_{i=1}^{n} \left[\frac{d}{dt} \left(\frac{\partial F}{\partial \dot{x}_i} \right) - \frac{\partial F}{\partial x_i} \right] \delta x_i \, dt \qquad \text{(A-15)}$$

Since the variations δx_i are all independent and arbitrary, the only way Eq. (A-15) can be satisfied is for each coefficient to vanish separately.

$$\frac{d}{dt} \left(\frac{\partial F}{\partial \dot{x}_i} \right) - \frac{\partial F}{\partial x_i} = 0 \quad (i = 1, \ldots, n) \qquad \text{(A-16)}$$

The n Eqs. (A-16) are the Euler-Lagrange equations which, together with the 2n boundary conditions, define a path through phase space which renders the functional I stationary. Incidentally, if the integrand F in Eq. (A-9) contains higher-order derivatives such as $\ddot{x}_i$, the same techniques of successive integration by parts may be used to derive the corresponding form of the Euler-Lagrange equations. Alternatively Eqs. (A-16) may still be used if new state variables are defined ($\dot{v}_j \equiv \ddot{x}_i$) which limit the derivatives in F to first order.

Isoperimetric Problems

More complicated problems arise when constraints are imposed on the state variables. One of the simplest forms of constraint arises in the so-called isoperimetric problems. An example would be to find the form of a planar closed curve of given length which encloses maximum area. In the field of low-thrust trajectory optimization, another example would be to find the trajectory between two sets of boundary conditions which minimizes the trip time while maintaining the integral $J = \int_0^T a^2 \, dt$ equal to a given constant.

The isoperimetric problem is stated formally as follows. Find n functions $x_i(t)$ subject to 2n boundary conditions such that

$$I = \int_0^T F(\dot{x}_i, x_i, t) \, dt \qquad \text{(A-17)}$$

is stationary subject to the constraint,

$$J = \int_0^T G(\dot{x}_i, x_i, t)\, dt = \text{CONSTANT} \tag{A-18}$$

$$\delta I = 0 = \int_0^T \sum_{i=1}^{n} \left[\frac{\partial F}{\partial x_i} - \frac{d}{dt}\left(\frac{\partial F}{\partial \dot{x}_i}\right) \right] \delta x_i\, dt \tag{A-19}$$

and since J must be constant regardless of the variations x_i,

$$\delta J = 0 = \int_0^T \sum_{i=1}^{n} \left[\frac{\partial G}{\partial x_i} - \frac{d}{dt}\left(\frac{\partial G}{\partial \dot{x}_i}\right) \right] \delta x_i\, dt \tag{A-20}$$

The variations δx_i are not completely arbitrary as before since the functions x_i cannot be varied so as to violate Eq. (A-20). The coefficients of the δx_i in Eq. (A-19), therefore, cannot be set separately equal to zero.

Consider the Hilbert space (i.e., function space) defined by the infinite set of all functions of t defined on the interval 0 to T and which have homogeneous boundary conditions at the endpoints. The functions

$$f_i(t) \equiv \frac{\partial F}{\partial x_i} - \frac{d}{dt}\left(\frac{\partial F}{\partial \dot{x}_i}\right)$$

and

$$g_i(t) \equiv \frac{\partial G}{\partial x_i} - \frac{d}{dt}\left(\frac{\partial G}{\partial \dot{x}_i}\right)$$

are all members of this Hilbert space. For brevity the following inner product notation is defined.

$$\left\langle f_i \middle| \delta x_i \right\rangle \equiv \int_0^T f_i(t)\, \delta x_i(t)\, dt \tag{A-21}$$

Now, interchanging the integration and summation operations, Eqs. (A-19) and (A-20) can be rewritten as follows.

$$\sum_{i=1}^{n} \left\langle f_i \middle| \delta x_i \right\rangle = 0 \tag{A-22}$$

$$\sum_{i=1}^{n} \left\langle g_i \middle| \delta x_i \right\rangle = 0 \qquad \text{(A-23)}$$

Although the variations δx_i are not completely arbitrary as before, they are still independent (i.e., δx_i can be changed independently of δx_j). In order for Eqs. (A-22) and (A-23) to be satisfied, each term in the sums must vanish separately. Therefore

$$\left\langle f_i \middle| \delta x_i \right\rangle = 0 \quad (i=1,\ldots,n) \qquad \text{(A-24)}$$

$$\left\langle g_i \middle| \delta x_i \right\rangle = 0 \qquad \text{(A-25)}$$

Equations (A-25) show that δx_i is any function orthogonal to g_i. But Eqs. (A-24) show that f_i is also orthogonal to δx_i. Therefore f_i and g_i must be related by a constant λ.

$$f_i + \lambda g_i = 0 \qquad \text{(A-26)}$$

or

$$\frac{d}{dt}\left[\frac{\partial(F+\lambda G)}{\partial \dot{x}_i}\right] - \frac{\partial(F+\lambda G)}{\partial x_i} = 0 \quad (i=1,\ldots,n) \qquad \text{(A-27)}$$

Equations (A-27), along with the constraint Eq. (A-18) and the boundary conditions, determine the functions x_i (t) and the constant value of the Lagrange multiplier which makes I stationary subject to the constraint. It is straight-forward to extend this derivation to the case of q constraints ($q < n$). In this case the function in the Euler-Lagrange equations would be

$$F + \sum_{j=1}^{q} \lambda_j G_j$$

Differential Constraints

Problems with differential constraints most frequently arise in trajectory optimization. The typical problem is stated formally as follows. Determine n state functions x_i (t), ($i = 1,\ldots,n$) and m control functions u_k, ($k = 1,\ldots,m$) which must satisfy certain differential constraints (equations of motion),

$$\phi_j(\dot{x}_i, x_i, u_k, t) = 0 \qquad (j = 1, \ldots, p < n+m) \tag{A-28}$$

and certain prescribed boundary conditions,

$$\begin{aligned} w_\ell(\dot{x}_i, x_i, 0) &= 0, \\ w_\ell(\dot{x}_i, x_i, T) &= 0 \end{aligned} \qquad (\ell = 1, \ldots, n) \tag{A-29}$$

such that the functional,

$$I = \int_0^T F(\dot{x}_i, x_i, u_k, t)\, dt \tag{A-30}$$

is stationary.

If any of the differential constraints, Eq. (A-28), contain higher-order derivatives, the system can always be reduced to first order by defining new state variables with further constraints of the form $\phi = \dot{x}_i - x_{i+c} = 0$. For the present, let it be assumed that the boundary conditions are given as fixed numbers rather than the more general case represented by Eqs. (A-29). The general case will be treated later.

The control variables are treated as additional state variables mathematically. In fact, the only thing that distinguishes them from state variables is that time derivatives of the control variables generally do not appear, although this would be perfectly acceptable. In the derivation to follow, therefore, the notation u_k distinguishing control variables will be suppressed, and both control and state variables will be denoted by x_i (t), (i = 1,...,n+m).

If the differential constraints (Eqs. (A-28)) are to be maintained, the ϕ_j must not change at any point in time with variations in the state functions.

$$\delta\phi_j = \sum_{i=1}^{n+m} \left[\frac{\partial \phi_j}{\partial \dot{x}_i} \delta\dot{x}_i + \frac{\partial \phi_j}{\partial x_i} \delta x_i \right] = 0 \quad (j = 1, \ldots, p) \tag{A-31}$$

There exists a unique set of functions of time, $\lambda_j(t)$ (j = 1,...,p) called adjoint

variables such that the functional,

$$J = \int_0^T \left(F + \sum_{j=1}^{p} \lambda_j \phi_j\right) dt \qquad \text{(A-32)}$$

has a stationary value subject to no constraints for the same set of functions $x_i(o,t)$ which make I stationary subject to the set of differential constraints of Eqs. (A-28).

A partial proof of this statement follows. For stationary J

$$\delta J = 0 = \int_0^T \sum_{i=1}^{n+m} \left[\frac{\partial F}{\partial \dot{x}_i} \delta \dot{x}_i + \frac{\partial F}{\partial x_i} \delta x_i \right] dt + \int_0^T \sum_{j=1}^{p} \lambda_j(t) \sum_{i=1}^{n+m} \left[\frac{\partial \phi_j}{\partial \dot{x}_i} \delta \dot{x}_i + \frac{\partial \phi_j}{\partial x_i} \delta x_i \right] dt \qquad \text{(A-33)}$$

The second integral of Eq. (A-33) is zero due to the fact that every integral in the sum contains $\delta\phi_j$ which is zero from Eq. (A-31). Therefore, the first integral of Eq. (A-33) is also zero. But it will be recognized as the variation of the original functional δI, and the proposition is proved. The variation of Eq. (A-32) vanishing subject to no constraints along with the p differential equations of Eqs. (A-28) determine the n state functions $x_i(t)$ and the p adjoint functions $\lambda_j(t)$ which make I stationary subject to the constraints. Note that the above proof did not establish the existence or the uniqueness of the $\lambda_j(t)$. Existence and uniqueness, however, may be implied by the fact that the problem has a solution in the local sense. Multiple stationary solutions which are not neighboring are generally obtained, however, so that in this large sense the $\lambda_j(t)$ are not unique.

The Euler-Lagrange equations for this problem are now obtained exactly as before. Define the variational Lagrangian (also called the fundamental or augmented function) to be the integrand of Eq. (A-32).

$$L(\dot{x}_i, x_i, \lambda_j, t) = F + \sum_{j=1}^{p} \lambda_j \phi_j \qquad \text{(A-34)}$$

Then the Euler-Lagrange equations are obtained from $\delta J = \delta \int_0^T L \, dt = 0$ in the same way as was demonstrated for the unconstrained problem.

$$\frac{d}{dt}\left(\frac{\partial L}{\partial \dot{x}_i}\right) - \frac{\partial L}{\partial x_i} = 0 \quad (i = 1, \ldots, n+m) \tag{A-35}$$

In the case of a control variable whose time derivative (generally) does not appear in the Lagrangian, $\partial L/\partial \dot{u}_k = 0$ and

$$\frac{\partial L}{\partial u_k} = 0 \quad (k = 1, \ldots, m) \tag{A-36}$$

Hamilton's Canonical Equations

As in classical mechanics, it is often more convenient and advantageous to work with a formulation that is independent of the velocities. Analogous to classical mechanics, a Legendre transformation may be performed on $L(\dot{x}_i, x_i, \mu_k, \lambda_j, t)$ to obtain the variational Hamiltonian, $H(x_i, \lambda_i, u_k, t)$, which is independent of the velocities, $\dot{x}_i$ (Ref. 8).

$$H = \sum_{i=1}^{n} \frac{\partial L}{\partial \dot{x}_i} \dot{x}_i - L \tag{A-37}$$

Hamilton's canonical equations, which replace the Euler-Lagrange equations in the new formulation, can be derived from the former as follows. Define a new adjoint variable conjugate to the state variable x_i.

$$\lambda_i \equiv \frac{\partial L}{\partial \dot{x}_i} \tag{A-38}$$

If the differential constraints, Eqs. (A-28), can be put into the form $x_i = f_i(\dot{x}_j, u_k, t)$, then the adjoint variables of the Hamiltonian formulation, λ_i, will be the same as those in the Lagrangian, λ_j, otherwise not.

In either case the variational Hamiltonian may be rewritten,

$$H(x_i, \lambda_i, u_k, t) = \sum_{i=1}^{n} \left[\lambda_i \dot{x}_i - L(\dot{x}_i, x_i, \lambda_j, u_k, t)\right] \tag{A-39}$$

The total differential of H can be written in two forms, the first from the

functional form of H and the second from the definition of H, Eq. (A-39).

$$dH = \sum_{i=1}^{n} \left[\frac{\partial H}{\partial x_i} dx_i + \frac{\partial H}{\partial \lambda_i} d\lambda_i \right] + \sum_{k=1}^{m} \frac{\partial H}{\partial u_k} du_k + \frac{\partial H}{\partial t} dt \tag{A-40}$$

$$dH = \sum_{i=1}^{n} \left[\lambda_i d\dot{x}_i + \dot{x}_i d\lambda_i \right] - \sum_{i=1}^{n} \left[\frac{\partial L}{\partial \dot{x}_i} d\dot{x}_i + \frac{\partial L}{\partial x_i} dx_i \right] + \sum_{k=1}^{m} \frac{\partial L}{\partial u_k} du_k + \frac{\partial L}{\partial t} dt \tag{A-41}$$

As a consequence of the definition of the conjugate adjoint variables, λ_i, the first and third sets of terms in Eq. (A-41) cancel.

$$\sum_{i=1}^{n} \left[\lambda_i - \frac{\partial L}{\partial \dot{x}_i} \right] d\dot{x}_i = 0 \tag{A-42}$$

Also, using the Euler-Lagrange equations (Eqs. (A-35)),

$$-\sum_{i=1}^{n} \frac{\partial L}{\partial x_i} dx_i = -\sum_{i=1}^{n} \frac{d}{dt} \left(\frac{\partial L}{\partial \dot{x}_i} \right) dx_i = -\sum_{i=1}^{n} \dot{\lambda}_i dx_i \tag{A-43}$$

Equation (A-41) can now be rewritten.

$$dH = \sum_{i=1}^{n} \left[-\dot{\lambda}_i dx_i + \dot{x}_i d\lambda_i \right] + \sum_{k=1}^{m} \frac{\partial L}{\partial u_k} du_k + \frac{\partial L}{\partial t} dt \tag{A-44}$$

Now since H (x_i, λ_i, u_k, t) is a unique function of its independent variables it must vary in a unique manner with changes in these variables. Therefore, comparing Eqs. (A-40) and (A-44), the coefficients of each independent differential may be equated.

$$\dot{x}_i = \frac{\partial H}{\partial \lambda_i} \quad (i = 1, \ldots, n) \tag{A-45}$$

$$\dot{\lambda}_i = -\frac{\partial H}{\partial x_i} \quad (i = 1, \ldots, n) \tag{A-46}$$

$$\frac{\partial H}{\partial u_k} = \frac{\partial L}{\partial u_k} = 0 \quad (k = 1, \ldots, m) \tag{A-47}$$

$$\frac{\partial H}{\partial t} = \frac{\partial L}{\partial t} \tag{A-48}$$

Equations (A-45) through (A-48) are Hamilton's canonical equations and supply the same necessary conditions as the Euler-Lagrange equations.

First Integral

When the variational Lagragian is formally independent of the time (autonomous system) there exists a first integral which is a constant of the motion. In classical mechanics this first integral is the total energy.

$$\frac{dL}{dt} = \sum_{i=1}^{n} \left[\frac{\partial L}{\partial \dot{x}_i} \frac{d\dot{x}_i}{dt} + \frac{\partial L}{\partial x_i} \frac{dx_i}{dt} \right] + \sum_{k=1}^{m} \frac{\partial L}{\partial u_k} \dot{u}_k + \frac{\partial L}{\partial t} \tag{A-49}$$

The partial derivative $\frac{\partial L}{\partial u_k} = \frac{d}{dt} \left(\frac{\partial L}{\partial \dot{u}_k} \right) = 0$, since L is independent of $\dot{u}_k$, and $\frac{\partial L}{\partial t} = 0$, since the variational Lagrangian does not contain the time. Using the Euler-Lagrange equations again, $\frac{\partial L}{\partial x_i} = \frac{d}{dt} \left(\frac{\partial L}{\partial \dot{x}_i} \right)$, Eq. (A-49 becomes

$$\frac{dL}{dt} = \sum_{i=1}^{n} \left[\frac{\partial L}{\partial \dot{x}_i} \frac{d\dot{x}_i}{dt} + \frac{d}{dt} \left(\frac{\partial L}{\partial \dot{x}_i} \right) \dot{x}_i \right] \tag{A-50}$$

$$\frac{dL}{dt} = \frac{d}{dt} \sum_{i=1}^{n} \frac{\partial L}{\partial \dot{x}_i} \dot{x}_i \tag{A-51}$$

$$\frac{d}{dt} \left[\sum_{i=1}^{n} \frac{\partial L}{\partial \dot{x}_i} \dot{x}_i - L \right] = 0 \tag{A-52}$$

But the quantity in the bracket of Eq. (A-52), is the variational Hamiltonian.

Therefore,

$$\frac{dH}{dt} = 0; \quad H = \text{CONSTANT} \tag{A-53}$$

that is, the Hamiltonian is constant in time. Equation (A-47) shows that the control must always be chosen such that this constant of the motion is an extremum. The pontryagin maximum principle asserts that H must always be maximized if the functional is to be minimized. Of course, if H contains time explicitly, it is no longer a constant of the motion.

Transversality Conditions

At each endpoint, n, boundary values must be given corresponding to the n state variables. Sometimes not all of these values are specified, but the boundary values of one or more of the state variables are constrained to lie on a surface or curve as given by Eqs. (A-29). In these cases the problem has additional degrees of freedom and the boundary values can be optimized with respect to the functional in question.

Assuming this new generality, let us again develop the necessary conditions for the Lagrange problem with differential constraints from the point where J is stated to be stationary.

$$\delta J = 0 = \delta \int_{t_1}^{t_2} L(\dot{x}_i, x_i, u_k, \lambda_j, t)\, dt \tag{A-54}$$

where the endpoints t_1 and t_2 are no longer fixed and the boundary values of the state functions $x_i(t)$ are prescribed to lie on certain hypersurfaces in phase space and time given by Eqs. (A-29). To simplify matters let us again suppress the separate notation for the control variables u_k and regard these as additional state variables x_i, $(i = n+1,\ldots,n+m)$.

For purposes of clarity, it is also advisable to abandon the variational notation and return to the original parametric representation of Eqs. (A-10) and (A-11).

$$x_i(\alpha_i, t) = x_i(0, t) + \alpha_i \eta_i(t) \tag{A-10}$$

$$\dot{x}_i(\alpha_i, t) = \dot{x}_i(0, t) + \alpha_i \dot{\eta}_i(t) \tag{A-11}$$

In this more general case the variations $\delta x_i = d\alpha_i \eta_i(t)$ not only change the state functions throughout but also change the endpoint times t_1 and t_2. Because of the endpoint constraints,

$$\begin{aligned} w_\ell(\dot{x}_i, x_i, t_1) &= 0 \\ w_\ell(\dot{x}_i, x_i, t_2) &= 0 \end{aligned} \qquad (\ell = 1, \ldots, n) \tag{A-29}$$

when x_i and $\dot{x}_i$ change, t_1 and t_2 must also change to preserve the equalities of Eqs. (A-29). Therefore, the endpoint times t_1 and t_2 can be regarded as functions of the variation parameters α_i.

The stationary quality of J is denoted parametrically by

$$\delta J = 0 = \sum_{i=1}^{n+m} \frac{\partial J}{\partial \alpha_i} d\alpha_i = \sum_{i=1}^{n+m} \frac{\partial}{\partial \alpha_i} \int_{t_1(\alpha_i)}^{t_2(\alpha_i)} L \, dt \, d\alpha_i \tag{A-55}$$

where $t(\alpha_i)$ means $t(\alpha_1, \alpha_2, \ldots, \alpha_{n+m})$.

Performing the differential indicated by Eq. (A-55) gives

$$\sum_{i=1}^{n+m} L \frac{\partial t}{\partial \alpha_i} d\alpha_i \Big|_1^2 + \int_{t_1}^{t_2} \sum_{i=1}^{n+m} \left[\frac{\partial L}{\partial \dot{x}_i} \dot{\eta}_i(t) + \frac{\partial L}{\partial x_i} \eta_i(t) \right] d\alpha_i \, dt = 0 \tag{A-56}$$

and

$$\sum_{i=1}^{n+m} L \frac{\partial t}{\partial x_i} d\alpha_i \Big|_1^2 + \sum_{i=1}^{n+m} \frac{\partial L}{\partial \dot{x}_i} \eta_i(t) \, d\alpha_i \Big|_1^2 - \int_{t_1(\alpha_i)}^{t_2(\alpha_i)} \sum_{i=1}^{n+m} \left[\frac{d}{dt}\left(\frac{\partial L}{\partial \dot{x}_i} \right) - \frac{\partial L}{\partial x_i} \right] \eta_i(t) \, d\alpha_i \, dt = 0 \tag{A-57}$$

The integrands of the last term of Eq. (A-57) will be recognized as the lefthand side of the Euler-Lagrange equations for problems with fixed endpoints.

It can be argued, however, that the same Euler-Lagrange equations are valid for variable endpoints as well. Once the variable-endpoint problem has been solved the endpoints can be fixed at their optimum values. If the problem were then solved again as a fixed-endpoint problem one would not expect the character of the solution to change. Therefore, the state functions in each case must satisfy the same set of differential equations, namely the Euler-Lagrange equations of Eqs. (A-35). The last term of Eq. (A-57), therefore, is zero and Eq. (A-57) becomes

$$L \sum_{i=1}^{n+m} \frac{\partial t}{\partial \alpha_i} d\alpha_i \Big|_1^2 + \sum_{i=1}^{n+m} \frac{\partial L}{\partial \dot{x}_i} \eta_i(t)\, d\alpha_i \Big|_1^2 = 0 \qquad \text{(A-58)}$$

For substitution into Eq. (A-58), the differential of Eq. (A-10) is now taken and rearranged.

$$dx_i = \frac{\partial x_i}{\partial \alpha_i} d\alpha_i + \frac{\partial x_i}{\partial t} dt$$

$$\eta_i(t)\, d\alpha_i = dx_i - \dot{x}_i\, dt \qquad \text{(A-59)}$$

Equation (A-59 is now substituted into Eq. (A-58), and using the fact that $dt = \sum_{i=1}^{n+m} \frac{\partial t}{\partial \alpha_i} d\alpha_i$, Eq. (A-58) becomes

$$\left[\left(L - \sum_{i=1}^{n+m} \frac{\partial L}{\partial \dot{x}_i} \dot{x}_i \right) dt + \sum_{i=1}^{n+m} \frac{\partial L}{\partial \dot{x}_i} dx_i \right]_1^2 = 0 \qquad \text{(A-60)}$$

Equation (A-60) is the general transversality condition for the Lagrange problem. The dt and the dx_i at points 1 and 2 represent variations in the time and the state variables at the endpoints. These are not all independent, however, but are related by the Eqs. (A-29). Through these equations the set of variations dt, dx_i in Eq. (A-60) can be reduced to a smaller set of independent variations. Then, in order for the transversality condition, Eq. (A-60), to be satisfied, the coefficients of each of these independent variations must vanish. The resulting equations supply the necessary conditions for optimality of the variable boundary values. Incidently, the variation, dx_i, of any state variable for which a fixed boundary value is specified, is zero, and the coefficient of dx_i does not have to vanish.

A brief illustration of why Eq. (A-60) is called a transversality condition may be useful. Consider the simple problem of finding the shortest path between a point and an infinite plane. It is known, of course, that the path is a perpendicular straight line between the point and the plane. If this problem were solved by calculus of variations, with the final point variable but constrained to lie on the plane, the Euler-Lagrange equations would admit a straight line solution while Eq. (A-60) would indicate that the path should be perpendicular (or transverse) to the plane at the final boundary. The same thing is true mathematically for more complicated hypersurfaces.

In the Hamiltonian formulation the transversality condition assumes a very simple form. The coefficient of dt in Eq. (A-60) is recognized as the negative of the Hamiltonian, and the coefficients of the dx_i are just the adjoint variables, λ_i, which are conjugate to the respective state variables x_i. The Hamiltonian form of the transversality condition is thus

$$\left[-H\, dt + \sum_{i=1}^{n+m} \lambda_i\, dx_i \right]_1^2 = 0 \qquad \text{(A-61)}$$

Weierstrass-Erdmann Corner Conditions

It may be that one or more of the state functions (or their time derivatives) which comprise an extremizing path undergo a finite number of discontinuities. The points at which these discontinuities occur are called corner points, and at corner points the Weierstrass-Erdmann corner conditions must be satisfied. By treating the corner points as internal boundaries where the two adjacent solutions must be matched, the corner conditions may be simply derived by using the development just presented for transversality conditions.

To be specific, consider the case where two corner points occur. The times of occurrence, T_1 and T_2, depend of course on the path chosen which is again represented parametrically by Eqs. (A-10) and (A-11). Therefore, T_1 and T_2 are functions of the n+m parameters α_i. The functional J, Eq. (A-32), can be rewritten as the sum of three integrals

$$J = \lim_{\epsilon \to 0} \left[\int_0^{T_1(\alpha_i)-\epsilon} L\, dt + \int_{T_1(\alpha_i)+\epsilon}^{T_2(\alpha_i)-\epsilon} L\, dt + \int_{T_2(\alpha_i)+\epsilon}^{T} L\, dt \right] \qquad \text{(A-32)}$$

Again for stationary J,

$$\delta J = 0 = \sum_{i=1}^{n+m} \frac{\partial J}{\partial a_i} \, da_i \tag{A-55}$$

Employing the same process as that of Eqs. (A-55) through (A-61) on Eq. (A-32) above, one obtains

$$\left[-H\,dt + \sum_{i=1}^{n+m} \lambda_i \, dx_i \right]_0^{T_1-\epsilon} + \left[-H\,dt + \sum_{i=1}^{n+m} \lambda_i \, dx_i \right]_{T_1+\epsilon}^{T_2-\epsilon} + \left[-H\,dt + \sum_{i=1}^{n+m} \lambda_i \, dx_i \right]_{T_2+\epsilon}^{T} = 0 \tag{A-62}$$

Since there are generally no relationships between the variations at the end-points and those at the corner points, the two terms at 0 and T can be separated from the rest of Eq. (A-62) and must vanish independently, giving the previously derived general transversality condition, Eq. (A-61). The variations on each side of the respective corner points must be equal, i.e., $dt(T_1-\epsilon) = dt(T_1+\epsilon)$, $dx_i(T_1-\epsilon) = dx_i(T_1+\epsilon)$ and similarly at T_2.

Therefore, Eq. (A-62) can be rearranged to give

$$\left[-H\,dt + \sum_{i=1}^{n+m} \lambda_i \, dx_i \right]_{T_1+\epsilon}^{T_1-\epsilon} + \left[-H\,dt + \sum_{i=1}^{n+m} \lambda_i \, dx_i \right]_{T_2+\epsilon}^{T_2-\epsilon} = 0 \tag{A-63}$$

Since no relation exists between the variations at T_1 and T_2, the two terms must separately vanish. Also since the variations on each side of the respective corner points are equal the respective coefficients must also be equal in order to satisfy Eq. (A-63). Thus $H(T_1-\epsilon) = H(T_1+\epsilon)$, $\lambda_i(T_1-\epsilon) = \lambda_i(T_1+\epsilon)$, $(i = 1,\ldots,n+m)$ and similarly at T_2. The fact that the Hamiltonian and all adjoint variables are continuous constitutes the Weierstrass-Erdmann corner conditions. The extension to more than two corner points is obvious.

The Pontryagin Maximum Principle

Two things that cause corner points are inequality constraints and discrete control variables. Only the latter are considered in this report. Consider the case where a certain control variable u_k is not continuous but may take on any one of a finite set of discrete values ℓ_s. According to the maximum principle the proper choice for u_k at any time is

$$u_k = \max_s H(x_i, \lambda_i, \ell_s, t) \tag{A-64}$$

that is, the discrete value ℓ_p which maximizes H at any point is the proper choice. In the limiting case of continuous control variables the maximum principle is consistent with $\partial H/\partial u_k = 0$ and the positive definite test of the Weierstrass excess function.

The Problem of Mayer

Up to now the development has centered almost exclusively on the Lagrange problem, although it has been shown earlier that the Lagrange problem can be transformed into a Mayer problem by simply defining a new state variable. It is reasonable to expect, therefore, that the same Euler-Lagrange equations will be valid for the Mayer problem.

That the same Euler-Lagrange equations are, in fact, valid for the Mayer problem is now shown. Starting with the original Lagrange problem of extremizing the functional

$$I = \int_0^T F(\dot{x}_i, x_i, t)\, dt \qquad (i = 1, \ldots, n+m) \tag{A-65}$$

subject to the differential constraints

$$\phi_j(\dot{x}_i, x_i, t) = 0 \quad (j = 1, \ldots, p < n+m) \tag{A-66}$$

a new state variable, z, is defined which obeys the new constraint

$$\dot{z} - F(\dot{x}_i, x_i, t) = 0 \tag{A-67}$$

Call the new state variable the $(n+m+1)$ variable $(z \equiv x_{n+m+1})$ and the additional constraint the $(p+1)$ constraint, ϕ_{p+1}.

As shown before, the problem can be transformed into the Mayer form,

$$I = \int_0^T \dot{z}\, dt = z\Big|_0^T \tag{A-68}$$

but the Lagrange form shall continue to be used in order to make use of previous developments. (Note that the new state variable Z is usually denoted by G or J in the literature.)

As before, the variational Lagrangian is formed.

$$L(\dot{x}_i, x_i, \lambda_j, t) = \dot{z} + \sum_{j=1}^{p+1} \lambda_j \phi_j \tag{A-69}$$

Since this is still a Lagrange problem the same Euler-Lagrange equations hold.

$$\frac{d}{dt}\left(\frac{\partial L}{\partial \dot{x}_i}\right) - \frac{\partial L}{\partial x_i} = 0 \quad (i = 1, \ldots, n+m) \tag{A-70}$$

$$\frac{d}{dt}\left(\frac{\partial L}{\partial \dot{z}}\right) - \frac{\partial L}{\partial z} = 0 \tag{A-71}$$

Inspection of the p+1 constraint, Eq. (A-67), and the Lagrangian, Eq. (A-69), reveals that L does not contain Z so that the second term in Eq. (A-71) is zero. Upon substituting Eq. (E-69), the first term becomes

$$\frac{d}{dt}(1 + \lambda_{p+1}) = 0 \tag{A-72}$$

or

$$\lambda_{p+1} = \text{CONSTANT} \tag{A-73}$$

Since neither Z nor $\dot{Z}$ appear in any of the other Euler-Lagrange equations (Eqs. (A-70) for $i \leq n+m$), or equations of constraint (Eqs. (A-66) for $j < n+m$), the equations involving Z and λ_{p+1}, Eqs. (A-67) and (A-72), are completely uncoupled from the rest of the system and Eq. (A-73) is a trivial result. With no

loss of generality or without changing the problem in any way, the constant of Eq. (A-73) can be chosen to be zero and the $\dot{Z}$ can be deleted from the Lagrangian,

$$L(\dot{x}_i, x_i, \lambda_j, t) = \sum_{j=1}^{p} \lambda_j \phi_j \qquad \text{(A-74)}$$

and the Euler-Lagrange equations for the Mayer problem are Eqs. (A-70) for $i = 1, \ldots, n+m$.

Using the same transformation device, the general transversality condition for the Mayer problem can be derived. Again the Lagrangian is used for the corresponding Lagrange problem,

$$L'(\dot{x}_i, x_i, \lambda_j, t) = \dot{z} + \sum_{j=1}^{p+1} \lambda_j \phi_j \qquad \text{(A-75)}$$

where the prime is introduced to distinguish Eq. (A-75) from the Mayer form of the Lagrangian which has been shown to be equivalent as far as the Euler-Lagrange equations are concerned. Since for the time being we are still dealing with a Lagrange problem with the functional in the form

$$I = \int_{t_1(\alpha_i)}^{t_2(\alpha_i)} \dot{z}\, dt \qquad \text{(A-76)}$$

where $\dot{Z} = F(x_i, x_i, t)$, the previously derived transversality condition, Eq. (A-63), is valid.

$$\left[\left(L' - \sum_{i=1}^{n+m+1} \frac{\partial L'}{\partial \dot{x}_i} \dot{x}_i \right) dt + \sum_{i=1}^{n+m+1} \frac{\partial L'}{\partial \dot{x}_i} dx_i \right]_1^2 = 0 \qquad \text{(A-77)}$$

Substituting Eq. (A-75) for L' and denoting the Mayer form of the variational Lagrangian by $L = \sum_{j=i}^{p} \lambda_j \phi_j$, Eq. (A-77) becomes

$$\left\{ \left[\dot{z} + L + \lambda_{p+1} \phi_{p+1} - \sum_{i=1}^{n+m} \frac{\partial L}{\partial \dot{x}_i} \dot{x}_i - (1+\lambda_{p+1}) \dot{z} \right] dt + \sum_{i=1}^{n+m} \frac{\partial L}{\partial \dot{x}_i} dx_i + (1+\lambda_{p+1}) dz \right\}_1^2 = 0 \quad \text{(A-78)}$$

Equation (A-78) can be simplified, ($\phi_{p+1} = 0$),

$$\left[dz + (L - \sum_{i=1}^{n+m} \frac{\partial L}{\partial \dot{x}_i} \dot{x}_i)\, dt + \sum_{i=1}^{n+m} \frac{\partial L}{\partial \dot{x}_i} dx_i \right]_1^2 = 0 \quad \text{(A-79)}$$

Equation (A-79) is the general transversality condition for the Mayer problem. Again this can be transformed into the Hamiltonian formulation.

$$\left[dz - H\, dt + \sum_{i=1}^{n+m} \lambda_i\, dx_i \right]_1^2 = 0 \quad \text{(A-80)}$$

If there exists no coupling between z and the other state variables, $dz = 0$ separately from the rest of Eq. (A-80).

Appendix A Nomenclature - Part I

a	Thrust acceleration
c	Exhaust velocity
F, f, G, g	Denote functional forms
H	Variational Hamiltonian
I, J	Integral functional
L	Variational Lagrangian (also called the augmented or fundamental function)
$m(t)$	Total vehicle mass at time t
P	Power available
T	A given instant of time
t	Time
u	Control variable
x	Position coordinate
z	Auxiliary state variable
α	Function variation parameter
$\delta x(t)$	Denotes variation of function $x(t)$
ϵ	Small quantity used for taking limits
$\eta(t)$	Arbitrary function of time
η_c	Thruster power conversion efficiency
λ	Lagrange multiplier
ϕ	Denotes functional form of a differential equation of constraint
ω	Denotes functional form of equation that the boundary values must satisfy

APPENDIX A - PART 2

VARIATIONAL FORMULATIONS OF FOUR POWER-LIMITED TRAJECTORY AND PROPULSION-SYSTEM OPTIMIZATION PROBLEMS

Detailed Description of Problems

The variational formulations of the problems are presented in the following sequence:

Problem 1: Three-dimensional trajectory and control optimization with the thruster constrained to constant exhaust velocity on-off operation. The power available is a given function of position and time corresponding to decaying radioisotope power or solar power. The objective is maximum final mass fraction for given values of powerplant specific weight, powerplant fraction, and exhaust velocity. The boundary conditions correspond to (a) planetary rendezvous, (b) planetary flyby, (c) flyby at a given radius, and (d) orbital transfer.

Problem 2: This problem includes all of problem 1, but in addition the powerplant fraction μ_w and the exhaust velocity C, as well as the trajectory and the associated steering program, are to be optimized. The objective function is maximum payload fraction, which is defined to be everything that is left at the end of the mission except the powerplant, thruster, and the structure.

Problem 3: In this problem two separate propulsion units are used, one before and one after the coast period. The exhaust velocity and powerplant fraction of each unit are optimized with respect to final payload fraction.

Problem 4: This problem is the same as problem 1 except that the thrust-acceleration vector is constrained to make a constant angle with respect to the radius vector. One constant angle is allowed before coast and another after coast. These two angles are to be separately optimized with respect to maximum final mass.

Problem 1

Maximizing the final mass fraction is equivalent to minimizing the objective function

$$z(T) = -K\mu(T) \equiv -K\mu_T \tag{A-81}$$

where K is an arbitrary positive constant. Let the power in the exhaust beam be denoted functionally by

$$P = -\frac{1}{2}\dot{m}c^2 = \eta_c P_0 f(\vec{r},t) \tag{A-82}$$

where η_c is the thruster efficiency, P_o is the power available to the thruster at Earth's orbital radius, and f is a given positive function of position and time. The time rate of change of the mass of the vehicle is given by

$$\dot{\mu}(t) = \frac{\dot{m}}{m_o} = -\frac{2\eta_c P_o f}{m_o c^2} = -\frac{2\eta\mu_w}{\alpha_w c^2} f \tag{A-83}$$

where α_w is the specific mass of the powerplant based on the initial power P_o.

The differential equations of constraint, corresponding to Eqs. (A-28), are now given.

$$\dot{x}_i = x_{i+3} \qquad (i = 1, 2, 3) \tag{A-84}$$

$$\dot{x}_4 = \frac{bcf}{\mu}\beta(t)\sin\theta\cos\phi - \frac{x_1}{r^3} \tag{A-85}$$

$$\dot{x}_5 = \frac{bcf}{\mu}\beta(t)\sin\theta\sin\phi - \frac{x_2}{r^3} \tag{A-86}$$

$$\dot{x}_6 = \frac{bcf}{\mu}\beta(t)\cos\phi - \frac{x_3}{r^3} \tag{A-87}$$

$$\dot{\mu} = -bf\beta(t) - \mu_* \delta(t - T_*) \tag{A-88}$$

Here, the state variables x_i (i = 1, 2, 3) are Cartesian position coordinates, the x_{i+3} are velocity components, and μ is the vehicle mass; $b \equiv 2\eta_c\mu_w/\alpha_w c^2$ and the control variables (denoted by u_k in Appendix A, Part 1) are θ, ρ, and $\beta(t)$. The latter is a discrete control variable corresponding to turning the thruster on and off.

$$\beta(t) = \begin{cases} 1 \text{ in powered regions} \\ \\ 0 \text{ in coasting regions} \end{cases} \tag{A-89}$$

The second term in Eq. (A-88) describes staging at time T_*. In this term μ_* is the mass fraction that is discarded and $\delta(t-T_*)$ is a Dirac delta function.

The variational Hamiltonian (Eq. (A-37)) is now formed.

$$H = \sum_{i+1}^{3} \left[\lambda_i x_{i+3} - \lambda_{i+3} \frac{x_i}{r^3} \right] + \frac{bcf\beta}{\mu} \left[(\lambda_4 \cos\phi + \lambda_5 \sin\phi) \sin\theta + \lambda_6 \cos\theta \right]$$
$$- \lambda_u \left[bf\beta + \mu_* \delta(t - T_*) \right] \tag{A-90}$$

The control variables can be determined in terms of the adjoint variables through the use of Eqs. (A-47) and (A-64).

$$\frac{\partial H}{\partial \phi} = 0 = - \frac{af\beta}{\mu} (\lambda_4 \sin\phi - \lambda_5 \cos\phi) \sin\theta \tag{A-91}$$

$$\frac{\partial H}{\partial \theta} = 0 = \frac{af\beta}{\mu} \left[(\lambda_4 \cos\phi + \lambda_5 \sin\phi) \cos\theta - \lambda_6 \sin\theta \right] \tag{A-92}$$

Equations (A-91) and (A-92) are satisfied if

$$\cos\phi = \pm \frac{\lambda_4}{\sqrt{\lambda_4^2 + \lambda_5^2}} , \qquad \sin\phi = \pm \frac{\lambda_5}{\sqrt{\lambda_4^2 + \lambda_5^2}} \tag{A-93}$$

and

$$\cos\theta = \pm \frac{\lambda_6}{p} , \qquad \sin\theta = \pm \frac{\sqrt{\lambda_4^2 \ \lambda_5^2}}{p} \tag{A-94}$$

where

$$\vec{p} \equiv \begin{pmatrix} \lambda_4 \\ \lambda_5 \\ \lambda_6 \end{pmatrix}$$

Investigation of the Pontryagin maximum principle, Eq. (A-64), indicates that the plus sign should be chosen in Eqs. (A-93) and (A-94).

The variational Hamiltonian, Eq. (A-90), can now be rewritten in more concise notation.

$$H = \sum_{i+1}^{3}\left[\lambda_i x_{i+3}\frac{x_i}{r^3}\right] + bf\beta\left[\frac{cp}{\mu} - \lambda_\mu\right] - \lambda_\mu \mu_* \delta(t - T_*) \tag{A-95}$$

When the discrete control variable $\beta(t)$ changes from 1 to 0 at a particular point, say T_1, the time derivatives of the state variables x_{i+3} ($i = 1, 2, 3$), i.e., the acceleration components, suffer discontinuities as shown by Eqs. (A-94) to (A-98). Thus a corner point occurs at T_1 and the Weierstrass-Erdmann corner conditions dictate that the Hamiltonian and all adjoint variables must be continuous across this point. Denoting by (-) the infinitesimal region just before the corner point where $\beta = 1$ and (+) just after the corner where $\beta = 0$,

$$\left\{\sum_{i=1}^{3}\left[\lambda_i x_{i+3} - \lambda_{i+3}\frac{x_i}{r^3}\right] + bf\left[\frac{cp}{\mu} - \lambda_\mu\right] - \lambda_\mu \mu_* \int (t - T_*)\right\}_- \tag{A-96}$$

$$= \left\{\sum_{i=1}^{3}\left[\lambda_i x_{i+3} - \lambda_{i+3}\frac{x_i}{r^3}\right] - \lambda_\mu \mu_* \delta(t - T_*)\right\}_+$$

Since there is no discontinuity in any of the state variables, x_i, x_{i+3}, and μ, and all of the adjoint variables must be continuous, the only way for Eq. (A-96) to be satisfied is for

$$\gamma \equiv \frac{cp}{\mu} - \lambda_\mu \tag{A-97}$$

to vanish at the corner point. The function γ is called a switching function (Ref. A-1) because it governs the discrete control variable β as follows. It is seen in Eq. (A-95) that the second term in the Hamiltonian is $bf\beta\gamma$. Note that b is a positive constant and f is a positive function of position and time. The maximum principle (Eq. (A-64)) states that β should always be chosen to maximize the Hamiltonian. It is quite evident that

$$\beta(t) = \begin{cases} 1 \text{ when } \gamma > 0 \\ 0 \text{ when } \gamma < 0 \end{cases} \tag{A-98}$$

is the proper choice.

The Hamiltonian canonical equations (Eqs. (A-45) and (A-46)) will now be determined in second-order form except for that for λ_μ.

$$\dot{\lambda}_{i+3} = -\frac{\partial H}{\partial x_{i+3}} = -\lambda_i \,, (i = 1,2,3) \tag{A-99}$$

$$\ddot{\lambda}_{i+3} = -\dot{\lambda}_i = \frac{\partial H}{\partial x_i} \quad , \tag{A-100}$$

$$\ddot{\lambda}_{i+3} = \frac{-\lambda_{i+3}}{r^3} + \frac{3x_i}{r^5} \sum_{k=1}^{3} \lambda_{k+3} x_k + b\beta \frac{\partial f}{\partial x_i} \left(\frac{cp}{\mu} - \lambda_\mu \right), \tag{A-101}$$

$$\dot{\lambda}_\mu = - \frac{\partial H}{\partial \mu} = \frac{bcf\beta p}{\mu^2} \tag{A-102}$$

The three Eqs. (A-101) and Eq. (A-102) are the complete set of Euler-Lagrange equations. Together with the equations of motion,

$$\ddot{x}_i = \frac{bcf\beta}{\mu} \frac{\lambda_{i+3}}{p} - \frac{x_i}{r^3} \quad (i = 1,2,3) \ , \tag{A-103}$$

and

$$\dot{\mu} = -bf\beta - \mu_* \delta (t - T_*) \ , \tag{A-88}$$

and prescribed boundary conditions, they determine the trajectory and thrusting program. The two first-order equations, Eqs. (A-102) and (A-88), can be reduced to one second-order equation by differentiation and substitution.

There still remains the question of boundary conditions on the state and adjoint variables. The boundary conditions depend upon the specific problem at hand (i.e., whether it is a planetary rendezvous, flyby, etc.). Assuming the rendezvous case with a single intermediate coast, for the moment, the following development indicates a condition on the primer vector magnitude at the two intermediate switching times, T_1 and T_2.

Integrate Eqs. (A-102) and (A-88).

$$\mu (t) = 1 - b \int_0^t f(\vec{r},\tau) \beta(\tau) \, d\tau - \mu_* \int_0^t \delta(\tau - T_*) \, d\tau \tag{A-104}$$

$$\lambda_\mu (t) = \lambda_\mu (0) + bc \int_0^t \frac{f(\vec{r},\tau)\beta(\tau)p}{\mu^2} \, d\tau \tag{A-105}$$

Since Eqs. (A-101) and (A-102) are homogeneous in the adjoint variables, the magnitude of the primer vector, p, and the mass adjoint variable λ_μ, may be arbitrarily scaled at any point, but not independently. In what follows let $p(T_1) = p_1$, $\mu(T_1) = \mu_1$, etc.

$$\gamma_1 = \frac{cp_1}{\mu_1} - \lambda_{\mu 1} = 0 \tag{A-106}$$

$$\lambda_{\mu 1} = \frac{cp_1}{\mu_1} = \lambda_{\mu 0} + bc \int_0^{T_1} \frac{f\beta p}{\mu^2}\, dt \tag{A-107}$$

$$\gamma_2 = \frac{cp_2}{\mu_2} - \lambda_{\mu 2} = 0 \tag{A-108}$$

$$\lambda_{\mu 2} = \frac{cp_2}{\mu_2} = \lambda_{\mu 0} + bc \int_0^{T_2} \frac{f\beta p}{\mu^2}\, dt \tag{A-109}$$

Since $\beta(t) = 0$, for $T_1 < t < T_2$, the integral terms in Eqs. (A-107) and (A-109) are equal. Therefore, the right-hand sides of these two equations are identical and

$$\frac{p_1}{\mu_1} = \frac{p_2}{\mu_2} \tag{A-110}$$

If no staging occurs during the coast period (i.e., if $\mu_* = 0$), then the primer vector magnitudes at the two switching times are equal, a well known result (Ref. A-2). If staging does take place,

$$\frac{p_1}{p_2} = \frac{\mu_1}{\mu_1 - \mu_*} \tag{A-111}$$

which indicates that the first switching time would occur earlier. The required scaling on λ_μ at $t = 0$ is given by Eq. (A-107),

$$\lambda_{\mu 0} = \frac{cp_1}{\mu_1} - bc \int_0^{T_1} \frac{fp}{\mu^2}\, dt \tag{A-112}$$

with arbitrary scaling on p at the initial point. Equation (A-112) shows that as T_1 decreases the scaling $\lambda_\mu(0)$ increases. This directly increases λ_μ at all points in time. Equation (A-97) shows that if λ_μ increases everywhere the switching function will become more negative and the second switching time T_2 will increase.

Thus the staging during the coast period has the effect of increasing the length of the coast, which is certainly reasonable.

Finally, the boundary conditions for the four cases must be considered. The first case of planetary rendezvous has already been discussed. For this case specific boundary values are given for the position vector x_i and the velocity vector $\dot{x}_i$ at both endpoints. This case usually results in one intermediate coast period and two switching points, although more than one coast period is certainly possible. In the latter case Eq. (A-110) holds over all coast periods and the mass (Eq. (A-88)) requires an additional δ function term for all staging points.

For the case of planetary flyby the general transversality condition, Eq. (A-80), is employed.

$$-K d\mu_T + \sum_{i=1}^{3} \left[\lambda_i \, dx_i + \lambda_{i+3} \, dx_{i+3} \right]_T + \lambda_{\mu_T} \, d\mu_T = 0 \qquad \text{(A-113)}$$

The final position is fixed ($dx_i = 0$) but the final velocity is open ($dx_{i+3} \neq 0$). Furthermore, Eq. (A-113) must be valid for any arbitrary set of independent weak variations. This is possible only if the coefficient of each independent variation separately vanishes.

$$\lambda_{i+3}(T) = 0 \quad (i = 1,2,3) \qquad \text{(A-114)}$$

$$\lambda_\mu(T) = K \qquad \text{(A-115)}$$

Equation (A-114) states that the primer vector at final time vanishes, while Eq. (A-115) implies an additional scaling requirement on λ_μ. It will be recalled, however, that K is an arbitrary positive constant, so Eq. (A-115) is satisfied by any positive final value of λ_μ, a fortunate circumstance since λ_μ is already completely determined by Eqs. (A-105) and (A-112).

For the flyby case $p(T) = 0$. Since λ_μ is everywhere positive, Eq. (A-97) shows that the switching function, Υ, will go negative and remain negative in the latter part of the trajectory. The final part of the trajectory, therefore, will always be a coasting region for the flyby case.

In the case of flyby at a given radius, R, the boundary condition corresponding to a solar probe, the location of the final boundary on the sphere of radius R is determined by two variables which are most conveniently defined to be the usual spherical polar coordinate angles θ and φ. In terms of these variables, the Cartesian coordinates are

$$x_1 = R \sin\theta \cos\phi \qquad \text{(A-116)}$$

$$X_2 = R \sin\theta \sin\phi \tag{A-117}$$

$$X_3 = R \cos\theta \tag{A-118}$$

The transversality condition, Eq. (A-113), is the same as the previous case except that the final position is not fixed and the dx_i are no longer zero. The variations dx_i are not all independent, however, but are related through Eqs. (A-116) to (A-118).

$$dx_1 = R\left[\cos\theta \cos\phi \, d\theta - \sin\theta \sin\phi \, d\phi\right] \tag{A-119}$$

$$dx_2 = R\left[\cos\theta \sin\phi \, d\theta + \sin\theta \cos\phi \, d\phi\right] \tag{A-120}$$

$$dx_3 = -R \sin\theta \, d\theta \tag{A-121}$$

Substituting Eqs. (A-119) to (A-121) into Eq. (A-113) one obtains Eqs. (A-114) and (A-115) as before, and in addition

$$(\lambda_1 \cos\theta \cos\phi + \lambda_2 \cos\theta \sin\phi - \lambda_3 \sin\theta)\, d\theta + (-\lambda_1 \sin\theta \sin\phi + \lambda_2 \sin\theta \cos\phi)\, d\phi = 0 \tag{A-122}$$

Since $d\theta$ and $d\varphi$ are independent variations, their respective coefficients must equal zero.

$$\lambda_1 \cos\phi + \lambda_2 \sin\phi = \lambda_3 \tan\theta \tag{A-123}$$

$$\lambda_1 (-\sin\phi) + \lambda_2 \cos\phi = 0 \tag{A-124}$$

Using Cramer's rule,

$$\lambda_1 = \lambda_3 \tan\theta \cos\phi \tag{A-125}$$

$$\lambda_2 = \lambda_3 \tan\theta \sin\phi \tag{A-126}$$

Equations (A-125) and (A-126) can be converted back to Cartesian coordinates and Eqs. (A-99) are substituted for the λ_i.

$$\frac{\lambda_1}{\lambda_3} = \frac{\lambda_4}{\lambda_6} = \frac{x_1}{x_3} \tag{A-127}$$

$$\frac{\lambda_2}{\lambda_3} = \frac{\dot{\lambda}_5}{\lambda_6} = \frac{x_2}{x_3} \tag{A-128}$$

The final boundary condition on position has three degrees of freedom. Equations (A-127) and (A-128) provide two conditions. The third condition is provided by

$$\sum_{i=1}^{3} x_i^2 = R^2 \tag{A-129}$$

where R is the given final radius.

For the case of orbital transfer in a given time, it is desired to depart from the best point in the initial orbit and arrive at the best point in the final orbit. At each end both the position and velocity of the given orbits are matched.

A Keplerian orbit in space can be specified by 5 parameters. In addition, a position in the given orbit is specified by one parameter, the central angle ξ. Once the orbit is specified, the position and velocity vectors of a certain point in the orbit are functions of the single parameter ξ.

$$x_i = f_i(\xi) \; ; \qquad \dot{x}_i = g_i(\xi) \qquad (i = 1, 2, 3) \tag{A-130}$$

The general transversality condition for orbital transfer is

$$-K d\mu_T + \left[\sum_{i=1}^{3} \left({}_i \frac{df_i}{d\xi} + \lambda_{i+3} \frac{dg_i}{d\xi} \right) d\xi \right]_0^T + \lambda_{\mu_T} d\mu_T = 0 \tag{A-131}$$

The variations $d\xi$ at the initial and final boundaries are completely independent. Therefore the respective coefficients must vanish separately.

$$\left[\sum_{i=1}^{3} \left(\lambda_{i+3} \frac{dg_i}{d\xi} - \lambda'_{i+3} \frac{df_i}{d\xi} \right) \right]_{t=0} = 0 \tag{A-132}$$

$$\left[\sum_{i=1}^{3} \left(\lambda_{i+3} \frac{dg_i}{d\xi} - \lambda'_{i+3} \frac{df_i}{d\xi} \right) \right]_{t=T} = 0 \tag{A-133}$$

Equations (A-132) and (A-133) along with Eqs. (A-130) are sufficient to determine the values of initial and final ξ and thus if x_i and $\dot{x}_i$. In case only one end is open Eqs. (A-132) and (A-133) are used and all the boundary values on the position and velocity vectors must be given for the other end.

Problem 2

Briefly, the only difference between this and the last problem is that now two constant parameters, the exhaust velocity, C, and the powerplant fraction, μ_w, are to be optimized in addition to the trajectory and thrusting program, and the payload fraction is to be maximized instead of just the final mass. The problem again can be most conveniently expressed in the Mayer form with the objective function.

$$z = -K\left[\mu(t) - \mu_w - \mu_F(C, \mu_w) - \mu_s\right] \tag{A-134}$$

to be minimized where K is again an arbitrary positive constant, μ_F is the thruster fraction (any continuous function of c and μ_w), and μ_s is the structure fraction.

The differential constraints, Eq. (A-28), for this problem are

$$\dot{x}_i = x_{i+3} \qquad (i = 1, 2, 3) \tag{A-135}$$

$$\dot{x}_{i+3} = \frac{2\mu_w \eta_c f(\vec{r},t)\beta(t)}{a_w C\, \mu(t)} \frac{\lambda_{i+3}}{p} - \frac{x_i}{r3} \tag{A-136}$$

$$\dot{\mu} = -\frac{2\mu_w \eta_c f(\vec{r},t)\beta(t)}{a_w C^2} - \mu_* \delta(t - T_*) \tag{A-137}$$

$$\dot{C} = 0 \tag{A-138}$$

$$\dot{\mu}_w = 0 \tag{A-139}$$

where the results of Eqs. (A-93) and (A-94) for the control variables have already been included in Eqs. (A-136).

The Hamiltonian, Eq. (A-39), can again be written in the concise form

$$H = \sum_{i=1}^{3}\left[\lambda_i x_{i+3} - \lambda_{i+3}\frac{x_i}{r^3}\right] + \frac{2\mu_w \eta_c f \gamma \beta}{a_w C^2} - \lambda_\mu \mu_* \delta(t - T_*) \tag{A-140}$$

where γ is the same switching function as before.

$$\gamma = \frac{Cp}{\mu} - \lambda_\mu \tag{A-97}$$

Application of the Pontryagin maximum principle, Eq. (A-56), again shows that

$$\beta(t) = \begin{cases} 1 \text{ for } \Upsilon > 0 \\ 0 \text{ for } \Upsilon < 0 \end{cases} \tag{A-98}$$

The Euler-Lagrange equations,

$$\lambda''_{i+3} = \frac{\lambda_{i+3}}{r^3} + \frac{3x_i}{r^3} \sum_{j=1}^{3} \lambda_{j+3} x_j + \frac{2\mu_w \eta_c}{a_w C^2} \frac{\partial f}{\partial x_i} \gamma\beta \tag{A-141}$$

$$\lambda'_{\mu} = \frac{2\mu_w \eta_c f p \beta}{a_w C \mu^2} \tag{A-142}$$

are the same as the previous problem. In this problem, however, there are two additional Euler-Lagrange equations for C and μ_w.

$$\lambda'_C = -\frac{\partial H}{\partial C} \tag{A-143}$$

$$\lambda'_{\mu_w} = -\frac{\partial H}{\partial \mu_w} \tag{A-144}$$

These equations may be integrated formally.

$$\lambda_C(T) - \lambda_C(0) = -\int_0^T \frac{\partial H}{\partial C} dt \tag{A-145}$$

$$\lambda_{\mu_w}(T) - \lambda_{\mu_w}(0) = -\int \frac{\partial H}{\partial \mu_w} dt \tag{A-146}$$

The general transversality condition for this problem are

$$dz + \left[-H dt + \sum_{i=1}^{3} (\lambda_i dx_i + \lambda_{i+3} dx_{i+3}) + \lambda_\mu d\mu + \lambda_C d + \lambda_{\mu_w} d\mu_w\right]_0^T = 0 \tag{A-147}$$

For the case of fixed-time rendezvous the variations dt, dx_i and dx_{i+3} are all zero at each end. Let the subscripts 0 and T denote the variation at the respective endpoints. Equation (A-147) can be rewritten as

$$dz + \lambda_{\mu T}\, d\mu_T + \lambda_{CT}\, dC_T - \lambda_{Co} dc_o + \lambda_{\mu wT}\, d\mu_{wT} - \lambda_{\mu wo}\, d\mu_{wo} = 0 \qquad \text{(A-148)}$$

Equations (A-138) and (A-139) insure that C and μ_w are constant throughout the trajectory. Therefore

$$dC_o = dC_T = dC \; ; \; d\mu_{wo} = d\mu_{wT} = d\mu_w \qquad \text{(A-149)}$$

Furthermore,

$$dz = K\left(d\mu_w + \frac{\partial \mu_F}{\partial C}\, dC + \frac{\partial \mu_F}{\partial \mu_w}\, d\mu_w - d\mu_T \right) \qquad \text{(A-150)}$$

Substitution of Eqs. (A-145), (A-146), (A-149), and (A-150) into Eq. (A-148) gives

$$K\left(d\mu_w + \frac{\partial \mu_F}{\partial C}\, dC + \frac{\partial \mu_F}{\partial \mu_w}\, d\mu_w - d\mu_T \right) + \lambda_{\mu T}\, d\mu_T - dC \int_0^T \frac{\partial H}{\partial C}\, dt - d\mu_w \int_0^T \frac{\partial H}{\partial \mu_w}\, dt = 0 \qquad \text{(A-151)}$$

and collecting coefficients of independent variations,

$$(\lambda \mu_T - K)\, d\mu_T + \left[K \frac{\partial \mu_F}{\partial C} - \int_0^T \frac{\partial H}{\partial C}\, dt \right] dC + \left[K \left(1 + \frac{\partial \mu_F}{\partial \mu_w} \right) - \int_0^T \frac{\partial H}{\partial \mu_w}\, dt \right] d\mu_w = 0 \qquad \text{(A-152)}$$

Each coefficient in Eq. (A-152) must vanish separately. The vanishing of the first coefficient shows that $\lambda_{\mu_T} = K$. If this relation is substituted into the last coefficient one obtains

$$\left[\lambda \mu_T \left(1 + \frac{\partial \mu_F}{\partial \mu_w} \right) - \int_0^T \frac{\partial H}{\partial \mu_w}\, dt \right] d\mu_w + \left[\lambda \mu_T \frac{\partial \mu_F}{\partial C} - \int_0^T \frac{\partial H}{\partial C}\, dt \right] dC = 0 \qquad \text{(A-153)}$$

It remains to determine the two partial derivatives in Eq. (A-153).

$$\frac{\partial H}{\partial \mu_w} = \frac{2 \eta_c f}{\alpha_w C^2}\, \gamma \beta \qquad \text{(A-154)}$$

Let us define a new variable μ_c such that

$$\dot{\mu}_c \equiv -\frac{2\mu_w \eta_c f \beta}{a_w c^2} \tag{A-155}$$

$\dot{\mu}_c$ will be recognized as the rate of mass loss of the vehicle associated with propulsion and not including the mass loss due to staging during coast. Then

$$\frac{\partial H}{\partial \mu_w} = -\frac{\dot{\mu}_c}{\mu_w}\left(\frac{Cp}{\mu} - \lambda\mu\right) \tag{A-156}$$

Now the integration indicated in Eq. (A-153) can be performed,

$$\int_0^T \frac{\partial H}{\partial \mu_w}\,dt = -\int_0^T \frac{\dot{\mu}_c}{\mu_w}\,\frac{Cp}{\mu}\,dt + \frac{1}{\mu_w}\int_0^T \dot{\mu}_c \lambda\mu\,dt\,, \tag{A-157}$$

and integrating the second term by parts gives

$$\int_0^T \frac{\partial H}{\partial \mu_w}\,dt = -\int_0^T \frac{\dot{\mu}_c}{\mu_w}\,\frac{Cp}{\mu}\,dt + \frac{1}{\mu_w}\left[\mu_c \lambda\mu\Big|_0^T\right] - \frac{1}{\mu_w}\int_0^T \mu_c \dot{\lambda}\mu\,dt \tag{A-158}$$

Inspection of Eq. (A-142) shows that

$$\dot{\lambda}\mu = -\frac{\dot{\mu}_c Cp}{\mu^2} \tag{A-159}$$

Equation (A-159) is substituted into Eq. (A-158).

$$\int_0^T \frac{\partial H}{\partial \mu_w}\,dt = \frac{1}{\mu_w}\left[\mu_c \lambda\mu\right]_0^T + \frac{C}{\mu_w}\int_0^T \dot{\mu}_c p\left(\frac{\mu_c}{\mu^2} - \frac{1}{\mu}\right)dt \tag{A-160}$$

For $0 \le t < T_*$, $\mu_c = \mu$, and for $T_* < t \le T$, $\mu_c = \mu + \mu_*$. The last term in Eq. (A-160) becomes

$$\begin{aligned}\frac{C}{\mu_w}\int_0^T \dot{\mu}_c p\left(\frac{\mu_c}{\mu^2} - \frac{1}{\mu}\right)dt &= \frac{C}{\mu_w}\int_0^{T_*} \dot{\mu}_c p\left(\frac{1}{\mu} - \frac{1}{\mu}\right)dt \\ &+ \frac{C}{\mu_w}\int_{T_*}^T \dot{\mu}_c p\,\frac{\mu_*}{\mu^2}\,dt = \frac{C\mu_*}{\mu_w}\int_{T_2}^T \frac{\dot{\mu}}{\mu^2}\,p\,dt\end{aligned} \tag{A-161}$$

The second equality of Eq. (A-161) is valid because from the staging time T_* to the end of the coast period T_2, $\dot{\mu}_c$ is zero, and after T_2, $\dot{\mu}_c = \dot{\mu}$. Equation (A-160) can finally be written as

$$\int_0^T \frac{\partial H}{\partial \mu_w} dt = \frac{1}{\mu_w}\left[(\mu_T + \mu_*)\lambda_{\mu T} - \lambda\mu_0\right] - \frac{2\eta_c \mu_*}{a_w C}\int_{T_2}^T \frac{pf\beta}{\mu^2} dt \qquad \text{(A-162)}$$

Turning attention to the other partial derivative in Eq. (A-153)

$$+\frac{\partial H}{\partial C} = -\frac{4\mu_w \eta_c f \gamma\beta}{a_w C^3} + \frac{2\mu_w \eta_c' f \gamma\beta}{a_w C^2} + \frac{2\mu_w \eta_c f p\beta}{a_w C^2 \mu} \qquad \text{(A-163)}$$

$$\frac{\partial H}{\partial C} = -\frac{2\mu_w \eta_c f \beta}{a_w C^3}\left[\left(2 - \frac{C\eta_c'}{\eta_c}\right)\left(\frac{cp}{\mu} - \lambda\mu\right) - \frac{cp}{\mu}\right] \qquad \text{(A-164)}$$

where it is assumed that the thruster efficiency η_c is a function of exhaust velocity, C, and η_c' represents $d\eta_c/dc$.

Equation (A-153) can now be rewritten as

$$\left\{\lambda_{\mu T}\left(1 + \frac{\partial \mu_F}{\partial \mu_w}\right) - \frac{1}{\mu_w}\left[(\mu_T + \mu_*)\lambda_{\mu T} - \lambda\mu_0\right] + \frac{2\eta_c \mu_*}{a_w C}\int_{T_2}^T \frac{pf}{\mu^2} dt\right\} d\mu_w$$

$$+\left\{\lambda_{\mu T}\frac{\partial \mu_F}{\partial C} + \frac{2\mu_w \eta_c}{a_w C^3}\int_0^T f\left[\left(2 - \frac{C\eta_c'}{\eta_c}\right)\left(\frac{cp}{\mu} - \lambda\mu\right) - \frac{cp}{\mu}\right]\beta(t)dt\right\} dc = 0 \qquad \text{(A-165)}$$

The two variations are independent so the coefficient of each is zero.

$$\left[\mu_T + \mu_* - \mu_w\left(1 + \frac{\partial \mu_F}{\partial \mu_w}\right)\right]\lambda_{\mu T} - \lambda\mu_0 = \frac{2\mu_u \eta_c \mu_*}{a_w C}\int_{T_2}^T \frac{pf\,dt}{\mu^2} \qquad \text{(A-166)}$$

$$\lambda_{\mu T}\frac{\partial \mu_F}{\partial C} = -\frac{2\mu_w \eta_c}{a_w C^3}\int_0^T f\left[\left(2 - \frac{C\eta_c'}{\eta_c}\right)\left(\frac{cp}{\mu} - \lambda\mu\right) - \frac{cp}{\mu}\right]\beta(t)\,dt \qquad \text{(A-167)}$$

Equations (A-166) and (A-167) determine the optimum values of C and μ_w with respect to payload fraction. Note that Eq. (A-166) depends upon μ_*, the fraction of mass dropped in staging. This is very reasonable. The more mass that is discarded during coast, the less will be the propulsion requirement from T_2 to T and the optimum values of C and μ will go up and down, respectively.

The scaling of the adjoint variables is the same as in Problem 1. The primer vector magnitude, p, is scaled arbitrarily at the initial boundary and the switching times T and T_2 must be such that

$$\frac{p_1}{\mu_1} = \frac{p_2}{\mu_2} \tag{A-110}$$

Once again $\mu(t)$ and $\lambda_\mu(t)$ can be determined by numerical quadrature.

$$\mu(t) = 1 - \frac{2\mu_w \eta_c}{a_w C^2}\int_0^t f(\vec{r},\tau)\beta(\tau)\,d\tau - \mu_* \int_0^t \delta(\tau - T_*)\,d\tau \tag{A-168}$$

$$\lambda\mu(t) = \lambda\mu_0 + \frac{2\mu_w \eta_c}{a_w C}\int_0^t \frac{f(\vec{r},r)p\beta(\tau)}{\mu^2}\,d\tau \tag{A-169}$$

The scaling on λ_μ is determined by the fact that the switching function is zero at $t = T_1$.

$$\lambda\mu(T_1) = \frac{cp_1}{\mu_1} \tag{A-170}$$

$$\lambda\mu(0) = \frac{cp_1}{\mu_1} - \frac{2\mu_w \eta_c}{a_w C}\int_0^{T_1} \frac{f(\vec{r},t)p\beta(t)}{\mu^2}\,dt \tag{A-171}$$

This completes the formulation of Problem 2 for fixed-time planetary rendezvous. Combining Eqs. (A-133) and (A-136), the equations of motion can be put into the second-order form of Eqs. (A-103). These equations, along with Eq. (A-168), are the equations of motion. The adjoint equations are Eqs. (A-141) and (A-169). Boundary values are given on the position and velocity vectors at both boundaries. Optimum values of c and μ_w are determined by Eqs. (A-166) and (A-167).

For the other cases of planetary flyby, flyby at a given radius, and orbital transfer the transversality conditions are the same as before.

Problem 3

In this problem the staging during coast consists of dropping the powerplant and thruster used during the initial powered phase as well as the empty propellant tank. Since two separate thrusters and powerplants are used in the two powered phases, there are now four parameters to be optimized: μ_{w1}, μ_{w2}, C_1 and C_2. The subscripts 1 and 2 refer to the first and second powered phases, respectively. The new objective function is the final payload-plus-structure fraction.

$$z = -K\left[\mu_T - \mu_{w2} - \mu_{F2}(\mu_{w2}, C_2) - \mu_s\right] \tag{A-172}$$

The rate of mass loss due to thrusting is

$$\dot{\mu}_c = -\frac{2\eta_{c\nu}\mu_{w\nu} f(\vec{r}_1 t)\beta(t)}{\alpha_{w\nu} C_\nu^2} \tag{A-173}$$

where

$$\nu = \begin{cases} 1 \text{ for } t < T_* \\ 2 \text{ for } t > T_* \end{cases} \tag{A-174}$$

The total rate of mass loss due to both propulsion and staging is

$$\dot{\mu} = \dot{\mu}_c - \left[\mu_{w1} + \mu_{F1}(C_1, \mu_{w1}) + \mu_* T_1\right]\delta(t - T_*), \quad (T_1 \le T_* \le T_2) \tag{A-175}$$

The subscripted powerplant specific weight α_w in Eq. (A-173) allows for the two powerplants μ_{w1} and μ_{w2} being different in this respect. The term $_*T_1$ in Eq. (A-175) represents an empty propellant tank, the mass of which is proportional to the propellant required for the first powered phase.

In addition to Eq. (A-175), the other differential constraints for this problem are

$$\dot{x}_i = \dot{x}_{i+3} \quad (i = 1,2,3) \tag{A-176}$$

$$\dot{x}_{i+3} = \frac{\dot{\mu}_c}{\mu} C_\nu \frac{\lambda_{i+3}}{\rho} - \frac{x_i}{r^3} \tag{A-177}$$

$$\dot{C}_\nu = 0 \tag{A-178}$$

$$\dot{\mu}_{w\nu} = 0 \tag{A-179}$$

From Eqs. (A-175) to (A-199), the variational Hamiltonian, Eq. (A-37), is formed.

$$H = \sum_{i=1}^{3}\left[\lambda_i x_{i+3} - \lambda_{i+3}\frac{x_i}{r^3}\right] + \frac{2\eta_{c\nu}\mu_{w\nu} f\beta}{\alpha_{w\nu} C_\nu^2}\left[\frac{C_\nu P}{\mu} - \lambda\mu\right] \tag{A-180}$$

$$-\lambda\mu\left[\mu_{w1} + \mu_{F1} + \mu_* T_1\right]\delta(t - T_*)$$

Except for the new subscripts ν the Euler-Lagrange equations in λ_{i+3} and λ_μ are exactly the same as in Problem 2.

$$\ddot{\lambda}_{i+3} = -\frac{\lambda_{i+3}}{r^3} + \frac{3x_i}{r^5}\sum_{j=1}^{3}\lambda_{j+3}x_j + \frac{2\mu_{w\nu}\eta_{c2}}{a_{w\nu}C_\nu^2}\frac{\partial f}{\partial x_i}\beta\left(\frac{C_\nu P}{\mu} - \lambda_\mu\right) \tag{A-181}$$

$$\dot{\lambda}_\mu = \frac{2\mu_{w\nu}\eta_{c\nu} f P \beta}{a_{w\nu} C_\nu \mu^2} \tag{A-182}$$

Again the continuity of the Hamiltonian at the corner points T_1 and T_2 requires that the switching function

$$\gamma = \frac{C_\nu P}{\mu} - \lambda_\mu \tag{A-183}$$

must vanish at these two points. Referring to conditions at T_1 by subscript 1 and similarly at T_2,

$$\gamma_1 = \frac{C_1 P_1}{\mu_1} - \lambda_{\mu_1} = 0 \tag{A-184}$$

$$\lambda_{\mu_1} = \frac{C_1 P_1}{\mu_1} = \lambda_{\mu c} + \frac{2\mu_{w1}\eta_{c1}}{a_{w1}C_1}\int_0^{T_1}\frac{Pf}{\mu^2}\,dt \tag{A-185}$$

$$\gamma_2 = \frac{C_2 P_2}{\mu_2} - \lambda_{\mu 2} = 0 \tag{A-186}$$

$$\lambda_{\mu 2} = \frac{C_2 P_2}{\mu_2} = \lambda_{\mu c} + \frac{2\mu_{w1}\eta_{c1}}{a_{w1}C_1}\int_0^{T_1}\frac{Pf}{\mu^2}\,dt + \frac{2\mu_{w\nu}\eta_{c\nu}}{a_{w\nu}C_\nu}\int_{T_1}^{T_2}\frac{Pf\beta}{\mu^2}\,dt \tag{A-187}$$

The last term of Eq. (A-187) is zero since $\beta = 0$ for $T_1 \le t \le T_2$. Since the right-hand sides of Eqs. (A-185) and (A-186) are identical, the left-hand sides may be equated.

$$\frac{C_1 P_1}{\mu_1} = \frac{C_2 P_2}{\mu_2} \tag{A-188}$$

Equation (A-188) corresponds to Eq. (A-110) for problem 1.

The Euler-Lagrange equations for C_ν and $\mu_{w\nu}$ are

$$\dot{\lambda}_{C\nu} = -\frac{\partial H}{\partial C_\nu} \; ; \; \dot{\lambda}_{\mu w\nu} = -\frac{\partial H}{\partial \mu_{w\nu}} \tag{A-189}$$

which can be integrated formally over their respective regions.

$$\lambda_{C1}(T_*) - \lambda_{C1}(0) = -\int_0^{T_*} \frac{\partial H}{\partial C_1}\, dt \tag{A-190}$$

$$\lambda_{C2}(T) - \lambda_{C2}(T_*) = -\int_{T_*}^{T} \frac{\partial H}{\partial C_2}\, dt \tag{A-191}$$

$$\lambda_{\mu w1}(T_*) - \lambda_{\mu w1}(0) = -\int_0^{T_*} \frac{\partial H}{\partial \mu_{w1}}\, dt \tag{A-192}$$

$$\lambda_{\mu w2}(T) - \lambda_{\mu w2}(T_*) = -\int_{T_*}^{T} \frac{\partial H}{\partial \mu_{w2}}\, dt \tag{A-193}$$

Regarding T_* as an internal boundary the general transversality condition is written

$$\begin{aligned} dz + \left[-H\,dt + \sum_{i=1}^{3} \left(\lambda_i dx_i + \lambda_{i+3}\, dx_{i+3}\right)\right]_0^T + \lambda_\mu\, d\mu \Big|_0^{T_*-\epsilon} \\ + \lambda_\mu\, d\mu \Big|_{T_*+\epsilon}^{T} + \lambda_{C1}\, dC_1 \Big|_0^{T_*-\epsilon} + \lambda_{C2}\, dC_2 \Big|_{T_*+\epsilon}^{T} + \lambda_{\mu w1}\, d\mu_{w1} \Big|_0^{T_*-\epsilon} + \lambda_{\mu w2}\, d\mu_{w2} \Big|_{T_*+\epsilon}^{T} \end{aligned} \tag{A-194}$$

In the case of fixed-time rendezvous $dt = dx_i = dx_{i+3} = 0$ at $t = 0$ and T so the second term in Eq. (A-194) vanishes. Differentiation of Eq. (A-172) gives

$$dz = K\left(d\mu_{w2} + \frac{\partial \mu_{F2}}{\partial C_2}\, dC_2 + \frac{\partial \mu_{F2}}{\partial \mu_{w2}}\, d\mu_{w2} - d\mu_T\right. \tag{A-195}$$

At $t = T_*$ the mass fraction μ decreases by an amount $(\mu_{w_1} + \mu_{F_1} + \mu_* T_1)$, i.e.,

$$\mu(T_*+\epsilon) = \mu(T_* + \epsilon) - (\mu_{w1} + \mu_{F1} + \mu_* T_1) \tag{A-196}$$

and

$$d\mu(T_* + \epsilon) = d\mu(T_* - \epsilon) - d\mu_{W1} - \frac{d\mu_{F1}}{dC_1}\, dC_1 - \frac{\partial \mu_{F1}}{\partial \mu_{W1}}\, d\mu_{W1} \tag{A-197}$$

Equations (A-178) and (A-179) ensure that C_1, C_2, μ_{W_1} and μ_{W_2} are all constant in time. Therefore

$$\begin{gathered} dC_1(0) = dC_1(T_*)\ ;\ dC_2(T_*) = dC_2(T)\ ; \\ d\mu_{W1}(0) = d\mu_{W1}(T_*)\ ;\ d\mu_{W2}(T_*) = d\mu_{W2}(T) \end{gathered} \tag{A-198}$$

Substitution of Eqs. (A-190) to (A-195), (A-197), and (A-198) into the transversality condition, Eq. (A-194), gives

$$\begin{aligned} &K\left(d\mu_{W2} + \frac{\partial \mu_{F2}}{\partial C_2}\, dC_2 + \frac{\partial \mu_{F2}}{\partial \mu_{W2}}\, d\mu_{W2} - d\mu_T\right) + \lambda_{\mu 1} d\mu_1 - \lambda_{\mu 1}\left(d\mu_1 - d\mu_{W1} - \frac{\partial \mu_{F1}}{\partial C_1}\, dC_1 - \frac{\partial \mu_{F1}}{\partial \mu_{W1}}\, d\mu_{W1}\right) \\ &+ \lambda_{\mu T}\, d\mu_T - dC_1 \int_o^{T_*} \frac{\partial H}{\partial C_1}\, dt - dC_2 \int_{T_*}^{T} \frac{\partial H}{\partial C_2}\, dt \\ &- d\mu_{W1} \int_o^{T_*} \frac{\partial H}{\partial \mu_{W1}}\, dt - d\mu_{W2} \int_{T_*}^{T} \frac{\partial H}{\partial \mu_{W2}}\, dt = 0 \end{aligned} \tag{A-199}$$

and collecting coefficients of independent variations,

$$\begin{aligned} &(\lambda_{\mu T} - K)\, d\mu_T + \left[\lambda_{\mu 1} \frac{d\mu_{F1}}{dC_1} - \int_o^{T_*} \frac{\partial H}{\partial C_1}\, dt\right] dC_1 + \left[K \frac{d\mu_{F2}}{dC_2} - \int_{T_*}^{T} \frac{\partial H}{\partial C_2}\, dt\right] dC_2 \\ &+ \left[\lambda_{\mu 1}\left(1 + \frac{\partial \mu_{F1}}{\partial \mu_{W1}}\right) - \int_o^{T} \frac{\partial H}{\partial \mu_{W1}}\, dt\right] d\mu_{W1} \left[K\left(1 + \frac{\partial \mu_{F2}}{\partial \mu_{W2}}\right) - \int_{T_*}^{T} \frac{\partial H}{\partial \mu_{W2}}\, dt\right] d\mu_{W2} = 0 \end{aligned} \tag{A-200}$$

The partial derivatives in Eq. (A-200) are now determined.

$$\begin{aligned} \frac{\partial H}{\partial C_\nu} = &- \frac{2\eta_{C\nu}\, \mu_{\omega\nu} f \beta}{\alpha_{\omega\nu}\, C_\nu^3} \left[\left(2 - \frac{C \eta'_{C\nu}}{\eta_{C\nu}}\right)\left(\frac{C_{\nu p}}{\mu} - \lambda_\mu\right) - \frac{C_{\nu p}}{\mu}\right] \\ &- \lambda_\mu\, \delta_{\nu 1} \frac{\partial \mu_{F1}}{\partial C_1}\, \delta(t - T_*),\ (\nu = 1, 2) \end{aligned} \tag{A-201}$$

$$\frac{\partial H}{\partial \mu_{w\nu}} = \frac{2\eta_{c\nu} f\beta}{x_{w\nu} C_\nu^2}\left(\frac{C_2 p}{\mu} - \lambda_\mu\right) - \lambda_\mu \delta_{\nu 1}\left(1 + \frac{\partial \mu_{F1}}{\partial \mu_{w1}}\right)\delta(t - T_*) \qquad (\nu = 1, 2) \qquad \text{(A-202)}$$

where $\delta_{\nu 1}$ is the Kronecker delta.

Since the first term of each of the partial derivatives contains β, which is zero between T_1 and T_2, the limits on the integrals of these terms in Eq. (A-200) can be changed from 0-T_* and T_*-T to 0-T_1 and T_2-T, respectively. The contributions of the second terms are

$$-\int_0^{T_*} \lambda_\mu \frac{\partial \mu_{F1}}{\partial C_1}\,\delta(t - T_*)\,dt = \lambda_\mu(T_*)\frac{\partial \mu_{F1}}{\partial C_1} = -\lambda_{\mu 1}\frac{\partial \mu_{F1}}{\partial C_1} \qquad \text{(A-203)}$$

$$-\int_0^{T_*} \lambda_\mu \left(1 + \frac{\partial \mu_{F1}}{\partial \mu_{w1}}\right)\delta(t - T_*) = \lambda_{\mu_1}\left(1 + \frac{\partial \mu_{F1}}{\partial \mu_{w1}}\right) \qquad \text{(A-204)}$$

Since each of the variations of Eq. (A-200) is independent, the coefficient of each variation must vanish independently. The first term indicates that $\lambda_{\mu_T} = K$ and this can be substituted into the last term. If these operations are performed, Eq. (A-200) becomes

$$\lambda_{\mu 1}\frac{\partial \mu_{F1}}{\partial C_1} + \frac{2\eta_{c1}\mu_{w1}}{\alpha_{w1} C_1^3}\int_0^{T_1} f\left[\left(2 - \frac{C\eta'_{c1}}{\eta_{c1}}\right)\left(\frac{C_1 p}{\mu} - \lambda_\mu\right) - \frac{C_1 p}{\mu}\right]dt = 0 \qquad \text{(A-205)}$$

$$\lambda_{\mu T}\frac{\partial \mu_{F2}}{\partial C_2} + \frac{2\eta_{c2}\mu_{w2}}{\alpha_{w2} C_2^3}\int_{T_c}^{T} f\left[\left(2 - \frac{C\eta'_{c2}}{\eta_{c2}}\right)\left(\frac{C_2 p}{\mu} - \lambda_\mu\right) - \frac{C_2 p}{\mu}\right]dt = 0 \qquad \text{(A-206)}$$

$$\lambda_{\mu 1}\left(1 + \frac{\partial \mu_{F1}}{\partial \mu_{w1}}\right) - \frac{2\eta_{c1}}{\alpha_{w1} C_1^2}\int_0^{T_1} f\left(\frac{C_1 p}{\mu} - \lambda_\mu\right)dt = 0 \qquad \text{(A-207)}$$

$$\lambda_{\mu T}\left(1 + \frac{\partial \mu_{F2}}{\partial \mu_{w2}}\right) - \frac{2\eta_{c2}}{\alpha_{w2} C_2^2}\int_{T_2}^{T} f\left(\frac{C_2 p}{\mu} - \lambda_\mu\right)dt = 0 \qquad \text{(A-208)}$$

The four subsidiary conditions, Eqs. (A-205) to (A-208), determine the optimum values of the four parameters, C_1, C_2, μ_{w_1}, and μ_{w_2}.

It is interesting to note that, although a definite time for discarding the initial propulsion system was defined in formulating the problem (i.e., T_*), the results turn out to be independent of T_*. These results are satisfying from a physical point of view since it should not matter where in the coast period the propulsion system is discarded.

Problem 4

This problem has been motivated by the desire to find a practical thrusting program for a solar-powered vehicle. Such a program has been presented in a two-dimensional analysis in Ref. A-3, where the thrust vector is constrained to make a constant angle (in time) with the radius vector from the sun to the vehicle. Two different angles were allowed before and after coast, and these constant angles were optimized.

In the present three-dimensional problem a vehicle is envisioned with an array of solar panels (or a huge parabolic reflector), which is always maintained perpendicular to the radius vector for maximum efficiency. Rigidly attached to this array at certain definite angles are two electric thrusters, one on either side of the panels. By rotating the whole spacecraft about the radius vector, the thrust vector can be changed while maintaining the solar panels perpendicular to the direction of the solar radiation. The thrust vector is thus constrained to a conical surface about the radius vector, the constant angle of which can be optimized. In a rendezvous mission one thruster is used before coast and the other after, thereby avoiding exhausting propellant through the solar panels.

Consider the typical spherical coordinate system in the sketch below.

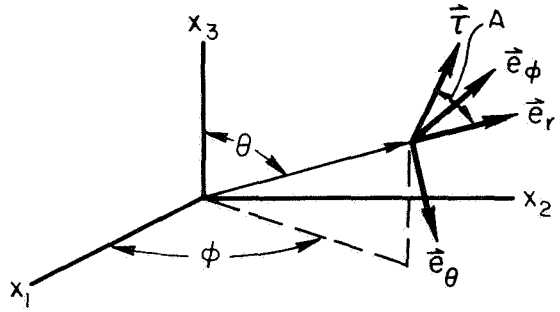

$\vec{\tau}$ is a unit vector in the direction of the thrust which makes a constant angle with respect to the unit radius vector $\vec{r}$. If $\vec{\tau}$ is projected into the plane perpendicular to the radius vector (i.e., the plane defined by the unit vectors $\vec{e}_\theta$ and $\vec{e}_\varphi$), the projection makes a variable angle ψ with respect to the unit vector $\vec{e}_\theta$. Positive ψ is defined as the angle that the unit vector must pass through for it to coincide with the projection of $\vec{\tau}$ when the triad is rotated about $\vec{e}_r$ such that a right-hand screw would move in the direction of the positive $\vec{e}_r$.

The following vector relations are used.

$$\vec{\tau} = \vec{e}_r \cos A + \vec{e}_\theta \sin A \cos\psi + \vec{e}_\phi \sin A \sin\psi \tag{A-209}$$

$$\vec{e}_r = \vec{i}\,\frac{x_1}{r} + \vec{j}\,\frac{x_2}{r} + \vec{k}\,\frac{x_3}{r} \tag{A-210}$$

$$\vec{e}_\theta = \vec{i}\,\frac{x_1 x_3}{r\rho} + \vec{j}\,\frac{x_2 x_3}{r\rho} - \vec{k}\,\frac{\rho}{r} \tag{A-211}$$

$$\vec{e}_\phi = -\vec{i}\,\frac{x_2}{\rho} + \vec{j}\,\frac{x_1}{\rho} \tag{A-212}$$

Where ρ is the projection of the radius vector, $\vec{r}$, onto the ecliptic plane.

Substituting Eqs. (A-210) to (A-212) into Eq. (A-209) $\vec{\tau}$ can be expressed in terms of the Cartesian vector components.

$$\begin{aligned}\vec{\tau} = {} & \vec{i}\left[\frac{x_1}{r}\cos A + \frac{x_1 x_3}{r\rho}\sin A\cos\psi - \frac{x_2}{\rho}\sin A\sin\psi\right] \\ & + \vec{j}\left[\frac{x_2}{r}\cos A + \frac{x_2 x_3}{r\rho}\sin A\cos\psi + \frac{x_1}{\rho}\sin A\sin\psi\right] \\ & + \vec{k}\left[\frac{x_3}{r}\cos A - \frac{\rho}{r}\sin A\cos\psi\right]\end{aligned} \tag{A-213}$$

Using Eq. (A-213) the differential equations of constraint, Eqs. (A-28), may be written.

$$\dot{x}_i = x_{i+3} \qquad (i = 1, 2, 3) \tag{A-214}$$

$$\dot{x}_4 = \frac{bC}{\mu} f\beta\left[\frac{x_1}{r}\cos A + \frac{x_1 x_3}{2\rho}\sin A\cos\psi - \frac{x_2}{\rho}\sin A\sin\psi\right] - \frac{x_1}{r^3} \tag{A-215}$$

$$\dot{x}_5 = \frac{bC}{\mu} f\beta\left[\frac{x_2}{r}\cos A + \frac{x_2 x_3}{r\rho}\sin A\cos\psi + \frac{x_1}{\rho}\sin A\sin\psi\right] - \frac{x_2}{r^3} \tag{A-216}$$

$$\dot{x}_6 \quad \frac{bC}{\mu} f\beta\left[\frac{x_3}{r}\cos A - \frac{\rho}{r}\sin A\cos\psi\right] - \frac{x_3}{r^3} \tag{A-217}$$

$$\dot{\mu} = -bf\beta - \mu_* \delta(t - T_*) \tag{A-218}$$

$$\dot{A} = 0 \tag{A-219}$$

Furthermore, impose the restriction that

$$A = \begin{cases} A_1 \text{ for } t < T_1 \\ A_2 \text{ for } t > T_2 \end{cases} \tag{A-220}$$

Once again it is most convenient to express the problem in the Mayer form. The objective function will be maximum final mass for given values of C and μ_W. These last factors could again be optimized, but this is not considered to be warranted at the present stage. Other factors besides payload optimization may determine μ_W.

$$Z = K\mu_T \tag{A-221}$$

where again K is any positive constant.

The variational Hamiltonian, Eq. (A-37), is now written.

$$\begin{aligned} H = \sum_{i=1}^{3} \left[\lambda_i x_{i+3} - \lambda_{i+3} \frac{x_i}{r^3}\right] + \frac{bCf\beta}{\mu} \Bigg[\cos A \sum_{i=1} \lambda_{i+3} \frac{x_i}{r} \\ + \frac{\sin A \cos\psi}{r\rho} (x_i x_3 \lambda_4 + x_2 x_3 \lambda_5 - \rho^2 \lambda_6) \\ + \frac{\sin A \sin\psi}{\rho} (x_1 \lambda_5 - x_2 \lambda_4)\Bigg] - \lambda_\mu bf\beta - \lambda_\mu \mu_* \delta(t - T_*) \end{aligned} \tag{A-222}$$

The control variables are ψ and $\beta(t)$. The continuous control variable ψ may be determined in terms of the state and adjoint variables through the use of Eq. (A-47).

$$\frac{\partial H}{\partial \psi} = 0 = \frac{bCf\beta \sin A}{\mu\rho} \left[-\frac{\sin\psi}{r} (x_1 x_3 \lambda_4 + x_2 x_3 \lambda_5 - \rho^2 \lambda_6) + \cos\psi (x_1 \lambda_5 - x_2 \lambda_4)\right] \tag{A-223}$$

$$\tan\psi = \frac{r(x_2\lambda_4 - x_1\lambda_5)}{x_3(x_1\lambda_4 + x_2\lambda_5) - \rho^2\lambda_6} \tag{A-224}$$

Whereas before the control variables only depended on the adjoint variables, in this problem an additional coupling has been introduced by the thrusting constraint.

In determining the thrusting angle ψ from Eq. (A-224), there is a choice of two quadrants. One will minimize the Hamiltonian while the other will maximize it. The Pontryagin maximum principle, Eq. (A-64), states that the choice must be the latter.

Next, the Weierstrass-Erdmann corner conditions, Eq. (A-63), are examined at the switching points T_1 and T_2 where β changes from 1 to 0 and vice versa. In order for H to be continuous at T_1 and T_2 the coefficient of β in Eq. (A-222) must vanish at these points since all other terms are continuous. The switching function, γ, for this problem can be written in concise form as

$$\gamma = \frac{C}{\mu}\left[\frac{\cos A}{r}\,\vec{p}\cdot\vec{r} + \frac{\sin A\cos\psi}{r\rho}\,\vec{\rho}\cdot\vec{r}' - \frac{\sin A\sin\psi}{\rho}\,\vec{k}\cdot(\vec{p}\times\vec{r})\right] - \lambda_\mu \qquad \text{(A-225)}$$

where

$$\vec{r}' = \begin{pmatrix} 0 & -\lambda_6 & \lambda_5 \\ -\lambda_6 & 0 & \lambda_4 \\ \lambda_5 & \lambda_4 & 0 \end{pmatrix}\begin{pmatrix} x_1 \\ x_2 \\ x_3 \end{pmatrix} \qquad \text{(A-226)}$$

and

$$\vec{\rho}' = \begin{pmatrix} 0 & 1 & 0 \\ 1 & 0 & 0 \\ 0 & 0 & 0 \end{pmatrix}\begin{pmatrix} x_1 \\ x_2 \\ x_3 \end{pmatrix} \qquad \text{(A-227)}$$

The Hamiltonian can again be written as

$$H = \sum_{i=1}^{3}\left[\lambda_i x_{i+3} - \lambda_{i+3}\frac{x_i}{r^3}\right] + bf\beta\gamma - \lambda_\mu \mu_* \delta(t - T_*) \qquad \text{(A-228)}$$

Applying the maximum principle it is seen that the same condition holds for the discrete control variable β.

$$\beta = \begin{cases} 1 \text{ for } \gamma > 0 \\ 0 \text{ for } \gamma < 0 \end{cases} \qquad \text{(A-98)}$$

The Euler-Lagrange equations are now determined.

$$\ddot{\lambda}_{i+3} = \frac{\partial H}{\partial x_i} = -\frac{\lambda_{i+3}}{r^3} + \frac{3x_i}{r^5}\sum_{j=1}^{3}\lambda_{j+3}\,x_j + b\beta\gamma\frac{\partial f}{\partial x_i} + b\beta f\frac{\partial \gamma}{\partial x_i} \qquad \text{(A-229)}$$

$$\dot{\lambda}_\mu = -\frac{\partial H}{\partial \mu} = \frac{bCf\beta}{\mu^2}\left[\frac{\cos A}{r}\,\vec{p}\cdot\vec{r} + \frac{\sin A\cos\psi}{r\rho}\,\vec{\rho}'\cdot\vec{r}' - \frac{\sin A\sin\psi}{\rho}\,\vec{k}\cdot(\vec{p}\times\vec{r})\right] \qquad \text{(A-230)}$$

$$\dot{\lambda}_A = -\frac{\partial H}{\partial A} = -\frac{bCf\beta}{\mu^2}\left[\frac{\sin A}{r}\,\vec{p}\cdot\vec{r} - \frac{\cos A\cos\psi}{r\rho}\,\vec{\rho}'\cdot\vec{r}' + \frac{\cos A\sin\psi}{\rho}\,\vec{k}\,(\vec{p}\times\vec{r})\right] \qquad \text{(A-231)}$$

The last equation will be used along with transversality conditions to determine the optimum values of A_1 and A_2 on either side of the coast period. The partials $\partial\gamma/\partial x_i$ in Eqs. (A-229) are rather involved and will not be presented here. In taking the partial derivative of Eq. (A-225) with respect to x_i, it must be remembered that ψ is a function of x_i through Eq. (A-224).

The general transversality condition, Eq. (A-80), for this problem is

$$-K\,d\mu_T + \left[-H\,dt + \sum_{j=1}^{6}\lambda_j\,dx_j + \lambda_\mu\,d\mu\right]_0^T + \lambda_{A_1}\,dA_1\Big|_0^{T_1} + \lambda_{A_2}\,dA_2\Big|_{T_2}^{T} = C \qquad \text{(A-232)}$$

where the switching times T_1 and T_2, as far as the angles A_1 and A_2 are concerned, are regarded as internal boundaries. For the case of fixed-time planetary rendezvous, $dt = dx_j = 0$, $(J = 1\ldots6)$, and since both A_1 and A_2 are constant in time,

$$\text{and} \qquad \begin{aligned} dA_1(0) &= dA_1(T_1), \\ dA_2(T_2) &= dA_2(T) \end{aligned} \qquad \text{(A-233)}$$

Equation (A-232) becomes

$$\left(-K + \lambda_\mu(T)\right)d\mu_T + \left(\lambda_{A_1}(T_1) - \lambda_{A_1}(0)\right)dA_1 + \left(\lambda_{A_2}(T) - \lambda_{A_2}(T_2)\right)dA_2 = C \qquad \text{(A-234)}$$

Since $d\mu_T$, dA_1 and dA_2 are independent variations, their respective coefficients in Eq. (A-234) must each be zero.

$$\lambda_{A_1}(T_1) - \lambda_{A_1}(0) = \int_0^{T_1}\lambda'_A\,dt = 0 \qquad \text{(A-235)}$$

$$\lambda_{A_2}(T) - \lambda_{A_2}(T_2) = \int_{T_2}^{T}\lambda'_A\,dt = 0 \qquad \text{(A-236)}$$

Using Eqs. (A-220) and (A-231), Eqs. (A-235 and (A-236) become

$$\sin A_{\substack{1\\2}} \int_{\substack{0\\T_2}}^{\substack{T_1\\T}} \frac{\vec{p}\cdot\vec{r}}{\mu r}\, f\, dt - \cos A_{\substack{1\\2}} \int_{\substack{0\\T_2}}^{\substack{T_1\\T}} \frac{\left[\cos\psi\, \vec{\rho}'\cdot\vec{r}' - r\sin\psi\, \vec{k}\cdot(\vec{p}\times\vec{r})\right] f\, dt}{\mu\, r\rho} = 0 \quad \text{(A-237)}$$

where Eq. (A-237) represents two equations, one for the upper subscripts on A and the upper limits of integration and the other for the lower quantities. Transposing Eq. (A-237), one obtains

$$\tan A_{\substack{1\\2}} = \frac{\int_{\substack{0\\T_2}}^{\substack{T_1\\T}} (\mu r\rho)^{-1}\left[\cos\psi\, \vec{\rho}'\cdot\vec{r}' - r\sin\psi\, \vec{K}\cdot(\vec{p}\times\vec{r})\right] f\, dt}{\int_{\substack{0\\T_2}}^{\substack{T_1\\T}} (\mu r)^{-1}\, \vec{p}\cdot\vec{r}\, f\, dt} \quad \text{(A-238)}$$

Equations (A-238) determine the optimum constant values of A_1 and A_2.

The equations associated with mass, Eqs. (A-218) and (A-230), can be integrated by numerical quadrature.

$$\mu(t) = 1 - b\int_0^T f(\vec{r}_1, \tau)\,\beta(\tau)\, d\tau - \mu_* \int_0^T f(\tau - T_*)\, d\tau \quad \text{(A-239)}$$

$$\lambda_\mu(t) = \lambda_{\mu_0} + bC\int_0^T \frac{f(\vec{r},\tau)\,\beta(\tau)}{\mu^2}\left[\frac{\cos A}{r}\,\vec{p}\cdot\vec{r} + \frac{\sin A\cos\psi}{r\rho}\,\vec{\rho}'\cdot\vec{r}' - \frac{\sin A\sin\psi}{\rho}\,\vec{k}\cdot(\vec{p}\times\vec{r})\right] dt \quad \text{(A-240)}$$

Again p and λ_μ are not independently scaled. The same condition must be satisfied by the primer vector magnitude at the switching times.

$$\frac{p_1}{\mu_1} = \frac{p_2}{\mu_2} \quad \text{(A-110)}$$

Since $\gamma = 0$ at T, Eq. (A-225) shows that

$$\lambda_\mu(T_1) = \frac{C}{\mu_1}\left[\frac{\cos A_1}{r_1}\,\vec{p}_1\cdot\vec{r}_1 + \frac{\sin A_1\cos\psi_1}{r_1 p_1}\,\vec{\rho}_1'\cdot\vec{r}_1' - \frac{\sin A_1\sin\psi_1}{\rho_1}\,\vec{k}\cdot(\vec{p}_1\times\vec{r}_1)\right] \quad \text{(A-241)}$$

and the scaling of λ_μ at 0 can be determined from Eq. (A-240) with $t = T_1$.

For the other boundary conditions of planetary flyby, flyby at a given radius, and fixed-time orbital transfer, the results of Problem 1 may be consulted because the conditions are in each case the same. Of course, in the case of flyby, there is only one switching time T_1 and only one of Eqs. (A-238) is required.

REFERENCES

A-1 Leitmann, G.: "Variational Problems with Bounded Control Variables," Optimization Techniques edited by G. Leitmann (Academic Press, Inc., New York, 1962), Chap. 5, pp. 172-203.

A-2 Lawden, D. F.: Optimal Trajectories for Space Navigation (Butterworths, London, 1963).

A-3 Melbourne, W. G. and C. G. Sauer, Jr.: "Constant Attitude Thrust Program Optimization," American Institute of Aeronautics and Astronautics Preprint 63-420, August 1963.

Appendix A Nomenclature - Part 2

A	Angle between thrust vector and radius vector
a_o	Initial thrust acceleration
b	Fractional time rate of change of vehicle mass
C	Exhaust velocity
$\vec{e}_r$, $\vec{e}_\theta$, $\vec{e}_\phi$	Conventional orthonormal vector basis for spherical coordinates
$f(\vec{r}, t)$	Power available function of position and time
$f(\xi)$, $g(\xi)$	Planetary position and velocity functions of central angle
H	Variational Hamiltonian
$\vec{i}$, $\vec{j}$, $\vec{k}$	Conventional orthonormal vector basis for Cartesian coordinates
K	Arbitrary positive constant
m	Vehicle mass
P	Power available
$\vec{p}$	Primer vector
R	Radius (given constant)
$\vec{r}$	Radius vector
T	Given instant of time
t	Time
x	Position coordinates
z	Objective function (corresponds to the auxiliary state variable, z_1 of the Appendix)
α_w	Powerplant specific mass
β	Discrete control variable
γ	Switching function

NOMENCLATURE (cont'd)

$\delta(t-T_*)$	Dirac delta function
$\delta_{i\nu}$	Kroneker delta $= \begin{cases} 1 \text{ for } \nu = 1 \\ 0 \text{ for } \nu \neq 1 \end{cases}$
ϵ	Small quantity
η_c	Thruster power conversion efficiency
θ	Standard spherical coordinate angle
λ_i	Adjoint variable (or Lagrange multiplier) conjugate to position coordinate x_i
λ_{i+3}	Adjoint variable conjugate to velocity component x_i
λ_μ	Adjoint variable conjugate to the mass
μ	Vehicle mass fraction (based on initial mass)
μ_f	Thruster fraction
μ_w	Powerplant fraction
μ_s	Structure fraction
μ_*	Fraction of initial mass discarded at staging point
ξ	Orbital central angle
ρ	Projection of radius vector onto ecliptic plane
τ	Time - (dummy integration variable)
$\vec{\tau}$	Unit vector in the direction of thrust
ϕ	Standard spherical coordinate angle
ψ	Angle between unit vector $\vec{e}_\theta$ and the projection of $\vec{\tau}$ onto the $\vec{e}_\theta$ and $\vec{e}_\phi$

APPENDIX B

DERIVATION OF PLANETOCENTRIC EQUATIONS FOR HIGH-LOW THRUST OPERATIONS

The first integrals of the equation of motion in differential form which describes the trajectory of a thrusting vehicle within a planetary gravitational field are derived. The form of the vehicle thrust acceleration is displayed.

The basic equation of motion in polar coordinates for vehicles thrusting in a planetary gravitational field is:

$$\ddot{\bar{\zeta}} = -\frac{1}{\zeta^2}\,\bar{i}_\zeta + \tilde{\sigma}\,\bar{i}_V \qquad \text{(B-1)}$$

where ζ = nondimensional radial distance

$\tilde{\sigma}$ = nondimensional vehicle thrust acceleration

$\bar{i}_\zeta$ = unit vector in radial direction

$\bar{i}_V$ = unit vector in direction of instantaneous velocity

Consider the two vector operations $\dot{\bar{\zeta}} \cdot (\quad)$ and $\bar{\zeta} \times (\quad)$:

$$\dot{\bar{\zeta}} \cdot \ddot{\bar{\zeta}} = -\frac{1}{\zeta^2}\,\dot{\bar{\zeta}} \cdot \bar{i}_\zeta + \tilde{\sigma}\, V\, \bar{i}_V \cdot \bar{i}_V \;,\quad \dot{\bar{\zeta}} = V\bar{i}_V$$

$$\frac{d}{d\tau}\,\frac{V^2}{2} = -\frac{1}{\zeta}\,\frac{d\zeta}{d\tau} + \tilde{\sigma}\, V$$

and

$$\frac{d}{d\tau}\,\frac{V^2}{2} - \frac{1}{\zeta} = \tilde{\sigma}\, V$$

but,

$$\frac{V^2}{2} - \frac{1}{\zeta} = E$$

where E is vehicle total energy.

Therefore,

$$\frac{dE}{d\tau} = \tilde{\sigma} V \tag{B-2}$$

Now,

$$\bar{\zeta} \times \ddot{\bar{\zeta}} = \bar{\zeta} \times \left(-\frac{1}{\zeta^2}\right) \bar{i}_\zeta + \tilde{\sigma} (\bar{\zeta} \times \bar{i}_V)$$

but,

$$\ddot{\bar{\zeta}} = (\ddot{\zeta} - \zeta \dot{\eta}^2) \bar{i}_\zeta + \frac{1}{\zeta} \frac{d}{d\tau} (\zeta^2 \dot{\eta}) \bar{i}_a$$

where η = azimuthal angle

$\bar{i}_a$ = unit vector in azimuthal direction

$\bar{i}_z = \bar{i}_\zeta \times \bar{i}_a$

and

$$\bar{\zeta} \times \ddot{\bar{\zeta}} = \frac{d}{d\tau} (\zeta^2 \dot{\eta}) \bar{i}_z$$

Also,

$$\bar{i}_V = \frac{\dot{\zeta}}{V} \bar{i}_\zeta + \frac{\zeta \dot{\eta}}{V} \bar{i}_a$$

and

$$\bar{\zeta} \times \bar{i}_V = \frac{\zeta^2 \dot{\eta}}{V} \bar{i}_z$$

Therefore,

$$\frac{d}{d\tau}\left(\zeta^2\ \dot{\eta}\right) = \frac{\tilde{\sigma}\left(\zeta^2\ \dot{\eta}\right)}{V}$$

Let

$$H \equiv \zeta^2\ \dot{\eta} \qquad \text{(instantaneous vehicle angular momentum)}$$

so that

$$\frac{d}{d\tau}(H) = \frac{\tilde{\sigma}\ H}{V} \tag{B-3}$$

The conversion from dimensional variables to nondimensional variables may be made as follows:

$$\zeta = r/r_{P0}$$

$$V = v/v_{c_{P0}}$$

$$\tilde{\sigma} = \tilde{g}/g_{P0}$$

$$\tau = t\ v_{c_{P0}}/r_{P0}$$

$$E = e/v_{c_{P0}}^2$$

$$H = h/r_{P0}\ v_{c_{P0}}$$

$$C = I_{sp}\ g_{\oplus}/v_{c_{P0}} \tag{B-4}$$

The thrust acceleration of the vehicle is either

$$\sigma(\tau) = \sigma \tag{B-5a}$$

or,

$$\sigma(\tau) = \begin{cases} \sigma_i/\left(1 - \frac{\sigma_i\ \tau}{C}\right), & \tau \geq 0 \text{ (Departure)} \\ \sigma_{B0}/\left(1 - \frac{\sigma_{B0}\ \tau}{C}\right), & \tau \leq 0 \text{ (Capture)} \end{cases} \tag{B-5b}$$

where, σ = constant thrust acceleration ($C \rightarrow \infty$)

σ_i = initial thrust acceleration of vehicle

σ_{B_0} = final thrust acceleration of vehicle

C = exhaust speed

APPENDIX C

CONSTANT LOW-THRUST PLANETOCENTRIC SPIRAL

Perkins' Generalized Equations of Motion

The problem of analyzing the performance of an electrically propelled vehicle departing from or arriving onto a parking orbit has been studied by Perkins (Ref. C-1) and extended by Edelbaum (Ref. C-2). The approach to be discussed is based largely on the results of Perkins and Edelbaum and is oriented primarily towards simplifying the analytical techniques as much as possible.

The low-thrust vehicle of mass, m, is under constant thrust, F, which is applied tangentially, thereby resulting in the instantaneous velocity vector, V, along the path. The thrust is applied at an angle, θ, to the local horizontal and at a radial distance, R, from the center of the planet (Fig. C-1).

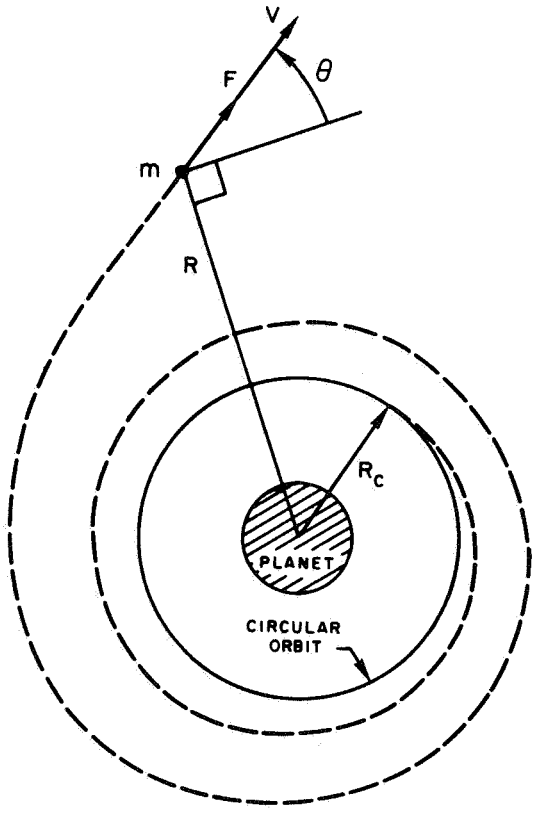

Fig. C-1 Low-Thrust Spiral

The total acceleration along the radius is given by

$$\ddot{R} = \left(\frac{V^2}{R}\right) - \frac{\dot{R}^2}{R} - \frac{\mu}{R^2} + \frac{F}{m}\,\frac{\dot{R}}{V}$$

where μ is the planet's gravity constant. The first two terms on the right are the centrifugal acceleration, the third term is the acceleration of gravity at R, and the last term is the vertical component of thrust acceleration.

The total acceleration along the flight path is given by

$$\dot{V} = \frac{F}{m} - \frac{\mu}{R^2}\,\frac{\dot{R}}{V}$$

The rate of change of mass is

$$\dot{m} = -\frac{F}{C} = -\frac{F}{I_{SP}\,g_0}$$

where C is the exhaust velocity and g_0 is the standard acceleration of gravity on the Earth's surface.

To express the differential equations in a form independent of the gravity constant and thrust acceleration, Perkins introduces the following dimensionless parameters; radius, X; velocity, Y; and time, T, defined according to

$$X \triangleq \left(\frac{F/m_E}{\mu}\right)^{1/2} R,$$

$$Y \triangleq \left(\mu\,\frac{F}{m_E}\right)^{-1/4} V,$$

and

$$T \triangleq \frac{(F/m_E)^{3/4}}{\mu^{1/4}}\,t,$$

where the thrust acceleration, F/m_E, is referenced to escape conditions by using the mass of the vehicle at escape, m_E. To account for the variation in mass, Edelbaum defines a dimensionless exhaust velocity, Z, and a characteristic velocity, W, by

$$Z \triangleq \left(\mu \frac{F}{m_E}\right)^{-1/4} C,$$

and

$$W \triangleq Z \ln\left(\frac{m_E}{m}\right)$$

Introducing the foregoing parameters into the differential equations of motion and making W the independent variable yields

$$e^{2W/Z}\left(X'' + \frac{X'}{Z} - \frac{X}{Y}\right) = \frac{Y^2}{X} - \frac{(X')^2}{X} - \frac{1}{X^2}$$

and

$$Y' = 1 - \frac{X'}{X^2 Y},$$

where the prime notation indicates differentiation with respect to W. Because these equations are independent of the thrust-to-weight ratio, specific impulse, and mass of the planet, any solution of these equations represents a family of solutions of the original differential equations corresponding to different values of thrust-to-weight ratio, specific impulse, and initial conditions. Further, where the solution is independent of the initial conditions, one solution curve will suffice for all cases. This circumstance occurs when the local flight conditions approximate a circular orbit.

If the vehicle thrust-to-weight ratio is less than 10^{-2} starting on a circular orbit, X and its derivatives are small and the first of the above differential equations becomes $Y^2 = 1/X$. This relationship defines circular orbital flight and, hence, for very small local thrust-to-weight ratios, the trajectory is quasi-circular. Consequently, the vehicle will pass through the initial conditions of other low-thrust trajectories with the same mean velocity, radius, and flight path angle regardless of the starting time and position. Thus, any low-thrust spiral trajectory may be represented by one curve of Y versus X or Y versus W, each of which depends only on Z.

The results of a numerical integration of the generalized equations are presented in Figs. C-2, C-3, and C-4. Positive values of Z correspond to departure from a circular orbit while negative values correspond to approach. The constant thrust-acceleration results of Ref. 1 are included in these figures and correspond to the case of $Z \rightarrow \infty$.

From Fig. C-3 it can be seen that the curves approach a slope of -1 at high circular velocities and a slope of +1 at high hyperbolic velocities. Thus it is possible to utilize simple linear expressions for the dimensionless characteristic

velocity, W, (referenced to escape) required to reach a mean path velocity, Y. As an example, if the lower asymptotes are used (conservative basis), then

$$Y = +W + 0.941 = Z \ln\left(\frac{m_E}{m}\right) + 0.941,$$

for either starting from (+Z) or arriving at (-Z) escape conditions with final or initial, respectively, high hyperbolic speeds. Also

$$Y = -W + 0.805 = -Z \ln\left(\frac{m_E}{m}\right) + 0.805$$

for either starting from (+Z) or arriving onto (-Z) a circular orbit with final or initial, respectively, escape speed.

A region of validity can be described depending on a given tolerable error. If an error of about 5% is acceptable, then

$W < -1.0$ and $Y > 1.8$ between circular and escape velocity,
$W > +1.0$ and $Y > 1.95$ between escape and hyperbolic velocity.

Thus, to use the simplified expressions it is necessary to assure that no case is encountered which leads to W's and Y's which violate the above restrictions.

Use of Simplified Expressions

The following discussion presents the results of translating the dimensionless equations into vehicle system and trajectory terms.

Planetary Departure

If the vehicle starts from a circular orbit and goes to escape conditions, the equation is

$$Y = -Z \ln\left(\frac{m_E}{m_C}\right) + 0.805$$

Substituting the definitions of Y and Z, and after some manipulating, the mass ratio required is

$$\frac{m_C}{m_E} = \exp\left\{\frac{V_C}{C}\left[1 - 0.805\left(\frac{F/m_C}{\mu/R_C^2}\right)^{1/4}\left(\frac{m_C}{m_E}\right)^{1/4}\right]\right\} \quad \text{circular orbit to escape}$$

where m_C is the initial mass on the circular orbit, V_C is the circular speed, and m_E is the mass at escape. The term F/m_C is the initial thrust-to-weight ratio. Note that because the thrust-to-weight ratio is usually known at the initiation of low thrust rather than at burnout, an iterative procedure is required to determine m_C/m_E. Alternatively, an explicit form may be obtained by expanding the exponential and using the fact that m_C/m_E is approximately 1.0.

If the vehicle starts from escape velocity and is to achieve a hyperbolic velocity, V_H, at infinity, the appropriate equation is

$$Y = Z \ln\left(\frac{m_E}{m_H}\right) + 0.941$$

This can be translated into system terms. Thus

$$\frac{m_E}{m_H} = \exp\left[\frac{V_H}{C} - \frac{0.941}{C}\left(\mu\frac{F}{m_E}\right)^{1/4}\right] \qquad \text{escape to hyperbolic}$$

where m_H is the mass at infinity and F/m_E is the initial thrust-to-weight ratio. Since F/m_E is known initially, m_E/m_H may be computed directly.

The mass ratio required to achieve a hyperbolic speed starting from a circular parking orbit may be found by combining the two foregoing portions of the overall trajectory. Hence

$$\frac{m_C}{m_H} = \exp\left\{\frac{V_H}{C} + \frac{V_C}{C}\left[1 - 1.746\left(\frac{F/m_C}{\mu/R_C^2}\right)^{1/4}\left(\frac{m_C}{m_E}\right)^{1/4}\right]\right\} \qquad \text{circular to hyperbolic}$$

where m_C/m_E is found from the circular orbit-to-escape equation and F/m_C is the initial thrust-to-weight ratio.

The corresponding limitations on velocity, assuming an allowable error of about 5%, become

$$V_C \geq 1.8\left(\mu\frac{F}{m_C}\right)^{1/4}\left(\frac{m_C}{m_E}\right)^{1/4} \qquad \text{circular to escape}$$

$$V_H \geq 1.95\left(\mu \frac{F}{m_E}\right)^{1/4} \qquad \text{escape to hyperbolic}$$

Planetary Capture

For a vehicle at infinity approaching the planet with some hyperbolic speed, the corresponding linear equation is

$$Y = Z \ln\left(\frac{m_E}{m_H}\right) + 0.941$$

Substituting the definitions for Y and Z and accounting for Z being negative for capture, the mass ratio equation becomes

$$\frac{m_H}{m_E} = \exp\left[\frac{V_H}{C} - \frac{0.941}{C}\left(\mu \frac{F}{m_H}\right)^{1/4}\left(\frac{m_H}{m_E}\right)^{1/4}\right] \qquad \text{hyperbolic to escape}$$

where m_H is the initial mass and F/m_H the initial thrust-to-weight ratio. Again, because the thrust-to-weight ratio is known at startup rather than at burnout, an iterative procedure is necessary to determine m_H/m_E.

Using the same procedure as before, the mass ratio necessary to achieve a circular orbit from an initial escape velocity is given by

$$\frac{m_E}{m_C} = \exp\left\{\frac{V_C}{C}\left[1 - 0.805\left(\frac{F/m_E}{\mu/R_C^2}\right)^{1/4}\right]\right\} \qquad \text{escape to circular}$$

The two foregoing expressions are combined to obtain the mass ratio required for capturing onto a circular orbit from a hyperbolic velocity at infinity. Thus

$$\frac{m_H}{m_C} = \exp\left\{\frac{V_H}{C} + \frac{V_C}{C}\left[1 - 1.746\left(\frac{F/m_H}{\mu/R_C^2}\right)^{1/4}\left(\frac{m_H}{m_E}\right)^{1/4}\right]\right\} \qquad \text{hyperbolic to circular}$$

where m_H/m_C is the ratio of the initial mass to the mass on the circular orbit and m_H/m_E is obtained from the hyperbolic-to-escape equation.

The appropriate limitations on velocity for a low-thrust planetary capture spiral are given by

$$V_C \geq 1.8\left(\mu \frac{F}{m_E}\right)^{1/4} \qquad \text{circular to escape}$$

$$V_H \geq 1.95\left(\mu \frac{F}{m_E}\right)^{1/4}\left(\frac{m_H}{m_E}\right)^{1/4} \qquad \text{hyperbolic to escape}$$

As can be seen, the utility of the foregoing overall approach to the analysis of low-thrust planetocentric operations is in the relatively simple equations involved; it is not necessary to solve a system of differential equations. The limitation of this simplified approach, however, is in the restriction of circular and hyperbolic speeds required by the linearized dimensionless equations. An example of this restriction is shown in Table C-1. Note that some values of Y are less than the maximum of 1.95 allowed for thrusting to some hyperbolic speed. An additional basic limitation is the assumption that the vehicle possesses a given hyperbolic velocity at the planet's sphere of influence rather than at infinity.

APPENDIX C REFERENCES

C-1. Perkins, F. M.: "Flight Mechanics of Low-Thrust Spacecraft," Journal of Aerospace Sciences, Vol. 26, No. 5, May 1959, p. 291-297.

C-2. Edelbaum, T. N.: "A Comparison of Nonchemical Propulsion Systems for Round-Trip Mars Missions," United Aircraft Research Laboratories, Report E-1383-2, October 1960.

TABLE C-1

RADIUS DISTANCE WHERE HYPERBOLIC SPEED IS ACHIEVED

Hyperbolic speed = 4.5 km/sec
Ion thrustor, d = 20 km/sec
Powerplant specific mass = 20 kg/kw
Earth's activity sphere = 116 Earth Radii

C, km/sec	W	Y	R_{BO}, Earth radii
40	0.006	3.04	134
	0.020	2.25	41.6
	0.100	1.51	6.6
100	0.006	3.72	296
	0.020	2.75	96
	0.100	1.84	18

FIG. C-2

MEAN PATH PARAMETRIC VELOCITY AND RADIUS DISTANCE

CONSTANT LOW-THRUST PLANETOCENTRIC SPIRAL

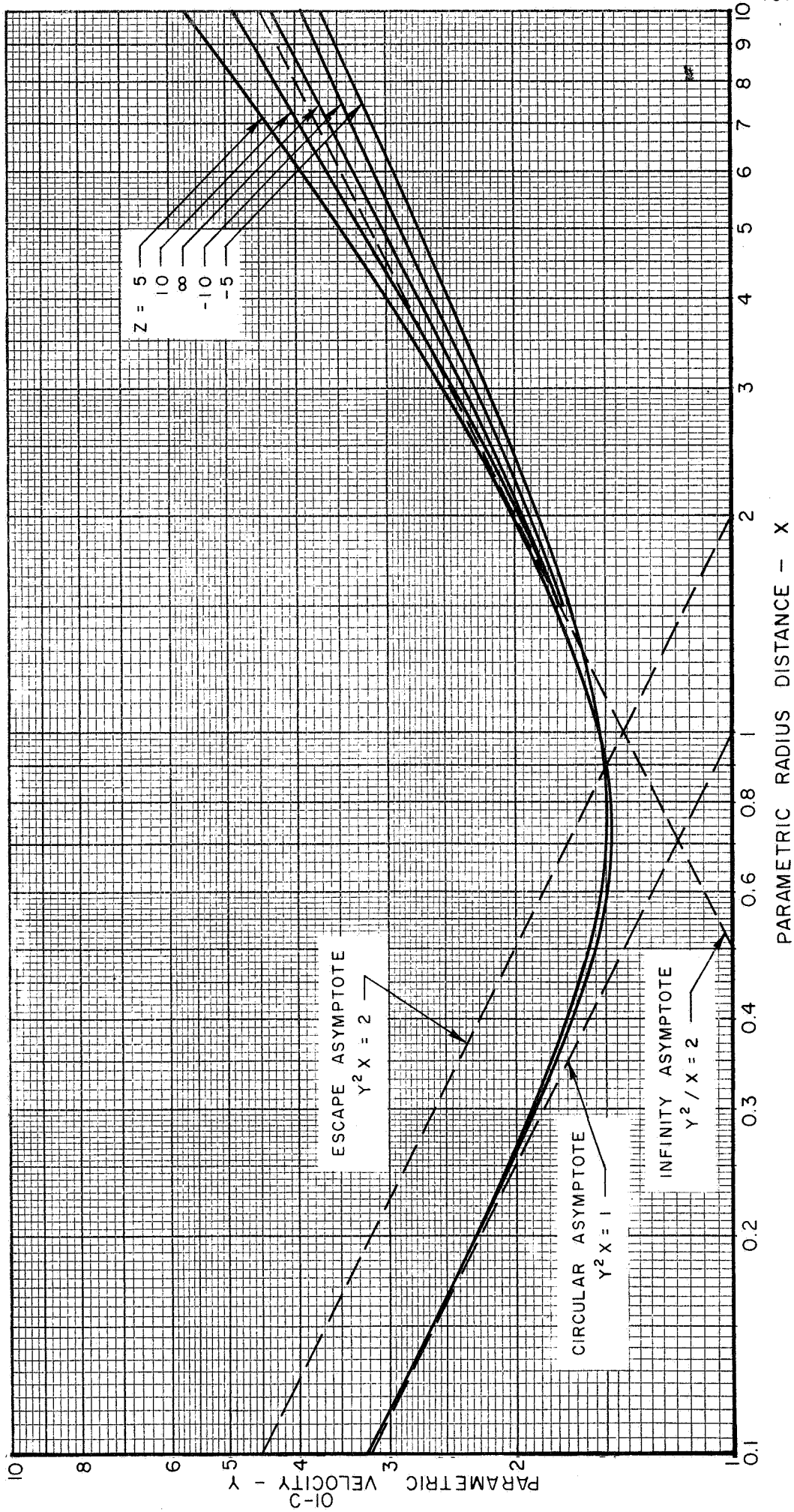

FIG. C-3

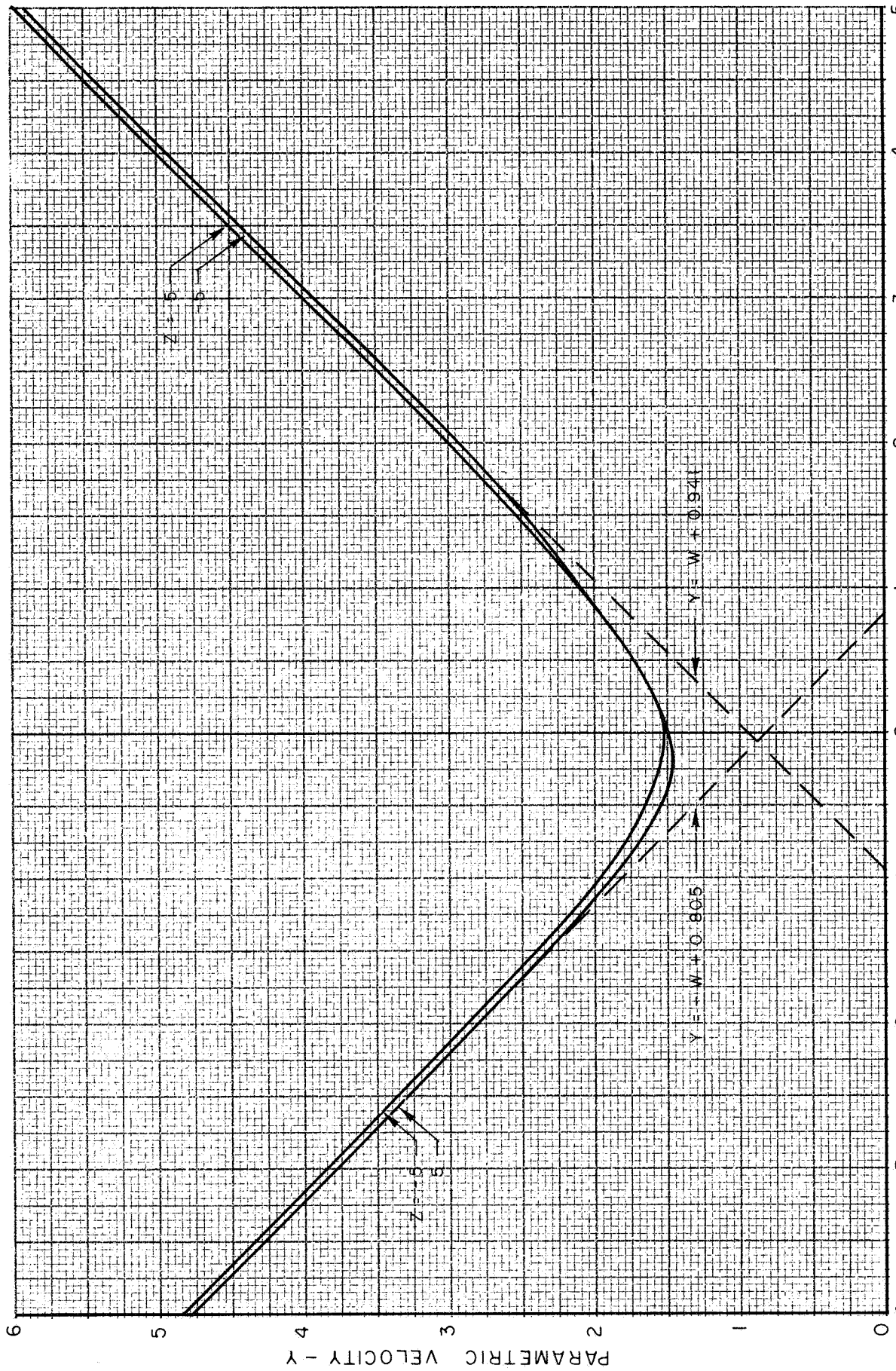
DEPENDENCE OF MEAN PATH VELOCITY ON CHARACTERISTIC VELOCITY
CONSTANT LOW-THRUST PLANETOCENTRIC SPIRAL
PARAMETRIC VELOCITY - γ
CHARACTERISTIC VELOCITY REFERENCED TO ESCAPE - W = Z ln(m_E/m)
γ = W + 0.941
γ = W + 0.805
Z = 6
Z = 5
6
5
4
3
2
1
0
-4
-3
-2
-1
0
1
2
3
4
5

FIG. C-4

FLIGHT PATH ANGLE AT VARIOUS RADIUS DISTANCES

CONSTANT LOW-THRUST PLANETOCENTRIC SPIRAL